DESIGN, SYNTHESIS AND BIOLOGICAL ASSESSMENT OF MOLECULAR TRANSPORTERS FOR TARGETED DELIVERY OF ANTI-CANCER DRUGS

Thesis Submitted to Academy of Scientific and Innovative Research (AcSIR)
for the Award of the Degree of
DOCTOR OF PHILOSOPHY
in Chemical Sciences

By

JYOTHI B. NAIR

Registration No: 10CC15A39011

Under the guidance of

Dr. KAUSTABH KUMAR MAITI

CSIR-NATIONAL INSTITUTE FOR INTERDISCIPLINARY SCIENCE AND TECHNOLOGY (CSIR-NIIST)
THIRUVANANTHAPURAM-695019, KERALA, INDIA

July, 2018

Dedicated to

My Beloved Family

Declaration

I hereby declare that the matter embodied in the thesis entitled: "**Design, synthesis and biological assessment of molecular transporters for targeted delivery of anti-cancer drugs**" is the result of the investigations carried out by me at the Organic chemistry section, Chemical Sciences and Technology Division, CSIR-National Institute for Interdisciplinary Science and Technology (CSIR-NIIST), Trivandrum, under the supervision of Dr. Kaustabh Kumar Maiti and the same has not been submitted elsewhere for any other degree.

In keeping with the general practice of reporting scientific observations, due acknowledgement has been made wherever the work described is based on the findings of other investigators.

Jyothi B. Nair

National Institute for Interdisciplinary Science and Technology (NIIST)
Council of Scientific and Industrial Research (CSIR)
Industrial estate P.O., Thiruvananthapuram- 695019
Kerala, India

Dr. Kaustabh Kumar Maiti
Senior Scientist
Chemical Sciences and Technology Division

Tel: 0471-2515475
Mob: +91-8547761544
e-mail: kkmaiti@niist.res.in
kkmaiti29@gmail.com

July, 2018

Certificate

This is to certify that the work embodied in this Ph.D. thesis entitled "**Design, synthesis and biological assessment of molecular transporters for targeted delivery of anti-cancer drugs**" submitted by **Ms. Jyothi B. Nair** to Academy of Scientific and Innovative Research (AcSIR), in partial fulfilment of the requirements for the award of the **Degree of Doctor of Philosophy in Chemical Sciences**, has been carried out under my supervision and guidance at the Organic chemistry Section, Chemical Sciences and Technology Division of the CSIR-National Institute for Interdisciplinary Science and Technology (CSIR-NIIST), Thiruvananthapuram. I further certify that this work has not been submitted to any other University or Institution in part or full for the award of any degree or diploma.

Jyothi B. Nair

Dr. Kaustabh Kumar Maiti
(Thesis Supervisor)

Acknowledgements

It is with great pleasure that I extend my deep sense of gratitude to Dr. Kaustabh Kumar Maiti, my thesis supervisor, for suggesting the research problem, for his valuable guidance, support, encouragement and scientific freedom of thought and action, leading to the successful completion of this work.

I thank Dr. A. Ajayaghosh, Dr. Gangan Prathap, and Dr. Suresh Das, present and former Directors of CSIR- NIIST, Trivandrum, for providing me the necessary facilities for carrying out this work.

I express my deep sense of gratitude to our collaborator Dr. Surajith Ghosh from CSIR-IICB- Kolkata and Dr. T.T. Sreelekha for biological studies and valuable suggestions.

My sincere thanks are also due to:

- *Dr. Mangalam S. Nair and Dr. R. Luxmi Varma, former and present AcSIR coordinators.*
- *Dr. K. R. Gopidas, Dr. D. Ramaiah Former Head, Chemical Sciences and Technology Division for their support*
- *Dr. L. Ravi Shankar, Dr Priya S. and Dr. R. Luxmi Varmamy DAC members*
- *Dr. G. Vijay Nairand Prof. M. V. George, for their inspiring presence*
- *Dr. K. V. Radhakrishnan, Dr. B. S. Sasidhar and Dr. Sunil Varughese Scientists of Organic Chemistry Section, for their help and support extended to me*
- *Dr. Raghu K. G for providing initial cell culture facilities.*
- *Dr. Jubi John and Dr. Ganesh Chandra Nandi for their valuable suggestions and support*
- *Sincere thanks to Dr. Manu M. Joseph, Dr. Vandanashanker, Ms. Varsha Karunakaran and Mr. Saswat Mohaptra for teaching and helping biological experiments.*
- *Special thanks to Ms.Sreedevi, Dr. Dhanya, Dr. Sajin, Dr. Parvathy, Mr. Preethanuj, Dr. Saranya, Dr. Shimi, Dr. Sarath, Dr. Vineeth Vijayan, and Dr. Susan Alex for their timely help and support.*

- *Mrs. M. Saumini, Mr. P. Saran and Mr. R. Gokul, Mr. Syam for NMR, Mrs. S. Viji, Ms. Athira for mass spectral analyses and Mr. Kiran M. and Mr. Robert Philip for TEM analysis*
- *Ms. Tanwista, Ms. Chinju, Mr. Jagadeesh , Mr. Rajeev, Mr. Thejus, Ms. Jayanthy, Ms. Ramya, Ms. Reshma, my classmates and roommates*
- *Sincere thanks to my group members Mr. Santhi Maniganda, Dr. Nisha N., Ms. Ramya A.N., Mr. Sujai P.T., Ms. Saranya Giridharan, Ms. Arya J.S., Mr. Syamjith S., Ms. Deepika S., Dr. Vishnupriya M. and Mr. Madhukrishnan M. for their love, friendship and support.*
- *Ms .Safeera M, Ms. Priya S., Ms. Monica Antony for assisting me in conducting some of the experiments reported in this thesis*
- *Special thanks to Mr. V.T Mathew my Plus two teacher for the inspiration*
- *All my beloved teachers at every stages of my academic career.*
- *All students of organic chemistry section.*
- *All my friends at NIIST.*
- *(UGC) & CSIR for the financial assistance.*

I am deeply and forever indebted to and my husband Mr. Sreekanth for his constant source of love, care, motivation and support.

Special thanks to my son Mr. Avaneeth for adjusting with me for finishing my works.

I would like to thank my parents, sister, brother and my husband's parents for their love and prayers.

I would like to thank my teachers and friends starting from my school days to those at NIIST, who motivated and blessed me.

Above all, I bow to Almighty for bestowing his blessings upon me.

Jyothi B. Nair

CONTENTS

List of Schemes

List of Figures

by Annexin-V staining after treating HeLa and A549 cells without and with laser Flow cytometry analysis showing Annexin-V-FITC staining in the x-axis and PI in the y-axis. Percent of annexin-positive (apoptotic) cells is indicated in the respective quadrants. a) HeLa without, b) with laser and c) represents cumulative effects. d) A549 without, e) with laser and f) represents cumulative effects.

List of Abbreviations

a.u.	Arbitrary unit
ACN	Acetonitrile
Ala	Alanine
AO	Acridine orange
Arg	Arginine
Asp	Asparticacid
AuNPs	Gold nanoparticles
BBB	blood–brain barrier
BTB	blood tumor barrier
CathB	Cathepsin B
CCD	Charge-coupled device
$CDCl_3$	Deuterated chloroform
$CHCl_3$	Chloroform
cm	Centimeter
CNTs	Carbon nanotubes
CO_2	Carbondioxide
CPPs	Cell-penetrating peptides
cRGD	Cyclic RGD
d	Doublet
DCM	Dichloromethane
DIC	N,N'-diisopropylcarbodiimide
DIPEA	N,N-diisopropylethylamine
DLS	Dynamic light scattering

DMEM	Dulbecco's modified eagle's medium
DMF	Dimethyl formamide
DMSO	Dimethyl sulfoxide
DNA	Deoxyribonucleic acid
DOX	Doxorubicin
ε	Molar extinction coefficient
EDC	3-(dimethylamino)-propyl)-N′-ethylcarbodiimide
EGF	Epidermal growth factor
EGFR	Epidermal growth factor receptor
EPR	Enhanced permeability and retention
EDTA	Ethylene di amine tetra acetic acid
eq.	Equivalent
EtOAc	Ethyl acetate
FBS	Fetal bovine serum
FITC	Fluorescein isothiocyanate
Fl	Fluorescein
FR	Folate receptor
Glu	Glutamic acid
Gly	Glycine
GSH	Glutathione
GSSG	Glutathione disulfide
H_2O	Water
H9C2	Cardiac cell line
HATU	1-[Bis(dimethylamino)methylene]-1H-1,2,3-triazolo[4,5-b]pyridinium 3-oxide hexafluorophosphate

HCl	Hydrochloric acid
HeLa	Cervical Cancer cell line
HER2	Human epidermal growth factor receptor2
HGNPs	Hollow gold nanoparticles
HPLC	High performance liquid chromatogrphy
HRMS	High resolution mass spectrometry
HR-TEM	High-resolution transmission electron microscopy
Hz	Hertz
J	Coupling constant
λ	Wavelength
Leu	Leucine
λ_{ε}	Excitation wavelength
Lys	Lysine
m	Multiplet
$\mathbf{M^+}$	Molecular ion
MALDI-TOF	Matrix-assisted laser desorption ionization-time of flight
max	Maximum
MDR	Multiple drug resistance
mg	Milligram
MHz	Mega hertz
min	Minutes
mL	Millilitre
mm	Millimeter
mM	Millimolar

mmol	Milli mole
MMP	Matrix metalloproteinases
mol	Mole
MSNs	Mesoporous silica nanoparticles
MTT	3-(4,5-dimethylthiazol-2-yl)-2,5-diphenyltetrazolium bromide
MW	Molecular weight
NA	Numerical aperture
NaOAc	Sodium acetate
Na_2SO_4	Sodium sulfate
NaCl	Sodium chloride
NaOH	Sodium hydroxide
NGF	Neural growth factor
NHS	N-hydroxysuccinimide
NIR	Near-infrared
nm	Nanometer
nM	Nanomolar
NMR	Nuclear Magnetic resonance
NO	Nitric oxide
NPs	Nanoparticles
PABC	P-aminobenzyloxycarbonyl
PAI	Photoacoustic imaging
PBS	Phosphate buffered saline
PCB	Poly carboxybetaine methacrylate
PD	Pharmacodynamic

PDPA	Poly (2-(diisopropylamino)ethyl methacrylate)
PDT	Photodynamic therapy
PEG	Poly(ethylene glycol)
PGs	Prostaglandins
pH	Hydrogen ion concentration at logarithmic scale
Phe	Phenyl alanine
PI	Propedium iodide
PK	Pharmacokinetic
ppm	Parts per million
PS	Photo sensitizer
PSA	Prostate specific antigen
PTT	Photothermal therapy
PTX	Paclitaxel
QDs	Quantum dots
RES	Reticulo-endothelial system
RGD	Arg-Gly-Asp sequence
RNA	Ribonucleic acid
ROS	Reactive oxygen species
rpm	Revolutions per minute
RT	Room temperature
s	Seconds
SERS	Surface-enhanced Raman scattering
SKOV3	Ovarian Canccer cell line
SPR	Surface plasmon resonance

SPPS	solid phase peptide synthesis
T	Temperature
t	Triplet
TDDS	Targeted drug delivery system
TEA	Triethylamine
THF	Tetrahydrofuran
TMS	Tetramethylsilane
UV	Ultraviolet
µg	Microgram
µm	Micrometer
µM	Micromolar
$\boldsymbol{\nu_{em}}$	Frequency of emission
$\boldsymbol{\nu_{ex}}$	Frequency of excitation
NSCLC	non-small cell lung carcinoma
SPPS	solid phase peptide synthesis

PREFACE

In Cancer therapy the development of drug delivery vectors are accountable to resolve a number of issues associated with conventional delivery of anticancer drugs, e.g. nonspecific distribution, poor water solubility, lack of targeting capacity, systemic toxicity, low therapeutic index and many more. In this regard, the design of targeted delivery systems holds special interest among researchers in multidisciplinary expertise. The present thesis describes the design, synthesis and biological evaluation of targeted drug delivery carriers and investigated their utility for efficient cancer therapy. Chapter 1 of the thesis gives an overview about the recent developments with targeted drug delivery systems towards efficient cancer therapy with special emphasis on basic fabrication strategies. In addition, specific objectives of the present thesis were briefly described at the end of this chapter.

Although significant efforts were made for the design of targeted drug delivery vehicles in the present decade, majority of the delivery vectors faces failure to get translated for the bed-side applications. Chapter 2 of the thesis deals with design and synthesis of octa-guanidine appended poly (propylene imine) based dendron carrier for targeted delivery of doxorubicin (DOX) towards cancer cells. The delivery vector was found to be non-toxic, displayed higher cellular uptake compared to the well-known cell penetrating peptide, Arg-8-mer and exhibited excellent selectivity towards lysosomes in cathepsin B expressing HeLa cells. The DOX loaded carrier showed significant cytotoxicity to cancer cells without affecting the non-cancerous cells. This new approach is expected to appreciably augment the likelihood of cell killing and potentially overcome drawbacks of current chemotherapeutic agents, making it a promising approach to cancer therapy.

Chapter 3 of the thesis describes the application of the as-synthesized delivery carrier towards dual targeted therapy. The skeleton of the delivery system consists of cathepsin B specific peptide substrate appended with lysosome-targeting octa

guanidine molecular transporter and further functionalized with surface targeting ligand folic acid. The platform specifically enabled the delivery of DOX towards folate over expressing cancer cells. The system exhibited excellent biocompatibility and demonstrated tumor-targeting in the *in vivo* murine models with an optimal bio-distribution pattern.

The construction of sorbitol octa-guanidium appended transporter for targeted delivery of paclitaxel (PTX) is the subject matter of chapter 4. The cell surface receptor $\alpha_v\beta_3$ integrin targeting ligand cRGD and lysosome specific peptide substrate was conjugated on the molecular transporter and applied for PTX delivery towards U-87 MG glioma cells. The alteration of microtubular networking of the cancer cell with the drug conjugate was more prominent than free drug. The enzyme assisted delivery was monitored *via* high performance liquid chromatography (HPLC) and surface enhanced Raman scattering (SERS) modalities. As a new insight the time dependent SERS fingerprinting and imaging enabled accurate monitoring of internalization as well as release of the PTX. The cytotoxicity profiling, cell cycle analysis, apoptosis assays and bio-compatibility evaluation revealed the potency of the delivery system. The as-synthesised delivery system provides greater promise for their applications in tumor-targeted drug delivery and imaging.

Nanoparticle based delivery systems holds an excellent cell penetrating ability, bio-compatibility and many other features compared with the bulk material. Fifth chapter of the thesis demonstrated a nanoparticle based drug delivery system for dual sub cellular compartment targeted delivery to reduce cardio toxicity as well as drug resistance of anti cancer drug DOX towards cancer cells. Hollow gold nanoparticle modified with p-sulfonato calyx[4]arene has been used as the nanocarrier delivery system. The high photo thermal ability of the carrier was used for both NIR laser triggered drug release and combined photo thermal chemotherapy. A combination of DOX and mitochondria targeted peptide appended DOX (Mt-DOX) has been associated within the carrier system and modified with cell surface targeting folic acid ligand. Mt-DOX can induce mitochondria depolarisation and cell death in cancer cells but not

towards cardiac cells in comparison with free DOX. The *in vitro* SERS imaging and fluorescence technique predicted the intracellular localisation pattern. The combined photo thermal chemotherapy and selective targeting ability studied in cancer cells, drug resistant cancer cells and cardiac cell line. The NIR triggered drug release synergistically exerted both nano-transporter mediated photo thermal ablation and cytotoxicity by free DOX and Mt-DOX. These results confirmed the potential of delivery system to overcome cardio toxicity and drug resistance in long-time anticancer chemotherapy.

In summary, the various possibilities of utilizing a number of targeted drug carriers were explored which provided a promising tool for the delivery of anticancer drugs towards target site. Using in-depth biological evaluation, the detailed mechanistic insights were made in each delivery vectors. The synthetic and nano carriers are not specific to the delivery of particular anti-cancer or localized phototherapy; the specificity can be tuned by varying targeting ligands in order to accomplish selectivity towards desired cancer treatment keeping the normal cells and tissues unaffected.

References

1. **Nair, J. B.;** Mohapatra, S.; Ghosh, S.; Maiti, K. K. Novel Lysosome Targeted Molecular Transporter Built on a Guanidinium-Poly-(propylene Imine) Hybrid Dendron for Efficient Delivery of Doxorubicin into Cancer Cells. ***Chem. Commun.*** **2015,** *51* (12), 2403–2406.
2. **Nair, J. B.;** Joseph, M. M.; Mohapatra, S.; Safeera, M.; Ghosh, S.; Sreelekha, T. T.; Maiti, K. K. A Dual-Targeting Octaguanidine-Doxorubicin Conjugate Transporter for Inducing Caspase-Mediated Apoptosis on Folate-Expressing Cancer Cells. ***ChemMedChem*** **2016**, *11* (7), 702–712.
3. **Nair, J. B**.; Mohapatra, S Joseph, M. M.; V.Gupta, Ghosh, S. Maiti, K. K, SERS Guided Targeted Paclitaxel Delivery in to Glioblastoma using Peptide-Sorbitol Conjugate **, 2018**,Manuscript submitted
4. **Nair, J. B.;** Joseph ; Maiti, K. K. A combination of doxorubicin and mitochondria targeted doxorubicin synergistically augments drug resistance and cardio toxicity with targeted theranostic nano probe ,**2018,** Manuscript under preparation

List of Publications

1. Maniganda, S.; Sankar, V.; **Nair, J. B**.; Raghu, K. G.; Maiti, K. K. A Lysosome-Targeted Drug Delivery System Based on Sorbitol Backbone towards Efficient Cancer Therapy. ***Org. Biomol. Chem.*** **2014,** *12*, 6564–6569.

2. **Nair, J. B.;** Mohapatra, S.; Ghosh, S.; Maiti, K. K. Novel Lysosome Targeted Molecular Transporter Built on a Guanidinium-Poly-(propylene Imine) Hybrid Dendron for Efficient Delivery of Doxorubicin into Cancer Cells. ***Chem. Commun.*** **2015,** *51* (12), 2403–2406.

3. **Nair, J. B.;** Joseph, M. M.; Mohapatra, S.; Safeera, M.; Ghosh, S.; Sreelekha, T. T.; Maiti, K. K. A Dual-Targeting Octaguanidine-Doxorubicin Conjugate Transporter for Inducing Caspase-Mediated Apoptosis on Folate-Expressing Cancer Cells. ***ChemMedChem*** **2016**, *11* (7), 702–712.

4. Ramya, A. N.; Joseph, M. M.; **Nair, J. B.;** Karunakaran, V.; Narayanan, N.; Maiti, K. K. New Insight of Tetraphenylethylene-Based Raman Signatures for Targeted SERS Nanoprobe Construction towards Prostate Cancer Cell Detection. ***ACS Appl. Mater. Interfaces*** **2016**, *8* (16), 10220–10225.

5. K. Nabeela, R. T. Thomas**, J. B. Nair**, K. K. Maiti, K. G. K. Warrier and S. Pillai, TEMPO-Oxidized Nanocellulose Fiber-Directed Stable Aqueous Suspension of Plasmonic Flower-like Silver Nanoconstructs for Ultra-Trace Detection of Analytes. ***ACS Appl. Mater. Interfaces*****, 2016**, 8, 29242–29251.

6. Mathai, B. M.; Joseph, M. M.; Santhi, M.; **Nair, J. B**.; J.S, A.; Karunakaran, V.; Radhakrishnan, k v; Maiti, K. Guanidinium Rich Dendron- Appended Hydnocarpin Executes Superior Anti-Neoplastic Effects Through Caspase Mediated Apoptosis. ***RSC Adv.*** **2016**, *6*, 52772–52780.

7. Narayanan, N.; Nair, L. V.; Karunakaran, V.; Joseph, M. M.; **Nair, J. B**.; N, R. A.; Jayasree, R. S.; Maiti, K. K. Investigation of Apoptotic Events at Molecular Level

Induced by SERS Guided Targeted Theranostic Nanoprobe. ***Nanoscale* 2016**. DOI:10.1039/C6NR03385G

8. Joseph, MM**, J. B. Nair,** Ramya ,AN., Hari,N, Pillai,R.K, Nair,A.J, Maiti,K.K,Sreelekha ,T.T, Exploration of Biogenic Nano-chemobiotics Fabricated by Silver Nanoparticle and Galactoxyloglucan with an Efficient Biodistribution in Solid Tumor Investigated by SERS Fingerprinting ***ACS Appl. Mater. Interfaces*, 2017**, 9, 19578–19590.

9. Joseph M.M, **Nair J.B,** Maiti K.K, Sreelekha T.T.; Plasmonically Enhanced Galactoxyloglucan Endowed Gold Nanoparticles Exposed Tumor Targeting Biodistribution Envisaged in a Surface-Enhanced Raman Scattering Platform; **Biomacromolecules, 2017**, 18(12):4041-4053 doi: 10.1021/acs.biomac.7b01109

10. Joseph M.M,, Nisha N, **Nair J.B**, Karunakaran V., Ramya A.N., Sujai P.T, Saranya G., Arya J.S; Vineeth V.M, Maiti K.K; Exploring the Margins of SERS in Practical Domain: An Emerging Diagnostic Modality for Modern Biomedical Applications (Review);Biomaterials,**2018,***181*,140-181; doi:10.1016/j.biomaterials.2018.07.045.

11. Sreedevi P, **Nair, J. B** Preethanuj P, Jeeja B.S Cherumuttathu H. Suresh C.H, Maiti K.K. Luxmi R.V; Calix[4]arene Based Redox Sensitive Molecular Probe for SERS Guided Recognition of Labile Iron Pool in Tumor Cells, ***Analytical chemistry*, 2018,**90,7148-7153

12. **Nair, J. B**.; Mohapatra, S Joseph, M. M.; V.Gupta, Ghosh, S. Maiti, K. K, SERS Guided Targeted Paclitaxel Delivery in to Glioblastoma using Peptide-Sorbitol Conjugate **,Acs Medicinal chemistry letters,2018,***M*anuscript under revision

13. **Nair, J. B.;** Joseph ; Maiti, K. K. A combination of doxorubicin and mitochondria targeted doxorubicin synergistically augments drug resistance and cardio toxicity with targeted theranostic nano probe ,**2018,** Manuscript under preparation

14. Saranya G. Joseph M.M, Karunakaran V, **Nair J.B.**, Saritha V.N, ,⊥ Vamadevan S. Veena V.S., Sujathan K., Ajayaghosh A., Maiti K.K; Enzyme-Driven Switchable Fluorescence-SERS Encoded Antitag Cocktail for the Multiplex Detection of Lung

Cancer Biomarkers, ***ACS Appl. Mater. Interfaces,*** **2018,** doi:10.1021/acsami.8b15583.

15. Sujai P.T, Joseph M.M, Karunakaran V., Saranya G., Ramya A.N., S. Shamjith**, Nair J.B**; Kumar Maiti K.K , A Targeted Three-in-One Nanotheranostic probe Built on Biogenic-cluster Encased Gold Nanorod for SERS Recorded Photo-Chemotherapy on Metastatic Melanoma ,**2018,** communicated.

16. Karunakaran V., Saritha V.N, **Nair J.B,** Saranya G., A New insight on non invasive label free digagonosis of te metabolomics and genomics profiling of cervical precancer prognosis by differential SERS fingerprinting, Manuscript under preparation

List of Posters & Conferences

1. Presented poster in 6th Internatinal Conference on Current Trends in Drug Discovery and Research (CTDDR-2016), Organized by CSIR-CDRI Lucknow(Feb, 25-28th, 2016); Cancer Cell-Specific Induction of Apoptosis By Precise Delivery of Doxorubicin using a dual targeting Dendron based transporter; Poster presentation : Jyothi B Nair, Manu M Joseph and Kaustabh Kumar Maiti.

2. Presented poster in The Ramanbhai Foundation 7th International Symposium onCurrent Trends in Pharmaceutical Sciences ”Advances in New Drug Discovery & Development”; Organized by Zydus Research Centre, Ahmedabad, India (Feb, 2- 4th, 2015); An Efficient Approach on Guanidium Appended Molecular Transporter For Targeted Delivery of Doxorubicin Towards Malignant Cells: A Future Prospect in Cancer Therapy; Poster presentation : Jyothi B Nair, Santhi Maniganda, Varsha Karunakaran, Kaustabh Kumar Maiti.

3. Participated in The International Symposium on Photonics Applications and Nanomaterials; Organized by Sree Chitra Tirunal Institute for Medical Sciences & Technology , Thiruvananthapuram (Oct, 28-30th, 2015); A New Insight of Squaraine Based Raman Reporters for Construction of Diagnostic SERS Nano-Probe in Cancer Screening, Poster presentation : Nisha Narayanan, Ramya A N, Varsha Karunakaranand, Kaustabh K. Maiti.

4. Presented poster in Transending frontiers in organic chemistry(October,2014) An Efficient Approach on Guanidium Appended Molecular Transporter For Targeted Delivery of Doxorubicin Towards Malignant Cells, Poster presentation: Jyothi B Nair, Santhi Maniganda, Vandana Sanker, Kaustabh Kumar Maiti.

5. Participated in 6th International Conference on Nano Science and Technology (ICONSAT 2014); Organized by Institute of Nano Science and Technology (INST), Mohali, Punjab (March, 2-5th, 2014); New Insight of Squaraine Based Raman Reporters for Construction of Diagnostic SERS Nano-Probe In Cancer Screening; Poster presentation: Nisha N, Jyothi B Nair, Kaustabh Kumar Maiti.

6. Participated in 2nd International Conference on Advanced Functional Materials (ICAFM 2014), Organized by CSIR-NIIST, Trivandrum (February, 19-21st, 2014); New Insight of Squaraine Based Raman Reporters for Construction of Diagnostic SERS Nano-Probe In Cancer Screening. Poster presentation: Nisha N, Jyothi B Nair, Kaustabh Kumar Maiti

Chapter 1

Trends in Targeted Drug Delivery System towards Therapeutic Oncology

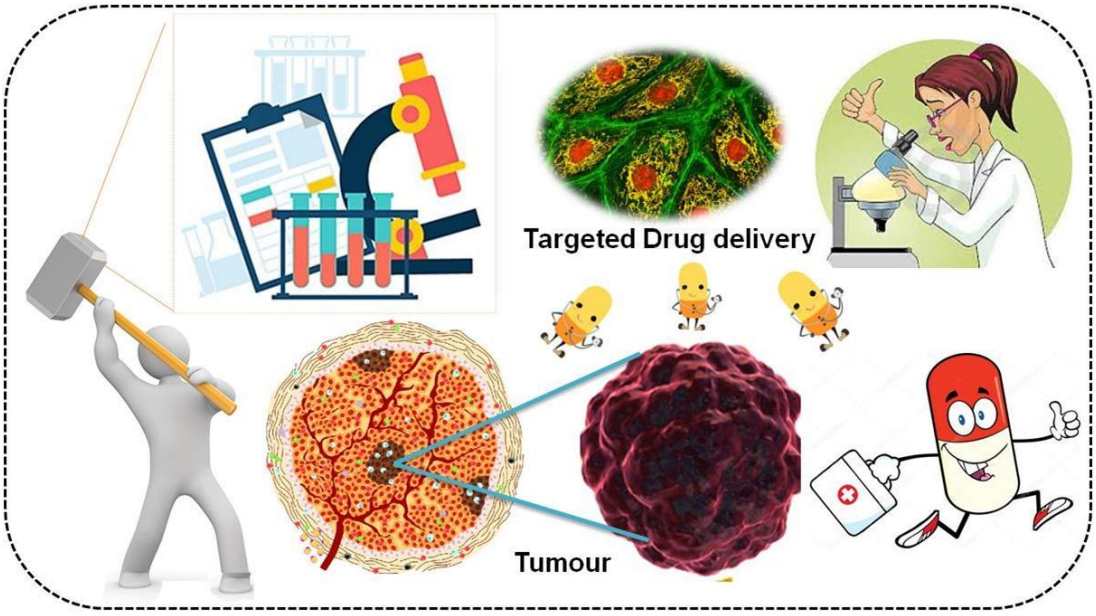

Abstract: *In biology and medicine, development of drug delivery vectors has sparked rapid attention as it promises solution to a number of problems coupled with conventional therapy especially in oncology which includes their nonspecific distribution, poor water solubility, lack of targeting capacity, low therapeutic index and systemic toxicity. Remarkable advancement has been made in the area of drug delivery system during the last decade in order to address all the issues associated with currently available treatment modalities. Therapeutic warheads have been integrated with synthetic and nano delivery carriers with definite structure, size, shapes, and surface properties to enlarge their solubility, prolong their circulation, improve their bio-distribution, targeting ability etc. The carriers with their payloads have also been satisfactorily delivered into target sites by taking advantage of the pathophysiological conditions, such as the spatial variations in the pH value and the enhanced permeability and retention (EPR) effect. By taking these advantages, lot of targeting approaches has been emerged with the aid of antibodies, peptides, nucleic acids, small organic molecules etc. Subsequently multiple therapeutic agents and diagnostic agents*

could also been delivered with these drug carriers in order to achieve combination therapy with a potential to overcome the drug resistance and other disadvantages of single therapy. The scope of this chapter covers the importance of drug delivery carriers towards cancer therapy and also extended further to describe targeted strategies as well as various challenges encountered in combination therapy. It is anticipated that multi-component therapeutic modality and their accurate delivery towards target site will appear as an emerging next-generation platform for anti-cancer drug delivery.

1.1 Cancer

Cancer, a major public health problem, and called as second 'biggest killer, is defined as "a malignant tumour of potentially unlimited growth that expands locally by invasion and systemically by metastasis" in the Merriam – Webster dictionary[1]. Researchers have made remarkable breakthroughs for understanding origin and development of cancer in human body over the past few decades which made advancements in treatment as well as diagnosis. The overall mortality rate is showing a declining trend in last five years but the average incidence rate is still 20.2%. [2] The foremost reason for this high mortality rate is due to inefficient delivery strategy of the therapeutic agents specifically towards tumour sites without inducing severe adverse effects on healthy tissues and organs. The commonly used therapeutic methods for the treatment of cancer include surgery, radiation, photo therapies (photodynamic (PDT) and, photo thermal (PTT) therapy)[3], gene therapy[4], immunotherapy[5], and chemotherapy.[6] Primary treatment for most of the solid tumours includes surgery, which involves the removal of obvious cancerous tissue (ultrasonic and CD scanners were used to find out the margin).Radiation therapy[7] is widely used in conjunction with surgery and also an alternative for chemotherapy or it can be considered as neo-adjuvant therapy in surgery by reducing the size of tumour. Generally high energy X-Rays were used and it can be considered as local treatment modality because it affect only the tumour area. Another widely used modality involves light mediated treatment of diseases called phototherapy[3], which can be of two types photodynamic therapy (PDT)[8] and photo thermal therapy (PTT).This involves highly localized therapy, and among which PDT[9] involves the

generation of reactive oxygen species (ROS) by administrating a photo sensitizer (PS) to the target site, this will lead to excellent cytotoxicity. In PTT[10],a photo thermal agent mediated hyperthermia is generating cytotoxicity effects. Furthermore, gene therapy involves the correction of an inborn or acquired error of metabolism of malignant cells as well as tumour-associated cells, by selective transfer of recombinant DNA/RNA into the cells[11], there by changing or repairing an acquired genetic abnormality, and to provide a new function to a cell. Subsequently, immunotherapy[12]has emerged for the treatment of cancer by the activation of immune system, where in immunity suppresses the tumour growth conditions such as fast tumour replication and mutation rates. The tumour immuno editing or tumour surveillance is capable of detecting and eliminating cancer cells by discriminating force that can rework the cell composition of the tumour. Chemotherapy is the broadly used modality for the treatment of cancer. The term chemotherapy in a broad sense is used to refer the treatment using a drug or combination of drugs, and its effects are systemic.

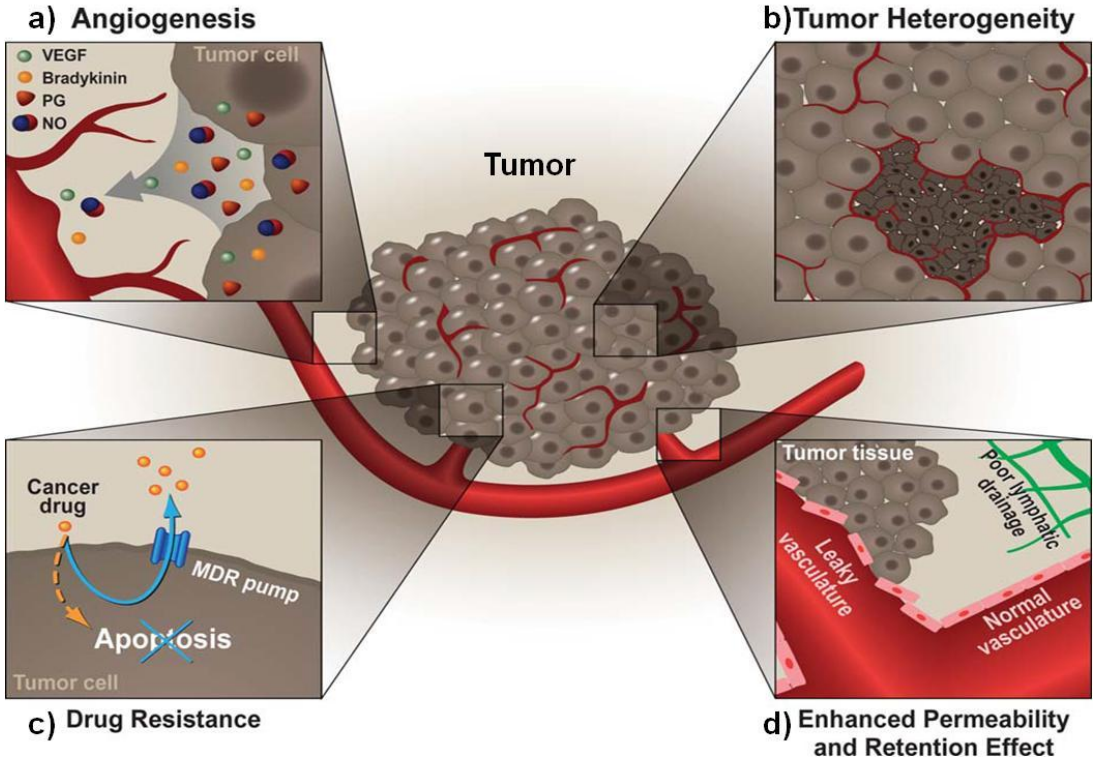

Figure1.1: Schematic representation of cellular compartments in tumour; a) Releasing factor for causing angiogenesis, such as vascular endothelial growth factor[VEGF], bradykinin, prostaglandins [PGs], and nitric oxide [NO]) since they stimulate the formation of new blood vessels. b) Tumour heterogeneity such as acidosis, presence of different

biomarkers etc. (c) Multiple drug resistance generated by different kind of efflux mechanisms, responsible for extruding chemotherapeutic drugs. (d) The enhanced permeability and retention (EPR) due to the combined effect of "leaky" defective vascular architecture and poor tumour lymphatic drainage. This allows chemotherapeutic drugs to leave the vasculature and accumulate at the site of the tumour.[13]

1.2 Treatments with different types of anticancer drugs

Chemotherapeutic drugs can be either synthetic or natural sources and are a powerful weapon to stop or decelerate the growth of cancer cells. There are quite a few different anticancer drugs categorized into different classes according to its mechanism of action, which includes a) inhibition of topomerase I or II[14], enzyme involved in unwinding DNA throughout replication and transcription; b)antibiotics that hamper the enzymes involved in DNA replication; c) mitotic inhibitors that hamper mitosis and cell division; d)anti-metabolites that change the normal building blocks of RNA and DNA; e) alkylating agents which break DNA etc. Patients with stage IV and metastatic cancer may benefit from (palliative) chemotherapy. According to current clinical scenario, first-line chemotherapeutic treatment consists of a platinum agent-based doublet, e.g. cisplatin or carboplatin in combination with a third-generation cytotoxic drug, gemcitabine, a taxane (paclitaxel, docetaxel), or vinorelbine. Several anticancer drugs applied to the treatment of cancer includes bleomycin, doxorubicin, etoposide (VP-16), camptothecine, methotrexate etc.[15]There are different types of cancers with common characteristics which makes diagnosis and therapy very difficult. The effectiveness of conventional chemotherapeutic agents is restricted by the unfocused distribution and quick clearance of several anti-cancer agents, multiple drug resistance at the tumour and cellular level, low efficiency, and significant toxicity due to higher dose administration. Subsequently in recent decades enormous hard work have been devoted for understanding the molecular and cellular mechanisms of cancer as well as to the design of drugs for its management This has prompted the exploration of new drug carriers that can overcome the foremost drawbacks of conventional treatment systems via specific internalization mechanisms and properties.

Anticancer drug	Clinical use	Drawbacks
Adriamycin	Soft-tissue and bone sarcomas, ovary, breast, Wilms' tumor, neuroblastoma, urinary bladder, thyroid, gastric, Hodgkin's disease	Nausea, vomiting, diarrhea, cardio toxicity, vomiting
Docetaxel	Breast, non-small cell lung carcinoma, HRPC, gastric adenocarcinoma, SCCHN	Acute toxicities like myelosuppression, are mild and never dose limiting fatigue/asthenia,excessive tearing and nail disorders
Cisplatin	Metastatic breast cancer, metastatic testicular tumours, anal canalglioblastoma, lung, lymphoma,	Decrease immunity to infections, allergic reactions, gastrointestinal disorders, hemorrhage, and hearing loss especially in younger patients
Etoposide	Lymphoma, Ewing's sarcoma SCLC, GCT, , ovary	Weak drug absorption
Paclitaxel	Advanced carcinoma of the ovary, breast, stomach, lung, head and neck, GCT, , urothelial, urinary bladder	Decrease blood cells, risk of infection or other diseases, hair loss,nausea, vomiting or diarrhea.
Methotrexate	Epidermoid cancer of the head and neck, gestational choriocarcinoma, ALL, breast, advanced mycosis	Liver damage, lung damage, and a decreased ability to fight off infections
Cyclophosphamide	Malignant lymphomas, Hodgkin's disease, lymphocytic lymphoma, CLL, CML, ALL, AML, osteosarcoma, GCT	Fatigue, nausea, diarrhea,bleeding from the bladder, loss of pregnancy
Cetuximab	Metastatic colorectal and non-small-cell lung carcinoma	Low affinity
Gemcitabine	Pancreas, breast, NSCLC, ovary, gallbladder, lymphoma, urinary bladder	Acute myositis. Patients present with painful symmetric weakness of the proximal muscles, with elevation of serum creatine kinase levels.

Ibritumomab	B-cell non-Hodgkin's lymphoma	Radiation induced damage
l-asparaginase	ALL	Allergic reactions and anaphylaxis.
Rituximab	CD20-positive B-cell non-Hodgkin's lymphoma	-
Tositumomab	CD20-positive B-cell non-Hodgkin's lymphoma	-
Transtuzumab	Metastatic breast cancer	Disease recurrence
Bevacizumab	Metastatic CRC, NSCLC, Metastatic breast cancer, glioblastoma, ovary, renal cell carcinoma	Retinal toxicity

Table1.1: Anticancer drugs currently in clinical use[16]

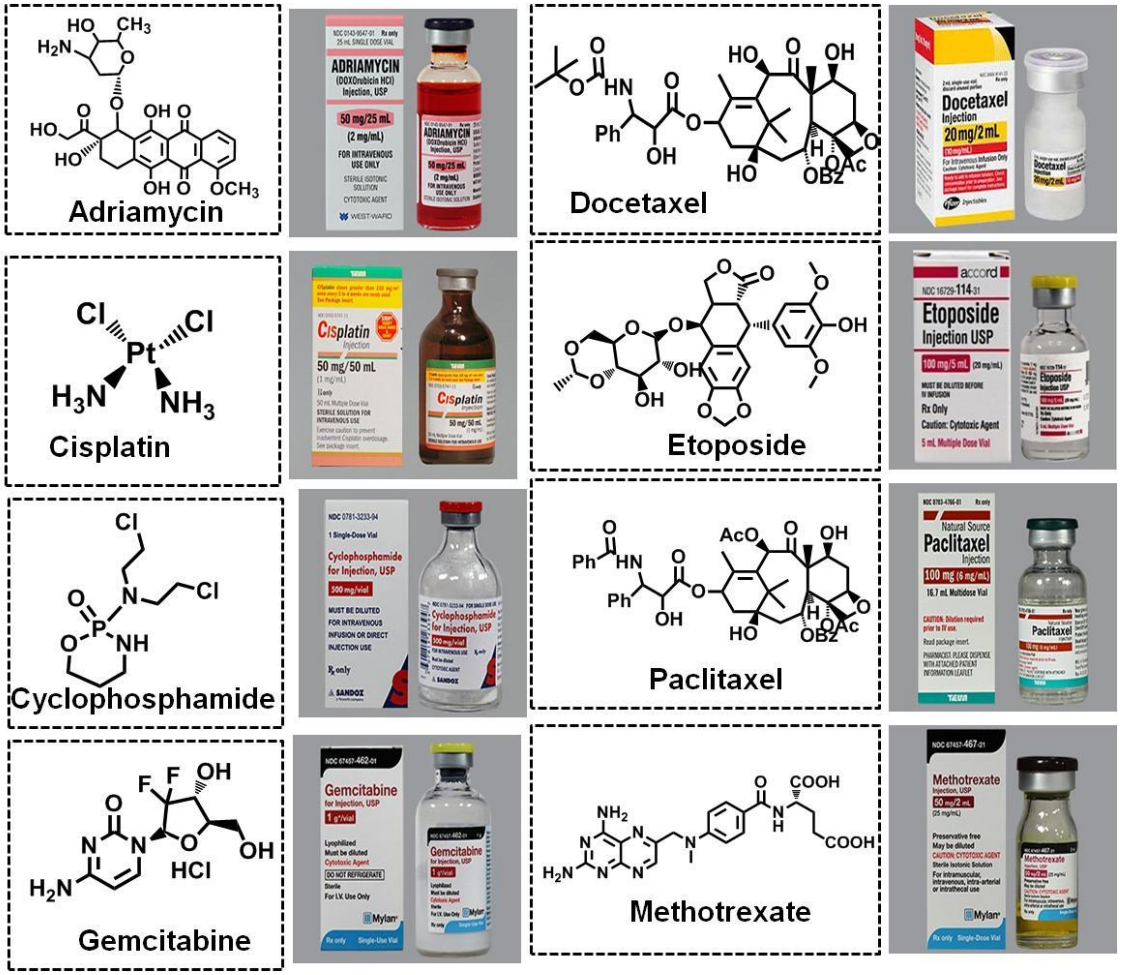

Figure 1.2: Chemical structure and clinically available forms of currently used anti-cancer drugs.

1.3 Advancement of drug delivery systems towards better therapeutic outcome

Drug delivery system can be defined as the method or process of administering a pharmaceutical agent to accomplish a better therapeutic effect in a particular disease condition in humans or animals. In therapeutic scenario, drug delivery system has grown up exponentionaly in order to overcome the conventional treatment modalities. Over the past several decades, remarkable progress has been made in the development and application of drug delivery vectors for the treatment of human communicable or non-communicable diseases. Remarkable breakthroughs have been made for the improvisation of "old" drugs with high safety efficacy using different methods such as individualizing or combining drug therapy, dose dependent therapeutic delivery, and therapeutic drugs ratio variation. Administrating drug molecules at controlled rate, targeted fashion and slow release profile, are other widely focused area for pharma and medicinal chemistry researchers, and the methods have been pursued vigorously. Advancements in carrier development have scrutinized an assortment after several decades of technological enlargement. The delivery vectors and their payloads have also been satisfactorily delivered into the site of action by taking advantage of the pathophysiological conditions, such as the enhanced permeability and retention effect (EPR) and other cellular environmental conditions. As shown in the Figure 3 drug delivery vehicles can be readily fabricated from either flexible (organic polymeric and dendritic) or rigid (inorganic) materials with their sizes being controlled and compositions/structures being fabricated to load different drugs in a number of configurations. The physicochemical parameters of the delivery systems can also be finely tuned by tailoring their chemical functionalization, surface properties, structures, sizes, shapes, and morphologies. A number of such delivery systems have been approved for providing therapeutic output in clinics, with many more currently under clinical trials or preclinical evaluations.

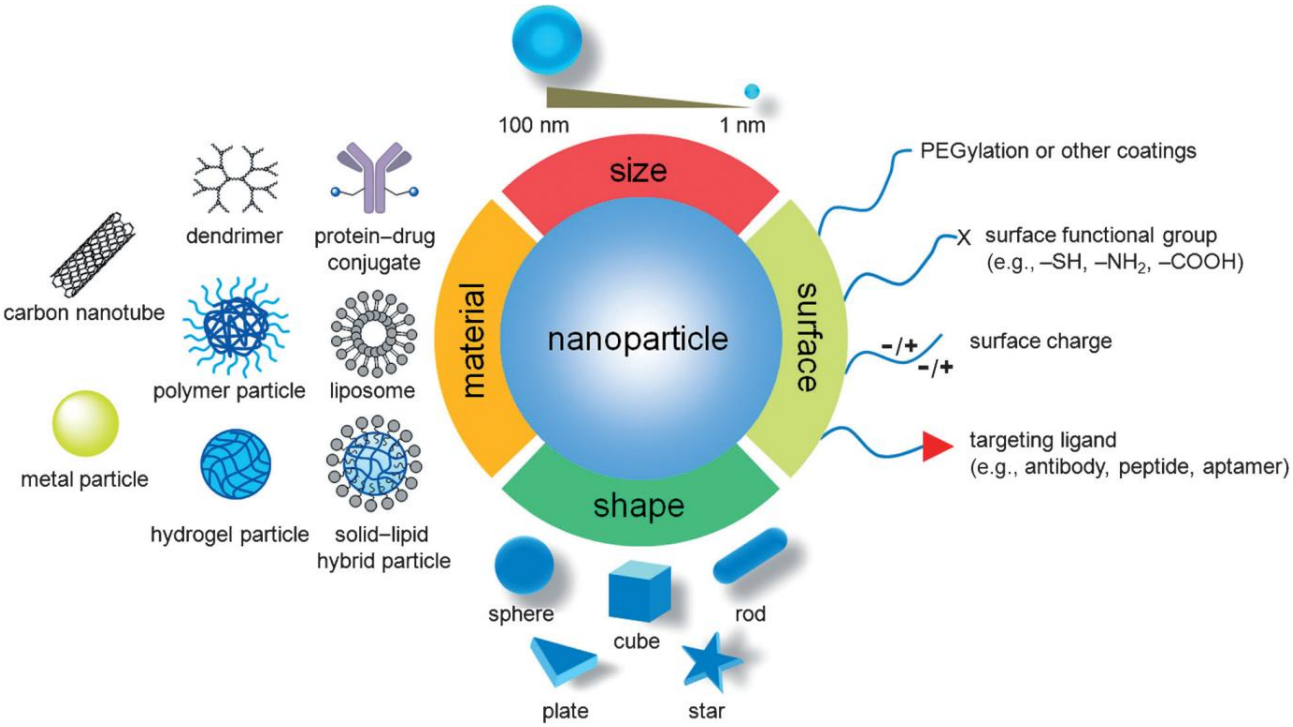

Figure 1.3: Schematic representation of carriers that have been explored as drug delivery vehicles in cancer therapy, along with illustrations of bio-physicochemical properties.[16]

1.3.1 Molecular carrier: Guanidium rich molecular transporter

The discovery of cell penetrating peptide from HIV –Tat opened a new avenue for the subsequent progressive development of molecular carriers based on guanidium rich motifs from arginine residues since more than a decade. The cell penetrating nature of Tat protein is presumed to be a core of 9 amino acid sequence i.e. $Tat_{49\text{-}57}$ (RKKRRQRRR)[17],especially the basic nature of the sequence which is mainly responsible for the cellular uptake mechanism.

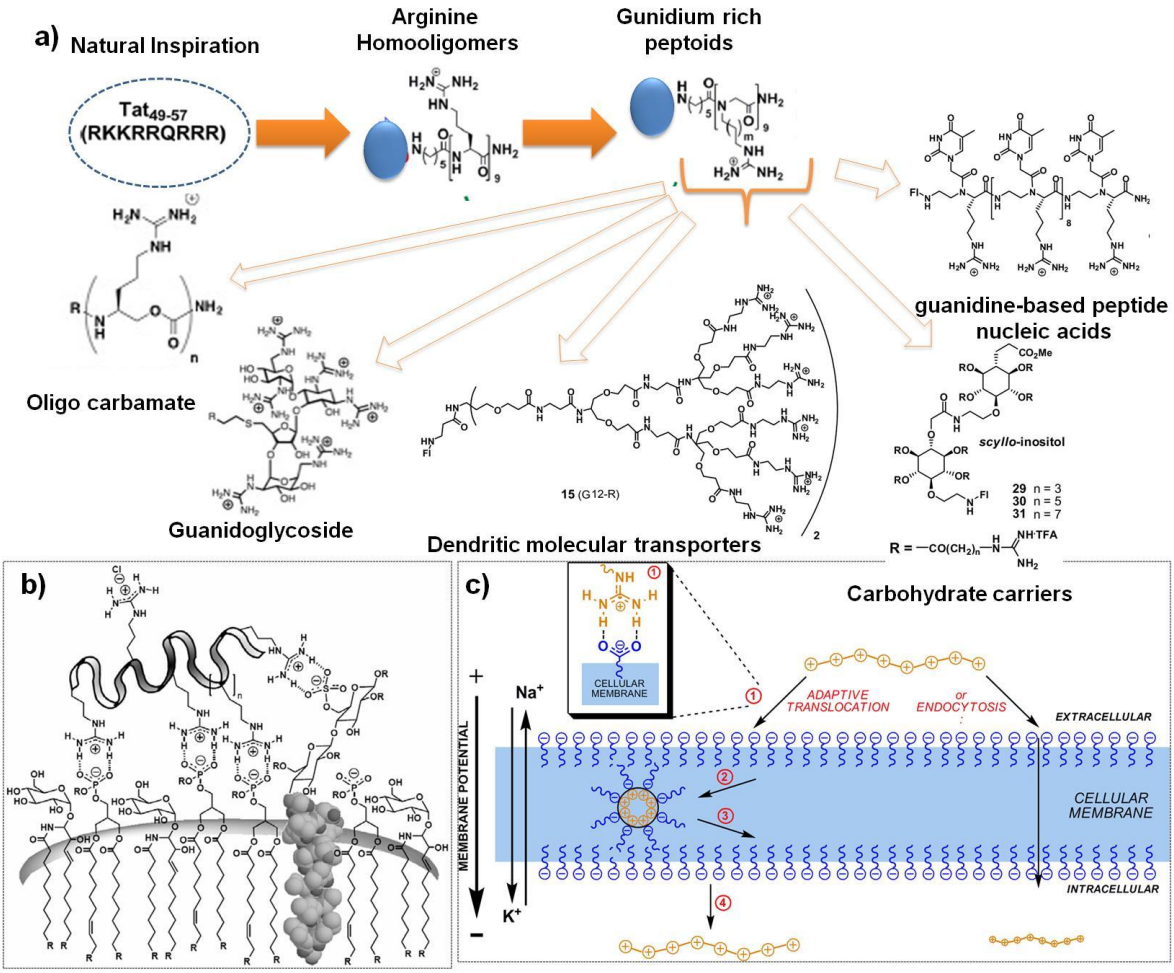

Figure 1.4: a) Different scaffolds for guanidinim-rich transporters. b) Associations of a polycationic guanidinium transporter with anionic cell membrane constituents.[18] b) Mechanisms of uptake, interaction of guanidium residues with negatively charged moieties on the cell surface.[19] c) Mechanism of internalisation (adaptive translocation and endocytosis). (1) The guanidinim-group forms a bidendate bond with negative phosphates, sulfates, and carboxylates on the cell surface. (2,3) The charge-neutralized species moves through the membrane, in a process termed "adaptive translocation," driven into the cell by the membrane potential. (4) In the reverse of (1), the oligo-guanidinium transporter dissociates from the membrane once inside the cell. [18]

The importance of lysine and arginine residues and importance of charge in cellular uptake mechanism was well demonstrated by Wender's group[17] by a series of functional and structural investigations. Later, detailed studies confirmed that the unique ability of arginine-oligomers to enter cells was attributable to the number and arrangement of attached guanidinium groups. The interaction of positively charged guanidium groups can help to form an electrostatic interaction and a

bidentate hydrogen bond with negatively charged species such as sulphates, phosphates, and carboxylates confirmed by decrease in cellular entry by methylation of guanidium groups[20]. The first designed cell-penetrating guanidinim-rich carriers were reported in 2000[21], numerous new classes of guanidinim-rich molecular transporters have been emerged including guanidinim- rich peptoids, carbamates, carbonates, carbohydrates, nucleic acids, and dendrimers. The guanidium rich molecular transporters have been used to deliver an array of cargos, including small molecules, proteins, peptides, imaging agents, siRNA, plasmids, quantum dots, xenon cages, and vesicles across a variety of cellular and tissue barriers, including bacterial, algal and mammalian cell membranes, human skin, and the blood brain barrier and the uptake efficiency can be tuned with the optimum number of guanidine unit. The special feature of guanidine based molecular carrier unfolds an opportunity for the desired delivery of polar and nonpolar drugs to the target site. Therefore, guanidinium-rich peptides (octa-arginine or R8)[22], peptoids[23], oligocarbamates[24], and dendrimers[25] turned out as a potential carrier platform and reached in advanced cases such as clinical trials. Like few notable examples, cyclosporine-heptaarginine conjugate has progressed to clinical trial for the treatment of psoriasis and subsequently RACK peptide transporter conjugate was used for the treatment of ischemic damage.

1.3.2 Nanoparticle delivery carrier based on polymeric core

Polymer nanoparticles stands among the most widely investigated carrier systems for drug delivery. Many synthetic polymers with hydrophilic or hydrophobic units (PLGA, PLA, PEG, PCL etc) among which few are turned out with biodegradable properties. Both hydrophobic and hydrophilic drugs can be accommodated into the particles according to the nature of core polymer. These particles usually contain dense matrices with well-defined degradation profiles and can result in a sustained release profile from the system. The preparation of an efficient delivery carrier with great tenability can be achieved with the aid of tunable physicochemical properties of polymer nanoparticles.[26]

1.3.3 Dendrimers as drug carrier:

Dendrimers are macromolecules with tree-like spherical structures having many branches emanating from a central core. It has been synthesized either by convergent synthesis or by divergent synthesis. Dendrimers are mostly well-suited for the delivery of drugs and imaging agents because of their mono dispersed size, high water solubility, and uniform composition. In addition, the unique branching structural design and availability of various functional groups can be utilized to either encapsulate or directly conjugate therapeutic candidates for effective delivery. However, controlling the encapsulated drug release remains a challenging task that depends on the hydrophobicity and size of the drug, functionalization on the surface of the dendrimer, and the generation number of the dendritic carrier. The future of the delivery system will focus on the rational design and synthesis of novel linkers that will be recognized by the heterogeneity of diseased site such as, selective cleavage by enzymes and other biological molecules present exclusively in the specific area. This approach can achieved by an extra degree of control over the site and rate of drug release from dendrimer-drug conjugates.[26]

1.3.4 Inorganic nanoparticles as drug carrier:

Inorganic nanoparticles comprise an important category of drug-delivery systems (Figure 5) because of their precision in size and shape control, rich variety, multi-functionality, and excellent physicochemical properties. The largely used inorganic nanoparticles include mesoporous silica nanoparticles (MSNs)[27], carbon-based nanostructures (fullerenes, carbon nanotubes or CNTs, and graphene)[28], noble metal (typically Au) nanostructures, porous silicon, hydroxyapatite and so on. Gold nanostructures possess pronounced photothermal properties which has an advantage for direct cancer therapy without involving an anticancer drug, in addition to a variety of optical properties (e.g., multiphoton luminescence for Au nanorods and nanocages, fluorescence for Au nanoclusters, and strong optical absorptions for all of them) for diagnostic as well as therapeutic applications. Therapeutic agents are loaded to the surface of solid Au nanostructures (e.g., nanosphere sand nanorods), Au structures with hollow interiors (e.g. hollow gold nanoparticles (HGNPs)[29], nanoshells[30] ,and nanocages[31]) which allow for a much more efficient encapsulation of drugs within the surface or in their cavities. hollow

gold nanoparticles represent a novel class of Au nanostructures with thin walls, and hollow interiors (Figure 5e) can readily prepared using a galvanic replacement reaction between Cobalt templates[32] and Au^{3+} in an aqueous solution. The wall thickness of HGNPs can be separately adjusted to tune an array of optical properties, including multi-photon luminescence and optical scattering/absorption, to the desirable wavelengths. HGNPs have been actively used for imaging based on photoacoustic tomography, and surface-enhanced Raman scattering (SERS).

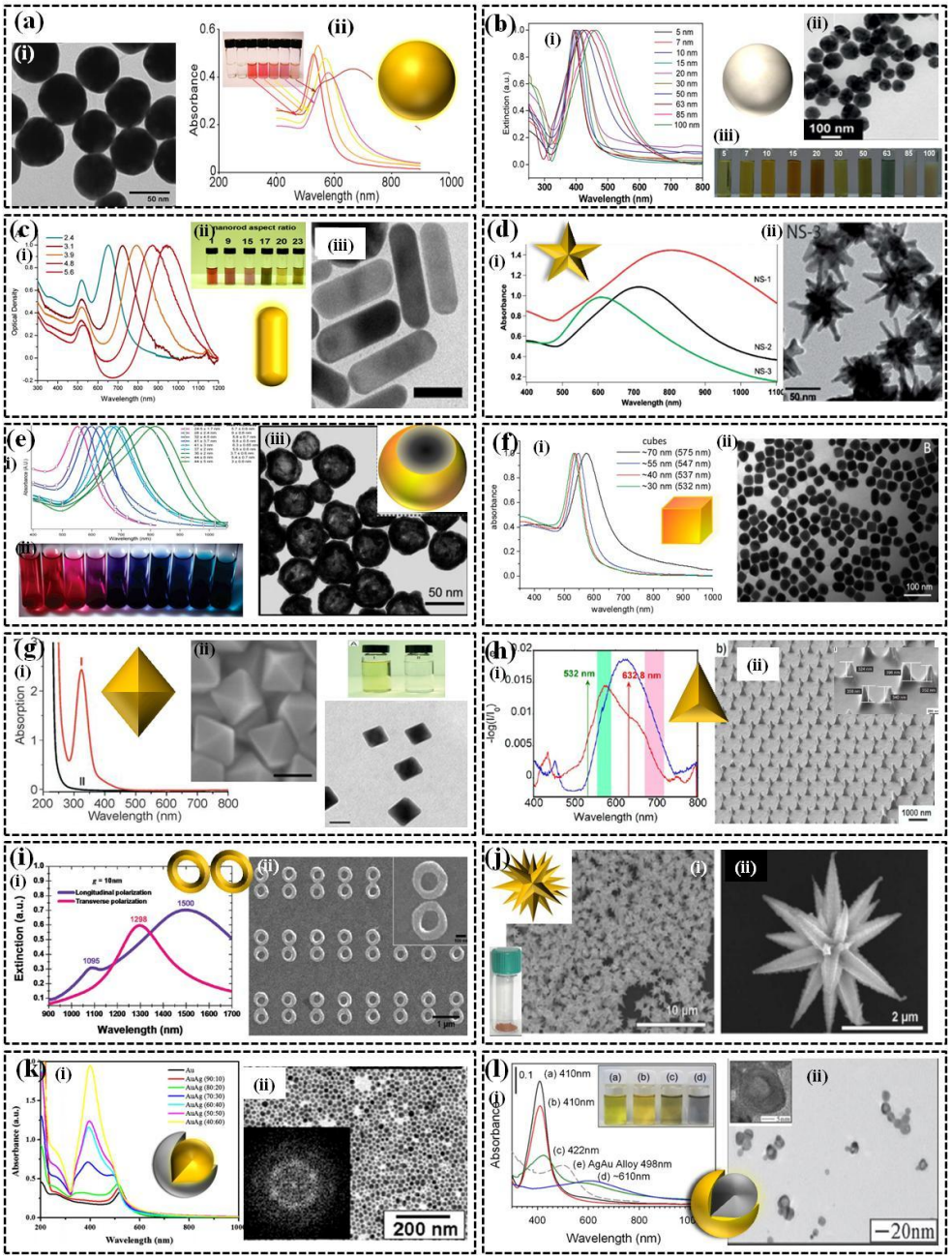

Figure 1.5: Different type of inorganic nanocarrier delivery system[33]

Any DDS, whether organic or inorganic, must satisfy certain number of general criteria, specially (i) avoid capture by cells of the reticulo-endothelial system (RES) and nonspecific interactions with the body or the induction of adverse reactions (ii) protect theloaded molecules from unfavorable effects such as enzymatic degradation, hydrolysis etc.(iii) facilitate the biologically active molecule's transport to the site of action (organ, tissue, cell, or organelle) from the site of administration in a high yield while keeping the active molecules in a safe (i.e. inactive) state during transport, iv) effective release of payloads at the site of action in a controlled manner, (v) enable elimination of all the by-products created during delivery (clearance from the body) after its function as a carrier has been fulfilled. Moreover, a targeting agent should be attached with the carrier system in order to achieve maximum therapeutic effect. A successful strategy requires specificity or high selectivity of binding to tumour cells. Thanks to advanced technology, many types of combination of anticancer agents against primary tumours have been developed, but the exploitation of anticancer drugs which completely cure cancer is still in research modality.

Trade Name	Carrier used	Therapeutic agent	Seller	Application	Development phase
Doxil	liposome	doxorubicin	Sequus Pharmaceuticals	Kaposi sarcoma	approved
Abraxane	albumin-bound nanoparticle	paclitaxel	Abraxis Bioscience, Inc.	metastatic breast cancer	approved
Myocet	liposome	doxorubicin	ZeneusPharma Ltd	metastatic breast cancer	approved
Genexol-PM	methoxy PEG-PLA	paclitaxel	Samyang Biopharmaceuticals	ovarian and lung cancer	phase II
BIND-014	polymer matrix	docetaxel	BIND Therapeutics,	prostate cancer	phase II

			Inc.		
CRLX101	cylodextrin -PEG micelle	camptothecin	Cerulean Pharma, Inc.	ovarian/tubal /peritoneal cancer, rectal cancer	phase I/II
NL CPT-11,	liposome	irinotecan	University of California	San Francisco solid tumour	phase I/II
DEPTM-Docetaxel	dendrimer	docetaxel	Starpharma Holdings, Ltd	breast, prostate, lung, and ovarian cancer	phase I
DaunoXome [12]	liposome	daunorubicin	Galen Ltd	Kaposi sarcoma	approved

Table 2: Different carrier based therapeutics in clinical use and under clinicaltrials[16]

1.4 Introduction of targeting ligands into drug carriers

Introduction of targeting ligands into drug carriers promote the therapeutic agent towards the target site at a high precision level with potential personalized treatment option. Each delivery vectors should be encroached specifically to diseased cells keeping away to healthy cells. The most attractive strategy for achieving the desired goal is to link the therapeutic or diagnostic agents to a specific target ligand that can selectively recognize the pathological cell and tissue. The term "drug targeting" (or "targeted drug delivery") used in drug delivery is discrete from "targeted therapy" that is frequently used in drug discovery. The predominant drug accumulation, which is completely independent of route of administration and methods with in target zone, is referred to as targeted drug delivery whereas specific interaction between the receptor and corresponding drugs in the molecular level is called targeted therapy. Effective targeted drug delivery systems require mainly four key requirements: retain, evade, target and release. Targeted ligand appended drugs have several advantages over non-targeted counter parts,(i) they

can deliver the therapeutic payload selectively to diseased cell, thereby avoiding toxicity associated with non-specific uptake.(ii)therapeutic agents can produce highly potent therapeutic warheads, that exhibit no efficiency when administrated in a non-targeted fashion[34]. Researcher should identify the strategies required for understanding the events involving in drug carrier transport or drug effects at the target site for overcoming many challenges in development of targeted drug delivery systems. Drug targeting to specific sites in the body obviously required different delivery systems depending on the routes selected, example for the *i.v* administration people generally used two strategies such as passive and active targeting, among which passive targeting is based on the usage of tumour leaky vasculature for drug accumulation with the aid of EPR effect. Because of the EPR effect, both drugs in nano formulation or macro formulation can target tumours more powerfully than small molecular drugs, as the extravasation of particular size objects occurs in a tumour-selective manner. Taking advantage of high permeable nature of tumour tissue much new therapeutics were developed over past decades for cancer treatment. The presence of outsized gaps flanked by the endothelial cells on the tumour vascular walls was confirmed by direct visualization through optical and electronmicroscopy[35]. Opening on the tumour vasculature mainly depends on the tumour type and is ranging from 100-800 nm, where as in the case of MCa-IV mouse mammary carcinoma functional pore size of 1200-2000 nm has also been reported[36]. The nanoparticles with sizes in the range of 30–200 nm show better retention by the tissue resistance, shifting the equilibrium toward extravasation and leading to enhanced accumulation. Therefore, nanoparticles with sizes between 30–200 nm are supposed to be most favorable for passive targeting of most types of solid tumours by captivating on the EPR effect. Despite its widespread use in the clinic, the passive targeting strategy has many limitations. Passive targeting is the property of many carriers which highly depends on blood circulation and

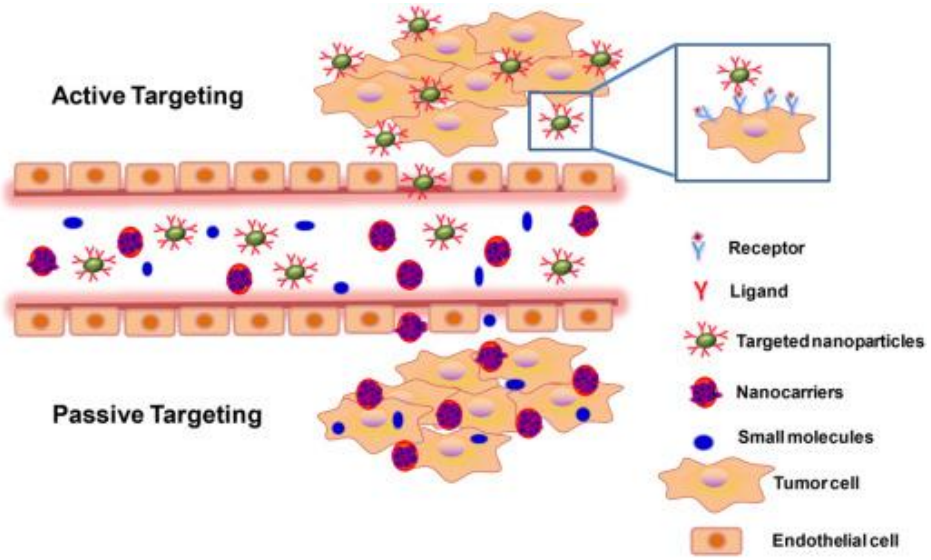

Figure 1.6: Different targeting approaches[37]

extravasations, leads to unintended accumulation on other organs like kidney, liver, spleen etc. Furthermore in the case of small tumours which is not showing angiogenesis is having limited access by EPR effect. Subsequently the blood vessels formed *via* angiogenesis is not uniformly distributed in tumour; therefore the accumulation of delivery agents will not be uniform. Flourishing therapeutic direction in the systemic circulation can be achieved through technologies such as localized delivery, where in the drug release or the action of drug can be limited to selective sites such as tumour but not to other organs. In such cases the term active targeting is important, which can be used to describe specific ligand-receptor interactions between drug carrier and the target sites. The biomedical property of cancer cells is different and this property can be utilized to target the same. So the usage of ligands such as peptides, proteins, antibody fragments, nucleic acids (aptamers), small molecules etc, may provide improved targeting efficiency of delivery agents. The conjugated ligand can increase the affinity of binding and thereby induce receptor-mediated endocytosis more effectively, which may lead to achieve higher intracellular drug concentration. Currently, the active targeting of tumours remains a tricky task and represents a bottleneck for cancer therapeutics.

1.4.1 Importance of targeting ligands for tumour targeted drug delivery systems

Active targeting system may be able to target individual tumours and their specific intra-cellular organelles. The selection of the targeting moiety for our interest should be guided by the detailed idea regarding over-expression of certain receptors or cell membrane proteins inside or outside the tumour area. The function of cell membrane receptors includes recognition of specific molecules, enabling transport of various molecules, serves as enzymes, control cell adhesion etc. A broad variety of ligands can be used for selective targeting and internalization of the delivery system into the cell. For example, mannose, fucose has been used to promote binding to kupfer cells,[38]galactose for parenchymal liver cells, the ligand folic acid is used for folate receptor expressing cancer cells. The most specific targeting ligands are antibodies which are widely used in clinical practice. For example, trastuzumab and rituximab which are antibodies now in clinic. Furthermore many endogeneous proteins can also recognize tumour motif specific receptors. For example, iron transporting protein Tf, which binds with transferrin receptor, has been used to deliver carriers into different cell types[26]. Alternatively, growth factors such as epidermal growth factor (EGF) and neural growth factor (NGF) attached to carriers are other examples of protein-targeted delivery vectors which enter cells and bring out specific molecular responses. Additionally, peptides have gained attention as targeting ligands due to their small size, easy preparation methods, relatively low immunogenicity as compared to larger proteins, high stability, and ease of conjugation to the organic and inorganic carrier surfaces. Combinatorial libraries have led to the breakthrough of short peptides (5–15 amino acids) that are capable to serve as a substrate to connect the targeted proteins, cells, or tissues precisely. One of the most studied peptide sequence is Arg-Gly-Asp (RGD) which binds to $\alpha_v\beta_3$ integrin receptors and are highly up-regulated on both tumour cells and angiogenic endothelial cells. RGD can be chemically synthesized, and is commercially available with various linker appended form that allow for its conjugation to carrier surfaces, biomaterials, or drugs. Some representative tumour cell membrane receptors and the corresponding receptor-binding ligands are listed in table 3. Every year numerous new-fangled receptors and their complementary binding ligand are being

introduced. The main criterion for selecting suitable ligands for a delivery system not only depends solely on its specificity but also with cost and availability. It is important to consider the cost and easy accessibility of the systems when attempting to develop a target specific carrier for practical applications. However, variety of chemical conjugation techniques is available in order to attach targeting ligands to different carrier motifs. Other targeting peptide substrates are also explored such as cathepsins, matrix metalloproteins (MMP), and prostate specific antigen binding sequence.

Ligand type	Receptor specific ligand	Target
Peptides	RGD, c(RGD),iRGD	Integrin (αvβ3, αvβ5)
	Cathepsins	Cathepsin proteases
	MMPs	Matrix mettalloproteinase
	PSA	Prostate specific antigen
	VEGF peptides	VEGF receptor
	NLS	Nuclear receptor
	Mitocondriatargeting peptides	**Mitocondria**
Antibodies	Transferrin antibody	Tranferrin receptor
	Anti EGFR	EGFR
	Anti-P16	cytoplasm
	Anti-Ki67	Nucleus
	Anti HER2-scFv	ErbB2 receptor
	Anti-VEGF Antibody	
	Anti-CD44	CD44antigen
Other small molecular ligands	Folic acid (vitamin B9)	Folate receptor
	Biotin	Biotin receptor
	Mannose, fucose	Kupfer cells
	Galactose, galactosamine, glucose	Asialoglycoprotein receptor
Aptamers	A10 RNA apt	Prostate specific membrane antigen
	Sgc8c DNA apt	Protein tyrosine kinase 7 receptor

	35mer DNA apt	Platelet derived growth factor

Table 1.3: Commonly used ligands for targeted drug delivery

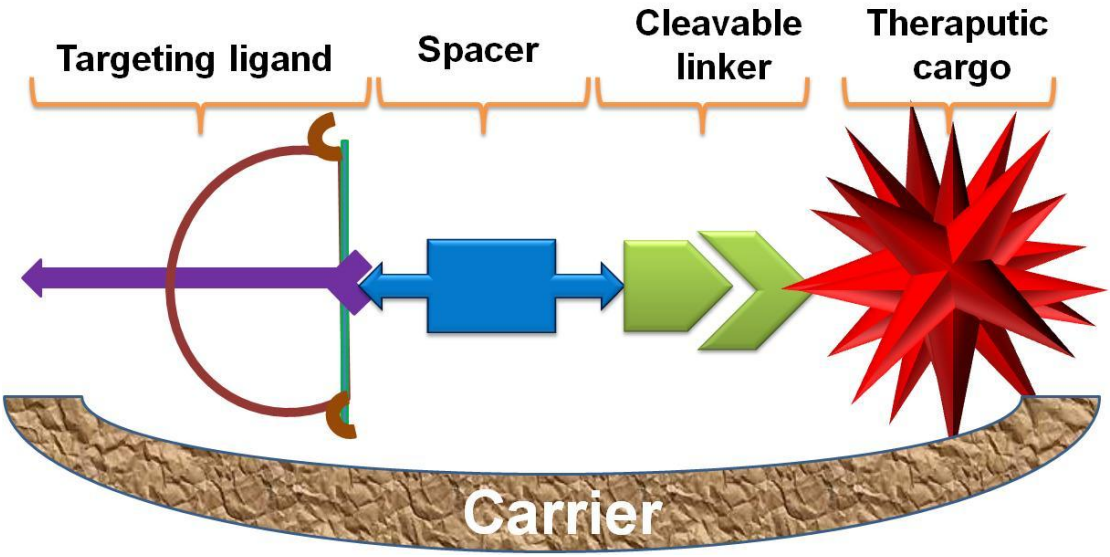

Figure 1.7: Design of ideal targeted drug delivery system

1.4.2 Introduction of spacers and cleavable linkers into delivery carrier

An optimally designed spacer is very important for connecting between the ligand and therapeutic payloads in order to minimize steric hindrance as well as improving the pharmacokinetic (PK) and pharmacodynamic (PD) properties of the targeted carrier systems. The main criterion for selecting a spacer is to balance the lipophilic nature of carrier. The global hydrophobicity/hydrophilicity of a targeted system easily adjustable by tuning the nature of the spacer because playing with therapeutic payloads may change the net efficiency of the systems. The concept of therapeutic delivery is mainly based on the combination of three key mechanistic elements, each thought to play an essential role for efficient delivery (i) specific cellular binding with ligands, (ii) intracellular uptake of drug-carrier in targeted cells, and (iii) controlled release of carried drug molecules in an active form among which the third step is very essential because it involves the drug release, which display its biological activity in the targeted cell. The release can be achieved with the aid of good cleavable linkers (Figure 8). A cleavable linker is usually required between the

drug or therapeutic payloads and the ligand appended carrier, and the payload should be released upon internalization in to target cell. Generally in the case of delivery of diagnostic agents, non-cleavable linkers are often preferred because the imaging agent should be retained in the site, and should be resistant towards efflux pumping. But a linker with cleavage property should be attached while delivering therapeutic drugs, because it should be released in order to accomplish promising actions at the target site. Any linker should obey some of the major requirements such as it should be stable in systemic circulation, it should be cleaved after uptake and it should release active drugs at the target site. The cleavage of the linker can be triggered by low endosomal pH, disulfide reduction, intracellular enzyme hydrolysis, etc.

1.4.3 Use of acid cleavable linkers

One of the frequently exploited strategies of intracellular drug release involves the use of an acid cleavable linker which is readily hydrolyzed in tumour microenvironment. Acidosis is a major heterogeneity within the tumour cells (~6.5-6.8). Many pH cleavable linkers have been reported including hydrazone, hydrazide, oxime, acetal etc. For example, anti-cancer drug doxorubicin is modified with hydrazone at the carbonyl position and hydrolysis of the linker within endosomal or lysosomal compartment afforded the release of unmodified drug. In another case, asymmetric ring opening of a p-alkoxybenzylideneacetal was used for the drug release via utilizing electron donating effect of the p-alkoxy substituent in thearomatic ring imparts increased sensitivity to hydrolysis under mild acidic condition[16]

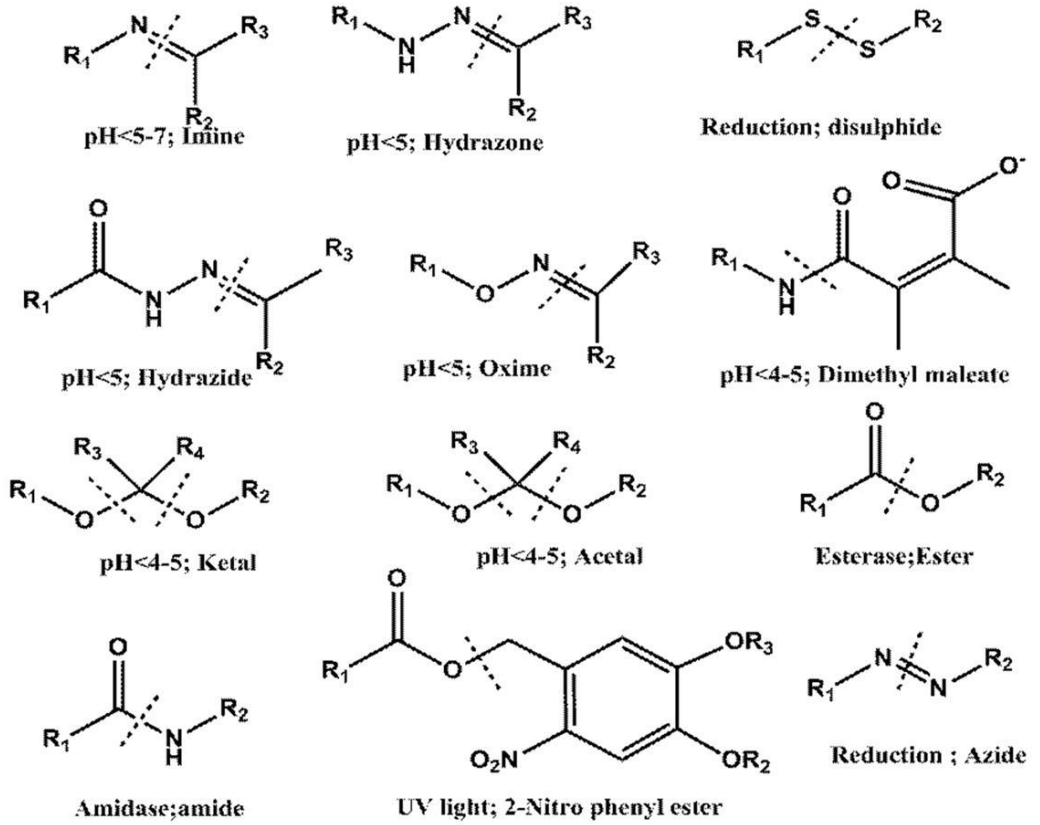

Figure 1.8: Stimuli responsive linkers, conditions and their cleavable sites.

1.4.4 Use of reduction-responsive cleavable linkers.

The presence of reducing agents glutathione (GSH) / glutathione disulfide (GSSG) can be used as a trigger for releasing drugs in the intra cellular milieu. Intracellular glutathione concentration varies between 2 to 10 mM which triggers the recognition of chemically degradable materials containing disulphide bonds with the aid of its difference in reduction potential. A number of delivery systems already explored based on this approach, for example a doxorubicin-peptide conjugate delivery vector (pHLIP-SS-DOX NPs) was developed by Song *et al.* overcoming multiple drug resistance (MDR) and increased therapeutic potential.[39]

1.4.5 Use of enzyme sensitive cleavable linkers

A vast array of important human genome encoded proteases such as mettallo, cysteine, threonine, serine etc. is performing important functions inside the body. However the down regulation is a main output for pathogenic mechanisms underlying cancer and other diseases. This has made proteases attractive targets for drug development. Cathepsins constitute a ubiquitous lysosomal cysteine protease

involved in many pathological and oncological processes in human cells and tissues and also considered to be one of the best examples of intracellular proteases. Different types of cathepsins like cathepsin B,C,D,E,F,G,H,J,K,L,O,S,T,V,W,Y,Z were identified in various organisms among which cathepsin B is involved in oncogenic process especially in the invasive and metastatic stages of cancers. The enzyme is in harmony with malignant transformation, and its regulation is altered thereby resulting in over expression of cathepsin B. The over expression of cathepsin B has been observed in different malignancies, including lung, liver, prostate, cervical, breast, and colorectal cancer.[40]Lysosomally cleavable peptides which recognize cathepsin has been widely used for drug carriers as linkers, because of its significant potential for slow drug release and comfortable solubility. Cathepsin B enzyme cleaves Leu, Arg-Arg, Ala-Leu, Phe-Arg, Phe-Lys, Ala-Phe-Lys, Gly-Leu-Phe-Gly, Gly-Phe-Leu-Gly and Ala-Leu- Ala-Leu[41] In 2001 Shiah*et al.* demonstrated the synthesis of N-(2-hydroxypropyl) methacrylamide (HPMA) copolymer-doxorubicin conjugates (P-DOX). The conjugate was attached with a tetrapeptide Gly-Phe-Leu-Gly and N2 ,N5–bis(N-methacryloyl-glycyl-phenylalanyl-leucyl-glycyl) ornithine cross-linker, with different molecular weights were prepared. The clearance of the system depending on molecular weight was well demonstrated and the therapeutic potential of the system is evaluated in nude mice bearing subcutaneous OVCAR-3 xenografts.[42] A number of delivery vectors conjugated to cath B specific peptide substrates were emerged.[43] In 2015, Maiti et.al reported a lysosome targeted delivery system based on sorbitol scaffold for effective delivery of doxorubicin.[44]

Another multigene family of enzymes called matrix metalloproteinases (MMPs), a zinc-dependent extracellular matrix (ECM) re-modeling endo peptidases generally seen in pathological processes, such as carcinogenesis. Increased cell proliferation and tumour size is correlated with high expression of MMPs in extracellular matrix. MMPs are abundant nearly all human cancers. Pharma and biotech industries have invested substantial attempts over the past 20 years aiming to build up and secure in effectual agents targeting MMPs. In this regard, multiple MMPs have been developed, in an attempt to control the synthesis, secretion, activation and enzymatic activity of MMPs. Several generations of synthetic non peptidomimetics,

peptidomimetics, and tetracycline derivatives of MMPs were tested in phase III clinical trials. In 2010 Yi *et al*. reported MMP sensitive targeted gold nanorods for effective photothermal therapy. They have conjugated MMP specific peptide sequence (Gly-Pro-Leu-Gly-Val-Arg-Gly-Cys) with NIR fluoresent dye Cyanine 5 and decorated on gold nanorod for the delivery of therapeutic agents in SSC-7 tumour xenograft model[45]. Recently Maiti et.al reported a targeted theranostic nanoprobe for MMP targeted delivery of doxorubicin and an imaging agent towards cervical cancer[46].

Prostate specific antigen (PSA) is an over-expressed biomarker in prostate cancer. Extensive research have been devoted in identifying the potential of prostate cancer-specific antigens and corresponding ligands, such as monoclonal antibodies/fragments, peptides, aptamers, or small molecules. Among them PSA, a serine protese[47], member of the family of zinc-dependent exo-peptidases with a bi-nuclear zinc active site, and belongs to kallikrein gene family and it can work as a glutamate carboxypeptidase and its expression level is 100 to 1000 fold higher in prostate cancer cells compared to normal tissues.[48]Therefore PSA represents an attractive candidate for selectively targeted therapies for prostate and/or other solid tumors. Many PSA targeting aptamers, mAb or peptides have been developed and employed in prodrug or nanoparticles to improve their targeting efficiency to prostate cancer cells[48]. In 2010 Elsadek *et al*. reported an albumin-binding prodrug of doxorubicin that with p-aminobenzyloxycarbonyl (PABC) as a self-immolative spacer in and a PSA specific peptide sequence, Arg-Ser-Ser-Tyr-Tyr-Ser-Leu. The prodrug exhibited good water solubility and was bound rapidly to the cysteine-34 position of human serum albumin[47]. In recent years, Maiti *et.al.* developed a tetra phenyl ethylene based fluorophore appended with PSA peptide for the detection of PSA in prostate cancer with a limit of detection of 0.5ng[49].

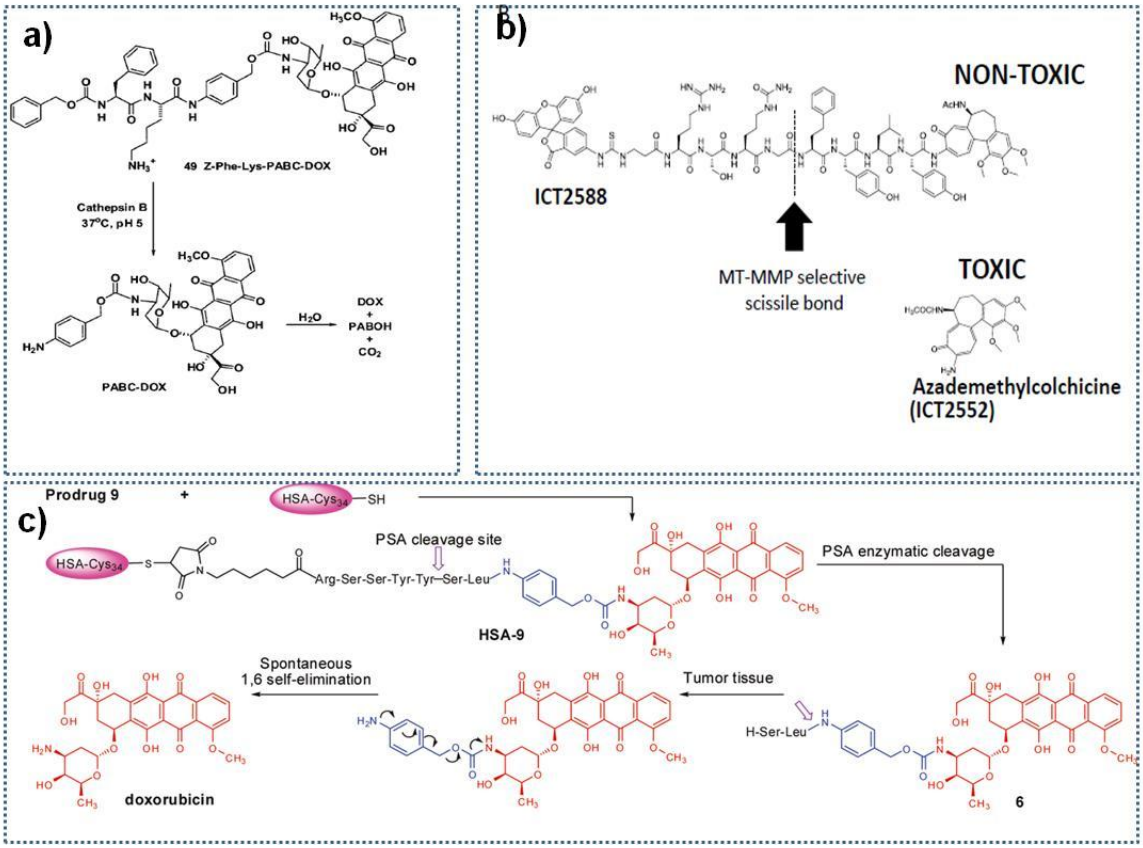

Figures 1.9: Enzyme responsive prodrug constructs; a) Cathepsin B responsive doxorubicin conjugate with PABC linker[50], b)MMP responsive prodrug for ICT2552 delivery[51], c)PSA responsive doxorubicin prodrug for selective killing of prostate cancer[47].

1.5. Strategies involved in targeted drug delivery systems towards cancer therapy

In a targeted drug delivery system, generally tumour targeted ligand attached to the carrier -drug conjugate undergo internalization by the process of receptor-mediated endocytosis. Endocytosis includes different pathways *viz,* phagocytosis (cell eating), pinocytosis (cell drinking), clathrin-mediated endocytosis (receptor mediated), and caveolae or the lipid-rafts pathway (clathrin independent).[51]The carrier may choose any of these pathways depending on the physicochemical properties. Finally, the whole carrier-drug complex crosses the cell membrane. Inside the cell, the carriers begin to release the chemotherapeutic drug depending on the releasing strategy, to efficiently suppress the propagation of the tumour relative to the untargeted tumour

cells. The whole mechanism of targeting cancer cells using drug carrier[52] is illustrated in figure 1.10

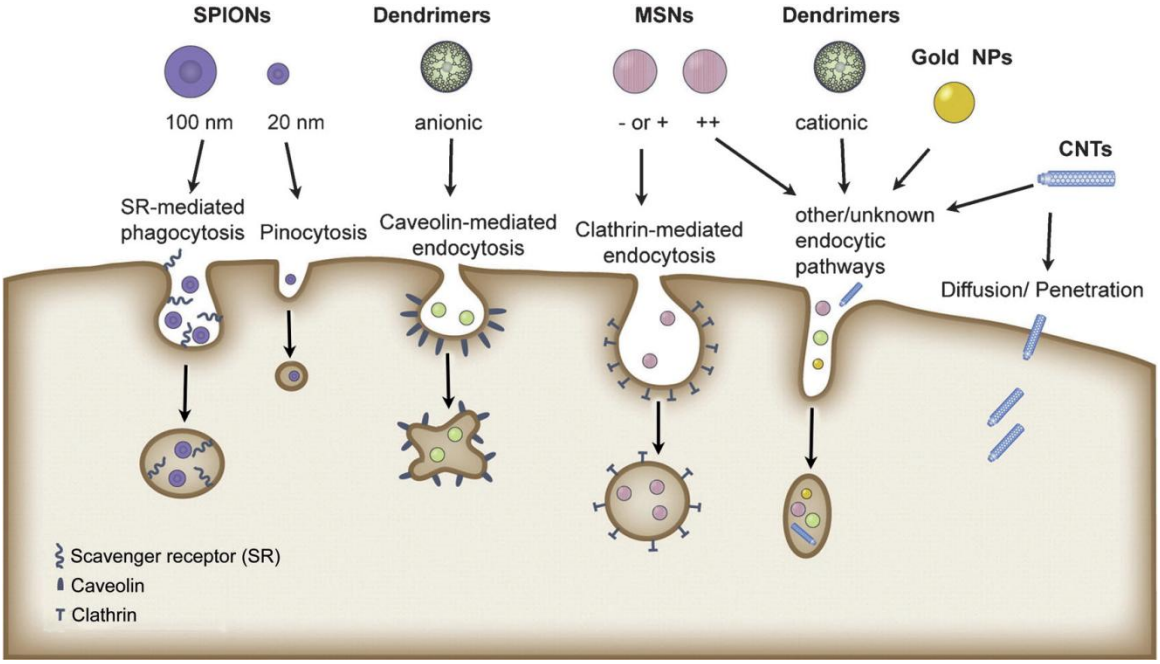

Figure 1.10: Cellular internalization pathways for cellular internalization according to size and surface properties of the particles.[52]

Bushman *et al*. reported a targeted delivery system for paclitaxel (PTX) by taking advantage of pre-targeted radio immunotherapy which employed the advantage of the specific antibodies for targeted cell populations and delivers a localized dose of a biotinylated (targeting ligand) radionuclide that is most frequently administered following binding of a biotinylated antibody and streptavidin (StA) to the target cells. The authors described the development of ABA type copolymer based nanosphere comprising of a tyrosine-derived oligomer as the B-block and poly (ethylene glycol) (PEG).The targeted nanoprobe was loaded with anticancer drug paclitaxel. The system has showed excellent targeting efficiency towards CD44 positive cells.[52]

In 2014, Hauang and colleagues established an acid induced disassembly of integrin targeted polymeric particle for the delivery of Dox. The authors synthesized a block co polymer of poly carboxy betaine methacrylate (PCB) and poly (2-(diisopropylamino) ethyl methacrylate) (PDPA) wherein PCB is responsible for increased circulation and PDPA is used as an acid triggering group. The polymer was

attached with Arg-Gly-Asp (RGD), an integrin targeting ligand, and co-loaded with anticancer drug dox. The therapeutic response of the drug was evaluated at pH 5-6 whereas in pH7.4 the system was intact.[53]

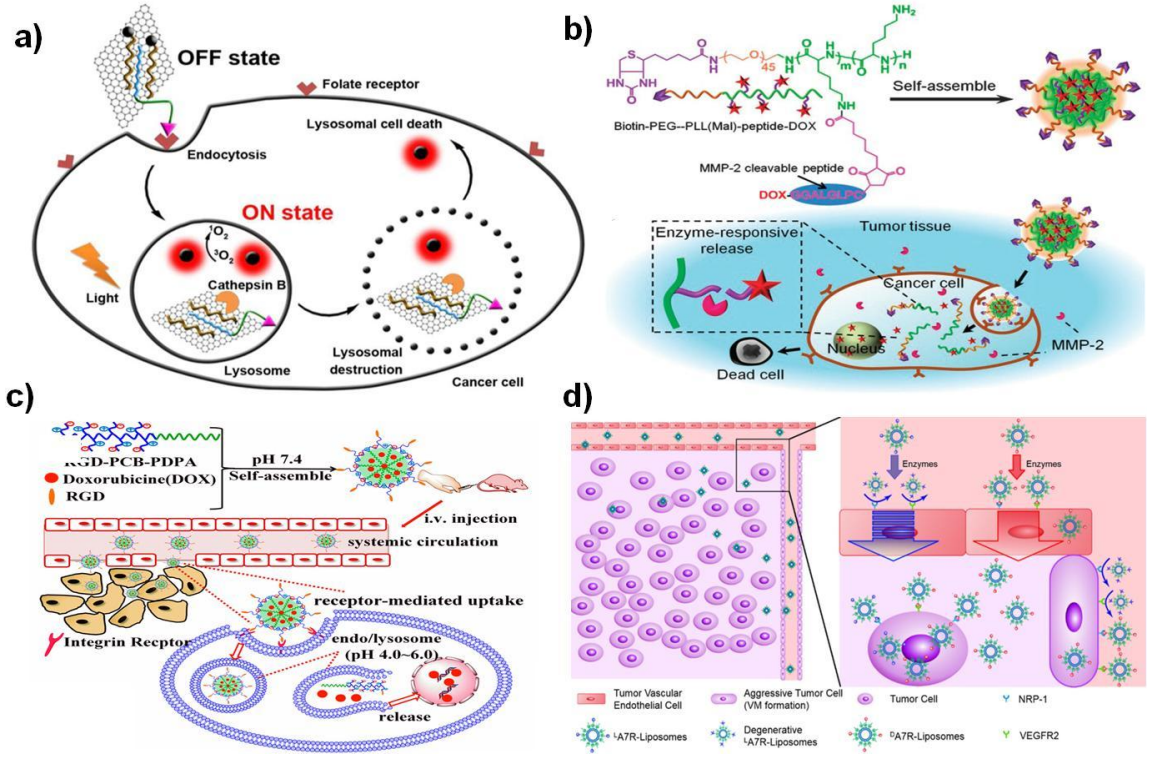

Figure 1.11. a) FR-targeted delivery and cathB activation for photosensitive lysosomal cell death and *in situ* therapeutic monitoring.[54]b)Schematic representation of the formation of micelles and intracellular drug releasae. (A) The formation of micelles with amphiphilic Biotin-PEG-b-PLL (Mal)-peptide-DOX via self-assembly. (B)The uptake of nanoparticles via active targeting and triggering release of drug upon interaction with MMP-2.[55]c) synthesis of RGD-PCBPDPA/DOX NPs, and targeted accumulation, and receptor-mediated endocytosis and stimuli responsive drug release.[53]Schematic demonstration liposome stabilized with Heptapeptide A7R-based delivery vector.[56]

Ju and co-workers demonstrated a cathepsin B activatable folate targeted delivery probe for photosensitizer delivery and therapy in 2015. The nanoprobe was prepared on graphene oxide by attaching peptide labeled photosensitizer (Ce6-GRRGKGGFFFF) and folate decorated phospholipid-poly(ethylene oxide)*via* a non-covalent assembly. The probe was internalized via recognizing folate receptor on the cell surface and subsequent release of photosensitizer happened via peptide

destruction in the lysosome by the over expressed cathB enzyme. Both therapeutic monitoring and cell death can be monitored by triggering the photosensitizer release from the nano probe.[54]

In 2017 Han *et al*. reported a dual enzymatic reaction assisted delivery of gemcitabine(GEM), a well-known anticancer drug towards pancreatic cancer. The authors used CdSe/ZnS Quantum dots (QDs) as both MMP-9 and Cath B responsive nano vector and the whole system is decorated with integrin targeting ligand Cyclo-RGD. The drug was conjugated with the QDs via cathB specific peptide GFLG, and the whole system is protected with polyethylene glycol chains via MMP-9 responsive peptide GGPLGVRGK-NH_2. In their system the RGD will recognize the integrin ligand and allow internalization inside the cancer cell. Subsequently the MMP-9 over expressed in extracellular matrix will cleave the peptide and leads to removal of PEG from the nanosystem. Furthermore the vector will go towards the lysosome, and free gemcitabine will release upon exposure with up-regulated cathB enzyme by ensuring maximum therapeutic effect.[54]

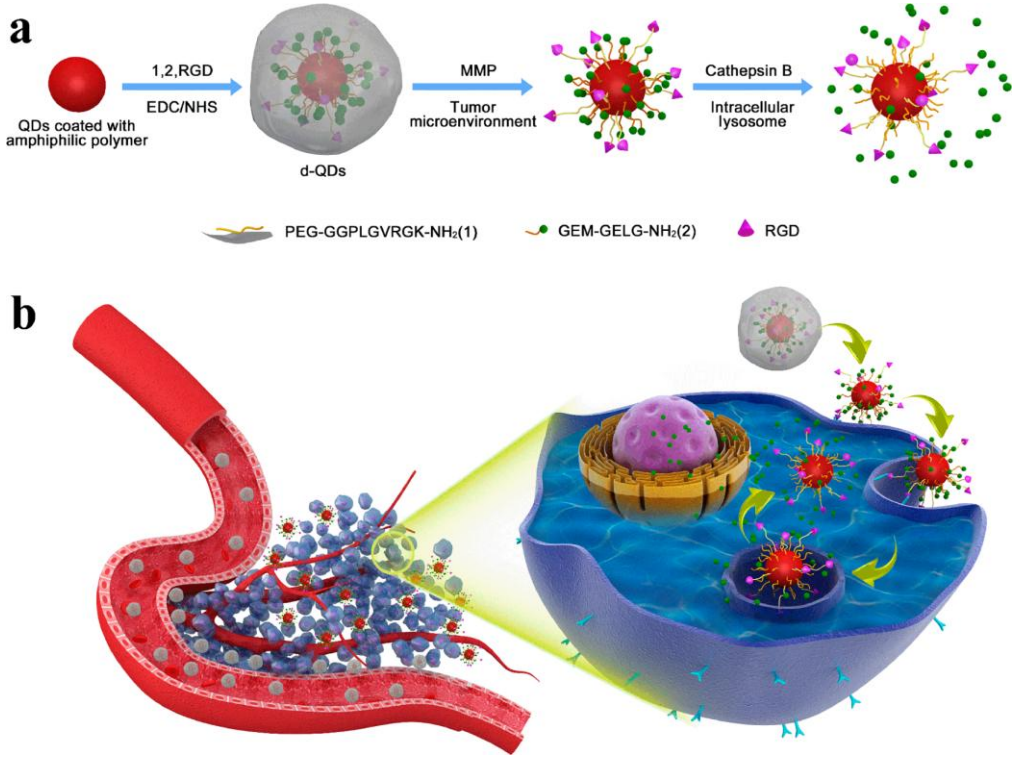

Figure 1.13: GEM nanovectors for multistage dual enzymatic reaction assisted drug release (a) synthesis of nanovector and its releasing property (b)schematic representation of targeting ability of nanovectors.[54]

1.6. Current trends in the development of drug carriers.

Development of carriers in recent years involves multi-disciplinary approaches where different novel trends are emerging by considering several aspects.

1.6.1 Multi targeted carriers

Recent developments in targeted carriers systems have revealed that the single-target drugs may not be always adequate to produce the the maximum therapeutic effect to diseased cells and tissues. If two or more targeting ligands were used to recognize different receptors present in the tumour site, the approach become a muti-targeted delivery system. This method can improve the uptake of carrier by cancer cells with the aid of ‘‘two-punch’’ (or ‘‘three-punch’’) approach. Many of the targets have associations with the others (at least with one drug) through target–target network visualization, which further confirms the significance of multi-target drugs. The targets can be a resident of the same or separate pathways within an individual cell, or in separate tissues. The components bind in separate sites to create a combination effect and increase the pharmacological action.

1.6.2 Combination therapy

Combination therapy governed by co-delivering multiple drugs/other therapeutic agents encapsulated in the same targeted carrier is projected to address the challenges of single-agent chemotherapy. Combinations of two or more types of chemotherapeutic drugs are often preferred, which can reduce the therapeutic dosages and side effects. Chemoradiotherapy[54], chemophototherapy[54] and other combinational modalities are emerging to control the individual side effects, synergistic anti-cancer effects, reduced drug related toxicity, inhibit efflux mechanisms, and reduce multiple drug resistance via different mechanisms. Therefore, the use of multi modalities or a variety of methods for comprehensive treatment or a method to support the treatment management has become a new trend in cancer therapy. One of the promising approaches for non-invasive therapy to eradicate tumour constitutes NIR- phototherapy, owing to its minimal side effects and high efficiency. Phototherapy is classified in to PDT and PTT according to the conversion of light into chemical energy or heat energy to achieve cytotoxic effects to the disease cells. The therapy requires a photoactive agent and light to generate either reactive oxygen species or heat. PDT requires administration of a

photosensitizer with wavelength of our interest to produce various photochemical reaction assisted apoptosis of cancer cells. Whereas in PTT the photoactive agent will generate a locally elevated temperature to eradicate tumour cells under NIR laser irradiation. The combination of phototherapy and chemotherapy qualifies as an alternative treatment modality for chemo- and radio-resistant cancer cells which enables a different cytotoxic mechanisms.

Peng *et al* in 2009 reported chlorine core polymeric micelle loaded with anti-cancer drug SN-38 for effective destruction of colon cancer. Herein self-assembled micelle not only act as photosensitizer but also as carrier for chemotherapeutic agent, confirm the dual therapy (both chemo and PDT) in a synergistic way.[57] The PTT induced chemotherapy with hollow gold nano particle (HGNP) was established by You *et al* in 2010.The HGNP acted as nanocarrier, photothermal agent as well as triggering PTT induced release of anticancer drug doxorubicin. The authors compared photothermal ablation efficiency as well as chemotherapeutic efficiency with bare HGNP and PEGylated HGNPs.[58] Further more in 2017 Davids and co-workers established a combinational effect of PDT and chemotherapy in metastatic melanoma with the aid of hypericin-based PDT and dacarbazine based chemotherapy. This combination therapy decreases melanoma cell viability and it abrogates the renewal capacity of melanoma cells – a characteristic that these cells used to induce clonogenic growth and tumourigenicity.[59]Subsequently *Lao et al*. described the effective delivery of doxorubicin co-loaded polymersomes *via* gold nanorod carrier, a well-known photothermal agent where in co-therapy showed more apoptotic tumour cells in presence of 808 nm laserexposure.[60]

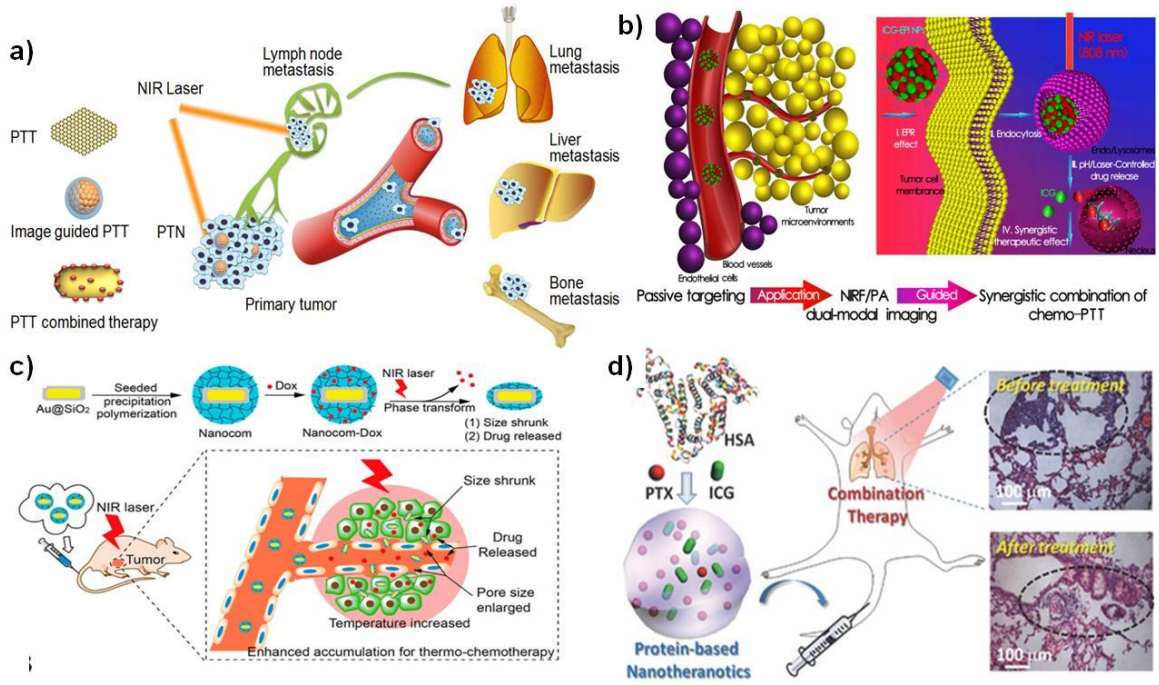

Figure 1.14: a) The Schematic representation of curing cancer metastatis via different photothermal nanoparticles (PTN)[10]. b) ICG-EPI NPs for dual-modal imaging-guided synergistic chemo-PTT. The particles were internalized via passive targeting, pH and photo responsive drug release[61]. c) pH sensitive polymer functionalized silica coated gold nanorod for synergestic photothermal chemo therapy. [10] d) Paclitaxel nanodrug for dual therapy of metastatic breast cancer. [10]

1.6.3 Sub-cellular targeting

The subcellular organelles, for example, mitochondria, nucleus, lysosome, etc are the vital organelle which plays an important role in pathological processes such as cell operation, intracellular transportation, metabolism and other cellular functions. The dysfunction in any of the organelle leads to chronic disorders such as cancer. To investigate the molecular mechanism and the unambiguous role of the organelles numerous organelle targeting molecules and ligands were developed.[62]**.** Lysosomes are of particular interest, and considered as potential target for the design and delivery of pH-dependent as well as cathepsin B cleavable pro-drugs, for enhancing selectivity and developing strategies. In 2014. Maiti *et al.* reported a lysosome-targeted sorbitol doxorubicin conjugate for efficient cancer therapy. The carrier octaguanidine sorbitol scaffold was conjugated with lysosome specific peptide sequence and decorated with anti neoplastic drug doxorubicin.[62] Lysosomal targeting transporting nanocarriers to the mitochondria is also an emerging

platform in cancer therapy. The commonly used ligands targeting to mitochondria are the mitochondrial targeting sequence peptides, lipophilic cations like triphenylphosphonium cation etc. Over the past decade, the covalent modification of compounds to mitochondria-targeting "vehicles" has gained much attraction, due to straight forward chemical synthesis and the high targeting efficiency. The pioneering work, which underwent in the early 1990s, verified that mitochondria-localized anti-apoptotic proteins could be blooming targets for cancer therapy[62,63].Nucleus is also a key target for cancer therapy. Many small molecules and nuclear localization peptide sequence were used to demonstrate nuclear targeted delivery. In 2012 Pan *et al*. reported a TAT peptide modified mesoporous silica nanoparticles for nuclear targeted drug delivery of doxorubicin. [64] .

1.7 Therapeutic delivery monitoring modalities

Different multi modal therapies are emerging for the efficient treatment of cancer, so there is an increasing need of monitoring the progression and response of therapeutic effect to desired target site. A number of factors ranging from the type of delivery carrier and their response and type of therapeutic modality play an important role in intrinsic biology of the tumour, all of which can aid in the ideal course of treatment, profiling of toxicity and progression of disease. Therefore, it is very important to monitor the response of diseased cell towards therapy, and should be ideally optimized. This can be achieved by tuning unique optical properties of the delivery system and can select a tool without harming the rest of the body. Depending on the fabrication of drug-carrier conjugate several imaging techniques are adopted viz., , fluorescence microscopy, photoacoustic imaging (PAI), magnetic resonance imaging, surface enhanced Raman spectroscopy (SERS) etc[65].

1.7.1 Fluoresence microscopy

Fluorescent microscopy is a special type of optical microscopy where a fluorescent molecule is illuminated with light at a certain wavelength (sample-dependent), and the emitted photons are measured. It has become an indispensable technique in cell biology. This technique permits researchers to study the dynamics of cells in real time, individual organelles, tissue etc. Unfortunately, fluorescence microscopy has many limitations such as the high-intensity excitation light required for excitation of

fluorophores, many of the fluorophores with high quantum yield is having toxicity issues, so the system is not completely "noninvasive"[66]

1.7.1 Optical microscopy (eg; Dark filed microscopy)

Metallic carriers having high surface plasmon resonance (SPR) by interacting with light produce enhanced scattering and it can be viewed through optical microscopy e.g., dark filed microscopy. In this modality a source of light, mainly white light is applied to the sample, which is having strong scattering power. The corresponding SPR will be reflected from the sample, and can be collected and imaged through a confocal microscope. The colored image with black background will be created.[67]

1.7.3 Photoacoustic imaging

Photoacoustic imaging is a recent imaging technique, providing deeper penetration via enhanced spatial resolution through the production of acoustic signal from light absorbing biologically relevant molecules. This imaging technique not only relies on light but also with sound and can be a powerful combination, i.e, it is a combination of ultrasound with NIR radiation. The principle is attributed to non-radiative relaxation of a molecule or a probe after excitation of light. The non-radiative pathways include vibrational relaxation resulting in generation of heat, this local heating creating a pressure buildup and releasing ultra sound waves[68].

1.7.4 Surface enhanced Raman spectroscopy (SERS) based monitoring

Surface-enhanced Raman scattering (SERS) has been well taken by the researchers, as an alternative to fluorescence-based spectroscopy, for characterization, bio-imaging, cancer diagnostics and monitoring therapeutic progression. After the excitation with Vis-NIR light the vibrational modes undergo relaxation and produces Raman scattering. The probability of scattering is nearly 14 orders smaller than that of fluorescence. But when the molecule is in close proximity with the nano-roughened metal surface such as nanoparticles the situation will be different. The enhancement of Raman scattering occurs *via* fields generated from SPR, as a result of which a sharp increase in signal intensity was observed. It can be able to overcome the peak overlapping, photobleaching, increase signal to noise ratio especially in biological samples, thereby enabling even single molecule detection.

The development of NIR active Raman probes provide a new avenue for *in vivo* imaging techniques[69]

1.8 Opportunities and challenges for the development of targeted drug delivery carriers

In oncology drug delivery platform holds a large impact, where attempt on cells or tissue targeting to the molecular level furnish an effective delivery of cytotoxic drugs. Nowadays, cancer drugs generally administered either intravenously or orally become systemically distributed without preferential distribution in cancer tissue. The prevalent bio-distribution of cancer drugs results in both therapeutic anti-cancer effects as well as off target undesirable side effects on healthy and proliferating non-cancer cells. The primary goal of targeted therapeutics is to deliver the drugs in more controlled and specific manner. Although fabulous advancement has been made over the past few decades for constructing various delivery agents assays for killing cancer, most of these advancement are merely proof-of-concept manifestations and their feasibility are only reachable under highly optimized circumstances in a lab. A number of outstanding challenges stay behind for translating these delivery vectors from sparkling buffered resolution in a research environment to real-world clinical patients and to further practical settings. Commonly the molecularly targeted cancer drugs were modulating signaling pathways that are unusually activated in cancer cells. These therapeutic agents were found to: (i) interact with their targets reversibly, (ii)be dosed daily,(iii)be administered orally, and (iv) limited in their effectiveness as single vector due to emergence of multiple resistance, high network robustness etc. Targeted drug delivery technologies may facilitate the co-delivery of multiple molecularly targeted drugs, making an integrative pharmacologic effect among individual drugs, thereby adjusting numerous pathways that may transform into more prolonged and successful anti-cancer therapies. Eventually a number of factors need to be addressed for successful design of targeted delivery agents, which include optimization of biophysicochemical characteristics and the demonstration of the usefulness of targeted vectors in a clinical setting on their impact on patient outcomes. Apart from ligand identification and key targets for selective targeting, many challenges are still there in the development of targeted therapeutic agents,

which includes (i) easy and reproducible chemistries for bioconjugation, (ii) biocompatible, biodegradable and eliminable delivery carrier development, (iii) avoiding multistep and multi purification techniques, (iv) optimization of release profile, long retention time and distribution kinetics, (v) scalable protocol development for manufacturing materials in industrial level for clinical development and commercialization. Very recently the interest of researchers has been changed to tune the properties of carriers such as size, shape, surface areas and hydrophilicity or hydrophobicity for key understanding of improved carrier design. By tailoring the above parameters with minimum toxicity profile, avoiding unfavorable interactions with biological systems such as immune systems, renal clearance etc, will lead to the development of intelligent delivery system for changing current modalities. However extensive clinical trials are needed for demonstrating marketed improvement of the developed systems. Beyond this, demonstrating efficiency, safety, cost effectiveness and quality are the main regulatory requirements in the current scenario. Additional challenges should be investigated by case studies in order to address the tremendous potential of new class of delivery therapeutics.

1.9 Conclusion

Targeted drug delivery carriers have shown significant therapeutic potential in clinical practice. Delivery carriers having predicted biological properties based on their size, shape and structural property, which permit them to absorb, bind and carry therapeutic molecules such as small molecule drugs, DNA, RNA, siRNA, proteins, and molecular probes effectively. Their distinctive characteristics have allowed clinicians to suggest them either as new treatments (mono therapy) or as addition to current treatments (combined therapy) to improve therapeutic efficacy. Even though some delivery carriers have not been flourishing when being clinically translated, several new and promising carriers are currently in expansion stage and show great promise, thereby providing great anticipation for new treatment options in the near future. Nevertheless all newly developed carriers, whether they are used as carriers for small drugs, therapeutic or imaging agents, will need to be systematically characterized the physiochemical, pharmacological, and immunological properties prior to their approval for use in humans. Hence, short-

term and long-term toxicity studies also essential to undertake in both cell culture and living animal models before translate into clinical trials.

1.10. Objectives of the Present Investigation

Inspired by the recent progress in the design of drug delivery carriers based on organic and inorganic nanomaterials, the thesis is planned to explore the possibility of developing different drug delivery carriers and explore their different target specific approaches for maximum therapeutic benefit. It is well known in the literature that the guanidium rich carriers possessed excellent cell penetrating property as well as biocompatibility than other relevant organic carriers. Though these carriers were previously utilized for the delivery of therapeutic carriers, several new and promising candidates are in the expansion stage.

Our first aim was to synthesize a guanidium rich poly propylene imine based new drug carrier with good water solubility and excellent biocompatibility and transformed into a targeted drug delivery system with the core skeleton. After tuning the properties of the carrier we aimed to demonstrate its utility as dual targeted delivery system. Exploration of previously developed octa guanidium sorbitol scaffolds as dual targeted delivery system towards paclitaxel delivery consisted the subject matter of next investigation. In this way possibility of making different delivery system and tuning its carrier potential were developed. Recently nano therapeutic carriers gave wide attention in the field of drug delivery have been widely used for different sub cellular organelle targeted delivery. Therefore, next objective of the thesis was to design a nanocarrier which can target cancer and subsequently penetrating in to sub cellular organelle for overcoming current drawbacks of anticancer drugs. We have planned to use a targeted NIR absorbing, sulfocalix[4]arene appended hollow gold nano particle as carrier for mitochondria mediated apoptosis. The present thesis is a systematic investigation on the development of potential candidates for targeted delivery of therapeutic cargoes.

1.11. References

(1) Siegel, R. L.; Miller, K. D.; Jemal, A. Cancer Statistics. *CA Cancer J Clin* **2016**, *66* (1), 7–30.

(2) Release, P. Latest World Cancer Statistics Global Cancer Burden Rises to 14 . 1

Million New Cases in 2012 : Marked Increase in Breast Cancers Must Be Addressed. *International Agency for Research on Cancer, World Health Organization*. 2013, pp 1–3.

(3) Shibu, E. S.; Hamada, M.; Murase, N.; Biju, V. Nanomaterials Formulations for Photothermal and Photodynamic Therapy of Cancer. *J. Photochem. Photobiol. C Photochem. Rev.* **2013**, *15* (1), 53–72.

(4) Cross, D.; Burmester, J. K. Gene Therapy for Cancer Treatment: Past, Present and Future. *Clin. Med. Res.* **2006**, *4* (3), 218–227.

(5) Velpurisiva, P.; Gad, A.; Piel, B.; Jadia, R.; Rai, P. Nanoparticle Design Strategies for Effective Cancer Immunotherapy. *J Biomed(Syd)* **2017**, *2* (2), 64–77.

(6) Huang, C.-Y.; Ju, D.-T.; Chang, C.-F.; Muralidhar Reddy, P.; Velmurugan, B. K. A Review on the Effects of Current Chemotherapy Drugs and Natural Agents in Treating Non-Small Cell Lung Cancer. *BioMedicine* **2017**, *7* (4), 23.

(7) Camus, V. L.; Stewart, G.; Nailon, W. H.; McLaren, D. B.; Campbell, C. J. Measuring the Effects of Fractionated Radiation Therapy in a 3D Prostate Cancer Model System Using SERS Nanosensors. *Analyst* **2016**, *141* (17), 5056–5061.

(8) Hayden, S. C.; Austin, L. A.; Near, R. D.; Ozturk, R.; El-Sayed, M. A. Plasmonic Enhancement of Photodynamic Cancer Therapy. *J. Photochem. Photobiol. A Chem.* **2013**, *269*, 34–41.

(9) Allison, R. R.; Moghissi, K. Photodynamic Therapy (PDT): PDT Mechanisms. *Clin. Endosc.* **2013**, *46* (1), 24–29.

(10) Zou, L.; Wang, H.; He, B.; Zeng, L.; Tan, T.; Cao, H.; He, X.; Zhang, Z.; Guo, S.; Li, Y. Current Approaches of Photothermal Therapy in Treating Cancer Metastasis with Nanotherapeutics. *Theranostics*. 2016, pp 762–772.

(11) Higashi, T.; Khalil, I. A.; Maiti, K. K.; Lee, W. S.; Akita, H.; Harashima, H.; Chung, S.-K. Novel Lipidated Sorbitol-Based Molecular Transporters for Non-Viral Gene Delivery. *J. Control. Release* **2009**, *136* (2), 140–147.

(12) Immune, T. Principle of Cancer Treatment by Immunotherapy. *Surgery* **2009**, *27* (4), 1–2.

(13) Thakor, A. S.; Gambhir, S. S. Nanooncology : The Future of Cancer Diagnosis and Therapy. *CA Cancer J Clin C* **2013**, *63* (6), 395–418.

(14) Binaschi, M.; Zunino, F.; Capranico, G. Mechanism of Action of DNA Topoisomerase Inhibitors. *Stem Cells* **1995**, *13* (4), 369–379.

(15) Huang, C.-Y.; Ju, D.-T.; Chang, C.-F.; Muralidhar Reddy, P.; Velmurugan, B. K. A Review on the Effects of Current Chemotherapy Drugs and Natural Agents in Treating Non–small Cell Lung Cancer. *BioMedicine* **2017**, *7* (4), 23.

(16) Sun, T.; Zhang, Y. S.; Pang, B.; Hyun, D. C.; Yang, M.; Xia, Y. Engineered Nanoparticles for Drug Delivery in Cancer Therapy. *Angew. Chemie Int. Ed.* **2014**, *53* (46), 12320–12364.

(17) Wender, P. a; Galliher, W. C.; Goun, E. a; Jones, L. R.; Pillow, T. H. The Design of Guanidinium-Rich Transporters and Their Internalization Mechanisms. *Adv. Drug Deliv. Rev.* **2008**, *60* (4–5), 452–472.

(18) Stanzl, E. G.; Trantow, B. M.; Vargas, J. R.; Wender, P. A. Fifteen Years of Cell-Penetrating, Guanidinium-Rich Molecular Transporters: Basic Science, Research Tools, and Clinical Applications. *Acc. Chem. Res.* **2013**, *46* (12), 2944–2954.

(19) Wender, P. A.; Galliher, W. C.; Goun, E. A.; Jones, L. R.; Pillow, T. H. The Design of Guanidinium-Rich Transporters and Their Internalization Mechanisms. *Adv. Drug Deliv. Rev.* **2008**, *60* (4–5), 452–472.

(20) Wender, P. A.; Cooley, C. B.; Geihe, E. I. Beyond Cell Penetrating Peptides: Designed Molecular Transporters. *Drug Discov. Today. Technol.* **2012**, *9* (1), e49–e55.

(21) Stanzl, E. G.; Trantow, B. M.; Vargas, J. R.; Wender, P. A. FifteenYears of Cell-Penetrating,Guanidinium-Rich Molecular Transporters: Basic Science, Research Tools, and Clinical Applications. *Acc. Chem. Res.* **2013**, *46* (12), 2944–2954.

(22) Kloß, A.; Henklein, P.; Siele, D.; Schmolke, M.; Apcher, S.; Kuehn, L.; Sheppard, P. W.; Dahlmann, B. The Cell-Penetrating Peptide Octa-Arginine Is a Potent Inhibitor of Proteasome Activities. *Eur. J. Pharm. Biopharm.* **2009**, *72* (1), 219–225.

(23) Bolt, H. L.; Cobb, S. L. A Practical Method for the Synthesis of Peptoids Containing Both Lysine-Type and Arginine-Type Monomers. *Org. Biomol. Chem.* **2016**, *14* (4), 1211–1215.

(24) Wender, P. a; Rothbard, J. B.; Jessop, T. C.; Kreider, E. L.; Wylie, B. L. Oligocarbamate Molecular Transporters: Design, Synthesis, and Biological Evaluation of a New Class of Transporters for Drug Delivery. *J. Am. Chem. Soc.* **2002**, *124* (45), 13382–13383.

(25) Medina, S. H.; El-sayed, M. E. H. Dendrimers as Carriers for Delivery of Chemotherapeutic Agents. *chem soc rev* **2009**, *109* (734), 3141–3157.

(26) Caruso, F.; Hyeon, T.; Rotello, V. Targeted Polymeric Therapeutic Nanoparticles: Design, Development and Clinical Translation. *Chem. Soc. R ev* **2012**, *41* (7), 2971–3010.

(27) Huang, I.-P.; Sun, S.-P.; Cheng, S.-H.; Lee, C.-H.; Wu, C.-Y.; Yang, C.-S.; Lo, L.-W.; Lai, Y.-K. Enhanced Chemotherapy of Cancer Using pH-Sensitive Mesoporous Silica Nanoparticles to Antagonize P-Glycoprotein-Mediated Drug Resistance. *Mol. Cancer Ther.* **2011**, *10* (5), 761–769.

(28) Kumar, S.; Rani, R.; Dilbaghi, N.; Tankeshwar, K. Carbon Nanotubes : A Novel Material for Multifaceted Applications in Human Healthcare. *Chem. Soc. Rev.* **2016**, *46*, 158–196.

(29) Chem, J. M.; Preciado-flores, S.; Wang, D.; Wheeler, D. A.; Newhouse, R.; Hensel, J. K. Highly Reproducible Synthesis of Hollow Gold Nanospheres with near Infrared Surface Plasmon Absorption Using PVP as Stabilizing Agent. *J. Mater. Chem. B* **2011**, *21*, 2344–2350.

(30) Hooshmand, N.; Jain, P. K.; El-Sayed, M. A. Plasmonic Spheroidal Metal Nanoshells Showing Larger Tunability and Stronger near Fields than Their Spherical Counterparts: An Effect of Enhanced Plasmon Coupling. *J. Phys. Chem. Lett.* **2011**, *2* (5), 374–378.

(31) Skrabalak, S. E.; Chen, J.; Sun, Y.; Lu, X.; Au, L.; Cobley, C. M.; Xia, Y. Gold Nano Cages Synthesis, Properties, and Applications. *Acc. Chem. Res.* **2008**, *41* (12), 1587–1595.

(32) Schwartzberg, A. M.; Olson, T. Y.; Talley, C. E.; Zhang, J. Z. Synthesis, Characterization, and Tunable Optical Properties of Hollow Gold Nanospheres. *J. Phys. Chem. B* **2006**, *110* (40), 19935–19944.

(33) Wang, Y.; Yan, B.; Chen, L. SERS Tags: Novel Optical Nanoprobes for Bioanalysis. *Chem. Rev.* **2013**, *113* (3), 1391–1428.

(34) Srinivasarao, M.; Low, P. S. Ligand-Targeted Drug Delivery. *Chem. Rev.* **2017**, *117* (19), 12133–12164.

(35) Hashizume, H.; Baluk, P.; Morikawa, S.; McLean, J. W.; Thurston, G.; Roberge, S.; Jain, R. K.; McDonald, D. M. Openings between Defective Endothelial Cells Explain Tumor Vessel Leakiness. *Am. J. Pathol.* **2000**, *156* (4), 1363–1380.

(36) Haley, B.; Frenkel, E. Nanoparticles for Drug Delivery in Cancer Treatment. *Urol. Oncol. Semin. Orig. Investig.* **2008**, *26* (1), 57–64.

(37) Bhushan, B.; Khanadeev, V.; Khlebtsov, B.; Khlebtsov, N.; Gopinath, P. Impact of Albumin Based Approaches in Nanomedicine: Imaging, Targeting and Drug Delivery. *Adv. Colloid Interface Sci.* **2017**, *246*, 13–39.

(38) Ulbrich, K.; Holá, K.; Šubr, V.; Bakandritsos, A.; Tuček, J.; Zbořil, R. Targeted Drug Delivery with Polymers and Magnetic Nanoparticles: Covalent and Noncovalent Approaches, Release Control, and Clinical Studies. *Chem. Rev.* **2016**, *116* (9), 5338–5431.

(39) Song, Q.; Chuan, X.; Chen, B.; He, B.; Zhang, H.; Dai, W.; Wang, X.; Zhang, Q. A Smart Tumor Targeting Peptide–drug Conjugate, pHLIP-SS-DOX: Synthesis and Cellular Uptake on MCF-7 and MCF-7/Adr Cells. *Drug Deliv.* **2016**, *23* (5), 1734–1746.

(40) Gondi, C. S.; Rao, J. S. Cathepsin B as a Cancer Target. *Expert Opin. Ther. Targets* **2013**, *17* (3), 281–291.

(41) Zhong, Y.-J.; Shao, L.-H.; Li, Y. Cathepsin B-Cleavable Doxorubicin Prodrugs for Targeted Cancer Therapy (Review). *Int. J. Oncol.* **2013**, *42* (2), 373–383.

(42) Shiah, J. G.; Dvořák, M.; Kopečková, P.; Sun, Y.; Peterson, C. M.; Kopeček, J. Biodistribution and Antitumour Efficacy of Long-Circulating N-(2-Hydroxypropyl)methacrylamide Copolymer-Doxorubicin Conjugates in Nude Mice. *Eur. J. Cancer* **2001**, *37* (1), 131–139.

(43) Zhong, Y.-J.; Shao, L.-H.; Li, Y. Cathepsin B-Cleavable Doxorubicin Prodrugs for Targeted Cancer Therapy (Review). *Int. J. Oncol.* **2013**, *42* (2), 373–383.

(44) Maniganda, S.; Sankar, V.; Nair, J. B.; Raghu, K. G.; Maiti, K. K. A Lysosome-Targeted Drug Delivery System Based on Sorbitol Backbone towards Efficient Cancer Therapy. *Org. Biomol. Chem.* **2014**, *12* (34), 6564–6569.

(45) Yi, D. K.; Sun, I.; Ryu, J. H.; Koo, H.; Park, C. W.; Youn, I.; Choi, K.; Kwon, I. C.;

Kim, K.; Ahn, C. Matrix Metalloproteinase Sensitive Gold Nanorod for Simultaneous Bioimaging and Photothermal Therapy of Cancer. *Bioconjugate Chem. 2010,* **2010**, *21*, 2173–2177.

(46) Narayanan, N.; Nair, L. V.; Karunakaran, V.; Joseph, M. M.; Nair, J. B.; N, R. A.; Jayasree, R. S.; Maiti, K. K.; Investigation of Apoptotic Events at Molecular Level Induced by SERS Guided Targeted Theranostic Nanoprobe. *Nanoscale* **2016**, *8* (22), 11392–11397.

(47) Elsadek, B.; Graeser, R.; Warnecke, A.; Unger, C.; Saleem, T.; El-Melegy, N.; Madkor, H.; Kratz, F. Optimization of an Albumin-Binding Prodrug of Doxorubicin That Is Cleaved by Prostate-Specific Antigen. *ACS Med. Chem. Lett.* **2010**, *1* (5), 234–238.

(48) Poulton, R.; Caspi, A.; Milne, B. J.; Thomson, W. M.; Taylor, A.; Sears, M. R.; Moffitt, T. E. Prostate Cancer Relevant Antigens and Enzymes for Targeted Drug Delivery. *J Control Release* **2013**, *360* (9346), 1640–1645.

(49) Ramya, A. N.; Joseph, M. M.; Nair, J. B.; Karunakaran, V.; Narayanan, N.; Maiti, K. K. New Insight of Tetraphenylethylene-Based Raman Signatures for Targeted SERS Nanoprobe Construction Toward Prostate Cancer Cell Detection. *ACS Appl. Mater. Interfaces* **2016**, *8* (16), 10220–10225.

(50) Dubowchik, G. M.; Firestone, R. A.; Padilla, L.; Willner, D.; Hofstead, S. J.; Mosure, K.; Knipe, J. O.; Lasch, S. J.; Trail, P. A. Cathepsin B-Labile Dipeptide Linkers for Lysosomal Release of Doxorubicin from Internalizing Immunoconjugates: Model Studies of Enzymatic Drug Release and Antigen-Specific In Vitro Anticancer Activity. *Bioconjug. Chem.* **2002**, *13* (4), 855–869.

(51) Vandooren, J.; Opdenakker, G.; Loadman, P. M.; Dylan, R. Proteases in Cancer Drug Delivery. *Adv. Drug Deliv. Rev.* **2016**, *97*, 144–55.

(52) Kunzmann, A.; Andersson, B.; Thurnherr, T.; Krug, H.; Scheynius, A.; Fadeel, B. Biochimica et Biophysica Acta Toxicology of Engineered Nanomaterials : Focus on Biocompatibility , Biodistribution and Biodegradation ☆. *Biochim. Biophys. Acta J.* **2011**, *1810* (3), 361–373.

(53) Huang, P.; Song, H.; Wang, W.; Sun, Y.; Zhou, J.; Wang, X.; Liu, J.; Liu, J.; Kong, D.; Dong, A. Integrin-Targeted Zwitterionic Polymeric Nanoparticles with Acid-Induced Disassembly Property for Enhanced Drug Accumulation and Release

in Tumor. *Biomacromolecules* **2014**, *15*, 3128–3138.

(54) Tian, J.; Ding, L.; Wang, Q.; Hu, Y.; Jia, L.; Yu, J.; Ju, H. Folate Receptor-Targeted and Cathepsin B - Activatable Nanoprobe for In Situ Therapeutic Monitoring of Photosensitive Cell Death. *Anal Chem* **2015**, *87*, 3841–3848.

(55) Chen, W. H.; Luo, G. F.; Lei, Q.; Jia, H. Z.; Hong, S.; Wang, Q. R.; Zhuo, R. X.; Zhang, X. Z. MMP-2 Responsive Polymeric Micelles for Cancer-Targeted Intracellular Drug Delivery. *Chem. Commun.* **2015**, *51* (3), 465–468.

(56) Ying, M.; Shen, Q.; Liu, Y.; Yan, Z.; Wei, X.; Zhan, C.; Gao, J.; Xie, C.; Yao, B.; Lu, W. Stabilized Heptapeptide A7R for Enhanced Multifunctional Liposome-Based Tumor-Targeted Drug Delivery. *ACS Appl. Mater. Interfaces* **2016**, *8* (21), 13232–13241.

(57) Peng, C.; Lai, P.; Lin, F.; Wu, S. Y.; Shieh, M. Biomaterials Dual Chemotherapy and Photodynamic Therapy in an HT-29 Human Colon Cancer Xenograft Model Using SN-38-Loaded Chlorin-Core Star Block Copolymer Micelles. *Biomaterials* **2009**, *30* (21), 3614–3625.

(58) Gold, H.; Light-, N. N. Exceptionally High Payload of. *ACS Nano* **2010**, *4* (2), 1033–1041.

(59) Biteghe, F. A. N.; Davids, L. M. Journal of Photochemistry & Photobiology , B : Biology A Combination of Photodynamic Therapy and Chemotherapy Displays a Differential Cytotoxic Effect on Human Metastatic Melanoma Cells. *JPB* **2017**, *166*, 18–27.

(60) Liao, J.; Li, W.; Peng, J.; Yang, Q.; Li, H.; Wei, Y.; Zhang, X. T H E R a N O S T I c S Combined Cancer Photothermal-Chemotherapy Based on Doxorubicin / Gold Nanorod-Loaded Polymersomes. *Theranostics* **2015**, *5* (4), 345–356.

(61) Li, Y.; Liu, G.; Ma, J.; Lin, J.; Lin, H.; Su, G.; Chen, D.; Ye, S.; Chen, X.; Zhu, X.; Hou, Z. Chemotherapeutic Drug-Photothermal Agent Co-Self-Assembling Nanoparticles for near-Infrared Fl Uorescence and Photoacoustic Dual-Modal Imaging-Guided Chemo-Photothermal Synergistic Therapy. *J. Control. Release* **2017**, *258*, 95–107.

(62) Maniganda, S.; Sankar, V.; Nair, J. B.; Raghu, K. G.; Maiti, K. K. A Lysosome-Targeted Drug Delivery System Based on Sorbitol Backbone towards Efficient Cancer Therapy. *Org. Biomol. Chem.* **2014**, *12*, 6564–6569.

(63) Fesik, S. W. Promoting apoptosis as a strtegy for cancer drug discovery. *Nat. Rev. Chem.* **2005**, *5*, 876–885.

(64) Pan, L.; He, Q.; Liu, J.; Chen, Y.; Ma, M.; Zhang, L.; Shi, J. Nuclear-Targeted Drug Delivery of TAT Peptide-Conjugated Monodisperse Mesoporous Silica Nanoparticles. *J. Am. Chem. Soc.* **2012**, *134* (13), 5722–5725.

(65) Doane, T. L.; Burda, C. The Unique Role of Nanoparticles in Nanomedicine: Imaging, Drug Delivery and Therapy. *Chem. Soc. Rev.* **2012**, *41* (7), 2885.

(66) Ellinger, B. Y. P. Fluoresence microscopy in biology *Bilogical Rev.* **1940**, *15* (3), 323–347.

(67) Panikkanvalappil, S. R.; Hira, S. M.; Mahmoud, M. A.; El-sayed, M. A. Unraveling the Biomolecular Snapshots of Mitosis in Healthy and Cancer Cells Using Plasmonically-Enhanced Raman Spectroscopy. *J. Am. Chem. Soc.* **2014**, *136*, 15961–15968.

(68) Qu, M.; Mehrmohammadi, M.; Truby, R.; Graf, I.; Homan, K.; Emelianov, S. Photoacoustics Contrast-Enhanced Magneto-Photo-Acoustic Imaging in Vivo Using. *Biochem. Pharmacol.* **2014**, *2* (2), 55–62.

(69) Xie, W.; Schlücker, S. Medical Applications of Surface-Enhanced Raman Scattering. *Phys. Chem. Chem. Phys.* **2013**, *15* (15), 5329–5344.

Chapter 2

Fabrication of Molecular Transporter on a Guanidinium-Poly-(Propylene-Imine) Hybrid Dendron for Efficient Delivery of Doxorubicin into Cancer Cells

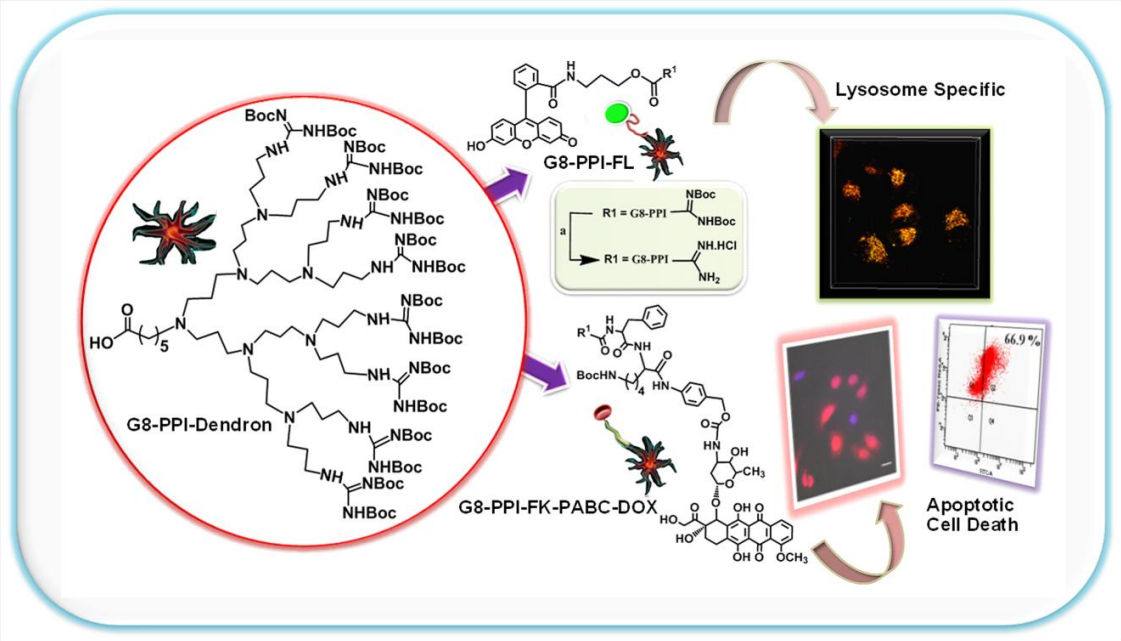

2.1 Abstract: *An efficient synthetic approach has been adopted to construct a new poly (propylene imine) dendron -based octa-guanidine molecular transporter with a lysosomal targeted cathepsin B specific peptide-substrate appended doxorubicin conjugate. The transporter alone (G8-PPI-FL) is found to be non-toxic, showed higher cellular uptake compared to well known cell penetrating peptide, Arg-8-mer and exhibited excellent selectivity towards lysosomes in cathepsin B over expressing HeLa cells, while the Dox-conjugate showed controlled drug release kinetics and significant cytotoxicity in cancer cells without affecting the normal cells.*

2.2 Introduction

Over the last few decades, target specific drug delivery of anticancer drugs has gained huge interest in the pharma industry as in some cases it has been demonstrated to successfully deliver at the right target with the required dose, which minimizes the dose limiting toxicity.[1] Most of the widely used anticancer drugs are highly hydrophobic (poor bioavailability) in nature and exhibit lack of specificity to particular tumor sites, causing severe toxicity to normal tissues and organs.

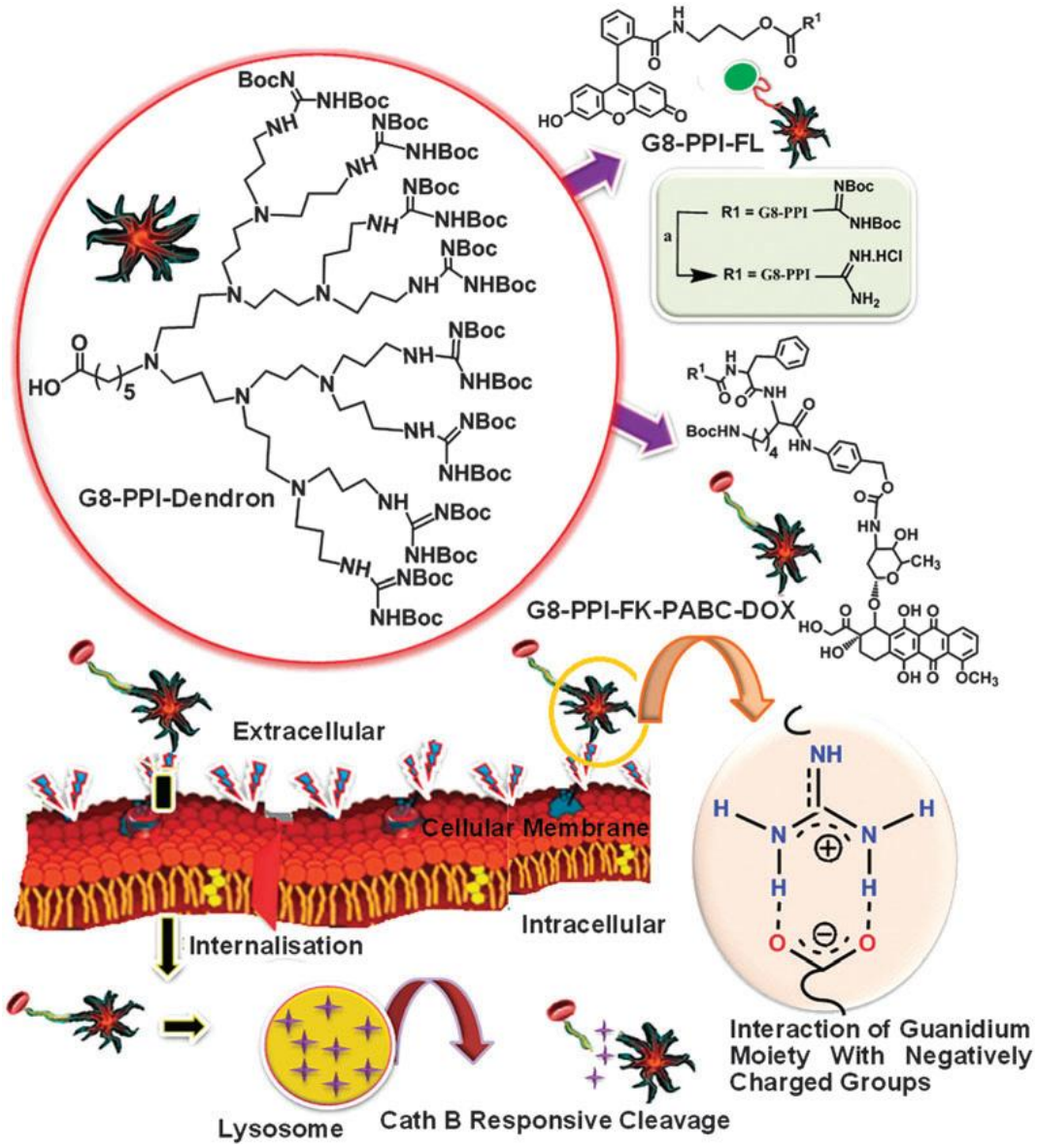

Scheme 2.1: Schematic representation of the drug delivery mechanism by TDDS based on G8-PPI dendron scaffold

It is therefore a challenging task for pharmaceutical and medicinal chemistry researchers to come up with an efficient targeted drug delivery system (TDDS) which selectively ferries the cargo molecule to the diseased cells and tissues in order to achieve the maximum therapeutic effect by possessing minimum pernicious concomitant effects to normal tissues. Encouraged by well-established cell-penetrating peptides (CPPs) like Tat (49–57) and arginine-octamer (Arg-8-mer)[2] that cross biological barriers efficiently, research on molecular transporters is significantly progressing towards TDDS development that is directed towards the delivery to intracellular organelles of diseased cells and tissues.[3] A probable mechanism emphasized that the guanidine group of arginine residues leads to the formation of bi-dentate hydrogen bonds between cell surface phosphates, carboxylates and/or sulphates, which facilitates cellular entry. [3] Therefore, extensive work on guanidine appended synthetic molecular transporters[4–7] has been progressing over the years for the development of new delivery carriers with improved submissive targeting systems that can actively reach the cancer cells after extravasation.[8] Attempts have also been made for improving the pharmacokinetic profiles of poorly bio available drugs.[9–13] Recently, focus on TDDS construction has increasingly considered various cellular proteases as target sites. Among these proteases cathepsin B (Cat B),[14,15] a ubiquitous lysosomal cysteine protease that plays an active role in cancer invasion, which is up-regulated in several malignant tumor cells but is in extremely low concentrations in normal cells. Thus, Cat B is considered as a vital candidate for targeted cancer therapy.

2.3 Present work

We have introduced a new class of synthetic octa-guanidine molecular transporter built on a poly-(propylene imine) dendron starting from aminocaproic acid as the focal point and G8-PPI (Scheme 1) for the target specific delivery of doxorubicin (Dox), which is an anthracycline-based DNA intercalator[16] and is one of the most typical anticancer drugs commonly employed in the clinic.[17]

2.4 Results and discussions

2.4.1 Synthesis of poly (propylene imine) dendron -based octa-guanidine molecular transporter: Targeted Drug Delivery System (TDDS)

The straight forward synthetic construction was initiated with PPI dendron growth by sequential Michael addition of acrylonitrile followed by reduction with RANEYs-Ni. Next, eight units of the free amine terminal were coupled with a Boc-protected guanidine residue affording the G8-PPI skeleton. Finally, fluorescein (FL) was attached via an amino propanol linker to G8-PPI. Similarly, the G8-PPI dendron was further conjugated to a Cat B specific small peptide substrate Phe (F)–Lys(K) for synthetic ease as well as potential systemic stability which was linked by 4-aminobenzyloxy carbonyl (PABC), a self-immolative spacer, bridging with Dox resulting the desired TDDS,

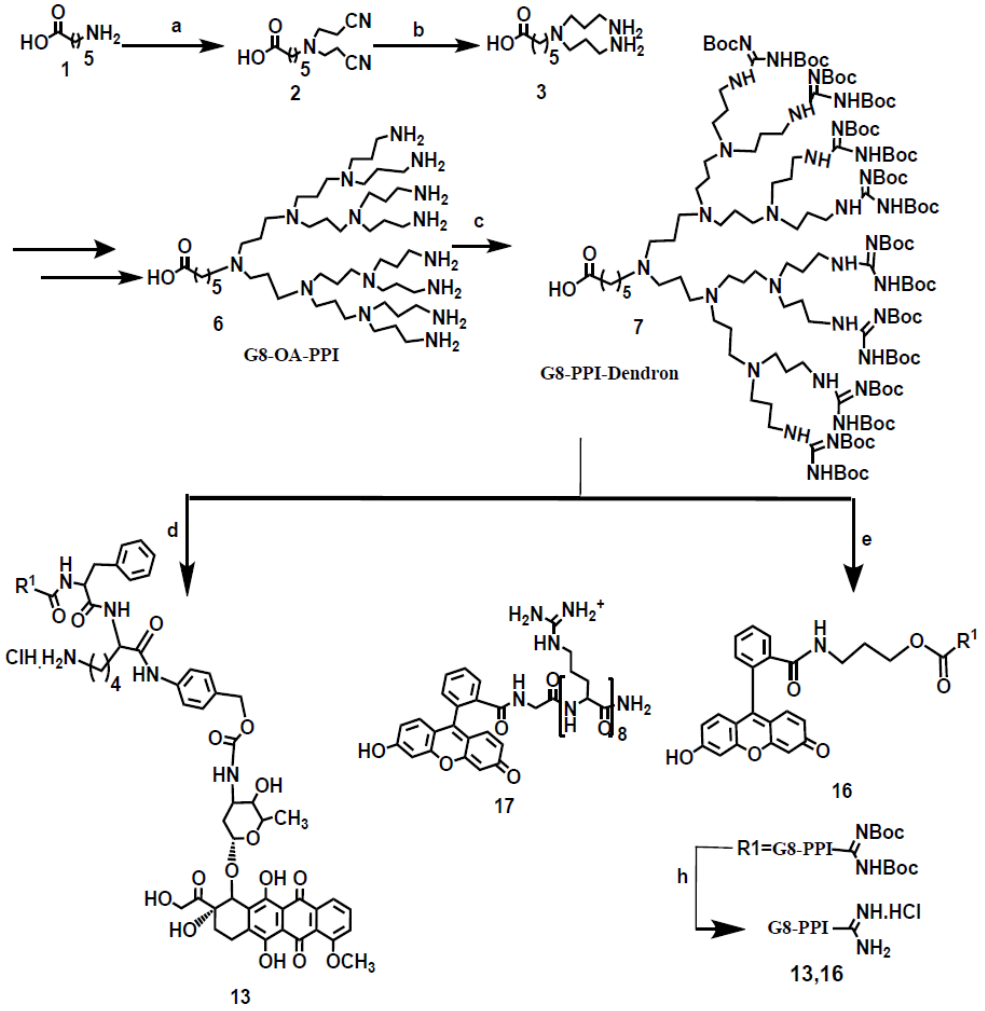

Scheme 2.2: Schematic representation of G8-PPI-FL, G8-PPI-FK-PABC-DOX and (Arg)8-G-FL . Elaborated synthetic procedures: scheme 2, 3, 4, 5 & 6(experimental section) h) HCl (g), EtOAc, RT, 4 h. 17) Control compound prepared by solid phase peptide synthesis.

G8-PPI-FK-PABC-Dox. In this synthetic construction the ratio of drug to carrier was maintained 1:1. A cellular internalization study has been compared with fluorescein labelled arginine- octamer (Arg-8-G-FL) as a standard cell-penetrating peptide obtained by solid phase peptide synthesis (SPPS)[18] using manual coupling of a Rink amide resin. The final target transporter molecules G8-PPI-FL and G8-PPI-FK-PABC-Dox were transformed into HCl salts after removal of the Boc groups on the guanidine moieties by treating with ethyl acetate saturated with HCl gas (Scheme 1). The key intermediates and products, G8-PPI-FL and G8-PPI-FK-PABC-Dox, were characterized by HPLC, NMR spectroscopy and MALDI-TOF mass spectrometry. The stability of the Dox conjugated carrier was checked by HPLC at different time intervals (1, 2 and 4 months) (Figure 2.1d) and the *in vitro* stability was also investigated in PBS buffer (7.4) containing 10% FBS.

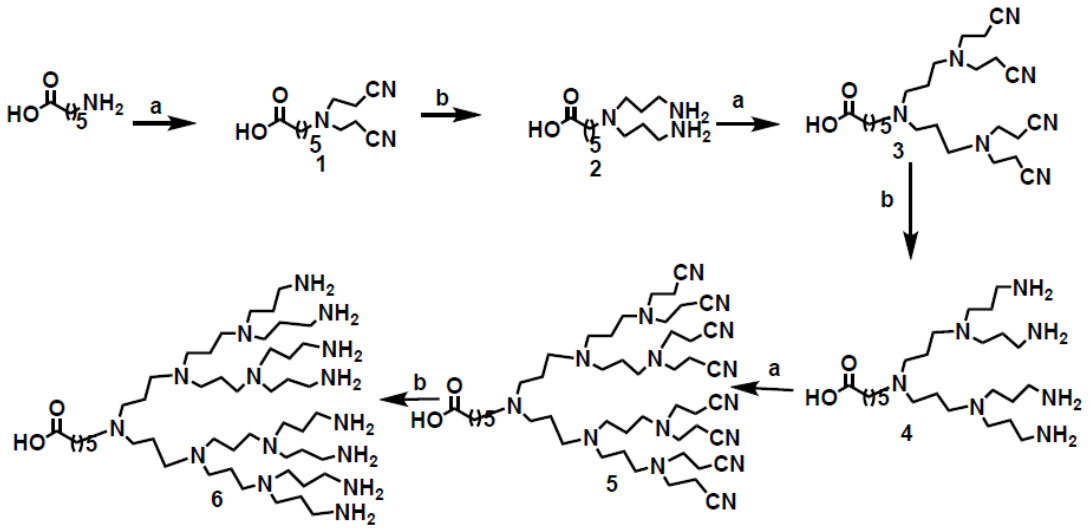

Scheme 2.3: Synthesis of G8-OA –PPI. Reagents and conditions: a) Acrylonitrile, Glc-AcOH, Reflux, 30 h, b) Raney Ni, EtOH, NaOH, 50 Psi, 24 h

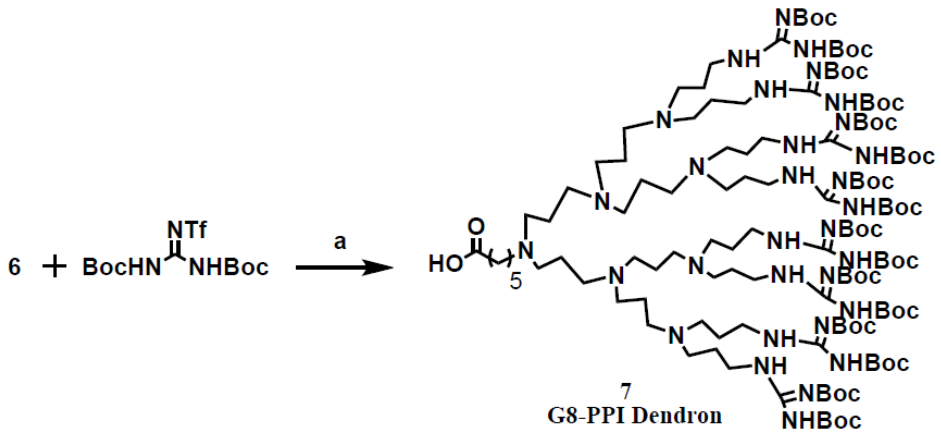

Scheme 2.4: Synthesis of G8-PPI Dendron. Reagents and conditions: a) N, N'-Di Boc -N"-trifluoro methane sufonyl Guanidine TEA in Dioxane /water.

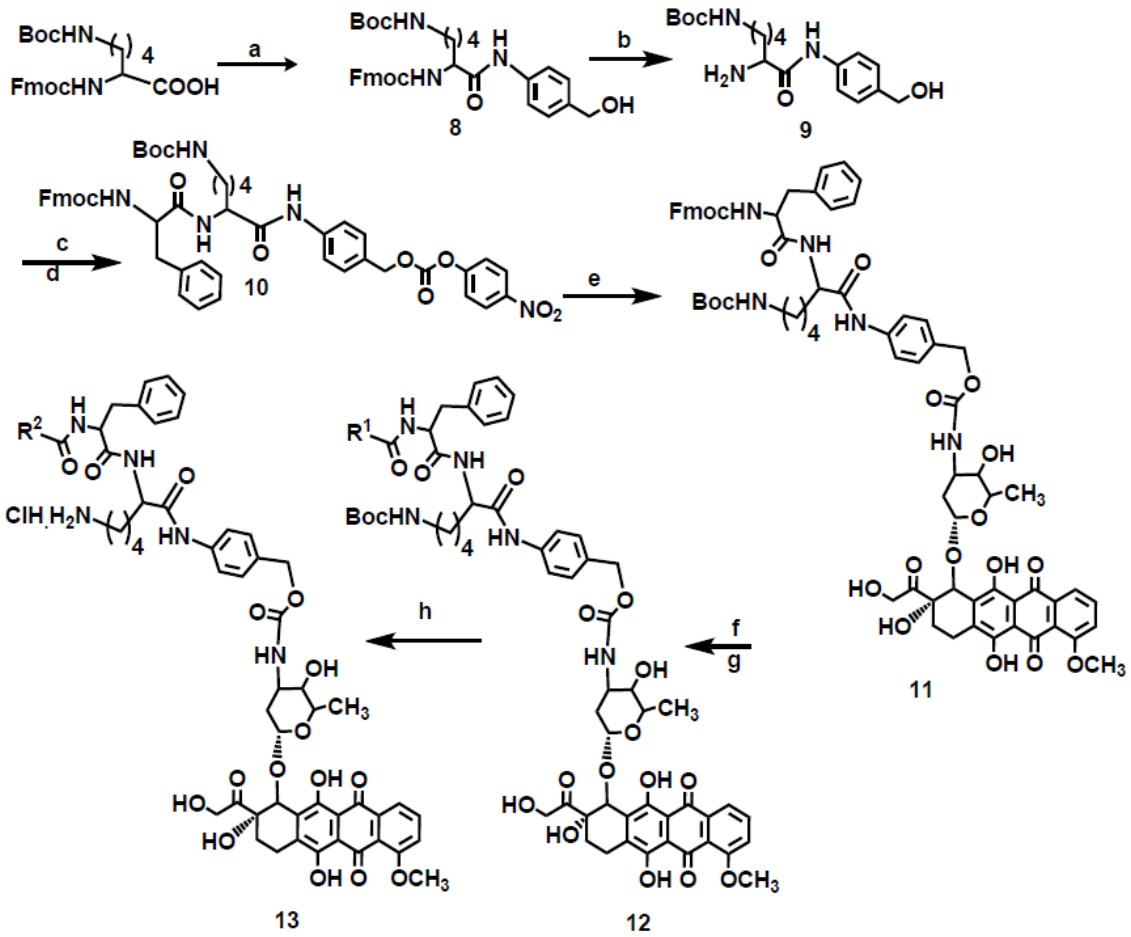

Scheme 2.5: Synthesis of G8-PPI-FK-PABC-Dox. Reagents and conditions: a) PABOH, EEDQ, Dry DCM, RT. b) 20% Piperidine in DMF. c) Fmoc Phe-OH, EDC, NHS, Dry DCM, TEA. d) Bis-PNP, Dry DCM, DIPEA, 0 °C, 48 h. e) Doxorubicin hyrochloride, DIPEA, Dry DMF. f) 20% Piperidine in DMF. g) EDC, HoBt, Dry DMF. h) HCl : EtOAc reagent.

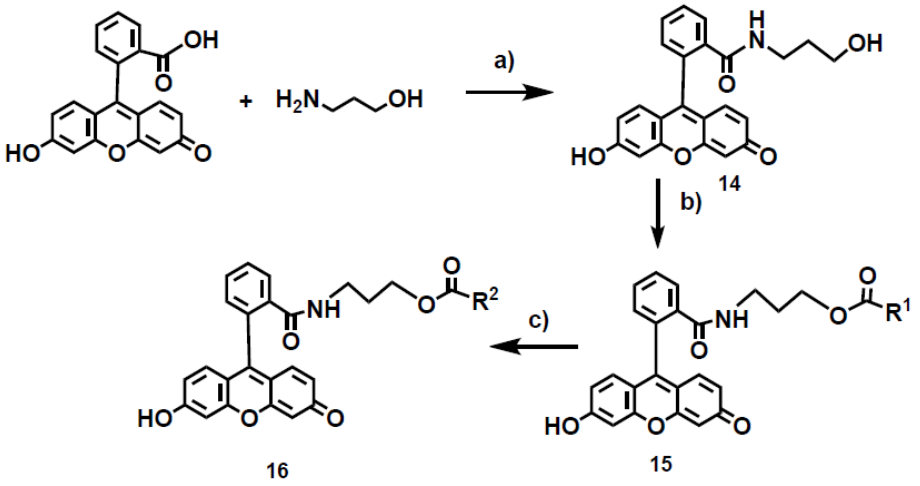

Scheme 2.6: Synthesis of G8-PPI. Reagents and conditions: a) EDC, HoBt, Dry DCM, 24 h. b) EDC, DMAP, Dry DCM, 24 h. c) Ethyl acetate saturated with HCl (g).

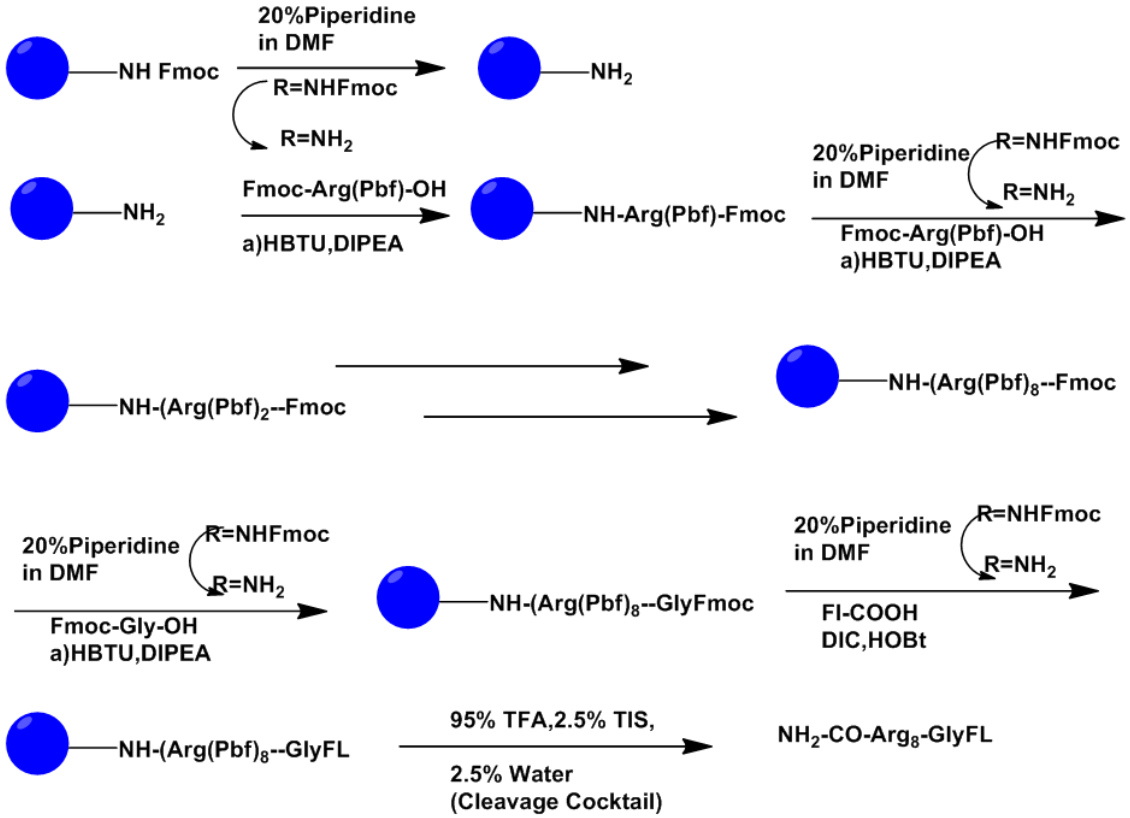

Scheme 2.7: Solid phase peptide synthesis of Arg-8-mer

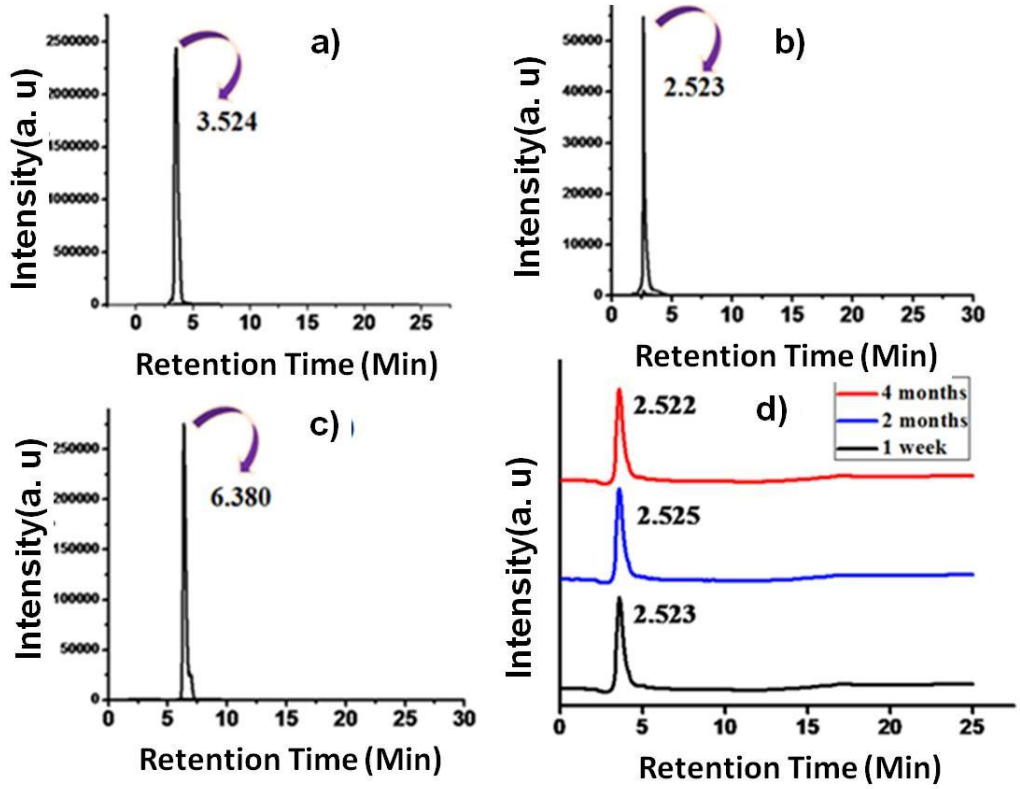

Figure 2.1: HPLC chromatogram of G8-PPI-FL (a), G8-PPI-FK-PABC-DOX (b) and (Arg) 8-G-FL (c), at different period of time stability of G8-PPI-FK-PABC-DOX (d).

2.4.2 Cellular uptake of the TDDS

We initially assessed the cellular uptake efficiency of the synthesized transporter G8-PPI-FL in HeLa cells by flow cytometery analysis and time dependent microscopy. In flow cytometry analysis a suspension of 1–5x10^5 HeLa cells was treated with 2 mM G8-PPI-FL and visually differentiated with Arg-8-G-FL for various time periods (figure 2.2. a-d). After incubation at 37 ^{0}C the cell suspension was washed properly with PBS, re-suspended in a colourless medium and analyzed using a BD LSRF or tessat instrument in FITC channels with emission filters at 530 nm. Flow cytometric analysis indicates that the cellular uptake of G8-PPI-FL increases with the time of incubation as is observed in the green coloured histogram shifted towards higher intensity. The cellular uptake efficiency was further quantified and found to be significantly higher for both G8-PPI-FL and G8-PPI-FK-PABC-Dox compared to Arg-8-G-FL (Figure 2.2e). The cellular uptake of G8-PPI-FL and Arg-8-G-FL in HeLa cells were observed using a fluorescent microscope for various time

periods (such as 60, 120 and 240 min) reveals that the green fluorescence intensity of G8-PPI-FL, increases with time compared to Arg-8-G-FL in HeLa cells (Figure 2.2 f). Therefore, both the flow cytometry analysis and microscopic images indicate that the cellular uptake ability of G8-PPI-FL is significantly higher than that of Arg-8-G-FL.

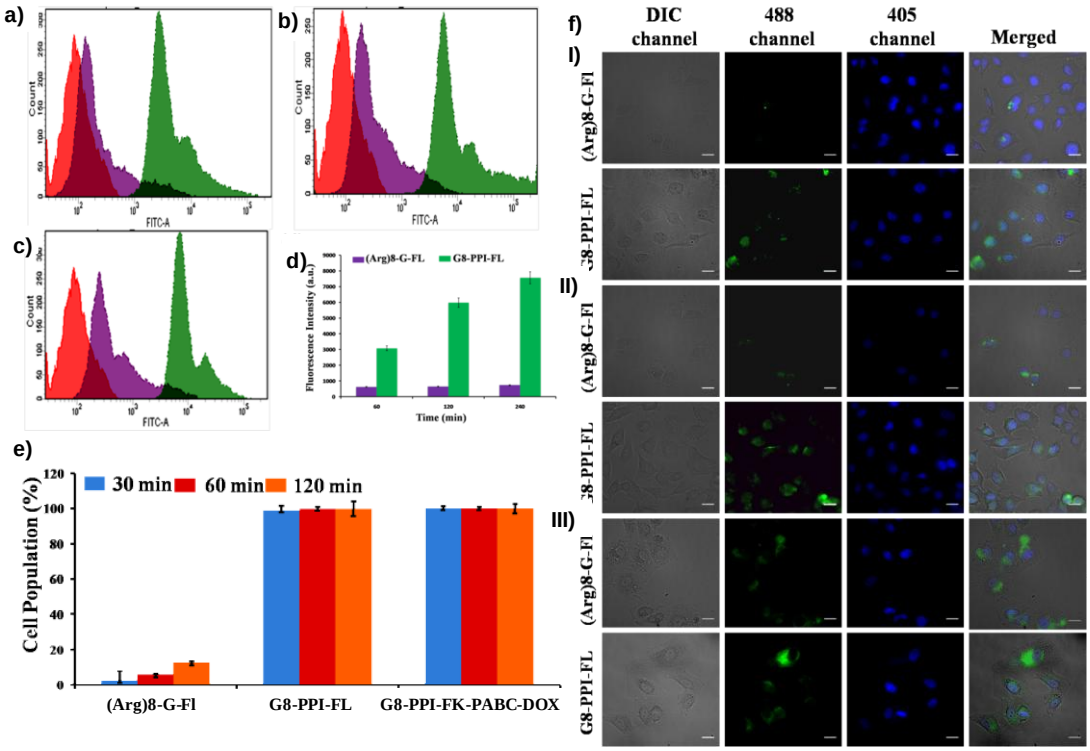

Figure 2.2: (a-c) Flow cytometric analysis of cellular uptake kinetics of G8-PPI-FL (transporter) (shown in green colour histogram) and (Arg)8-G-FL (shown in violet colour histogram) in 60 (a),120 (b), 240 (c) mins. Red graph represents untreated control of HeLa cells. (d) Bar diagram of FACS data reveals kinetics of cellular uptake of G8-PPI-FL and (Arg)8-G-FL. (e) Quantitative plot represents cellular uptake kinetics of HeLa cells after treatment with (Arg)8-G-FL, G8-PPI-FL and G8-PPI-FK-PABC-DOX for 30,60 and 120 min of incubation. Data represents G8-PPI-FL and G8-PPI-FK-PABC-DOX has similar uptake efficiency. (f) Microscopic images reveal cellular uptake kinetics of FITC labled (Arg)8-G-Fl and G8-PPI-FL (transporter) after 60 (I), 120 (II), 240 (III) mins incubation with HeLa cells. Scale bar corresponds to 20 µm.

2.4.3 Co- localization with sub-cellular compartments

Furthermore, we have investigated the intracellular localization of the transporter G8-PPI-FL and compared it with that of Arg-8-G-FL in HeLa cells using intracellular staining dyes such as lysotracker and mitotracker. G8-PPI-FL was found to be highly

co-localized with the lysotracker and the extent of co-localization is much higher than Arg-8-G-FL which reflects the lysosomal selectivity of the G8-PPI-FL carrier, representing a better delivery system than Dox (Figure 2.3). Again, we have evaluated the co-localization potency of G8-PPI-FL and Arg-8-G-FL in mitochondria. From the confocal image (Figure 2.3a) of G8-PPI-FL, we found no significant co-localization with mitotracker. Therefore, the above results clearly indicate that G8-PPI-FL has significant selectivity towards lysosomes of both normal and cancer cells. However, we did not find noticeable localization of G8-PPI-FL in the mitochondria.

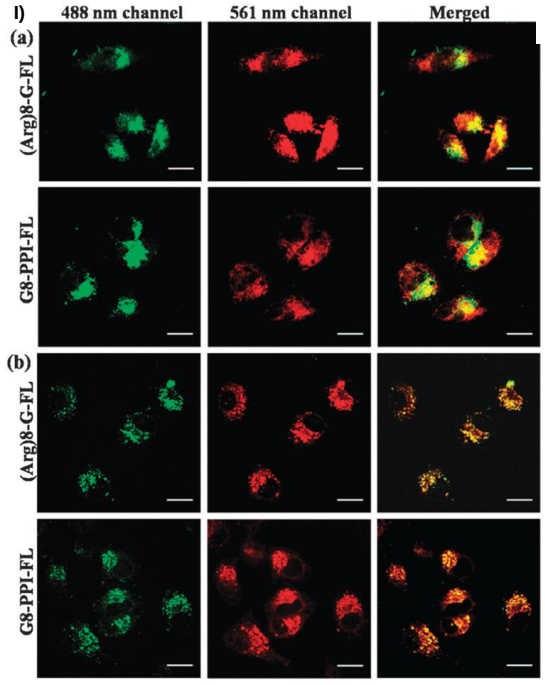

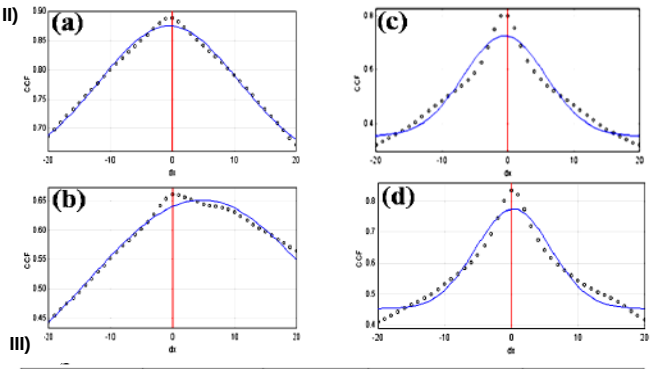

III)

Intracellular organelle	Fluorescently Labelled molecule	Pearson's Coefficient	Cross-correlation function(CCF)		P-value (Costes' method)
			Min. *(dx=-20)	Max. *(dx=0)	
Mitochondria	(Arg)8-G-FL	0.889	0.671	0.889	100%
	G8-PPI-FL	0.661	0.444	0.661	100%
Lysosome	(Arg)8-G-FL	0.801	0.32	0.801	100%
	G8-PPI-FL	0.836	0.41	0.836	100%

*Standard deviation or pixel shift (dx)

Figure 2.3. (I) Co-localization studies by confocal microscopy: the confocal images reveal co-localization of G8-PPI-FL and Arg-8-G-FL (green) with mitotracker (red) (a) and lysotracker (red) (b) in HeLa cells. Scale bar corresponds to 20 mm. (II) Curves (a-d) represents Van Steensel's cross correlation functions (CCFs) for (Arg)8-G-FL co-localization with mitochondria (a) and lysosome (b); G8-PPI-FL co-localization with mitochondria (c) and lysosome (III).Table.1: Pearson's coefficient, CCF and P-value of co-localization analysis represents higher co-localization of G8-PPI-FL with lysosme than the mitochondria in comparision to (Arg)8-G-FL .

2.4.4 Cellular uptake Kinetics

The flow cytometry data reveals that uptake of the Dox-conjugate reached a maximum after 120 min incubation (Figure 2.4a - c). We have also quantified this result and observed that significant release of Dox occurs from the conjugate

compared to free Dox. The microscopic images reveal that the red coloured fluorescence reaches a maximum intensity after 120 min incubation with the G8-PPI-FK-PABC-Dox conjugate compared to free Dox (Figure 2.4 d–f). However, there is significant uptake of the Dox conjugate shown compared to free Dox which starts from 30 min (Figure 2.4d). Moreover, the merged pink colour microscopic images indicate that Dox releases at the lysosome and approached to the nucleus where it binds with DNA (Figure 2.4d–f merged). Therefore, the above results clearly demonstrate that the G8-PPI-FK-PABC-Dox conjugate serves as an efficient drug-conjugate for the delivery of Dox into cervical cancer cell.

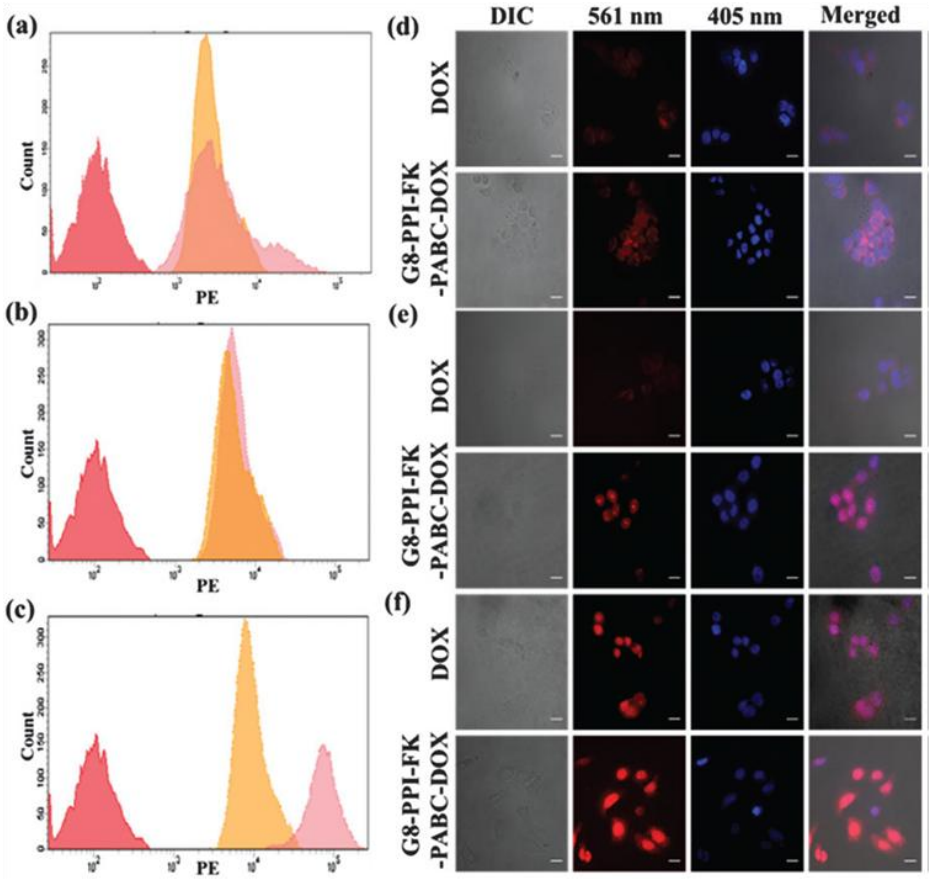

Figure 2.4. Flow cytometric analysis of the intracellular Dox release kinetics of G8-PPI-FK-PABC-Dox (shown in pink colour) and bare Dox (shown in yellow colour) at 30 (a), 60 (b) and 120 min (c). Microscopic analysis of the intracellular Dox release kinetics of G8-PPI-FK-PABC-Dox and bare Dox at 30 (d), 60 (e) and 120 min (f). Scale bar corresponds to 20 mm.

2.4.5 Drug release study

We have further examined the drug release ability of the Dox conjugated carrier by incubating G8-PPI-FK-PABC-Dox in a NaOAc/EDTA buffer with the Cat B enzyme[19] in

the ratio of 9 : 1. Capitalising on the benefits of the intrinsic fluorescence properties of Dox, its cumulative release from G8-PPI-FK-PABC-Dox was judged by fluorescence measurement at 590 nm (Figure 2.5a). Here we observed that above 70% of Dox release occurred in the presence of the enzyme after 28 h as we know that Cat B activity generally occurs in acidic pH which cleaves the specific peptide substrate, subsequently releasing Dox. Furthermore, the stability of the Cat B peptide substrate in the TDDS was evaluated under different pH conditions, which confirmed no significant drug release even at physiological pH (Figure 2.5b).

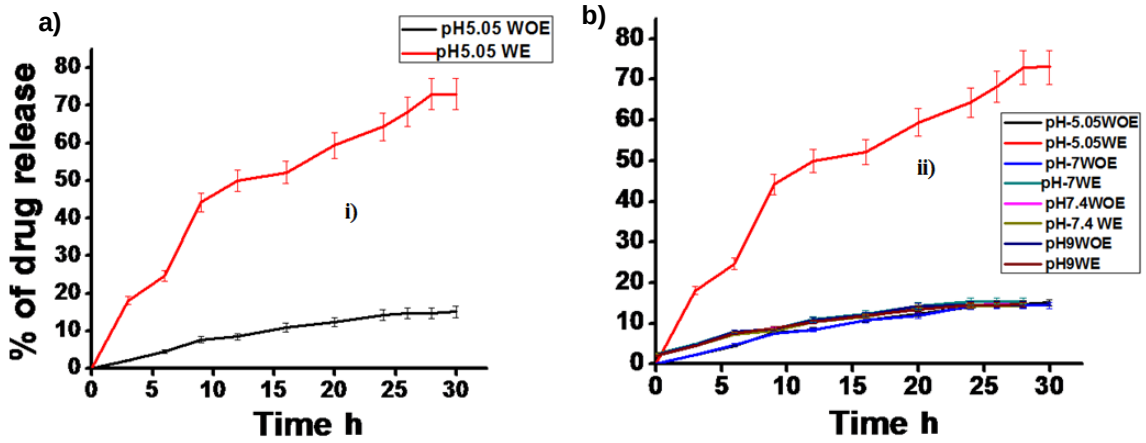

Figure 2.5. a) Line graph showing the release of Dox from G8-PPI-FK-PABC-DOX in the presence of cathepsin B enzyme at pH 5.05. WE denotes with enzyme and WOE denotes without enzyme .b) Drug release at different pH conditions (5.05, 7, 7.4 and 9).

2.4.6 Evaluation of cytotoxicity

Next, we investigated the *in vitro* cytotoxicity profile of the G8-PPI-FK-PABC-Dox conjugate using MTT assay. In this study G8-PPI-FL and free Dox were treated as controls. HeLa and WI-38 cells were incubated with various concentrations (0.5–4 mM) of G8-PPI-FK-PABC-Dox, G8-PPI-FL and free Dox for 24 hours. Interestingly, we found that the novel G8-PPI-FK-PABC-Dox conjugate showed higher cytotoxicity with an IC_{50}

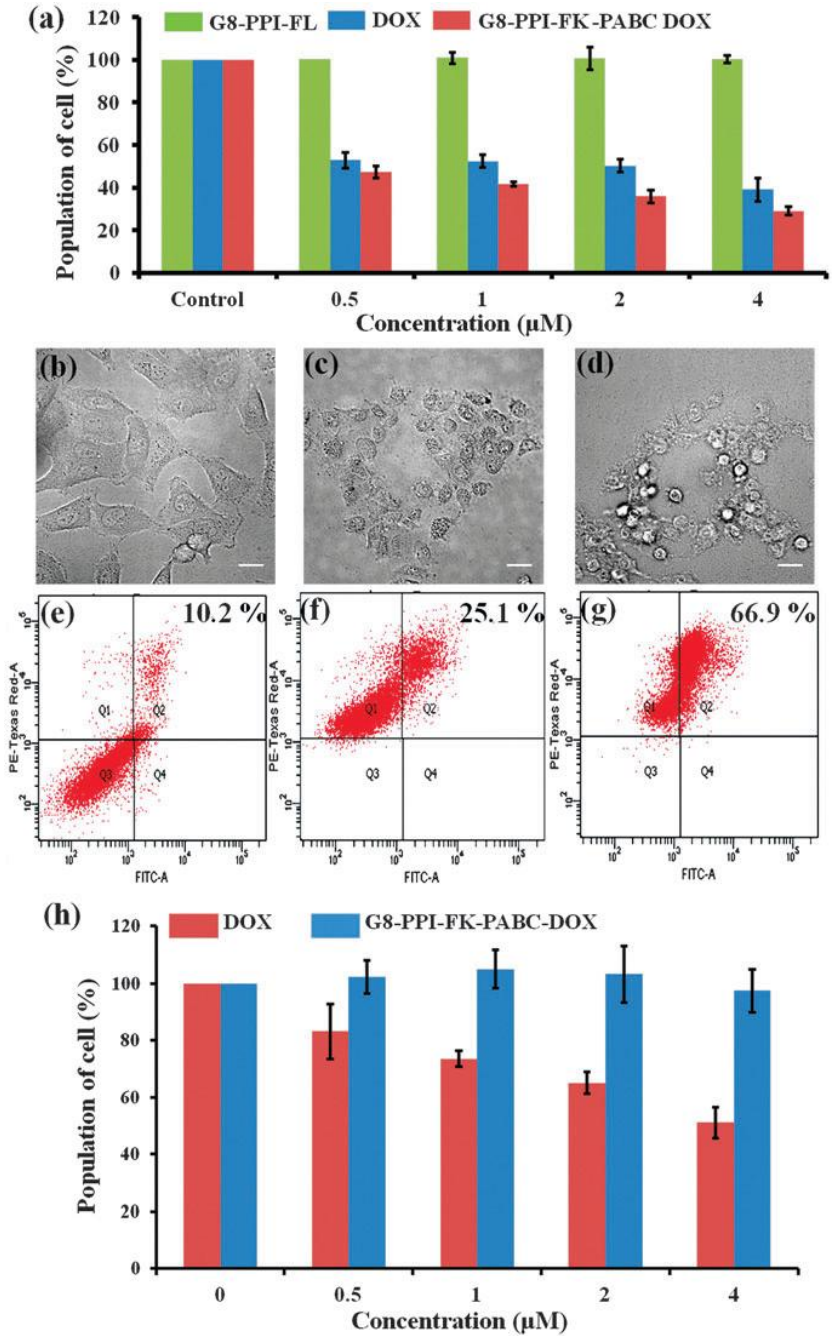

Figure 2.6. Survival of the HeLa cell line was assessed by MTT assay after treatment with G8-PPI-FL (transporter), Dox and G8-PPI-FKPABC- Dox (a). Cellular morphology of the HeLa cells incubated in the absence of each drug (b), after treatment with Dox (c) and after treatment with G8-PPI-FK-PABC-Dox (d). Scale bar corresponds to 20 mm. FACS analysis of the HeLa cells after treatment with annexin V and propidiumiodide: control cells (e), cells treated with 2 mM doxorubicin (f) and cells treated with 2 mMG8-PPI-FK-PABC-Dox (g). The MTT assay indicates that the G8-PPI-FK-PABC-Dox conjugate is non-cytotoxic against non-cancerouscell (WI-38) while free Dox shows significant cytotoxicity (h).

value of 0.40 ± 0.01 mM compared to that of free Dox with an IC_{50} value of 1.15±0.10 mM (Figure 2.6a) and was non-cytotoxic against the noncancerous cell line WI-38 (Figure 2.6h). We did not observe any cytotoxicity after treatment with the transporter G8-PPI-FL alone. Therefore, the above data clearly indicates that the enhanced cytotoxicity arises due to the release of Dox from the conjugate only in the cancer cells. Moreover, we have checked the cellular morphology after treatment with 4 mM of free Dox and the G8-PPI-FK-PABC-Dox conjugate for 4 h using a Nikon Ti-U microscope with a 40X objective in bright field. The morphology of the cells was compared with non-treated cells and we found extensive damage of the cellular morphology in the case of G8-PPI-FKPABC-Dox treated cells compared to the free Dox treated HeLa cells (Figure 2.6b-d).

2.4.6 Apoptotic evaluation

Finally, we investigated the type of cell death using flow cytometry by annexin V and propidium iodide (PI) method.[20] The flow cytometry data clearly indicates a higher proportion of apoptotic death of HeLa cells (66.99%) after treatment with G8-PPI-FK-PABC-Dox conjugate, while a lesser proportion of apoptotic death of HeLa cells (25.1%) occurred after treatment with free Dox (Figure 2.6e-g). This data absolutely supports the conclusion that the Dox conjugate, G8-PPI-FK-PABC-Dox, is more potent compared to free Dox against HeLa cells.

2.5 Conclusion

We have designed and synthesized a poly- (propylene imine) dendron based molecular transporter which showed significantly higher cellular uptake than Arg-8-mer and exhibited excellent selectivity towards lysosomes. Furthermore, we have constructed a TDDS and conjugated Dox through lysosomal targeting of Cat B specific peptide sequence Phe-Lys with a self-immolative linker PABC (G8-PPI-FK-PABC-Dox), which showed target specific cytotoxicity on cancer cells (HeLa) without affecting normal cells (WI-38). G8-PPIFK- PABC-Dox showed an equal uptake efficiency to G8-PPI-FL, enhanced cytotoxicity (IC_{50} value 0.40 ± 0.01 mM) compared to free Dox (IC_{50} value 1.15 ± 0.10 mM) and enhanced apoptotic cell death due to noticeable Dox release as shown by the annexin V and propidium iodide (PI) assay (66.99%).

2.6 Materials and Methods

2.6.1 Chemical synthesis

Unless otherwise indicated, all non-hydrolytic reactions were carried out in oven-dried glasswares under an inert atmosphere of dry argon or nitrogen. Protected amino acids were purchased from Nova bio chem. Doxorubicin Hydrochloride was obtained from Cal biochem, Cathepsin B was acquired from Enzo life science. All the other chemicals and solvents were purchased from sigma Aldrich, Merk, and Specrochem, used without further purification. Analytical TLC was performed on Merck 60 F254 silica gel plate (0.25 mm thickness), and visualization was done with UV light (254 nm and 365 nm), or by spraying with a 5% solution of phosphomolybdic acid or ninhydrine solution followed by charring with a heat gun. Column chromatography was performed on Merck 60 silica gel (60-120 or 100-200 mesh). HPLC was performed by Shimadzu HPLC system consisting of SCL-10Avp system controller, two LC-8A solvent delivery units, SPD-M20A UV-vis photo diode array (PDA) detector, equipped with Multi PDA- LC solution(software) on a 250 mm x 4.6 mm i.d, 5 μm, YMC-Pack R&D ODS analytical column (9YMC Co., Ltd. Japan).NMR spectra were recorded on a Bruker AMX 300 (1HNMR at 300MHz; 13C-NMR at 75 MHz) and Bruker AMX 500 (^{1}H-NMR at 500MHz; ^{13}CNMR at 125 MHz) spectrometers. Tetra methyl silane (TMS) was used as reference for ^{1}H NMR, and the chemical shift were reported in parts per million (ppm) and the coupling constant in Hz. High resolution mass spectra were determined on a HR-EMI analysis of Thermo Scientific Exactive system, and MALDI-TOF mass spectra on Shimadzu Biotech, AXIMA-CFR PLUS system. Liophilization was performed with lyophilizer Tenesis Wizard 2. For biological studies 2-[4-(2-hydroxyethyl) piperazin-1-yl] ethanesulfonic acid (HEPES) was purchased from Himedia. 3-(4, 5-dimethylthiazol-2-yl)-2, 5-diphenyltetrazolium bromide (MTT), dulbecco's modified eagle's medium (DMEM) trypsin-EDTA, dimethylsulfoxide (DMSO) for cell culture solution were purchased from Sigma Aldrich. Penicillin-Streptomycin, neutravidin, alexa fluor 568-carboxylic acid succinimidyl ester and fetal bovine serum (FBS), Mito Tracker red CMX Ros were purchased from Invitrogen. Annexin V and PI apoptosis detection kit were purchased from Santa Cruz Biotechnology. Bisbenzimide H 33258 (hoechst)

was purchased from Calbiochem. Lyso Tracker Deep Red was purchased from Life technologies.

2.6.1.1 Synthesis of compound 1

6-aminohexanoicacid (5g, 0.038mol), glacial acetic acid (43.7 mL, 0.764 mol) and acrylonitrile (188.58 mL, 2.867 mol) were added and kept in oil bath (105˚C), Refluxed for 30 h under N_2 atmosphere, the excess acrylonirile was concentrated under reduced pressure and co-evaporated repeatedly with toluene to remove residual acetic acid. Then the residue was dissolved in ethyl acetate washed several times with water, dried over Na_2SO_4 and concentrated .The crude product was purified by silica gel column chromatography to obtain compound 1 as brownish yellow sticky solid, Yield 84 %. ^{1}H NMR ($CDCl_3$): δ 1.260 (m, 2H), 1.383 (m, 2H), 1.670 (m, 2H), 2.357 (t, J = 5 Hz, 2H), 2.545 (t, J = 6 Hz, 4H), 2.859 ppm (t, J = 4 Hz 6H). HRMS m/z calculated 237.1477, $C_{12}H_{19}N_3O_2$, found 238.2316 $[M+H]^+$.

2.6.1.2 Synthesis of compound 2

To a solution of 1 (9.6 g) in anhydrous ethanol (125 ml) were added 1N NaOH solution 15 ml and approximately 4 g Raney-Ni catalyst. The mixture was hydrogenated in a Parr apparatus at 50 psi for 24 h at room temperature. The catalyst was filtered through celite column and eluted with ethanol. After evaporation of ethanol under rotary evaporator, to yield yellow sticky solid with 82 % yield. ^{1}H NMR (CD_3OD): δ 1.242 (m, 2H), 1.425 (m, 2H), 1.654 (m, 4H), 2.390 (m, 2H), 2.522 (m, 2H), 2.666 (t, J = 7.2Hz, 4H), 3.330 (m, 4H), 3.460 (t, J = 7.5 Hz, 2H). HRMS m/z calculated 245.2103, $C_{12}H_{27}N_3O_2$ found 246.3412 $[M+H]^+$.

2.6.1.3 Synthesis of compound 3

^{1}H NMR ($CDCl_3$): δ 1.384 (m, 2H), 1.397 (m, 2H), 1.646 (m, 4H), 2.319 (t, 6.5 Hz, 10H), 2.531 (t, J = 7 Hz ,8H), 2.640 (t, J = 5.5 Hz, 4H), 2.714 (t, J = 6.5 Hz, 4H), 3.212 ppm (t, J = 7.5 Hz, 6H); Yield=78%, HRMS m/z calculated, $C_{24}H_{39}N_7O_2$, 457.3165, found 458.5634 $[M+H]^+$ as sticky solid.

2.6.1.4 Synthesis of compound 4

^{1}H NMR (CD_3OD): δ 1.12 (m, 2H), 1.337 (m, 2H), 1.526 (m, 2H), 1.673 (m, 6H), 2.190 (t, J = 7.5 Hz, 2H,), 2.489 (t, J = 7.5 Hz, 20H), 2.676 (t, J = 6.5 Hz, 10H), 5.115 (br. s,

8H); Yield= 84%, HRMS m/z calculated: $C_{24}H_{55}N_7O_2$, 473.4417, found 474.8978 $[M+H]^+$as yellow solid.

2.6.1.5 Synthesis of compound 5

^{1}H NMR ($CDCl_3$): δ 1.228 (m, 2H), 1.434 (m, 2H) , 1.649 (m, 2H) ,1.540 (m, 12H) 1.873 (m, 12H) , 2.326 (t, J = 6 Hz, 2H), 2.525 (t, J = 6.5 Hz, 10H), 2.538 (t, J = 7.5 Hz, 8H), 2.813 (t, J = 6.5 Hz, 8H), 3.414 (m, 4H), 3.552 (m, 4H) , 3.655 (m, 4H) , 3.751 (m, 4H) **.** Yield=78%**,** HRMS m/z calculated: $C_{48}H_{79}N_{15}O_2$, 898.6541 found 899.7802 $[M+H]^+$as yellow sticky solid.

2.6.1.6 Synthesis of compound 6 (G8-OA-PPI)

Yellow sticky solid, **^{1}H NMR (CD_3OD):** δ 1.075-1.641 (m, 28H), 2.478 (m, 40H), 2.585 (m, 16H), 2.722,-2.819 (m, 20H); Yield 74%; HRMS m/z calculated $C_{48}H_{111}N_{15}O_2$, 929.9045, found 953.0321 $[M+Na]^+$.

2.6.1.7 Synthesis of compound 7

To a solution of 6 (176 mg, 0.19 x 10^{-3} mol) in 10 ml of water ,1N HCl solution was added drop wise to a neutral pH .To this solution dioxane were added (40 mL) and then N, N di Boc-N-tri fluorometane sulfonyl guanidine (600 mg, 1.5 x10^{-3} mol) and triethylamine (0.13 ml, 0.95 x 10^{-3} mol). After stirring for 72 h at RT, the reaction mixture was evaporated and residue was diluted with Ethyl acetate, water and brine. The organic layer was dried over Na_2SO_4 and concentrated. Yield 67%; **^{1}H NMR ($CDCl_3$):** δ 1.187 (m, 8H), 1.370 (m, 4H), 1.431 (s, 144H),1.523 (m, 10H), 2.489 (m, 20H), 2.537 (m, 16H), 3.088 (m, 16H), 3.349 (m, 8H), 3.506 (m, 2H), 3.564 (m, 6H), 3.656 (m, 4H, 8.0 (br. s, 8H). MALDI –TOF –MS m/z calculated $C_{136}H_{255}N_{31}O_{34}$, 2867.9211 found 2869.9601 $[M+H]^+$,light yellow solid.

2.6.1.8 Synthesis of G8-PPI –FK-PABC-DOX

2.6.1.8 .1 Synthesis of compound 8-13

Fmoc-Lys (Boc) OH (1g, 0.0078 mol) and N- Ethoxy carbonyl 1- 2- ethoxy - 1, 2 dihydroquinoline (EEDQ) (1.9 g, 0.0078 mol) was dissolved in anhydrous dichloromethane (100 mL). After stirring for few minutes at room temperature 4-amino bezyl alcohol (PAB-OH) (0.96 g, 0.0078 mol) was added and stirring was continued for 24 h. Completion of the reaction was monitored by TLC and DCM was evaporated under rotary evaporator and residue was purified on silica with $CHCl_3$:

MeOH) 0.5% to afford **8** as white powder. HRMS m/z calculated $C_{33}H_{39}N_3O_6$, 573.6832 found 578.7643 $[M+H]^+$. **8** (1.2g) was treated with a solution of 20% piperidine in DMF (5 mL) and reaction was stirred for 10- 15 min at room temperature . The product was precipitated with di-ethyl ether (150 mL) and washed with the same and dried over vacuum pump to afford **9** yield 83% as yellow powder. HRMS m/z calculated $C_{18}H_{29}N_3O_4$, 351.2234, found 352.2342 $[M+H]^+$. In the next step Fmoc-Phe OH (1.14 g, 2.96 mol) and N Hydroxy succinimide (NHS) (0.34 g, 2.96 mol) were dissolved in anhydrous DCM (50 mL) stirred at 0 ^{0}C for 5 min, then EDC was added in to it and stirred for 16 h and precipitate was filtered off. **9** (0.7 g, 2.96 mol) and triethyl amine TEA (0.22 mL, 2.96 mol) was added to the filtrate stirred for 4 hr. The volatiles were removed under reduced pressure and purified by silica. To a solution of the above (1.6 g, 2.28 mol) and 4 Nitro phenyl chloroformate (1.8 g, 9.12 mol) in anhydrous DCM 30 mL, N, N' di isopropyl ethyl amine (0.9 mL, 6.84 mol) was added at 0 ^{0}C and reaction was stirred for 48 hr, the volatiles were removed under reduced pressure and Purified by silica afforded 10. HRMS m/z calculated $C_{49}H_{51}N_5O_{11}$ 885.36, found 886.45 $[M+H]^+$. **^{1}H NMR ($CDCl_3$):** δ 1.25 (m, 2H), 1.43 (s, 9H), 1.518, (m, 2H), 1.90 (m, 2H), 3.125 (d, 2H), 3.266 (t, J=4.75 Hz, 1H), 4.709 (d. J=7.32 Hz, 2H), 4.692 (t, J=6.56 Hz, 1H), 5.075 (t, J=4.78 Hz, 1H), 5.103 (s, 2H), 7.16-7.71 (m, 23H), 8.03 (br. s, 4H). To a solution of **10** (5 mg, 5.6 x 10^{-6} mol) in anhydrous DMF (2 mL) Doxorubicin Hydrochloride (3.3 mg, 5.6 x 10^{-6} mol) and DIPEA (7 µL) were added and the reaction was stirred for 48 hr to yield Fmoc- Phe-Lys- PABC – DOX, **11** as red sticky solid. MALDI-TOF MS m/z calculated $C_{70}H_{75}N_5O_{19}$ 1290.3723 found 1313.8945 $[M+Na]^+$ **11** was treated with 20% piperidine in DMF and stirred for 30 min at room temperature and precipitated with diethyl ether and dried under vacuum . A solution of 11 in dry DCM , EDC (2 mg, 1.123 x 10^{-5} mol) were added under N_2 atmosphere and was stirred for 10 minutes and already prepared G8-PPI (16 mg, 6.72 x 10^{-6} mol) was added and stirred for 24 h the product was concentrated in rotary evaporator and purified by silica gel column chromatography to afforded **12**. Yield=70%, MALDI-TOF MS m/z calculated $C_{191}H_{318}N_{36}O_{50}$ 3918.78, found 3919.56 [M+H]+. Finally all the Boc deprotections were carried out using saturated HCl (g) - Ethyl acetate solution at room temperature. After 4 hr stirring the solution was concentrated and residue was washed with ethyl acetate and dried over vacuum pump. The residue was purified

by supelclean LC - 18 reverse phase silica gel, Sigma Aldrich. The purified product was dissolved in de-ionized water filtered through PTGE syringe filter (0.450 μm) and checks purity by HPLC and lyophilized to give final product **13** as brown sticky solid. Yield= 68%, MALDI-TOF MS m/z calculated $C_{106}H_{182}N_{36}O_{16}$, 2216.8102, found 2239.4512. $[M+Na]^+$. **^{1}H NMR (CD_3OD):** δ. 1.285 (m, 12H), 1.413 (m, 2H), 1.569 (m, 17H), 1.661 (m, 13H), 2.441-2.878 (m, 64H), 3.27-3.36 (m, 10H), 4.35-4.50 (m, 15H), 5.029 (s, 2H), 7.038-7.825 (m, 12H), 8.034 (br, s, 8H).

2.6.1.9 Synthesis of G8-PPI –FL

Fluorecein (221 mg, 1.5 x 10^{-4} mol) in DMF were activated with EDC (230 mg, 3 x 10^{-4} mol), HOBt (162 mg, 3 x 10^{-4} mol) for 2 mins then amino propanol (50 mg, 1.5 x 10^{-4}) was added, stirred under nitrogen atmosphere for 36 h. Completion of the reaction was monitored by TLC and purified by silica gel column chromatography to yield **14**, yield=85%**. 14** (26 mg, 6.8 x 10^{-5} mol) were coupled with G8-PPI (11 mg,5.2 x 10^{-5} mol) in presence of EDC (19 mg, 10.4 x 10^{-5} mol), DMAP (1 mg, 10 mol%) to yield **15, ^{1}H NMR ($CDCl_3$):** δ 1.25 (m, 4H), 1.439 (s, 144H), 1.344 (2H, m), 1.72 (m, 2H), 1.657 (2H, m), 1.539 (m, 12H), 2.41 (t, J=7.85 Hz, 40H), 2.227 (t, 2H), 3.041 (t, J=5.66 Hz, 2H), 3.611 (t, J=5.67 Hz, 2H), 2.953 (t, J=4.55 Hz, 16H), 6.532-7.711 (m, 10H), 8.22 (s, 8H). MALDI-TOF MS m/z calculated $C_{158}H_{270}N_{32}O_{38}$ 3225.25 found 3326.34 $[M+H]^+$. Finally all the Boc protected groups were removed using saturated HCl (g) Ethyl acetate solution at room temperature. After 4 hr stirring, the solution was concentrated and residue was washed with ethyl acetate and dried over vacuum pump. The residue was purified by supelclean LC -18 reverse phase silica gel. The purified product was dissolved in de-ionized water filtered through PTGE syringe filter (0.450 μ) and checked the purity by HPLC and lyophilized to give final product **16** as yellow solid. **^{1}H NMR (CD_3OD):** δ 1.286 (m, 4H), 1.3224 (m, 4H), 1.563 (m, 6H), 1.4535 (m, 6H), 1.574 (m, 10H), 1.721 (m, 8H), 1.821 (m, 8H), 2.176 (m, 2H), 2.656 (m, 26H), 2.75 3(m, 8H), 2.922 (m, 12H), 3.045 (m, 2H), 3.161-3.826 (m, 6H), 4.11 (m, 4H), 6.404-7.934 (m, 10H), 8.157 (s, 8H). MALDI –TOF –MS m/z calculated $C_{78}H_{142}N_{32}O_6$, 1624.1729 found 1625.9403 $[M+H]^+$, Yield 65%.

2.6.1.9 Synthesis of (Arg)8-G-FL by solid phase peptide synthesis

Synthesis of amide terminal (Arg) 8-G-FL started with deprotecting Fmoc group of Rink amide resin using 20% piperidine in DMF for 20 minutes. Then the resin was washed with DMF (3 x 3 mL), Fmoc- Arg (pbf) OH (276 mg, 4.2 x 10^{-4} mol.) dissolved in DMF along with activating agent(2-(1H-benzotriazol-1-yl)-1,1,3,3-tetramethyluronium hexafluorophosphate(HBTU) (161 mg, 4.2 x 10-4 mol) and 2- 3 drops of DIPEA charged to the resin bed. The reaction was continued for 8 hwith shaking, progress of the reaction was monitored by the Kaiser test. After completion of the coupling, the resin was washed with DMF (3 x 3 mL), and the Fmoc protection group was removed by treatment with piperidine in DMF (20%, 3 x 2 mL, 3 x 15 min). The reaction cycle was continued in a similar manner again seven times with Fmoc Arg (pbf) OH and Fmoc-Gly-OH (126 mg, , 4.2 x 10^{-4} mol). Finally fluorecein free acid (20 mg, 8.52 x 10^{-5} mol) activated with DIC (10 mg, 8.52 x 10-5 mol) and HoBt (11 mg, 8.52 x 10^{-5} mol) was added to the resin and shaken for overnight. Peptide was released from the resin bed by treatment with the most common cleavage cocktails that is, 95% trifluoro acetic acid, 2.5% triisopropyl silane, 2.5% water. The resin washing was combined and concentrated under reduced pressure, and the residue was co evaporated with toluene and precipitated with cold ether (3 mL) and filtered the residue peptide that afforded as shiny yellow solid. MALDI–TOF–MS m/z calculated $C_{70}H_{112}N_{34}O_{13}$, 1645.8583 found 1646.9023 $[M+H]^+$.

2.6.1.10 *In Vitro* drug release kinetics

Detailed studies were carried out by checking the Dox release from Dox-conjugated carrier. At first we incubated 0.05 mM G8-PPI-FK-PABC-DOX in NaOAc /EDTA buffer (with 50 mM NaOAc and 1 mM EDTA, pH=5.05) with Cat B enzyme (62.5 ng/µL) in the ratio of 9:1. Captivating the benefit of the intrinsic fluorescent property of Dox, its cumulative release from G8-PPI-FK-PABC-Dox as judged by fluorescence measurement at 590 nm. Dox release generally occurred in the presence of lysosomal cysteine protease, Cat B in acidic pH. The protease cleaves the specific peptide substrate, subsequently releasing Dox. The result indicated that the above 70% of Dox release occurred in the presence of enzyme after 28 h. Furthermore, stability of the Cat B peptide substrate in TDDS was evaluated at different pH conditions, which confirmed no significant drug release even at physiological pH. A

blank was carried out without Cat B enzyme, using 100 µL of G8-PPI-FK-PABC-DOX buffer solution. All measurements were carried out at different pH conditions (5.05, 7, 7.4 and 9) at specific time intervals from 0 to 30 h. Fluorescence was measured at different time intervals using BioTec Synergy 4 spectrophotometer at 590 nm, which has been reflected as % drug release (plotted in Y- axis) as shown in figure 2.4.

2.6.1.11 *In Vitro* stability

To evaluate the stability of G8-PPI-FK-PABC –DOX in blood circulation, we have dispersed the TDDS in PBS (pH=7.4) containing fetal bovine serum (FBS) and incubated at 37 °C. and checked HPLC at different intervals of time. The result indicates that there is no significant drug degradation providing possibility of enhancing drug accumulation in tumor tissue.

2.6.2 Cell and Cell Culture

Human cervical cancer cell line, HeLa (adenocarcinoma) and human lung fibroblast normal cell line WI-38 has been obtained from National Centre for Cell Science (NCCS) Pune, India. Cells are cultured on 25 cm^2 tissue culture flask in Dulbecco's modified eagle's medium (DMEM) containing 10% fetal bovine serum(FBS), kanamycin sulfate (110 mg/L), penicillin (50 units/mL), streptomycin (50 µg/mL) at 37 °C in the sterile condition of 5% CO_2 incubator with humidified atmosphere. Cells are exponentially cultured as monolayer up to 70-80% confluence. After optimal growth cells were detached using trypsin-EDTA (1X). All the cell culture work has been performed under sterile condition

2.6.2.1 Flow cytometric detection of cellular uptake and kinetics

To analyze the transporter G8-PPI-FL, cellular uptake kinetics was studied using flow cytometer. 1-5 × 10^5 density of cells were detached using trypsin and re-suspended in 200 µL cell culture serum free media containing G8-PPI-FL and (Arg) 8-G-FL at the concentration 2 µM for different time periods up to 4 hr mentioned in figure legend. After incubation at 37 °C cells suspension was diluted with 2 mL of PBS and centrifuged at 800 × g. The cell pellet was washed twice with PBS by centrifugation and resuspended in 500 µL of serum free media. Fluorescence analysis was performed with BD LSRFORTESA using FITC channels and emission filters at 530 nm. In order to characterize the drug (DOX) delivery efficiency of G8-

PPI-FK-PABC-DOX, cellular uptake kinetics of DOX was analyzed with respect to free drug DOX. We have followed above mentioned treatment protocol for G8-PPI-FK-PABC-DOX and DOX at the concentration 4 μM. After incubation for different time up to 120 min (mentioned in figure legend) cell suspension was washed twice with PBS. Fluorescence analysis was performed with BD LSRFORTESA using PE channels and emission filters at 561 nm.

2.6.2.2 Detection of cellular uptake and kinetics using fluorescent microscope

For qualitative analysis and localization of fluorescence tagged G8-PPI-FL and (Arg)8-G FL in HeLa cells, exponentially growing cells were seeded and harvested onto a cover glass bottom dish at an density of about 3000-5000 cells per dish. Then cells were either incubated with G8-PPI-FL or (Arg)8-G-FL for different time period up to 4h (mentioned in figure legends) in serum free media. Cell DNA was stained with Hoechst 33258 (1 μg/mL). Cells were washed by PBS and live cell imaging was carried out after different time using a Nikon Ti-U microscope on 37 $^{\circ}$C stage with a 40 X objective in 405 and 488 nm channel for FITC and Hoechst 33258 respectively and DIC mode for bright field. For analysis of DOX release from G8-PPI-FK-PABC-DOX conjugate in HeLa cells, similar protocol of kinetics study has been used as described above. Here, treatment of G8-PPI-FKPABC-DOX was carried out in serum free medium to 3000-5000 cells, already harvested in cover glass bottom dish. Bare DOX also treated in parallel experiment in similar way as G8- PPI-FK-PABC-DOX. After the incubation for different time period up to 120 min cells were washed. Nucleus was stained with Hoechst 33258. To visualize the cellular release, auto florescence of DOX was analyzed using Nikon Ti-U microscope after different time with a 40 X objective in 561 nm channel. Nuclear stain was analyzed by 405 nm channel.

2.6.2.3 Confocal analysis of cellular localization of G8-PPI-FL and (Arg)8-G-FL

To understand the mechanism of release of drug using G8-PPI-FL transporter containing cathepsin substrate, sub-cellular localization of this transporter need to be analyzed. HeLa cells and WI-38 at a density of 3000 were seeded on cover glass bottom dish for 24 hr followed by incubation with either in absence (negative control) or presence of fluorescence labeled G8-PPI-FL and (Arg)8-G-FL for 2 hr in serum free medium. After a single wash with serum free media live cells were

treated with either mitotracker or lysotraker at the concentration of 100 μM or Hoechst for 1 hr. Cell imaging was carried out using and or spinning disc confocal microscope using 60 X objective (Olympus) and an Andor iXon3 897 EMCCD camera in 488 and 561 nm wavelength lasers light.

2.6.2.4 Cell Viability assay

To analyze percentage of cell death MTT assay was performed after drugs treatments. 10000 cells were seeded onto 96 well tissue culture plates in sterile conditions. After harvesting for overnight cells were incubated for 24 hr in the absence or presence of 4 different concentrations (4 μM, 2 μM, 1 μM and 0.5 μM) of G8-PPI-FL (transporter), DOX and G8-PPI-FK-PABC-DOX. Treated cells were incubated for 4 hr in presence of MTT solution prepared from 5 mg/mL of 3-(4, 5-dimethylthiazol-2-yl)-2, 5 diphenyltetrazolium bromide in PBS. 1:1 (v/v) DMSO/MeOH was used as MTT solvent and cell population was analyzed by observing absorbance at 550 nm using microplate ELISA reader. Data analysis was performed using following formula:

% of Viable cells = $[(A550^{TC} - A550^{B})/(A550^{UC} - A550^{B})] \times 100$

(TC-Treated cells, B-Background, UC-untreated cells)

2.6.2.5 Analysis of cellular morphology

To study cellular morphology 3000 cells were seeded overnight onto a cover glass bottom dish. Then cells were incubated for 4 hr in absence and presence of 4 μM of DOX and G8-PPI-FK-PABC-DOX. After washing with fresh media, cells were incubated in colorless media for microscopic imaging. Live cells imaging was carried out using a Nikon Ti-U microscope with a 40 X objective in bright field mode at 37 $^{\circ}$C.

2.6.2.6 Detection of cellular death by flow cytometer

Cell death was analyzed by flow cytometer using annexin V and PI method. 1-5 × 10^5 density of HeLa cells were harvested on a 6 well plate for 24-48 h. Cells were first incubated with 2 μM of DOX and G8-PPI-FK-PABC-DOX for 24 h under sterile condition. After treatment, media containing drug was washed twice with PBS. Then cells were detached using trypsin-EDTA (1X) and washed once with 10% FBS containing DMEM. Cells pellet was resuspended in a 1X assay buffer (Santa Cruz Biotechnology). 5-6 ×106 cells in 100 μL assay buffer were incubated for 15-20 min

with 2.5 µL of Propidium iodide (PI) (stock conc. of 50 µg/mL) and annexin V (stock conc. of 200 µg/mL). Before analysis 400 µL of assay buffer has been added to make total volume of 500 µL of cell suspension. Flow cytometer analysis was carried out with respect to FITC fluorescence from annexin V-FITC and PI auto fluorescence intensity using FITC and PI channels of BD LSRFORTESA flow cytometer with emission filters at 530 and 610 nm respectively. To differentiate fluorescence and background noise both annexin V-FITC and PI positive and negative cells were analyzed. The untreated both positive controls were used to characterize the normal cells population.

2.6.2.7 Data analysis All the images were analyzed using Image J software.

2.7 References

(1) Sun, T.; Zhang, Y. S.; Pang, B.; Hyun, D. C.; Yang, M.; Xia, Y. Engineered Nanoparticles for Drug Delivery in Cancer Therapy. *Angew. Chemie Int. Ed.* **2014**, *53* (46), 12320–12364.

(2) Goun, E. a.; Shinde, R.; Dehnert, K. W.; Adams-Bond, A.; Wender, P. a.; Contag, C. H.; Franc, B. L. Intracellular Cargo Delivery by an Octaarginine Transporter Adapted to Target Prostate Cancer Cells through Cell Surface Protease Activation. *Bioconjug. Chem.* **2006**, *17* (3), 787–796.

(3) Rothbard, J. B.; Jessop, T. C.; Lewis, R. S.; Murray, B. A.; Wender, P. A. Role of Membrane Potential and Hydrogen Bonding in the Mechanism of Translocation of Guanidinium-Rich Peptides into Cells. *J. Am. Chem. Soc.* **2004**, *126* (31), 9506–9507.

(4) Stanzl, E. G.; Trantow, B. M.; Vargas, J. R.; Wender, P. A. FifteenYears of Cell-Penetrating,Guanidinium-Rich Molecular Transporters: Basic Science, Research Tools, and Clinical Applications. *Acc. Chem. Res.* **2013**, *46* (12), 2944–2954.

(5) Maiti, K. K.; Lee, W. S.; Takeuchi, T.; Watkins, C.; Fretz, M.; Kim, D.-C.; Futaki, S.; Jones, A.; Kim, K.-T.; Chung, S.-K. Guanidine-Containing Molecular Transporters: Sorbitol-Based Transporters Show High Intracellular Selectivity toward Mitochondria. *Angew. Chem. Int. Ed. Engl.* **2007**, *46* (31), 5880–5884.

(6) Maiti, K. K.; Jeon, O.-Y.; Lee, W. S.; Chung, S.-K. Design, Synthesis, and Delivery

Properties of Novel Guanidine-Containing Molecular Transporters Built on Dimeric Inositol Scaffolds. *Chem. Eur. J.* **2007**, *13* (3), 762–775.

(7) Paul A. Wender Christina B. Cooley, E. I. G. Beyond Cell Penitrating Peptides: Designed Molecular Transporters. *Drug Discov. Today. Technol.* **2012**, *9* (1), e49–e55.

(8) Rothbard, J. B.; Garlington, S.; Lin, Q.; Kirschberg, T.; Kreider, E.; McGrane, P. L.; Wender, P. a; Khavari, P. a. Conjugation of Arginine Oligomers to Cyclosporin A Facilitates Topical Delivery and Inhibition of Inflammation. *Nat. Med.* **2000**, *6* (11), 1253–1257.

(9) Tan, W.; Wang, H.; Chen, Y.; Zhang, X.; Zhu, H.; Yang, C.; Yang, R.; Liu, C. Molecular Aptamers for Drug Delivery. *Trends Biotechnol.* **2011**, *29* (12), 634–640.

(10) Jain, A.; Jain, A.; Gulbake, A.; Shilpi, S.; Hurkat, P.; Jain, S. K. Peptide and Protein Delivery Using New Drug Delivery Systems. *Crit. Rev. Ther. Drug Carrier Syst.* **2013**, *30* (4), 293–329.

(11) Cho, H.; Cho, Y.-Y.; Bae, Y. H.; Kang, H. C. Nucleotides as Nontoxic Endogenous Endosomolytic Agents in Drug Delivery. *Adv. Healthc. Mater.* **2014**, *3* (7), 1007–1014.

(12) Takakura, Y.; Nishikawa, M.; Yamashita, F.; Hashida, M. Development of Gene Drug Delivery Systems Based on Pharmacokinetic Studies. *Eur. J. Pharm. Sci.* **2001**, *13* (1), 71–76.

(13) Maniganda, S.; Sankar, V.; Nair, J. B.; Raghu, K. G.; Maiti, K. K. A Lysosome-Targeted Drug Delivery System Based on Sorbitol Backbone towards Efficient Cancer Therapy. *Org. Biomol. Chem.* **2014**, *12* (34), 6564–6569.

(14) Mohamed, M. M.; Sloane, B. F. Cysteine Cathepsins: Multifunctional Enzymes in Cancer. *Nat. Rev. Cancer* **2006**, *6* (10), 764–775.

(15) Dubowchik, G. M.; Firestone, R. A.; Padilla, L.; Willner, D.; Hofstead, S. J.; Mosure, K.; Knipe, J. O.; Lasch, S. J.; Trail, P. A. Cathepsin B-Labile Dipeptide Linkers for Lysosomal Release of Doxorubicin from Internalizing Immunoconjugates: Model Studies of Enzymatic Drug Release and Antigen-Specific *In Vitro* Anticancer Activity. *Bioconjug. Chem.* **2002**, *13* (4), 855–869.

(16) Yang, F.; Teves, S. S.; Kemp, C. J.; Henikoff, S. Doxorubicin, DNA Torsion, and

Chromatin Dynamics. *Biochimica et Biophysica Acta - Reviews on Cancer*. 2014, pp 84–89.

(17) Pisano, C.; Cecere, S. C.; Di Napoli, M.; Cavaliere, C.; Tambaro, R.; Facchini, G.; Scaffa, C.; Losito, S.; Pizzolorusso, A.; Pignata, S. Clinical Trials with Pegylated Liposomal Doxorubicin in the Treatment of Ovarian Cancer. *J. Drug Deliv.* **2013**, *2013*, 898146.

(18) Palomo, J. M. Solid-Phase Peptide Synthesis: An Overview Focused on the Preparation of Biologically Relevant Peptides. *RSC Adv.* **2014**, *4* (62), 32658–32672.

(19) Biniossek, M. L.; Nägler, D. K.; Becker-Pauly, C.; Schilling, O. Proteomic Identification of Protease Cleavage Sites Characterizes Prime and Non-Prime Specificity of Cysteine Cathepsins B, L, and S. *J. Proteome Res.* **2011**, *10* (12), 5363–5373.

(20) Rieger, A. M.; Nelson, K. L.; Konowalchuk, J. D.; Barreda, D. R. Modified Annexin V/Propidium Iodide Apoptosis Assay For Accurate Assessment of Cell Death. *J. Vis. Exp.* **2011**, No. 50, 2597.

Chapter 3

Cancer Cell-Specific Induction of Apoptosis by Precise Delivery of Doxorubicin Using Folate Targeted Lysosome Specific Octa- Guanidine Appended Molecular Transporter

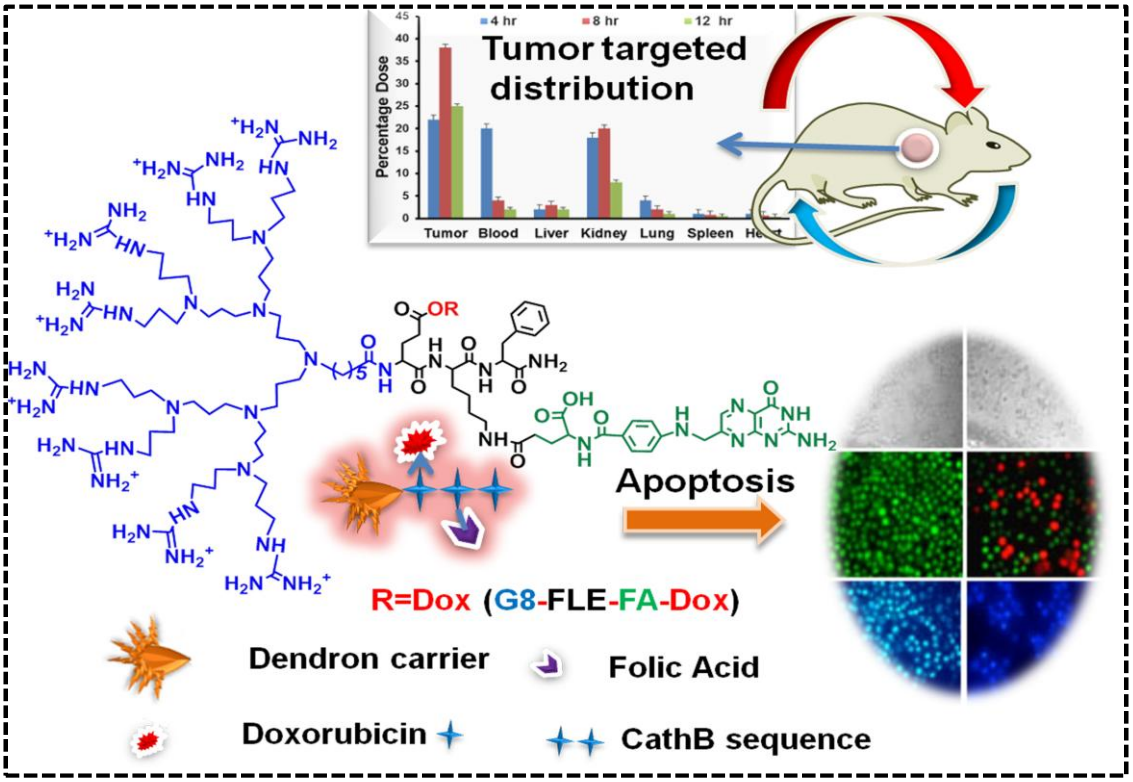

3.1 Abstract: *An efficient synthetic framework was assembled (G8-FKE-FA-Dox), consisting of a lysosome-targeting octa guanidine molecular transporter with a cathepsin B (cath B)-specific peptide substrate, folic acid, and the potent chemotherapeutic drug doxorubicin (Dox). Since the folate receptor (FR) and cath B are over expressed in malignant cells, the transporter-conjugate successfully executed lysosome-mediated transport of Dox into FR-positive tumour cells, illustrating this framework as an excellent targeted drug delivery system (TDDS). G8-FKE-FA-Dox was shown to exhibit selective toxicity toward FR-over expressing cancer cells, with an* IC_{50}

value superior to that of the US FDA approved Lipodox™ and proportional to that of free Dox via selective induction of apoptosis by the activation of caspases 8, 9, and 3. This TDDS was observed to be nontoxic to red blood cells and lymphocytes at neutral pH. Furthermore the tumor-targeting dissemination pattern of this system was revealed by monitoring the in vivo bio-distribution of the carrier (G8-FKE-FA-FL) in normal and FR-over expressing tumor-bearing mice.

3.2 Introduction

Cancer is a heterogeneous and fatal condition that remains the second leading cause of mortality worldwide,[1] despite the significant amount of progress made to combat the disease. Cancer cells mature rapidly, have defective vascular architecture, and are more permeable to macromolecules than normal tissues. The enhanced permeation and retention (EPR) effect[2] in the tumor microenvironment, owing to increased cell permeability and lack of lymphatic drainage, provides easier access by chemotherapeutic drugs[3] to tumor tissues. Targeted drug delivery systems (TDDS) with widely used anticancer drugs[4] such as doxorubicin (Dox), cisplatin, camptothecin, and methotrexate have been broadly examined in the past few decades. Among them, Dox[5] is widely used as the standard treatment against non-Hodgkin's lymphoma, acute lymphoblastic leukemia, breast cancer, and several other types of neoplasms, but is associated with severe side effects including alopecia, cardiotoxicity, and arrhythmia. TDDS,[6] as multidisciplinary approaches for the delivery[2,3,7] of therapeutics, have recently gathered greater enthusiasm generally, and particularly in cancer chemotherapy, given their capacity to direct active agents toward target sites at ideal times and doses, thereby maximizing therapeutic efficacy and minimizing undesired systemic side effects. Non-targeted therapeutic strategies, on the other hand, result in only 5–10% of the administered drug dose reaching the tumor site.[8] Various nanocarriers [9] have demonstrated the delivery of chemotherapeutic compounds to the targeted zone,[10] effecting the greatest EPR impact by enhancing the solubility, stability, and half-life of the drug to increase the overall therapeutic index. Active targeting of nanocarriers with specific target-cells specific ligands such as antibodies, small proteins, peptide substrates, carbohydrates, nucleic acids, and folic acid allow the selective distribution of a drug payload. Importantly, folic acid has several advantages as a targeting agent due to its

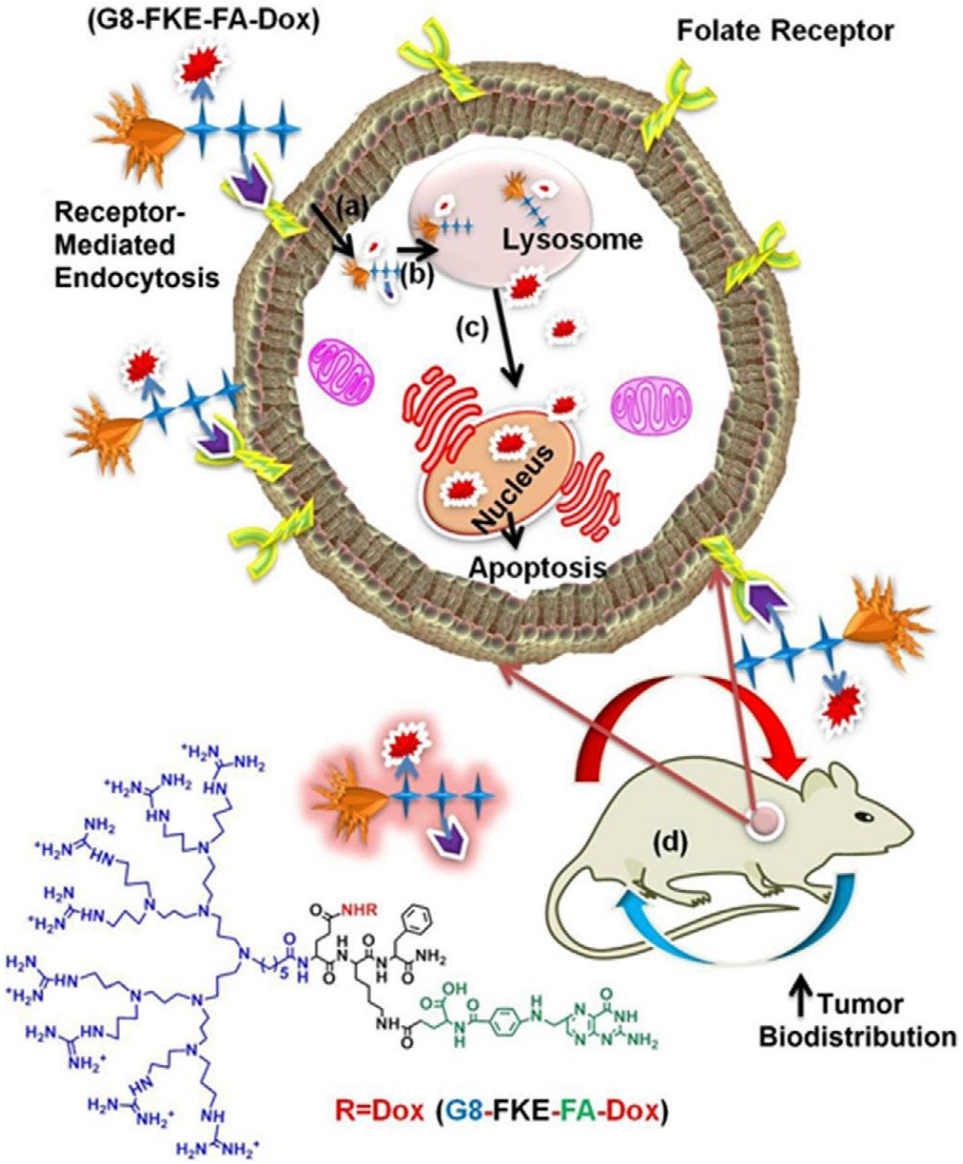

Scheme1: Thematic representation of the mode of action of G8-FLE-FA-Dox by (a) recognition of folate receptor and internalization by endocytosis (b) Cath B mediated drug release (c) diffusion of drug in to nucleus lead to death of cancer cells and (d) tumor targeted accumulation in mice.

low molecular weight, low immunogenicity, relatively high stability, and ease of synthetic modification. The folate receptor (FR)[11,12] is a well-studied tumor-associated receptor that is overexpressed in many cancer cell types (including those of the breast, lung, kidney, and brain) relative to normal cells. Normal cells transport folate only in its reduced form across their membrane, not folate conjugates of any type, whereas malignant cells transport folate conjugates via the FR, which is considered an alternative route.[13] Several folate–drug conjugates[14] have been developed and some have shown promising results in phase III clinical trials.[15] In

considering an effective TDDS, the encapsulated drug should be joined to the carrier through an enzyme-cleavable linker for ideal discharge at the target site. Cathepsin B (cath B),[16,17] a lysosomal cysteine protease over-expressed in tumor cells, has long been considered a target in cancer therapy and is widely used in many drug delivery systems in which a cath B peptide substrate is cleaved at lysosomal pH, thereby releasing the drug cargo molecule. Because the lysosome is the main organelle involved in FR-mediated endocytosis, a cath B peptide substrate could be a suitable linker for FR based targeting. Construction of TDDS with cell-penetrating peptides (CPPs) such as Tat and arginine octamers (Arg-8-mer) are well-known counterparts centered primarily on the number and spatial array of guanidine residues.[18] However, the EPR effect could not have been achieved with our TDDS via the CPP approach alone due to its lower molecular weight and size, but the FR-mediated targeting approach could lead to effective delivery of the drug. Molecular transporters containing octaguanidine[18] residues have been shown to enhance the cell-penetrating capacity most effectively, and have been shown to deliver a variety of cargos [19–22] including small molecules, peptides, proteins, imaging agents, siRNA, peptide nucleic acids (PNAs), plasmids, and vesicles. In the previous chapter a new guanidinium-rich poly(propylene imine) dendron-based molecular transporter[23] (G8-PPI-FL), has been revealed which was observed to be nontoxic with greater cellular uptake, in contrast with the Arg-8-mer, and showed a high degree of selectivity toward lysosomes in cath B overexpressing HeLa cells. The high cell-penetrating capacity of the G8-dendron has been utilized as a TDDS with a combination of folic acid and cath B peptide substrate as a linker for the efficient delivery of Dox into FR over expressing cancer cells. Therefore, in the present study a dual-targeted drug delivery construct built on an octaguanidine dendron based molecular transporter has been explored which specifically delivered Dox to FR-over expressing cancer cells while leaving normal cells unharmed.

3.3 Results and Discussion

3.3.1 Synthesis and characterization of TDDS: G8-FKE-FA-Dox and G8-FKE-FA-FL

The synthetic TDDS construct G8-FKE-FA-Dox is built on a poly-(propylene imine) dendron and is conjugated with a chemotherapeutic agent doxorubicin (an

anthracycline-based DNA intercalator), folic acid as a cell-surface FR-targeting ligand, and the cath B substrate peptide sequence i.e. Phe-Lys-Glu (FKE), a recognizing motive of cysteine protease over-expressed in lysosomes of tumor cells (Figure 3.1). The cath B substrate sequence FKE was synthesized by solid-phase peptide synthesis (SPPS) using manual coupling of Rink amide resin. Next, tert-butyloxycarbonyl (Boc)-deprotected lysine side chain amine groups were covalently linked to ɣ- carboxylic acid terminated folic acid (FA) via an amide bond. The N-terminus of Glu in the cath B substrate was conjugated with the octa guanidine transporter (G8-Boc-PPI) by amide coupling. The carrier G8-Boc-PPI Dendron was synthesized as per our previous report[23]i.e., by sequential Michael addition of acrylonitrile followed by reduction with Raney nickel; eight equivalents of free amine termini were coupled with Boc-protected guanidine residues to afford G8-Boc-PPI. Finally, Dox in free amine form was attached to the Glu side chain by amide coupling. Similarly, a control compound was synthesized by replacing Dox with fluorescein (FL) to give G8-FKE-FA-FL, in which FL is attached to the Glu residue via an aminopropanol linker. The control compound was used for tracking the internalization efficacy as well as to evaluate the cytotoxicity of the entire carrier system. The final target transporter molecules G8-FKE-FA-Dox and G8- FKE-FA-FL were transformed into their respective hydrochloride salts after removal of the Boc groups from the guanidine moieties by treatment with ethyl acetate saturated with HCl gas (Scheme 2). The elaborated scheme clearly outlines the stepwise synthesis strategy, key intermediates, and target products; G8-FKE-FA-Dox and G8-FKEFA- FL were purified and characterized by HPLC (Figure 3.1a,b), NMR spectroscopy, and MALDI-TOF mass spectrometry.

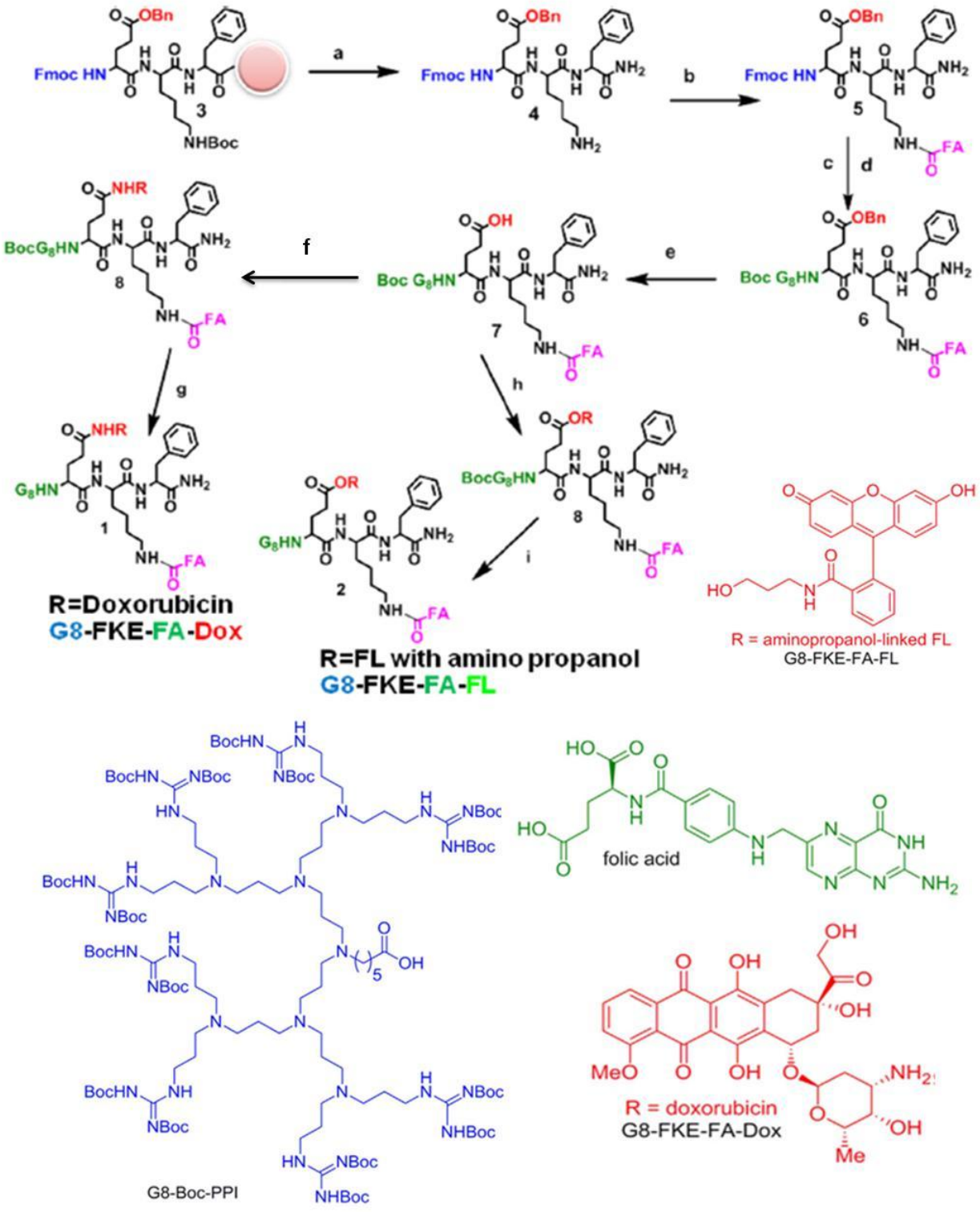

Scheme 2. Structure and synthesis of G8-FKE-FA-Dox and G8-FKE-FA-FL. Reagents and conditions: compound 3 was synthesized by SPPS, (a)Cathepsin B peptide cleavage from rink amide resin, by 95% TFA,2.5%TIS,2.5% water(cleavage cocktail for rink amide resin),(b)-folic acid, EDC, DMAP, Dry DCM: DMF(1:1), N_2 atm, RT, 24hrs (c) 20% piperidine in DMF(d)-G8-Boc-PPI ,EDC, HOBt ,Dry DCM: DMF(1:1), N_2 atm, RT, 24hrs.(e)Pd/C, EtOAc, H_2, CH_3COOH, 1.5hrs, 1atm, ,(f)- Doxorubicin, EDC, HOBt, Dry DCM: DMF(1:1), N_2 atm, RT,

24hrs, (g)-EtOAc saturated with HCl reagents. (h)-Fl with aminopropanol, EDC, DMAP, Dry DCM: DMF (1:1),N_2 atm, RT, 24h (i) EtOAc saturated with HCl reagents

The construct was found to be stable in 10% fetal bovine serum (FBS) in phosphate-buffered saline (PBS), which mimics *in vivo* fluid composition (Figure 3.1c).The stability of G8-FKE-FA-Dox was evaluated for up to four months and showed no significant degradation (Figure 3.1d).

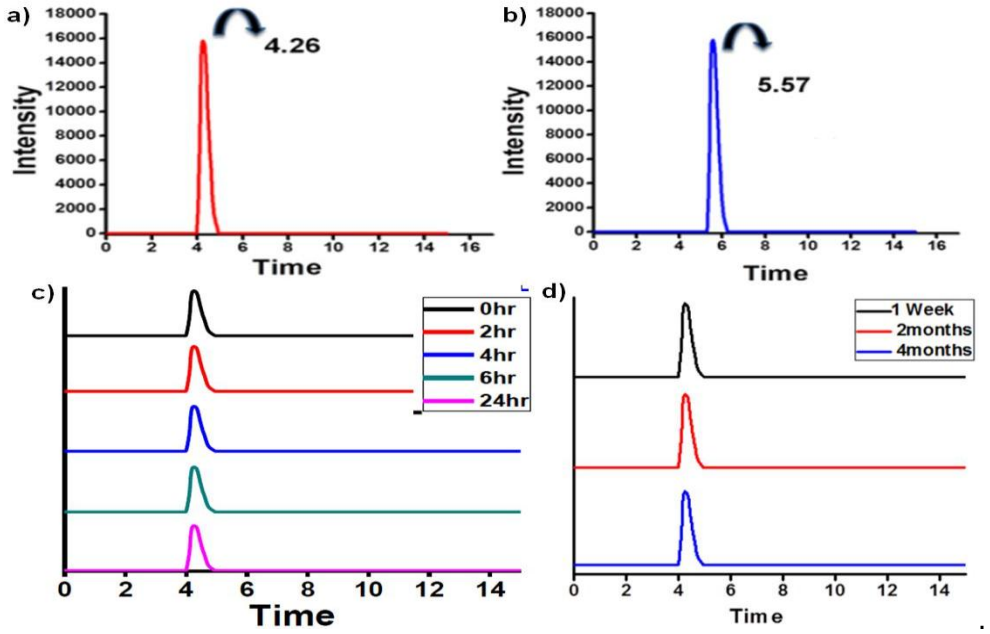

Figure 3.1. HPLC profiles of G8-FKE-FA-Dox (a) and G8-FKE-FA-FL (b) and stability of G8-FKE-FA-Dox up to 4 months(c) The stability of G8-FKE-FA-Dox in PBS (pH=7.4) containing 10% FBS at 37^0C for 24 h

3.3.2 Western blot analysis for FR expression and Hemolytic properties of TDDS

The FR-mediated targeted delivery system G8-FKE-FA-Dox is expected to deliver Dox to FR-expressing cancer cells; however the FR expression pattern varies widely between tumor subtypes. Therefore, we evaluated the FR expression status of five human and two murine cancer cell lines, along with one normal fibroblast cell line by western blotting analysis using antibodies directed against the FR. Quantitative evaluation of the resulting bands was performed after normalizing with those of

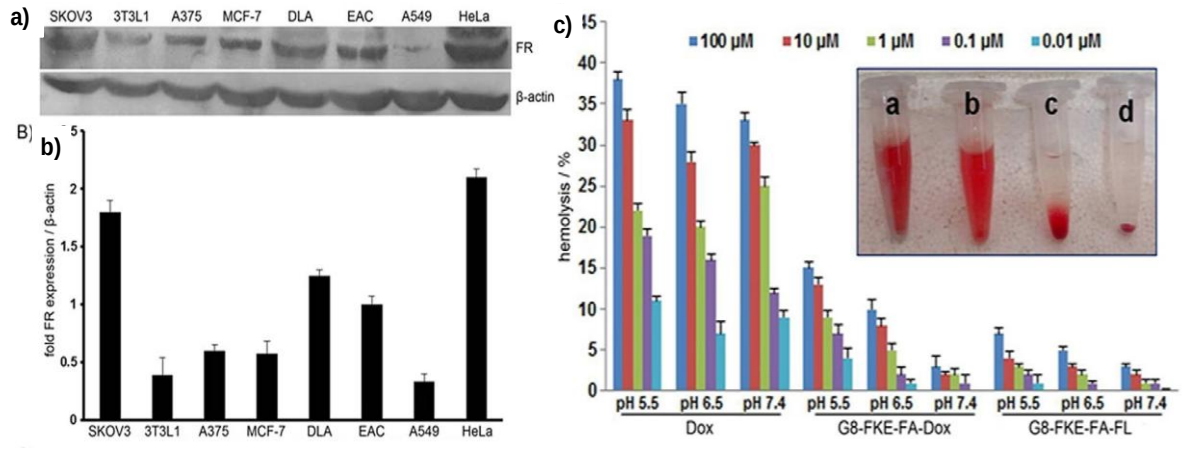

Figure 3.2. Folate receptor (FR) expression level analysis in various cell lines by western blotting and evaluation of hemolysis by various constructs. A) Western blot showing the expression levels of FR and β-actin in cancer and normal (3T3L1) cells. B) Quantitation of protein bands normalized to β-actin using Image J software. C) Hemolysis experiment performed with G8-FKE-FADox, G8-FKE-FA-FL, and free Dox at different concentrations and under various pH conditions; data are the mean SD of three independent experiments. Inset: representative experiment at pH 5.5showing: a) Triton X-100 (positive control), b) Dox (100 mm), c) G8-FKE-FA-Dox (100 mm), and d) G8- FKE-FA-FL (100 mm).

β-actin. Out of the eight cell lines examined, HeLa and SKOV3 cells showed significantly higher FR expression, whereas A549 and 3T3L1 showed minimum FR expression (Figure. 3.2a,b). The results correlated well with similar studies[24–26] and enabled us to select HeLa and SKOV3 as FR-positive and A549 as FR-negative cells for *in vitro* assays. Furthermore, Ehrlich ascites carcinoma (EAC) and Daltons lymphoma ascites (DLA) cells showed moderate levels of FR expression, and would therefore be suitable for in vivo assays with FR-targeting systems.

Because the initial encounter of any chemotherapeutic agent occurs with blood components, it is important to determine the carrier-conjugate hemolytic properties. Cytotoxic agents administered into the bloodstream may cause adverse side effects such as hemolysis and thrombogenesis. Therefore, hemolysis assays were performed to determine the toxicity of G8- FKE-FA-Dox, G8-FKE-FA-FL, and Dox· HCl on red blood cells (RBCs) under three different pH conditions (Figure 3.2c). The positive and negative control samples were prepared with Triton X-100 and PBS, respectively, and applied to RBCs; images of representative assays (inset photograph) containing the highest drug concentration tested (100 mM) at pH 5.5 are shown. The highest hemolytic activity was observed for free Dox, which demonstrates concentration-dependent pH-independent lysis. As high as 38%

hemolysis was observed for 100 mm Dox at pH 5.5, and even at 0.01 mM Dox causes 9% hemolysis at pH 7.4. G8-FKE-FA-Dox showed reasonably lower hemolysis than free Dox. It shows both concentration- and pH dependent lysis of RBCs: at the highest concentration of 100 mM, 15% lysis was observed at pH 5.5, whereas only 3% hemolysis was recorded at pH 7.4. Under slightly acidic conditions (pH 6.5) <10% lysis was observed even at 100 mM. The carrier G8-FKE-FA-FL was found to be devoid of any toxicity toward RBCs for all concentrations evaluated, and the same is true for cancer cells as well (Table 1) in evaluations by MTT assay. Cancer cells are characterized by an acidic extracellular pH, hence the mild hemolysis observed under acidic conditions might only affect RBCs within the tumor niche as opposed to those in circulation.[27] The haemolytic properties of Dox is well documented[28] along with its other deleterious effects. The significant decrease in the haemolytic properties of G8-FKE-FA-Dox might be due to the fact that Dox release from our TDDS is a lysosome-mediated process; as RBCs lack lysosomes, Dox remains conjugated to the carrier.

3.3.3 Cytotoxicity evaluation and FR inhibition studies of TDDS

Evaluation of cytotoxicity is an important step in the development of any cancer chemotherapeutic, and hence the cytotoxicity was evaluated on FR-positive and -negative cell lines by MTT assay. G8-FKE-FA-Dox, G8-FKE-FA-FL, free Dox, and

Compound	IC_{50} in µM											
	HeLa			SKOV3			A549			3T3L1		
	12 hr	24 hr	48 hr	12 hr	24 hr	48 hr	12 hr	24 hr	48 hr	12 hr	24 hr	48 hr
G8-FLE-FA-Dox	9 ± 0.5	2.5 ± 0.08	0.55 ± 0.1	25 ± 0.9	7 ± 0.6	1 ± 0.8	Nil	Nil	Nil	Nil	Nil	Nil
Dox	Nil	0.6 ± 0.07	0.1 ± 0.05	Nil	0.82 ± 0.06	0.3 ± 0.7	Nil	0.92 ± 0.8	0.17 ± 0.09	Nil	2.6 ± 0.8	0.1 ± 0.07
Lipodox	Nil	43.7 ± 1.2	7.4 ± 1	Nil	80 ± 1.7	26 ± 0.8	Nil	61 ± 1.1	9.2 ± 1.3	Nil	Nil	26 ± 0.8
G8-FLE-FA-FL	Nil	Nil	Nil	Nil	Nil	Nil	Nil	Nil	Nil	Nil	Nil	Nil

Table 1. The IC_{50} values of cell lines treated with various compounds calculated by using Easy Plot software after MTT assay

clinically used Lipodox ™ were assessed across a wide range of concentrations (0.01 nM to 100 mM) for 12, 24, and 48 h. G8-FKE-FA- Dox displayed cytotoxicity toward human cervical cancer (HeLa) and ovarian cancer (SKOV3) cell lines that overexpress FR, but was less toxic toward human lung adenocarcinoma (A549) and

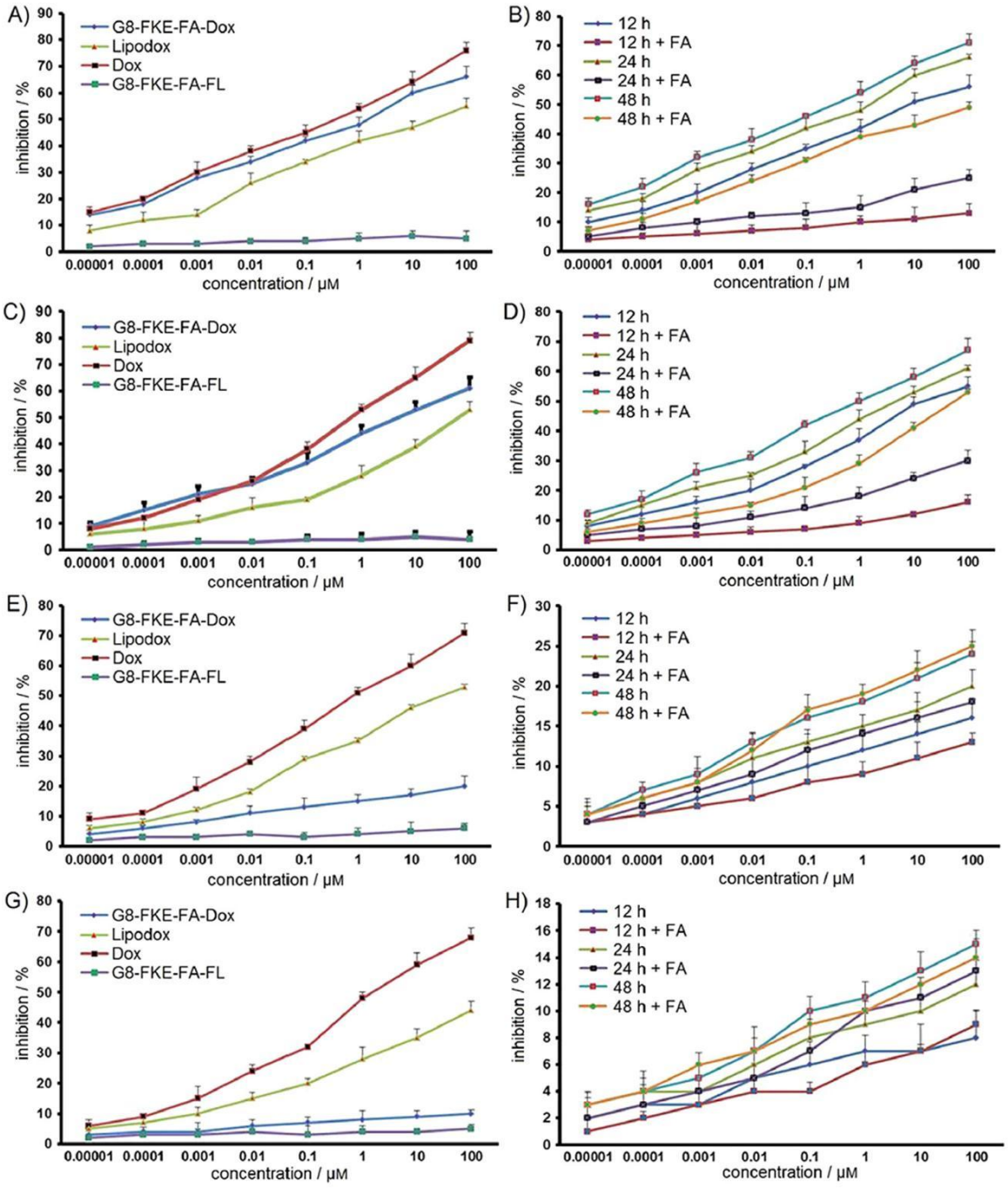

Figure 3.3. Cytotoxicity assay with cancer cells and normal cells treated with G8-FKE-FA-Dox, G8-FKE-FA-FL, Dox, and Lipodox ™ with and without external folic acid (FA; 2 mM for 2 h) after administration for 24 h. A) HeLa cells, B) HeLa cells + FA, C) SKOV3 cells, D) SKOV3 cells + FA, E) A549 cells, F) A549 cells + FA, G) 3T3L1 cells, and F) 3T3L1 cells + FA. Data are the mean SD of three independent experiments

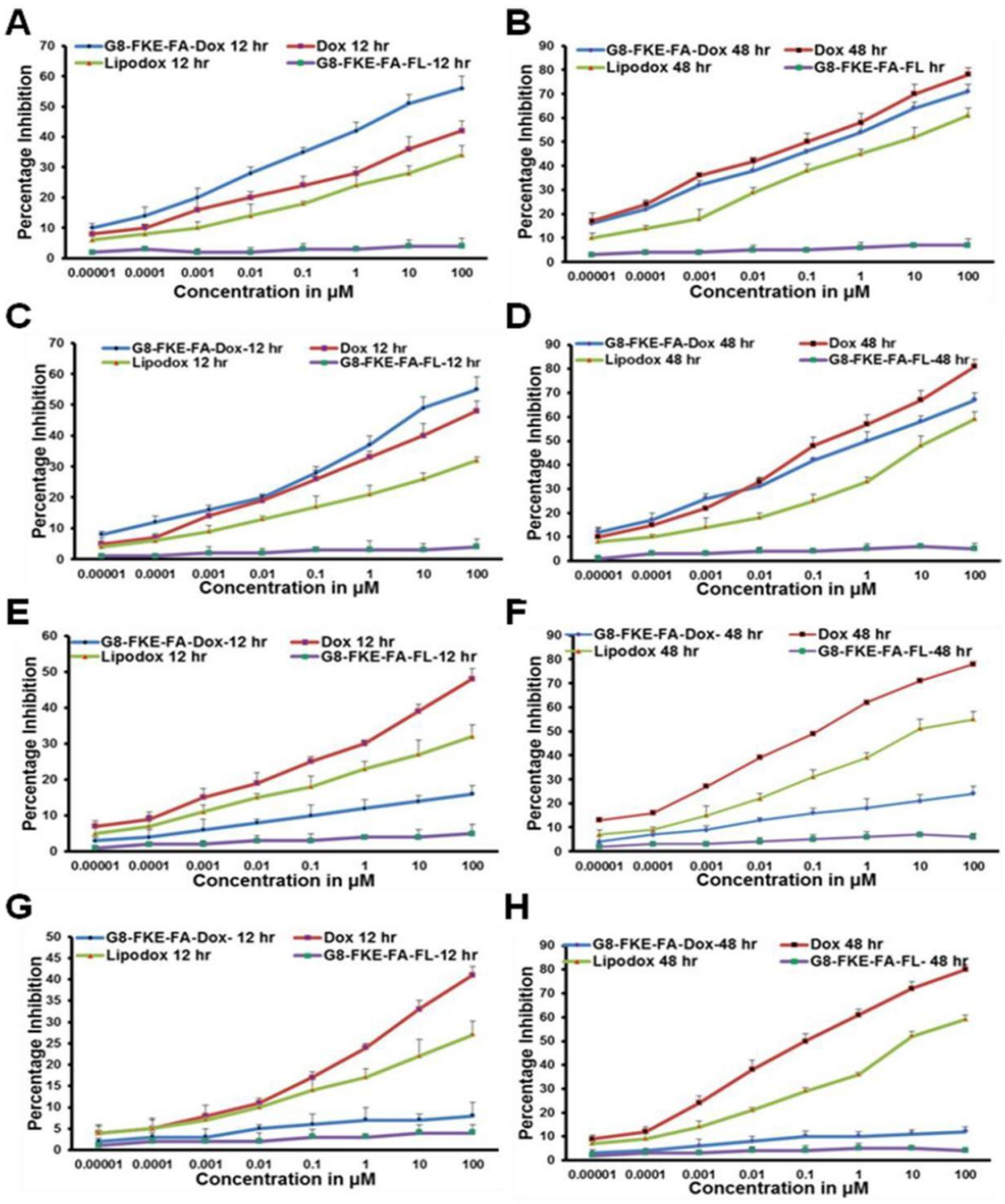

Figure 3.4. Assay for cytotoxicity in cancer cells and normal cells treated with G8-FKE-FADox, G8-FKE-FA-FL, Dox and Lipodox after 12 and 48 hrs of administration. (A)HeLa cells 12 h, (B) HeLa cells 48 h , (C) SKOV3 cells 12h, (D) SKOV3 cells 48 h , (E) A549 cells 12 h , (F) A549 cells 48 h, (G) 3T3L1 cells 12 h and (F) 3T3L1 cells 48 h.

murine fibroblasts (3T3L1) with minimal FR expression. HeLa and SKOV3 growth were arrested by G8-FKE-FA-Dox with an IC_{50} value of 90.5 and 250.9 mM at 12 h, whereas Dox and Lipodox™ could produce measurable IC_{50} values only at 24 h incubation. However, the IC_{50} values of Dox at 24 and 48 h are much lower than those of G8-FKE-FA-Dox and Lipodox™ (Table 1). G8-FKE-FA-Dox followed a

concentration- and time-dependent increase in cytotoxicity toward both HeLa (Figure 3.3A, Figure 3.4A,B) and SKOV3 cells (Figure 3.3C, Figure 3.4C,D). G8-FKE-FA-Dox showed higher cytotoxicity than Dox at 12 h, but Dox was more effective after 24 and 48 h. LipodoxTM, however, was found to be least cytotoxic under all concentrations and incubation times than G8-FKE-FADox and Dox (Figure 3.3 A, C,). FR-mediated targeted cytotoxicity of G8-FKE-FA-Dox was evidenced by the absence of IC_{50} values in A549 and 3T3L1 cells, where Dox and LipodoxTM exhibited IC_{50} values at 24 and 48 h (Table 1). Dox and Lipodox™ showed marked cytotoxicity on both A549 and 3T3L1 cell lines, but G8-FKE-FA-Dox was least toxic at lower concentrations and produced a maximum cytotoxicity of 241.2% on A549 and 120.9% on 3T3L1 cells after 48 h at 100 mM, whereas Dox and Lipodox ™ achieved 781.9 and 551.1% on A549, and 801.5 and 591.3% on 3T3L1 cells after 48 h at 100 mM (Figure 3.3 E,G, Figure 3.4E,F). The carrier itself (G8-FKE-FA-FL) was nontoxic to all four cell lines, regardless of FR expression (Figure 3.3A–H, Figure 3.4A–H). The FR-targeted cytotoxicity demonstrated by G8-FKE-FA-Dox was confirmed by MTT assay after the addition of 2 mM folic acid to the medium for 2 h, serving as a competitive inhibition study at the FR for G8-FKE-FA-Dox. There was a dramatic decrease in the cytotoxicity toward HeLa and SKOV3 cells after folic acid incubation, particularly at 12 and 24 h, but a slight increase at 48 h (Figure 3.3 B,D). There was no significant alteration in the cytotoxicity of G8-FKE-FA-Dox on the FR-negative cell lines A549 and 3T3L1 (Figure 3.3 F,H), further validating the FR-targeting capacity of G8-FKE-FA-Dox. The indiscriminate toxicity exhibited by Dox toward normal cells is well documented.[29] The decreased *in vitro* cytotoxicity of liposomal Dox–nanoparticle formulations such as Doxil™ and Lipodox™ relative to free Dox has already been reported,[30] and these formulations are more effective than Dox for in vivo applications, as they reduce hazardous effects toward normal cells, yet they are still not effective for targeted delivery approaches.

3.3.4 Cellular internalization of TDDS: G8-FKE-FA-Dox

Although G8-FKE-FA-Dox exhibited robust anticancer effects on FR-positive cells, it is still important to evaluate the internalization efficiency with respect to time and dosage. We initially assessed the intracellular localization of the transporter G8-FKE-FA-FL in HeLa cells using the intracellular staining dye LysoTracker™ (Figure

3.5A). G8-FKE-FA-FL was internalized rapidly and found to be with LysoTracker ™, which substantiates the cath B-mediated lysosomal drug release pattern. It is also evident from Figure 3.6A that the FL conjugate of G8-FKE-FA resides primarily in the cytoplasm, given the lack of co-localization with the nuclear dye DAPI. Cellular uptake and Dox release from G8-FKE-FA-Dox was evaluated in HeLa cells by confocal microscopy, clearly demonstrating the rapid Dox uptake and release in the nucleus. The Dox drug was delivered by G8-FKE-FA-Dox more effectively than from free Dox within 2 h of administration, as indicated by co-localization with DAPI (Figure 3.6B, C). Furthermore, cellular uptake of Dox from G8-FKE-FA-Dox estimated at various time points (0–4 h) in HeLa cells by flow cytometry demonstrated a time-dependent increase in Dox uptake, where a significant uptake was observed even after 30 min of treatment with a shift in histogram toward higher intensity (Figure. 3.5B). Increased cellular uptake of Dox from G8-FKE-FA-Dox than with free Dox, observed by confocal microscopy, was further confirmed by flow cytometry (Figure 3.5C). The FR-targeting capacity of G8-FKE-FA- Dox was tested after administration of the agent for 4 h in HeLa (Figure 3.6D) and A549 (Figure 3.6E) cells. There was a dramatic difference in drug uptake, with HeLa cells taking up significantly higher amounts of Dox ($p<0.001$) than A549 cells (Figure 3.6D–F).

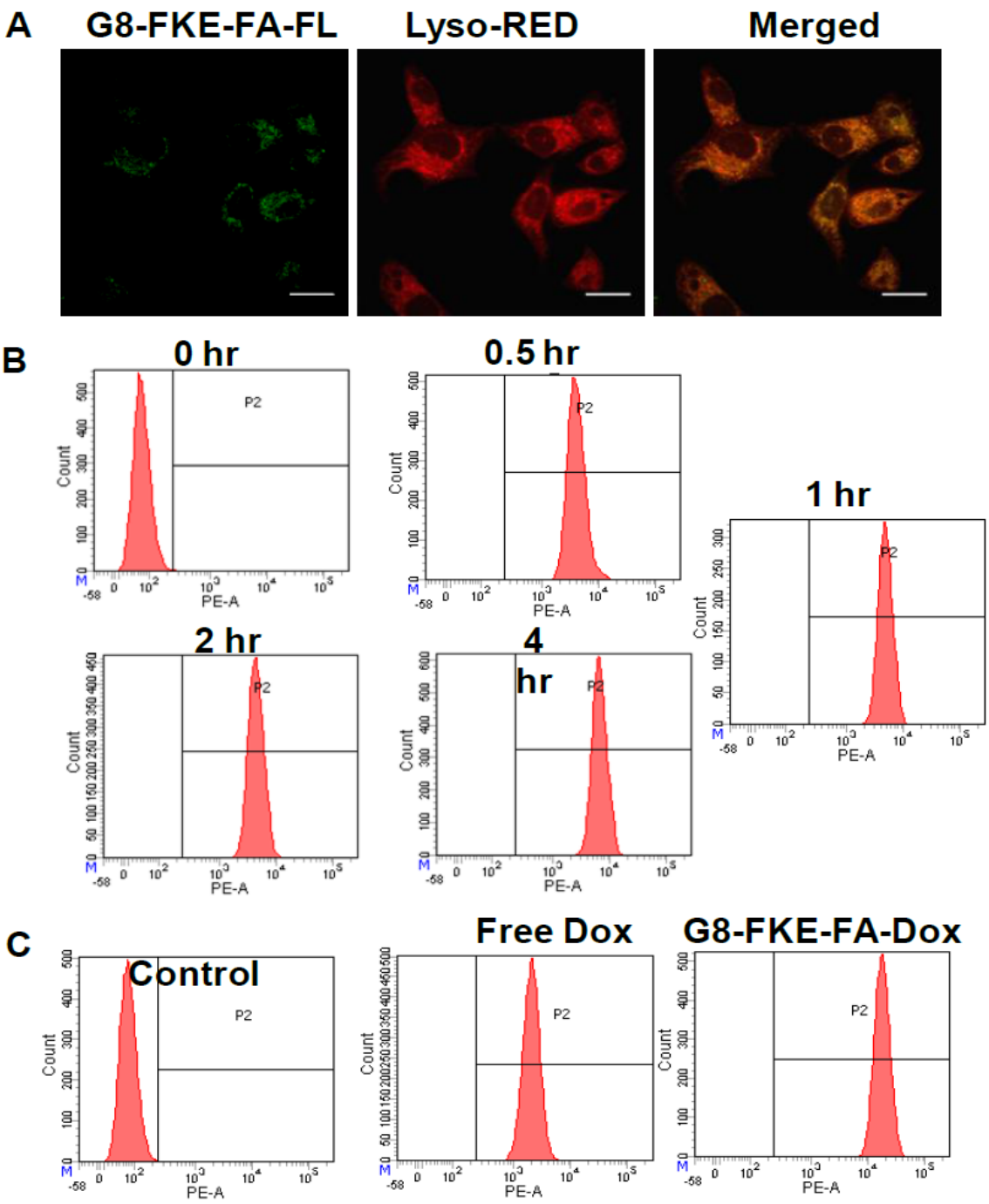

Figure 3.5: Cellular uptake studies by confocal microscopy and flow cytometry. (A) Colocalisation study of G8-FKE-FA-FL (2μM) with lysosome of HeLa cells after 4 h of incubation, Scale bar corresponds to 20 μM. (B) DOX uptake in HeLa cells after incubation of G8-FKE-FA Dox (2μM) with different time periods. (C) Dox uptake efficiency from free Dox (4 μM) and G8- FKE-FA-Dox (4μM) on HeLa cells

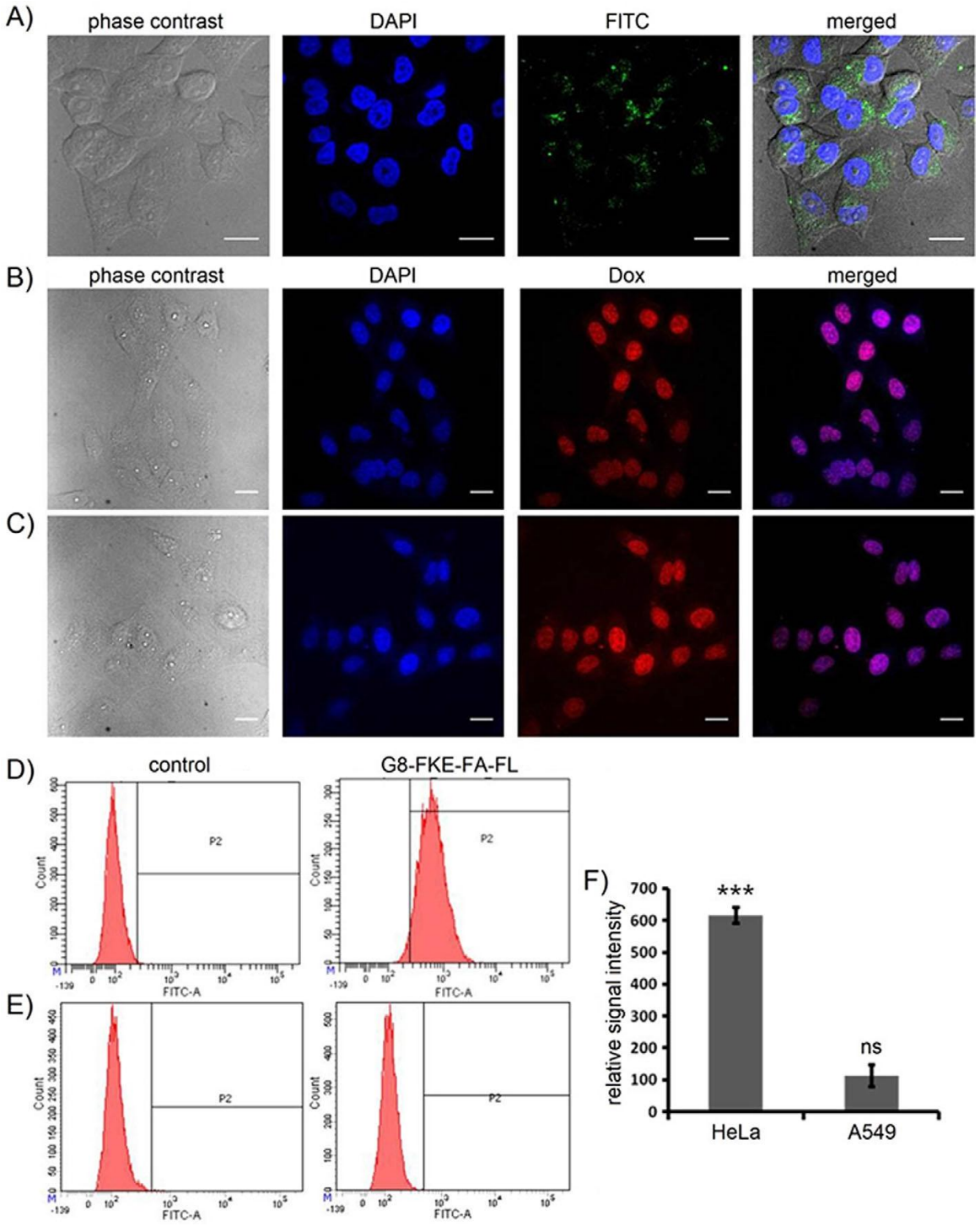

Figure 3.6. Cellular uptake studies with confocal microscopy and flow cytometry. A) Internalization of G8-FKE-FA-FL (2 mm) by HeLa cells after 4 h incubation. Release of Dox by B) free doxorubicin (2 mM) and C) G8-FKE-FA-Dox (2 mM) in HeLa cells after 4 h incubation. Scale bar: 20 mM. Cellular uptake of G8-FKE-FA-FL (20 mM) after 4 h incubation in D) HeLa and E) A549 cells. F) FR-targeted uptake by HeLa and A549 cells; data are the meanSD of three independent experiments; ***p<0.001, ns: not significant relative to control.

3.3.5 Evaluation of apoptosis by TDDS: G8-FKE-FA-Dox

To determine the mechanism of cell death induced by G8-FKE-FA-Dox in cancer cells, various apoptosis assays were conducted with HeLa, SKOV3 (FR-positive) and A549 (FR-negative) cells after administration of compound at 1 mM for 24 h. Evaluation of the cells by phase contrast microscopy revealed salient features of apoptosis such as distorted shape, membrane blebbing, and decreased cell number relative to control groups for HeLa and SKOV3 cells (Figure 3.7A upper panel). In comparison with the respective controls, acridine orange–ethidium bromide staining in FR-positive cells revealed a change in color from green to yellow/red, which is associated with other apoptotic features such as the presence of apoptotic bodies, damaged cell membrane, and nuclear condensation (Figure 3.7A, middle panel). Cells undergoing apoptosis demonstrated nuclear condensation and DNA fragmentation, which was detected by Hoechst 33342 nuclear staining. The percentage of chromatin condensation after G8-FKE-FA-Dox treatment was significantly higher in HeLa and SKOV3 cells, but no compelling transition was observed in A549 cells relative to its control (Figure 3.7A lower panel). The mechanism of cell death induced by G8-FKE-FA-Dox was further confirmed by terminal deoxynucleotidyl transferase (TdT) dUTP nick-end labeling (TUNEL) assay, in which propidium iodide (PI) was used as a counterstain. FR-positive cells displayed a green color, indicating TUNEL positivity, whereas FR-negative cells were found to be largely TUNEL negative (Figure 3.7B), indicating FR-targeted apoptosis induction by G8-FKE-FA-Dox.

Morphological changes that occur at the early onset of apoptosis were further detected by Annexin V–FITC staining using flow cytometry. Early-phase apoptotic cells stained with FITC are shown in the lower right quadrant of the FACS dot plot, whereas late-phase apoptotic cells stained with both FITC and PI are represented in the upper right quadrant. The percentage of apoptotic cells after drug treatment or negative control are represented in Figure 3.8d. There was a significant ($p<0.001$) increase in Annexin V positivity in treated HeLa and SKOV3 cells relative to control cells, but the change was insignificant for A549 cells (Figure 3.8a-c). One of the mechanistic features of apoptosis is the activation of caspases, a class of cysteine proteases. Many anticancer drugs including Dox have been reported to execute

apoptosis through a caspase-dependent pathway. [31]Because caspases are the effective mediators of apoptosis, the expression of caspases 3, 8, 9, and 2 was gauged by fluorimetry to thoroughly substantiate the mechanism of cell death induced by G8-FKE-FA-Dox. Both G8-FKE-FA-Dox and the parent Dox were expected to exhibit the same or very similar caspase profiling pattern. Both HeLa and SKOV3 cells presented a significant ($p<0.001$) increase in the expression of caspases 9, 8, and 3, but the change was insignificant for A549 cells (Figure 3.9A). Caspase 3 was the most over expressed, with 2.4- and 2.2-fold increases in HeLa and SKOV3 cells, respectively, relative to their controls. The expression pattern of caspase 2 was unaltered in all the cell lines examined, and activation of caspases 8 and 9 revealed that G8-FKE-FA-Dox activates both intrinsic and extrinsic apoptotic pathways.

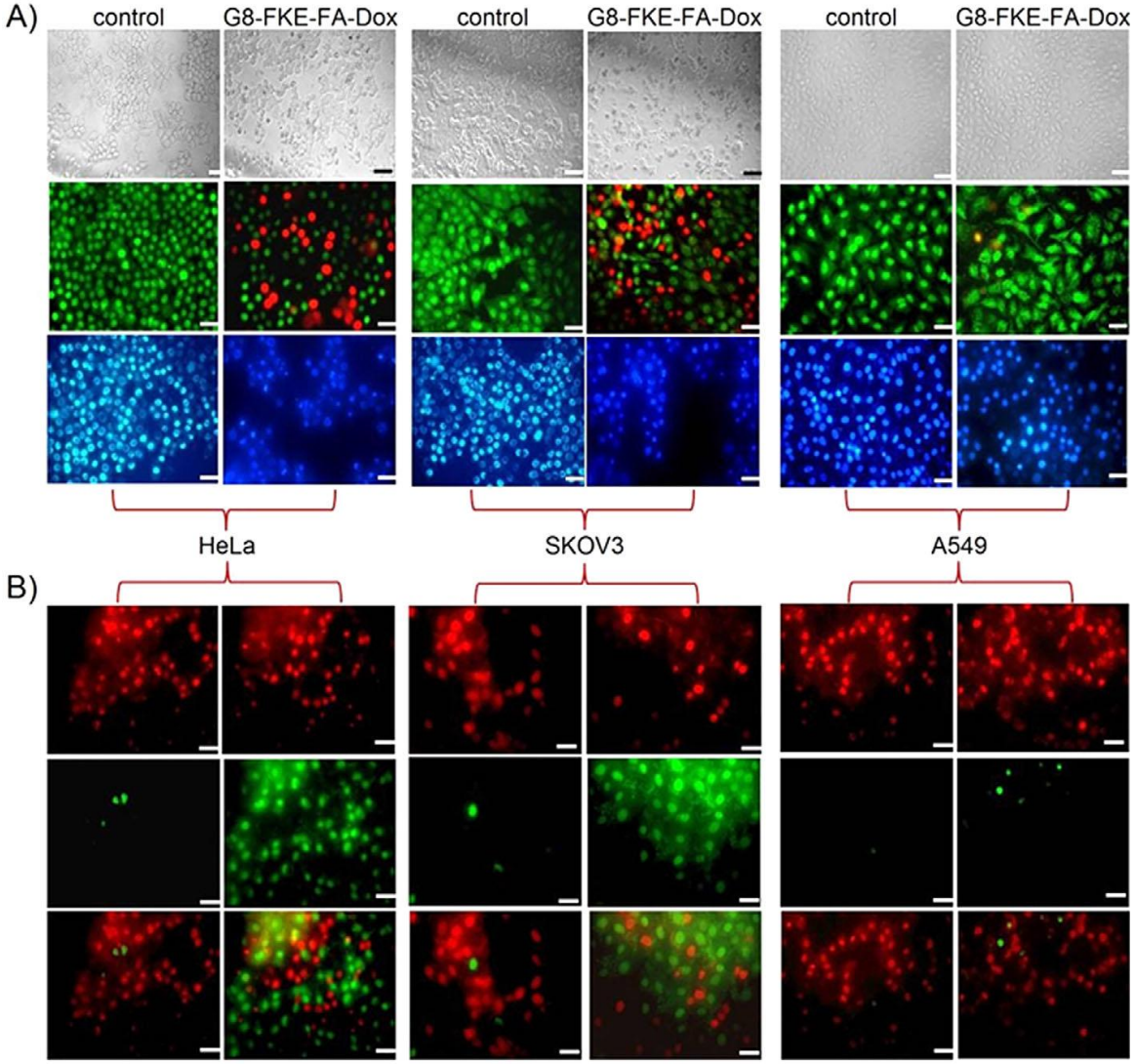

Figure 3.7. Evaluation of apoptosis after administration of G8-FKE-FA-Dox (1 mM) to HeLa, SKOV3, and A549 cells for 24 h. A) Upper row: phase contrast, middle row: acridine orange–ethidium bromide, lower row: Hoechst 33342 staining. B) Evaluation of apoptosis by TUNEL

staining assay; upper row: PI filter, middle row: FITC , lower row: merged images. Scale bar: 50 mM

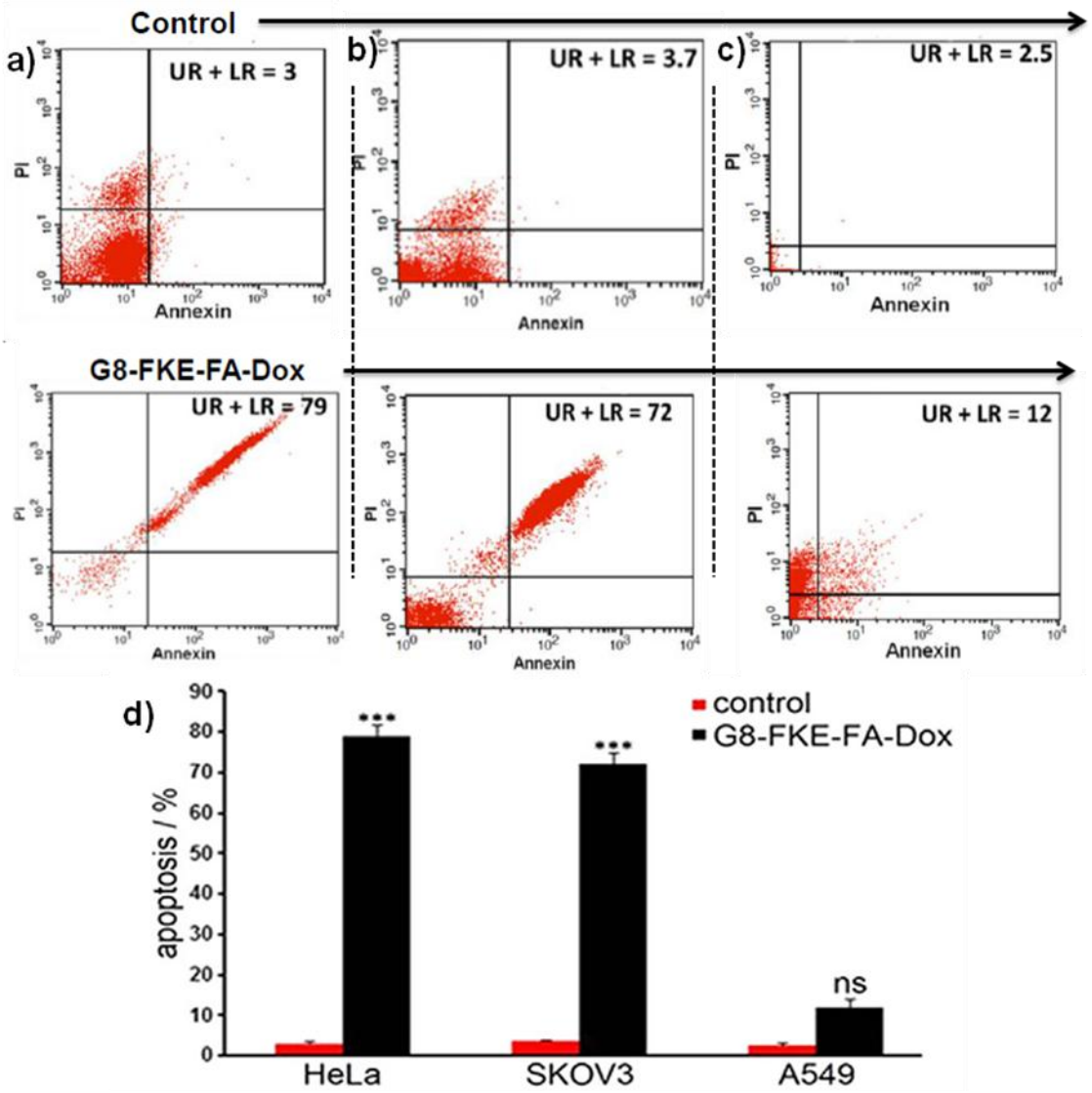

Figure 3.8. Morphological evaluation of apoptosis by the administration of G8-FKE-FA-Dox (1 μM) by Annexin V-FITC staining after 24 h on (A) HeLa, (B) SKOV3 and (C) A549 cells. D) Annexin V staining assay. Data are the mean SD of three independent experiments; ***p<0.001, ns: not significant relative to control.

3.3.6 Biodistribution studies

Finally, the tissue distributions of the carrier G8-FKE-FA-FL in normal and EAC-induced solid-tumor-bearing BALB/c mice were evaluated at various time intervals (4, 8, and 12 h). In the case of normal mice, blood (301.5%) and kidney (352.5%) showed maximum accumulation early on (4 h) and to a lesser extent in lungs (61%; Figure 3.9B). Intraperitoneal administration of G8-FKE-FA-FL to EAC-induced solid-tumor-bearing mice showed an interesting tissue distribution pattern, with an initial

distribution of 222.5, 201.9, and 183% in the tumor, blood, and kidney, respectively, at 4 h. After 8 h, the majority of the compound was found to be accumulated in the tumor area (383.4%) and kidney (203.2 %), with only 41.5% circulating in the bloodstream. Even after 12 h, 254.5% of the dose was gathered at the tumor site, with <81.8% in the kidney (Figure 3.9 C). Although tissue distribution was monitored for other organs such as thymus, stomach, and brain, the fluorescence signal was below measurable levels (data not shown).

The major limitations underlying the use of Dox are cardiotoxicity and hemotoxicity. Hemolysis experiments have clearly demonstrated the less toxic nature of G8-FKE-FA-Dox toward normal RBCs. The absence of G8-FKE-FA-FL accumulation in the heart ruled out the possibly of cardiotoxicity. Moreover, rapid clearance of the carrier within 12 h of administration in normal mice may facilitate the avoidance of systemic toxicity. Again, the high accumulation of carrier in the kidney is due to the high FR expression by renal tubular cells. It has been reported that the kidney has the highest concentration of FR expression on tubular epithelial cells,[32] and many FR-targeted drug delivery systems have shown renal accumulation and rapid clearance.[33] The efficiency of tumor targeting by TDDS was notable, particularly considering that the mice used in this study were fed a regular diet rather than a folate-free diet, which is usually necessary to increase the detection sensitivity of the FR-targeted delivery systems.[34]

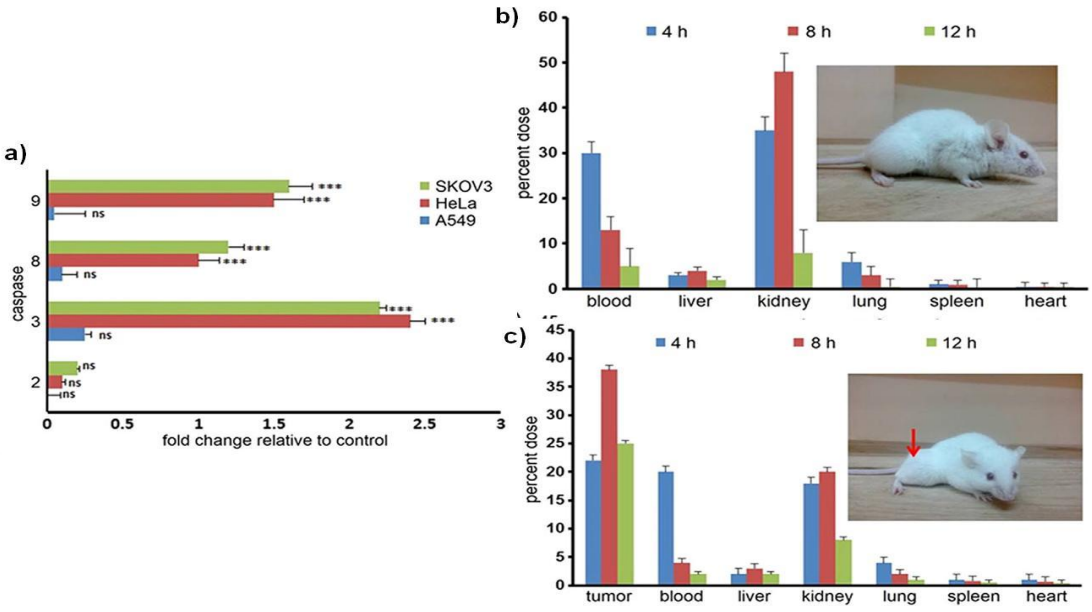

Figure 3.9. Caspase activity profiling and biodistribution analysis. A) Caspase activity related to apoptosis in cells treated with G8-FKE-FA-Dox (1 mM) for 24 h. Data are the mean

SD of three independent experiments; ***p<0.001, ns: not significant relative to control. In vivo biodistribution of G8-FKE-FA-Dox in B) normal and C) EAC solid-tumor-bearing mice; results are the mean SD of n=6 mice.

3.4 Conclusions

The TDDS outlined in this study, G8-FKE-FA-Dox, composed of an octa-guanidine-appended poly(propylene imine) dendron as transporter, showed a high degree of cellular uptake with efficient FR-targeting and intracellular lysosome-mediated delivery of Dox. G8-FKE-FA-Dox showed significant cytotoxicity via programmed cell death by activating both extrinsic and intrinsic caspase pathways, particularly on FR-overexpressing cancer cells, leaving normal and FR-negative cells unharmed. The IC_{50} values observed with G8-FKE-FA-Dox were superior to those of the clinically approved non-hemolytic LipodoxTM, and similar to those of free Dox, which is hemolytic to normal RBCs. The successful focused drug delivery observed with G8-FKE-FA-Dox could be due to its rapid FR-mediated cellular uptake and precise release of Dox triggered by lysosomal cath B activity. Assessment of the biodistribution in normal and FR-overexpressing EAC solid-tumor-bearing mice clearly illustrates the focused tumor-specific accumulation. Although further detailed investigations with this TDDS are warranted, the results of this study demonstrate the promise this system holds for further pre-clinical and clinical applications in cancer management.

3.5 Experimental Section

3.5.1 Chemical synthesis

All non-hydrolytic chemical reactions for the preparation of drug carrier constructs, unless otherwise indicated, were carried out in oven-dried glassware under an inert atmosphere of dry argon or nitrogen. Protected amino acids were purchased from Nova bio chem and SigmaAldrich. Doxorubicin Hydrochloride was obtained from Sigma Aldrich (St. Louis, MO, U.S.A.), Cathepsin B was acquired from Enzo life science. All the other chemicals and solvents werepurchased from Sigma Aldrich, Merk, and Specrochem and were used without further purification. Analytical TLC was performed on a Merck 60 F254 silica gel plate (0.25mM thickness), and visualization was done with UV light (254nm and 365nm), or by spraying with a 5% solution of phosphomolybdic acid or ninhydrine solution followed by charring with

a heat gun. Column chromatography was performed on Merck 60 silica gel (60-120 or 100-200 mesh).

HPLC was performed by Shimadzu HPLC system (Kyoto, Japan)consisting of SCL-10Avp system controller, two LC-8A solvent delivery units , SPD-M20A UV-vis photo diode array (PDA) detector, equipped with Multi PDA- LC solution software on a 250 mm x 4.6 mm i.d, 5µm, YMC-Pack R&D ODS analytical column (9YMC Co., Ltd. Japan). NMR spectra were recorded on a Bruker AMX 500 (1H-NMR at 500MHz; 13C-NMR at 125MHz) spectrometers (Falladen, Switzerland). Tetra methyl silane was used as reference for 1H NMR, and the chemical shift were reported in ppm and the coupling constant in Hz. High resolution mass spectra were determined on a HR-EMI analysis of Thermo Scientific Exactive system (Berman, Germany), and MALDI-TOF mass spectra on a Shimadzu Biotech, AXIMA-CFR PLUS system(Kyoto, Japan). Liophilization was performed with lyophilizer Tenesis Wizard 2(Germany)

3.5.1.1 Synthesis of compound 4

Rink amide resin (200mg, 0.142mmol) was swelled in dry dichloromethane (DCM). Then resin was washed with DMF (3×3mL) and the Fmoc protection group was removed by the treating with pipyridine in DMF (20%, 2×5mL, 2×25mins). The resin was again washed with DMF (3×3mL), Fmoc- Phe-OH (165mg, 0.426mmol) activated with HBTU (161mg, 0.426mmol), Di-isopropyl ethylamine (2 or 3 drops) were dissolved in DMF (7mL) and charged into the resin bed. The reaction was continued for 12 h under mechanical shaker. The progress of the reaction was monitored by Kaiser test. After completion of coupling the resin was washed with DMF (3×3mL) and Fmoc group was removed by the treatment with pipyridine in DMF as in the same manner. The reaction cycle was continued in the similar manner with Fmoc-Lys-(Boc)-OH (260mg, 0.426mmol) and Fmoc-Glu (OBn)-OH (195mg, 0.426mmol) amino acids were charged to the resin to yield **compound 3**. Finally peptide was released from the resin by treatment with 95% trifluro acetic acid, 2.5% triisopropyl silane, 2.5%(cleavage cocktail for Rink amide resin) water to yield compound **4**. **^{1}H NMR (500 MHz,$CDCl_3$):** 1.231, (2H), 1.514 (m, 2H), 1.625 (m, 2H), 2.340 (t, J=6Hz, 2H), 2.740 (t, 2H), 3.035 (t, J=6Hz, 2H), 3.659 (S, 2H), 4.125 (s, 3H), 4.310 (d, J=8Hz, 2H), 4.498 (m, 1H), 5.030(b, 2H), 7.053-7.880 (m, 18H); **HRMS/ESI** m/z calculated 733.3421,$C_{42}H_{47}N_5O_7$ and found m/z=734.5430 [M+H]+; Yield:67%.

3.5.1.2 Synthesis of compound 5 and 6

The Phe-Lys-Glu (compound **4**) peptide sequence , (20mg, 0.027mmol), EDC (10mg, 0.054mmol) and HOBt (7.36mg, 0.054mmol) were dissolved in dry DMF and stirred for 5 minutes under N_2 atmosphere. The folic acid (14.4mg, 0.033mmol) was added to the above mixture and kept for stirring for 36 hours at RT under N_2 atmosphere. The volatile components were removed and the residue was purified by silica gel column afforded yellow sticky solid **compound 5**. **HRMS/ESI** m/z calculated 1157.2413, $C_{61}H_{64}N_{12}O_{12}$ and found m/z =1180.8033 [M+Na]+; Yield:72%. Then the compound **5**(30 mg) was subjected to Fmoc deprotection using a solution of piperidine in DMF (20%, 2mL) and stirred for 30-45 minutes. The resulted mixture was concentrated to give yellow sticky product. **HRMS/ESI** m/z calculated 934.4053, $C_{46}H_{54}N_{12}O_{10}$ and found M/Z=935.5031 [M+H]+. G8-Boc -PPI (90mg, 0.031mmol), EDC (10.9mg, 0.057mmol) and HOBt (7.72mg, 0.057mmol) were added to Fmoc deprotected compound 5 (30mg, 0.029mmol) in dry DCM stirred for 36 hours at RT under N_2 atmosphere. The resulted mixture was concentrated to give crude product, which was then purified using column chromatography on silica gel to afford the product **6** as yellow sticky solid. **^{1}H NMR (500 MHz, $CDCl_3$):** 1.278 (m, 144 H), 1.334- 2.204 (m, 54 H), 2.401- 2.850 (m, 72 H), 3.037- 3.259 (m, 14 H), 4.035- 4.030(m, 6 H), 5.111- 5.372(b, 6 H), 6.850- 8.209 (m, 13 H).

3.5.1.3 Synthesis of Compound 2

The compound **6** was dissolved in distilled ethyl acetate to which Pd/C (catalytic amount) was carefully added along with a drop of CH3COOH, stirred for one and half hours at RT under H2 atmosphere. Pd/C was then removed by Celite column to yield **compound 7**.After the purification compound 7 (15mg, 0.004mmol), EDC (2mg, 0.008mmol), catalytic amount of DMAP were dissolved in dry DCM, stirred for 10 minutes. Then FLA (2mg, 0.005mmol) (FLA-preparation: Fluoroscein acid (50 mg,0.151 mmol) ,amino propanol (11.2mg,0.151mmol), EDC (58mg,0.302 m mol) and HO Bt (40mg,0.302mmol) were dissolved in dry DMF and stirred overnight in dark condition to give amino propanol linked fluorescein (FLA)) was added to the mixture and stirred in dark condition under N2 atmosphere for 36 hrs. The resulted mixture is concentrated and purified to yield product **8**. **^{1}H NMR** (**500 MHz**, $CDCl_3$)**:** 1.283 (m, 144H), 1.301-2.204 (m, 54H), 2.301-2.750 (m, 72H), 3.037-3.259 (m,

14H), 4.035-4.030 (m, 6H), 5.111-5.372 (b, 6H), 6.530-8.209 (m, 20H).Yield =72%. Ethyl acetate (4ml) saturated with gaseous HCl was added to a solution of 8 in ethyl acetate (1ml). The reaction mixture was stirred for 4h then the solution was concentrated and the residue was washed with ethyl acetate to remove less polar impurities. The residue was dried and purified by using MPLC on supelclean LC-18 reverse-phase silica gel (ACN/H2O). The purified product was then done HPLC and then dissolved in de-ionized water yielding product 2. **^{1}H NMR (500 MHz, CD_3OD):** 1.296 (m, 144H), 1.311- 2.371(m, 54H), 2.323-2.843(m, 72H), 3.162-3.684 (m, 14H), 4.214-4.322 (m, 6H), 5.136 (b, 6H), 7.276-8.017 (m, 15H).Yield=67%. MALDI –TOF –MS m/z calculated $C1_{19}H_{191}N_{43}O_{15}$, 2462.5521 found 2463.5720 [M+H]+

3.5.1.4 Synthesis of Compound 1

Compound 7 (5.4mg, 0.0014mmol), EDC (0.418mg, 0.0022 mmol) and N-Hydroxysuccinimide (0.251mg, 0.0022mmol) were dissolved in dry DMF and stirred for 10 minutes. Then Doxorubicin (0.791mg, 0.0014mmol) was added to it and stirred in dark condition for 36 hours at RT under N2 atmosphere. The resulted mixture was concentrated to give crude product as orange solid. **^{1}H NMR**(**500 MHz** , $CDCl_3$):1.196 (s,3H), 1.407 (s,144H),1.421-1.681(m, 56H), 2.045-2.849 (m,76H), 3.204-3.658(m,14H), 4.104-4.416 (m,6H),5.115(br,s,2H), 7.276-7.831(m,10H), 8.008 (br, s, 8H), 8.685 (s, 1H).Yield=65%, Ethyl acetate (4ml) saturated with gaseous HCl was added to a solution of 6 in ethyl acetate (1ml). The reaction mixture was stirred for 4h then the solution was concentrated and the residue was washed with ethyl acetate to remove less polar impurities. The residue was dried and purified by using MPLC on supelclean LC-18 reverse-phase silica gel (MeOH /H2O). The purified product was then done HPLC and then dissolved in de-ionised water yielding compound 1. **^{1}H NMR(500 MHz , CD_3OD)**:1.196 (s, 3H), 1.407 (s, 144H),1.421-1.681(m, 56H), 2.045-2.849 (m, 76H), 3.204-3.658 (m, 14H), 4.104 -4.416 (m, 6H),5.115 (br, s, 2H), 7.276-7.831(m, 10H), 8.008 (br, s, 8H), 8.685(s, 1H).Yield=65%. MALDI –TOF –MS m/z calculated $C_{123}H_{201}N_{43}O_{21}$, 2616.5981 found 2617.7232 [M+H]+

3.5.1.5 HPLC measurements

The HPLC analysis was conducted using Shimadzu RP- HPLC ODS column with mobile phase consisting of in MeOH (A) and in H2O (B).The gradient was linearly

increased from 0% to 80% B for 35 minutes at the flow rate of 1mL/min at ambient temperature. UV-VIS detection was monitored simultaneously at 254nm and 480nm wavelengths

3.5.1.6 *In vitro* stability by HPLC

To evaluate the stability of G8-FKE-FA-Dox in blood circulation, we have dispersed the TDDS in PBS (pH=7.4) containing 10% fetal bovine serum (FBS) and incubated at 370C, and checked HPLC at different intervals of time. The result indicates that there is no significant drug degradation providing possibility of enhancing drug accumulation in tumour tissue

3.5.2 Biological studies

3.5.2.1 Cell Culture

The human cancer cell lines HeLa (cervical cancer), MCF-7 (breast cancer), and A549 (lung adenocarcinoma) were obtained from American Type Culture Collection (ATCC, Manassas, VA, USA). SKOV3 (ovarian cancer) cells were generously provided by the Rajiv Gandhi Centre for Biotechnology (RGCB, Thiruvananthapuram, India). A375 (malignant melanoma) cells were obtained from NCCS (Pune, India). The fibroblast-like murine pre-adipocyte cell line 3T3L1 was obtained from the Inter-University Centre for Genomics and Gene Technology, University of Kerala (Thiruvananthapuram, India). Cells were maintained in DMEM with 10% FBS and under an atmosphere of 5% CO2 at 37 8C. The murine transplantable lymphoma cell lines, Ehrlich ascites carcinoma (EAC) and Daltons lymphoma ascites (DLA) were maintained in the peritoneal cavity of mice by intraperitoneal transplantation of $1X10^6$ cells per mouse. Animal experimentation protocols were reviewed and approved by the Institutional Animal Ethics Committee (IAEC) of the Regional Cancer Centre (Trivandrum, India).For biological studies 2-[4-(2-hydroxyethyl) piperazin-1-yl] ethanesulfonic acid (HEPES) was purchased from Himedia (Mumbai, India). 3-(4, 5-dimethylthiazol-2-yl)-2, 5-diphenyltetrazolium bromide (MTT), Dulbecco's modified eagle's medium (DMEM), trypsin- EDTA and dimethylsulfoxide (DMSO) for cell culture solution were purchased from Sigma Aldrich. Liposomal nano-formulation of doxorubicin (Lipodox) was generously gifted by Sun Pharma Advanced Research Company Ltd.(SPARC Ltd), Vadodara, Gujarat, INDIA.Penicillin-Streptomycin, neutravidin, alexafluor 568-carboxylic acid succinimidyl ester, fetal

bovine serum (FBS) and Mito Tracker red CMX Ros were purchased from Invitrogen (Merelbeke, Belgium). Annexin V-FITC apoptosis detection kit was purchased fromBD Pharmingen (#556547, BD Biosciences, San Jose, CA) and TUNEL assay kit from Promega, USA. Caspase assay was performed with ApoAlert ™ Caspase Profiling kit (Clontech, CA, USA). Bisbenzimide H 33258 (Hoechst) was purchased from Calbio chem (San Diego, CA, USA) and Lyso Tracker Deep Red was purchased from Molecular probes Life technologies.

3.5.2.2 Western blots

Proteins were extracted from 2X106 cells per petri dish using Pierce RIPA buffer (Thermo Scientific, Rockford, IL, USA). Protein concentrations were determined using Coomassie Plus protein assay reagent and bovine serum albumin (BSA) standards (Pierce, Rockford, IL, USA). Proteins (~50 mg) were separated by 10% SDS-PAGE and transferred to polyvinylidene difluoride (PVDF) membranes (Millipore, Billerica, MA, USA). Membranes were blocked with 5% BSA (Santa Cruz Biotechnology Inc., TX, USA) and incubated with the specific primary antibodies. The primary antibodies FOLR2 (folate receptor b) and b-actin were purchased from Sigma–Aldrich (St. Louis, MO, USA). Alkaline phosphatase conjugated secondary antibody (Sigma–Aldrich) was used for all primary antibodies and detected by the colorimetric substrate BCIP®/NBT (Sigma–Aldrich). The resulting bands were then quantitated using Image J software (version 1.48, NIH, USA) and normalized with β-actin.

3.5.2.3 Hemolysis assays:

The effect of constructs on normal red blood cells (RBCs) was evaluated by hemolysis assay as per previously reported protocols[35] with minor modifications. Briefly, EDTA-stabilized human blood samples were centrifuged at 700 g for 5 min, and blood plasma and the surface layer were removed. The remaining RBC pellet was washed with PBS (3–4X6 mL), and RBCs were diluted in 25 mL PBS. Test compounds at various concentrations in PBS (0.8 mL) were then added to RBC suspension (0.2 mL). Positive and negative control samples were also prepared by adding 0.8 mL 2% Triton X-100 and PBS, respectively, to 0.2 mL RBC solution. Samples were then incubated at room temperature for 2 h, shaken once every 30 min to resuspend the RBCs and compounds. After 2 h, the samples were centrifuged

at 700 g, and supernatants (100 mL) were transferred to a 96-well plate. Absorbance of hemoglobin in supernatants was measured with a microplate reader at λ 570 nm. Percent RBC hemolysis was calculated with the following formula [Eq. (1)]:

$$\text{Hemolysis } [\%] = \left(\frac{A_{\text{sample}} - A_{\text{negative control}}}{A_{\text{positive control}} - A_{\text{negative control}}} \right) \times 100 \qquad (1)$$

The experiments were performed after obtaining approval from the Human Ethical Committee, RCC, Trivandrum (India). Percent hemolysis values were calculated from three separate experiments.

3.5.2.4 Cytotoxicity assays: The growth inhibitory capacity of various constructs was evaluated by 3-(4,5-dimethylthiazol-2-yl)-2,5-diphenyltetrazolium bromide (MTT) assay as previously reported.[36] The absorbance was measured at λ 570 nm using a microplate spectrophotometer (BioTek, Power Wave XS) after incubation for 12, 24, and 48 h with test compounds. The percentage cell proliferation and growth inhibition were calculated with the following formulas [Eq. (2) and (3)]:

$$\text{Proliferation } [\%] = (A_{\text{sample}} / A_{\text{control}}) \times 100 \qquad (2)$$

$$\text{Inhibition } [\%] = 100 - \% \text{ Proliferation} \qquad (3)$$

Evaluation of the effect of folic acid on the growth inhibitory capacity of the constructs was also carried out by MTT assay after the addition of 2 mm folic acid to the medium for 2 h as reported.[37]

3.5.2.5 Internalization assays:

The cellular uptake efficiency, cell-line-specific, and organelle-specific localization of the transporter G8-FKEFA- FL as well as Dox-releasing efficacy of G8-FKE-FA-Dox were evaluated by confocal microscopy and flow cytometry

3.5.2.5.1 Cellular uptake and lysosomal targeting study

Cell internalization of G8-FKE-FA-FL was monitored by confocal microscopy with nuclear staining or LysoTracker™. HeLa cells were seeded in a covered glass bottom dish for 24 h and then incubated with G8-FKEFA-FL (20 mm) for up to 4 h. Cells were then washed with PBS and stained with either Hoechst 33258 for nuclei or 100

nm LysoTracker™ Red for lysosomes and incubated for 15–30 min. Imaging was performed with an Andor spinning disc confocal microscope with a 60X objective (Olympus) and an Andor iXon3 897 EMCCD camera at λ 405, 488, and 561 nm.

3.5.2.6 DOX release studies by confocal microscopy:

HeLa cells were seeded overnight in a covered glass-bottom dish, followed by incubation with G8-FKE-FA-Dox for 4 h. Cells were then fixed with formaldehyde and counter-stained with Hoechst 33258 to stain the nuclei. Imaging was performed with an Andor spinning disc confocal microscope with a 60X objective (Olympus) and an Andor iXon3 897 EMCCD camera at λ 405 and 561 nm.

3.5.2.7 Flow cytometric analysis of HeLa and A549 cell uptake of G8- FKE-FA-FL and G8-FKE-FA-Dox

Cells (1–5X105) were taken into suspension and incubated with 200 mL serum-free DMEM containing G8-FKE-FA-Dox at 20 mm for up to 4 h. Then cells were then washed with a sufficient quantity of 1X PBS via centrifugation at 800 g for 5 min. Cell pellets were washed again with 1X PBS via the same centrifugation protocol and then resuspended in 500 mL serum-free DMEM. Fluorescence analysis was performed with a FACS instrument (BD LSRFortessa) using FITC channels and emission filters at λ 530 nm. Similarly, Dox uptake in both HeLa and A549 cell lines was performed using the above-mentioned flow cytometric method. Here, cells were treated with 2 mm Dox for 4 h, and Dox release was quantified with respect to untreated controls. Fluorescence analysis (BD LSRFortessa) was carried out with PE channels and emission filters at λ 561 nm.

3.5.2.8 Apoptosis assays

Evaluation of the mode of cytotoxicity exhibited by the compounds was performed with various apoptosis assays[38]after administration of 1 mm G8-FKE-FA-Dox for 24 h. Morphological evaluation for apoptotic changes were performed by phase contrast microscopy under suitable magnification. Observation of nuclei for any changes was done with Hoechst 33342 staining, and cells were observed under an inverted fluorescence microscope using a DAPI filter (Olympus 1X51, Singapore). Assessment of apoptosis using the acridine orange–ethidium bromide dual-staining procedure was performed as described earlier. Cells were observed under an

inverted fluorescence microscope using a FITC filter (Olympus 1X51, Singapore) to view apoptotic or non-apoptotic cells. Furthermore, a TUNEL assay (DeadEnd™ fluorimetric TUNEL system, G3250, Promega, USA) was used to detect the incorporation of fluorescein-12–dUTP in the fragmented DNA of apoptotic cells, using the terminal deoxynucleotidyltransferase recombinant (rTdT) enzyme as per the manufacturer's instructions, using propidium iodide as counter-stain. Additionally, the evaluation of apoptosis by FITC–Annexin V staining (FITC–Annexin V apoptosis detection kit, BD Pharmingen #556547, BD Biosciences, San Jose, CA, USA) was also confirmed by flow cytometry, using kit-specified instructions. Signals were then detected using a FACSCalibur flow cytometer (BD Biosciences), and data were analyzed by Cell Quest Pro software (version 5.1).

3.5.2.9 Caspase assays:

The effect of both initiator caspases (caspases 8, 9, and 2) and executioner caspases (caspase 3) was determined by using Apo AlertTM Caspase Profiling kit (Clontech, CA, USA) as per the manufacturer's protocol. Cells were treated with 1 mm G8-FKEFA- Dox for 24 h, and samples were transferred to 96-well plates for fluorimetric reading (λ ex 380 nm, λ em 460 nm), and signals were recorded by spectrofluorimetry (FLx800, BioTek).

3.5.2.10 Biodistribution studies

BALB/c mice (5–6 weeks old) were used to probe the biodistribution pattern of our TDDS as described earlier.[39] The mice were maintained in well-ventilated cages with normal mouse chow and water available ad libitum. Mice were acclimatized for 1–2 weeks prior to all experiments. The temperature was maintained at 252 8C with a humidity of 505%, and the illumination cycle was set to 12 h light and 12 h dark. All animal experiments were reviewed and approved by the Institutional Animal Ethics Committee (IAEC) and the Committee for the Purpose of Control and Supervision of Experiments on Animals (CPCSEA), India. EAC cells were collected from the donor mouse, suspended in sterile isotonic saline, and viable cells were counted and adjusted to a concentration so that each animal receives $1X10^6$ cells per 100 mL intraperitoneal (i.p.) injection. For the development of solid tumors, viable EAC cells ($1X10^6$ cells per mouse) were injected subcutaneously into the hind limb with a very fine needle (31G). Each group consisted of six animals. To estimate the distribution

pattern, G8-FKE-FA-FL was administered i.p. to the animals, who were later sacrificed by cervical dislocation. Blood, tumor, and internal organs were collected at various intervals for further evaluation. Saline (0.9%) was added to each tissue by a threefold volume to its weight, homogenized and centrifuged at 900 g for 10 min. Supernatants were examined for fluorescence intensity using a spectro fluorimeter (FLx800, BioTek, USA) with excitation and emission wavelengths of 485 and 528 nm, respectively. For the negative control and normalization, normal tissues from control animals were used. The FITC concentration in each sample was determined from the net fluorescence intensity obtained by comparison with the standard curve. The initial dose administered was set at 100%.

3.5.2.11 Statistical analysis: The data are expressed as the mean standard deviation (SD) of three replicates and were analyzed by using GraphPad Prism software version 5.0 (Graph Pad, La Jolla, CA, USA). One-way analysis of variance (ANOVA) was used for the repeated measurements, and differences were considered to be statistically significant if $p<0.05$. IC_{50} values were calculated with Easy Plot software (version 2.8, Spiral Software, MD, USA).

3.6 References

(1) Siegel, R. L.; Miller, K. D.; Jemal, A. Cancer Statistics. *CA Cancer J Clin* **2016**, *66* (1), 7–30.

(2) Zhao, Z.; Meng, H.; Wang, N.; Donovan, M. J.; Fu, T.; You, M.; Chen, Z.; Zhang, X.; Tan, W. A Controlled-Release Nanocarrier with Extracellular pH Value Driven Tumor Targeting and Translocation for Drug Delivery. *Angew. Chem. Int. Ed. Engl.* **2013**, *52* (29), 7487–7491.

(3) Sun, T.; Zhang, Y. S.; Pang, B.; Hyun, D. C.; Yang, M.; Xia, Y. Engineered Nanoparticles for Drug Delivery in Cancer Therapy. *Angew. Chemie Int. Ed.* **2014**, *53* (46), 12320–12364.

(4) Remesh, A. Toxicities of Anticancer Drugs and Its Management. *Int. J. Basic Clin. Pharmacol.* **2012**, *1* (1), 2.

(5) Yokochi, T.; Robertson, K. D. Doxorubicin Inhibits DNMT1, Resulting in Conditional Apoptosis. *Mol. Pharmacol.* **2004**, *66* (6), 1415–1420.

(6) Albini, A.; Sporn, M. B. The Tumour Microenvironment as a Target for Chemoprevention. *Nat. Rev. Cancer* **2007**, *7* (2), 139–147.

(7) Pan, H.; Grow, M. E.; Wilson, O.; Daniel, M.-C. A New Poly(propylene Imine) Dendron as Potential Convenient Building-Block in the Construction of Multifunctional Systems. *Tetrahedron* **2013**, *69* (13), 2799–2806.

(8) Bosslet, K.; Straub, R.; Blumrich, M.; Czech, J.; Gerken, M.; Sperker, B.; Kroemer, H. K.; Gesson, J. P.; Koch, M.; Monneret, C. Elucidation of the Mechanism Enabling Tumor Selective Prodrug Monotherapy. *Cancer Res.* **1998**, *58* (6), 1195–1201.

(9) Danhier, F.; Ansorena, E.; Silva, J. M.; Coco, R.; Le Breton, A.; Préat, V. PLGA-Based Nanoparticles: An Overview of Biomedical Applications. *J. Control. Release* **2012**, *161* (2), 505–522.

(10) Pisano, C.; Cecere, S. C.; Di Napoli, M.; Cavaliere, C.; Tambaro, R.; Facchini, G.; Scaffa, C.; Losito, S.; Pizzolorusso, A.; Pignata, S. Clinical Trials with Pegylated Liposomal Doxorubicin in the Treatment of Ovarian Cancer. *J. Drug Deliv.* **2013**, *2013*, 898146.

(11) Nayak, S.; Lee, H.; Chmielewski, J.; Lyon, L. A. Folate-Mediated Cell Targeting and Cytotoxicity Using Thermoresponsive Microgels. *J. Am. Chem. Soc.* **2004**, *126* (33), 10258–10259.

(12) El-Gogary, R. I.; Rubio, N.; Wang, J. T. W.; Al-Jamal, W. T.; Bourgognon, M.; Kafa, H.; Naeem, M.; Klippstein, R.; Abbate, V.; Leroux, F.; Bals, S.; Van Tendeloo, G.; Kamel, A. O.; Awad, G. a S.; Mortada, N. D.; Al-Jamal, K. T. Polyethylene Glycol Conjugated Polymeric Nanocapsules for Targeted Delivery of Quercetin to Folate-Expressing Cancer Cells in Vitro and in Vivo. *ACS Nano* **2014**, *8* (2), 1384–1401.

(13) Lee, R. J.; Low, P. S. Folate-Mediated Tumor-Cell Targeting of Liposome-Entrapped Doxorubicin in-Vitro. *Biochim. Biophys. Acta-Biomembranes* **1995**, *1233* (2), 134–144.

(14) Zwicke, G. L.; Ali Mansoori, G.; Jeffery, C. J. Utilizing the Folate Receptor for Active Targeting of Cancer Nanotherapeutics. *Nano Rev.* **2012**, *3* (1), 18496.

(15) Christinat, a; Leyvraz, S. Oncotargets and Therapy. *Role trabectedin Treat. soft tissue sarcoma* **2009**, *2*, 105–113.

(16) Dubowchik, G. M.; Firestone, R. A.; Padilla, L.; Willner, D.; Hofstead, S. J.; Mosure, K.; Knipe, J. O.; Lasch, S. J.; Trail, P. A. Cathepsin B-Labile Dipeptide Linkers for Lysosomal Release of Doxorubicin from Internalizing

Immunoconjugates: Model Studies of Enzymatic Drug Release and Antigen-Specific In Vitro Anticancer Activity. *Bioconjug. Chem.* **2002**, *13* (4), 855–869.

(17) Giusti, I.; D'Ascenzo, S.; Millimaggi, D.; Taraboletti, G.; Carta, G.; Franceschini, N.; Pavan, A.; Dolo, V. Cathepsin B Mediates the pH-Dependent Proinvasive Activity of Tumor-Shed Microvesicles. *Neoplasia* **2008**, *10* (5), 481–488.

(18) Stanzl, E. G.; Trantow, B. M.; Vargas, J. R.; Wender, P. A. Fifteen Years of Cell-Penetrating, Guanidinium-Rich Molecular Transporters: Basic Science, Research Tools, and Clinical Applications. *Acc. Chem. Res.* **2013**, *46* (12), 2944–2954.

(19) Maiti, K. K.; Jeon, O.-Y.; Lee, W. S.; Chung, S.-K. Design, Synthesis, and Delivery Properties of Novel Guanidine-Containing Molecular Transporters Built on Dimeric Inositol Scaffolds. *Chem. Eur. J.* **2007**, *13* (3), 762–775.

(20) Maiti, K. K.; Jeon, O.-Y.; Lee, W. S.; Kim, D.-C.; Kim, K.-T.; Takeuchi, T.; Futaki, S.; Chung, S.-K. Design, Synthesis, and Membrane-Translocation Studies of Inositol-Based Transporters. *Angew. Chem. Int. Ed. Engl.* **2006**, *45* (18), 2907–2912.

(21) Maiti, K. K.; Lee, W. S.; Takeuchi, T.; Watkins, C.; Fretz, M.; Kim, D.-C.; Futaki, S.; Jones, A.; Kim, K.-T.; Chung, S.-K. Guanidine-Containing Molecular Transporters: Sorbitol-Based Transporters Show High Intracellular Selectivity toward Mitochondria. *Angew. Chem. Int. Ed. Engl.* **2007**, *46* (31), 5880–5884.

(22) Maniganda, S.; Sankar, V.; Nair, J. B.; Raghu, K. G.; Maiti, K. K. A Lysosome-Targeted Drug Delivery System Based on Sorbitol Backbone towards Efficient Cancer Therapy. *Org. Biomol. Chem.* **2014**, *12* (34), 6564–6569.

(23) Nair, J. B.; Mohapatra, S.; Ghosh, S.; Maiti, K. K. Novel Lysosome Targeted Molecular Transporter Built on a Guanidinium-Poly-(Propylene Imine) Hybrid Dendron for Efficient Delivery of Doxorubicin into Cancer Cells. *Chem. Commun.* **2015**, *51* (12), 2403–2406.

(24) Elnakat, H.; Ratnam, M. Distribution, Functionality and Gene Regulation of Folate Receptor Isoforms: Implications in Targeted Therapy. *Adv. Drug Deliv. Rev.* **2004**, *56* (8), 1067–1084.

(25) Santra, S.; Perez, J. M. Selective N -Alkylation of β-Alanine Facilitates the Synthesis of a Poly(amino Acid)-Based Theranostic Nanoagent. *Biomacromolecules* **2011**, *12* (11), 3917–3927.

(26) Sen, S.; Erba, E.; D'Incalci, M.; Bottero, F.; Canevari, S.; Tomassetti, a. Role of Membrane Folate-Binding Protein in the Cytotoxicity of 5,10-Dideazatetrahydrofolic Acid in Human Ovarian Carcinoma Cell Lines in Vitro. *Br. J. Cancer* **1996**, *73* (4), 525–530.

(27) Fais, S.; Venturi, G.; Gatenby, B. Microenvironmental Acidosis in Carcinogenesis and Metastases: New Strategies in Prevention and Therapy. *Cancer Metastasis Rev.* **2014**, *33* (4), 1095–1108.

(28) Se-woon Choea, David S. Termanb, Angela E. Riversc, Jose Riverad, R. L.; Sorg, and B. S. Drug-Loaded Sickle Cells Programmed Ex Vivo for Delayed Hemolysis Target Hypoxic Tumor Microvessels and Augment Tumor Drug Delivery. *J Control Release* **2014**, *171* (2), 184–192.

(29) Bar, H.; Yacoby, I.; Benhar, I. Killing Cancer Cells by Targeted Drug-Carrying Phage Nanomedicines. *BMC Biotechnol.* **2008**, *8* (37), 1–14.

(30) Kamimura, M.; Kim, J. O.; Kabanov, A. V.; Bronich, T. K.; Nagasaki, Y. Block Ionomer Complexes of PEG-Block-poly(4-Vinylbenzylphosphonate) and Cationic Surfactants as Highly Stable, pH Responsive Drug Delivery System. *J. Control. Release* **2012**, *160* (3), 486–494.

(31) Vaculova, A.; Kaminskyy, V.; Jalalvand, E.; Surova, O.; Zhivotovsky, B. Doxorubicin and Etoposide Sensitize Small Cell Lung Carcinoma Cells Expressing Caspase-8 to TRAIL. *Mol. Cancer* **2010**, *9*, 87.

(32) Gautam, N.; Puligujja, P.; Balkundi, S.; Thakare, R.; Liu, X.; Fox, H. S.; Mcmillan, J. Pharmacokinetics, Biodistribution, and Toxicity of Folic Acid-Coated Antiretroviral Nanoformulations. *Antimicrob. Agents Chemother.* **2014**, *58* (12), 7510–7519.

(33) Leamon, C. P.; Parker, M. a; Vlahov, I. R.; Xu, L.; Reddy, J. a; Vetzel, M.; Douglas, N. Synthesis and Biological Evaluation of EC20 : A New Folate-Derived , 99m Tc-Based Radiopharmaceutical. *Bioconj. Chem.* **2002**, *13* (ii), 1200–1210.

(34) Gravier, J.; Schneider, R.; Frochot, C.; Bastogne, T.; Schmitt, F.; Didelon, J.; Guillemin, F.; Barberi-Heyob, M. Improvement of Meta-Tetra(hydroxyphenyl)chlorin-like Photosensitizer Selectivity with Folate-Based Targeted Delivery. Synthesis and in Vivo Delivery Studies. *J. Med. Chem.* **2008**, *51* (13), 3867–3877.

(35) Dobrovolskaia, M. a.; Clogston, J. D.; Neun, B. W.; Hall, J. B.; Patri, A. K.; McNeil,

S. E. Method for Analysis of Nanoparticle Hemolytic Properties in Vitro. *Nano Lett.* **2008**, *8* (8), 2180–2187.

(36) Joseph, M. M.; Aravind, S. R.; Varghese, S.; Mini, S.; Sreelekha, T. T. Evaluation of Antioxidant, Antitumor and Immunomodulatory Properties of Polysaccharide Isolated from Fruit Rind of Punica Granatum. *Mol. Med. Rep.* **2012**, *5* (2), 489–496.

(37) Yoo, H. S.; Park, T. G. Folate-Receptor-Targeted Delivery of Doxorubicin Nano-Aggregates Stabilized by Doxorubicin-PEG-Folate Conjugate. *J. Control. Release* **2004**, *100* (2), 247–256.

(38) Joseph, M. M.; Aravind, S. R.; Varghese, S.; Mini, S.; Sreelekha, T. T. PST-Gold Nanoparticle as an Effective Anticancer Agent with Immunomodulatory Properties. *Colloids Surfaces B Biointerfaces* **2013**, *104*, 32–39.

(39) Joseph, M. M.; Aravind, S. R.; George, S. K.; Raveendran Pillai, K.; Mini, S.; Sreelekha, T. T. Galactoxyloglucan-Modified Nanocarriers of Doxorubicin for Improved Tumor-Targeted Drug Delivery with Minimal Toxicity. *J. Biomed. Nanotechnol.* **2014**, *10* (11), 3253–3268.

Chapter 4

Molecular Transporter Fabricated on Octa-Guanidium Sorbitol Scaffold Facilitates SERS Guided Dual Targeted Paclitaxel Delivery into Glioblastoma

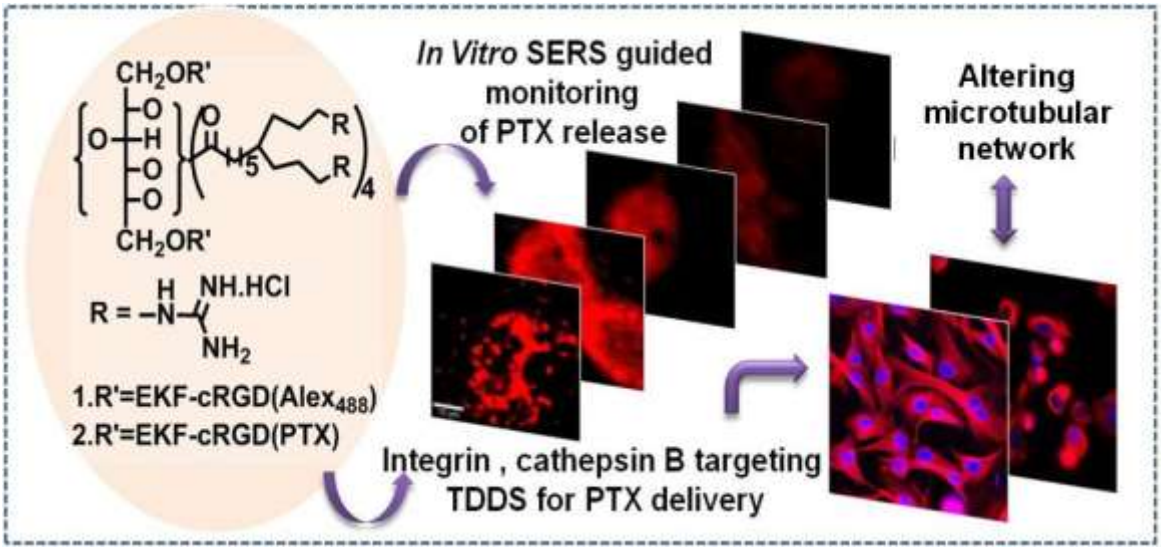

4.1 Abstract: *Target specific small peptide substrates were revamped on octa-guanidine-sorbitol (OG-S) scaffold to be termed as small molecular targeted drug delivery conjugate (SMTDDC). The carefully fabricated SMTDDC withdual targeting motifs altered the microtubule network of glioblastoma cells by the orchestrated release of cytotoxic drugpaclitaxel (PTX). The synthesized dual targeted SMTDDC altering the microtubular network of glioblastoma by the cumulative release of cytotoxic agent paclitaxel (PTX). Enzymatic reaction driven PTX delivery in presence of cathepsin B was monitored by high performance liquid chromatography (HPLC) and surface enhanced Raman scattering (SERS) spectral fingerprints. Moreover, intracellular drug release was illustrated with the aid of confocal Raman microscopy. The time dependent SERS fingerprinting and imaging revealed an accurate monitoring of cellular internalization as well as release of the PTX*

enabling profound cytotoxic profile, apoptosis and more precisely reducing microtubule networking in intracellular milieu. Furthermore the SMTDDC showed significant stability, biocompatibility to red blood cells and lymphocytes. Hence a small peptide-triggered OG-S appended PTX was able to (i) eradicate efficiently glioblastoma cells compared to free drug; (ii) enhance pharmacokinetic and pharmacodynamic properties, improve efficacy and safety profiles and allows for controlled drug release. The present investigation emphasizes on peptidomimectic sorbitol molecular transported enabling a great promise for further development of PTX delivery into glioblastoma towards clinical translation.

4.2 Introduction

Despite the immense progress made in the field of translational and clinical research, treatment of glioblastoma multiforme (GBM) still poses a great challenge in cancer therapy.[1] Although chemotherapy serves as one of the front line treatment options for cancer management, it is not an ideal candidate for treating glioblastoma[2] due to the inability of drugs to penetrate physiological barriers including blood–brain barrier (BBB)[3] and blood tumour barrier (BTB)[4]. To address these limitations, target specific delivery of anticancer drugs[5,6] has taken up in frontier drug delivery research by pharma and biotech industries. One of the attractive strategies for achieving this goal is to synthesis a stable ligand specific carriers either synthetic or nano-carriers having better biocompatibility under physiological condition and capable to promote moderate release profile of the cargo at the site of action[7]. In recent studies synthetic carriers built on sorbitol[8,9] and poly (propylene imine) dendron[10] scaffolds appended to octa-guanidium[7,11] motif exhibited excellent cellular internalization properties at par with the well known cell penetrating agents, viz Arg-8-mer[12] and Tat (49-57)[13] sequence. Molecular carrier having sorbitol backbone showed superior translocation across the cell membrane, mitochondria and blood brain barrier. An efficient class of adhesion receptors represents the integrins[14] ($\alpha_V\beta_3$, $\alpha_V\beta_5$), which evolved one of the key targets in cancer cells (viz., U-87MG cells), and are over expressed on tumour neovasculture and glioblastoma.[15]In addition, tumour-associated enzymes like matrix metallo proteases (MMP), cathepsin B (Cath B) are recognized as a trigger for specific prodrug activation with selective release of drug at the target site. The lysosomal cysteine

protease[16] cath B is one of the multiple proteases associated with tumour progression and elevated in malignant tumours including brain tumour[17]. Efficient release of drug at the tumour site can be achieved by tethering extracellular and intracellular target in a single synthetic construct[18] .

One of the most extensively used anticancer drug paclitaxel[19] (PTX) has been widely explored for its clinical efficacy against a wide variety of solid tumours such as breast[20,21], ovarian[22], non-small cell lung carcinoma (NSCLC)[23] and melanoma[24]. PTX, a well-known microtubule stabilizing agent binds to microtubules, stabilizes and blocks their dynamics, there by disrupting cell division[23]. A limited number of studies showed the potential of PTX to treat GBM[25–27], but there are few concerns restricts its use in brain tumour. In the present chapter, a synthetic PTX appended octa-guanidium-sorbitol (OG-S) framework has been introduced with dual targeting ligand viz. cath B, EKF (Glu-Lys-Phe) and a specific peptide substrate for lysosomal cysteine protease and a cyclic peptide (cRGD) targeting integrins as a tumour-homing motif appended to the OG-S framework (scheme1). PTX conjugate for glioblastoma therapy is named SMTDDC i.e, EKF-cRGD-PTX-OG-S (scheme 2) where as the control construct named as small molecule targeted delivery conjugate (SMC): EKF- cRGD -$Alex_{488}$- OG-S (Scheme 4). Investigation focused on the enzymatic release of PTX–conjugate in solution state mimicking physiological condition and intercellular milieu which was confirmed by HPLC and as a new insight established by intracellular Raman fingerprint analysis. Finally, the hemolytic activity, cellular toxicity, apoptotic activity and more precisely capability of changing microtubule network established the superiority of SMTDDC over free PTX which prompted its potential towards clinical applicability.

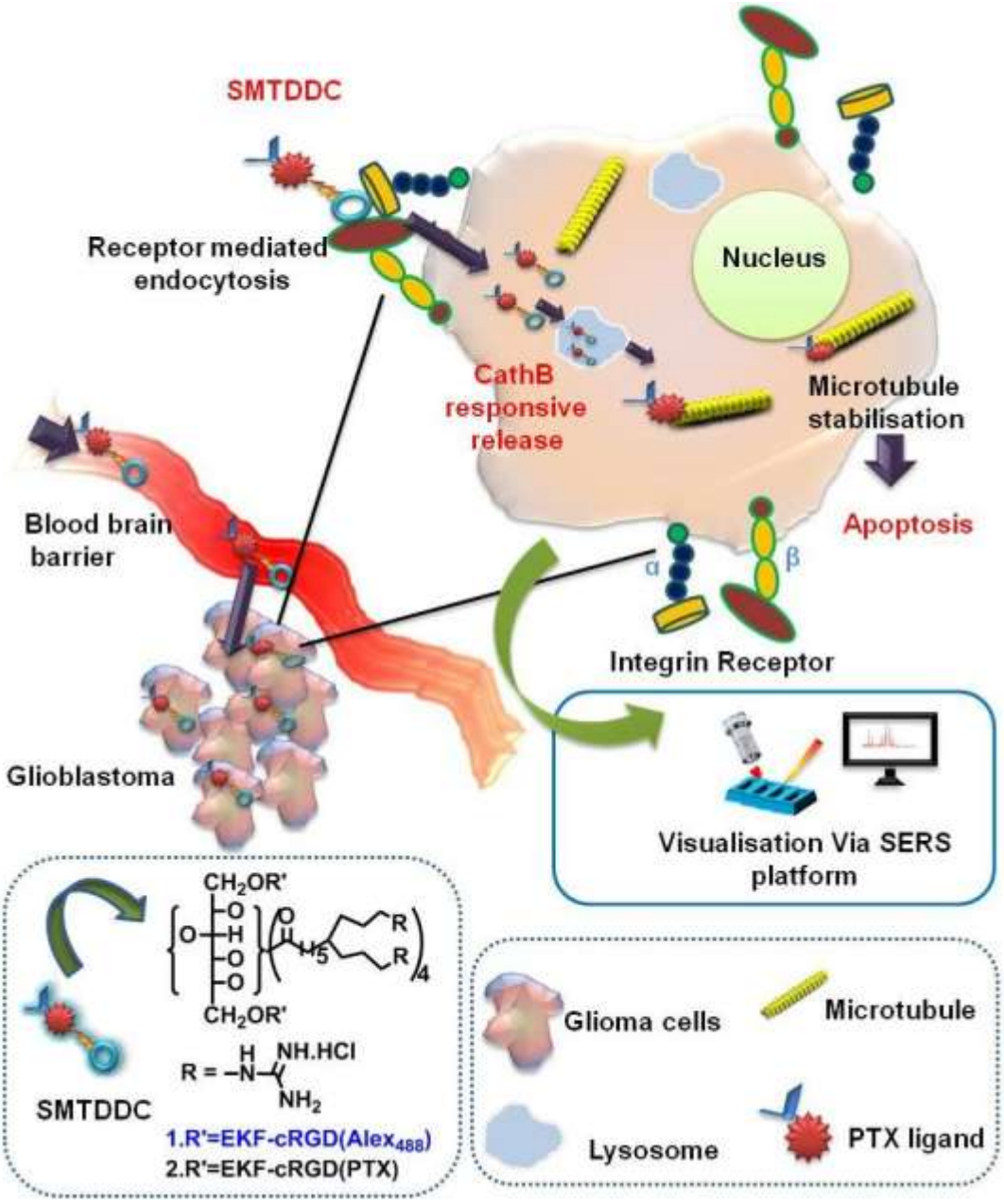

Scheme 4.1: Cellular internalization and mechanism of action of SMTDDC

4.3 Results Discussion

4.3.1 Synthesis and characterization of SMTDDC

The synthetic strategy initiated with the target PTX-conjugate in a convergent manner. Considering the steric factors, the 2'-hydroxyl of PTX side was first appended to hemisuccinate[28] by a known methodology to acquire a carboxylic group at the side chain. The cath B specific peptide substrate EKF was synthesized by solid phase peptide

synthesis (SPPS)[29] using manual coupling through HMPB-MBHA resin. Next, the lysine ε -amino terminal of integrin targeting peptide cRGD was coupled to the free carboxyl group of phenylalanine into C–terminus of cath B peptide substrate via an amide bond. Subsequently, Boc-group was de-protected from lysine ε -amino group of EKF sequence which was coupled with carboxylic acid terminal of PTX linked hemisuccinate[29]. In this synthetic route finally debenzylation was carried out using Pd/C from the benzyl protected β-carboxylic acid of glutamic acid residue of the peptidomimetic part [Glu-Lys (PTX)-Phe (cRGD)] and the free carboxylic group of the Glu was coupled through ester linkage with the primary hydroxyl group of octa-guanidium- sorbitol (OG-S) backbone. The final drug conjugate i.e. EKF-cRGD-PTX-OG-S was obtained after Boc-deprotection from guanidinium moiety of sorbitol backbone using ethyl acetate saturated with HCl (gas) generated the PTX conjugate SMTDDC as HCl salt. The elaborated scheme (scheme 2-6) described the step wise synthetic strategy of the key intermediates and target products, which were purified and characterized by High-performance liquid chromatography (HPLC), NMR spectroscopy and MALDI-TOF mass spectrometric analysis. Further the stability of SMTDDC was evaluated in 10% FBS in PBS which mimics *in vivo* fluid composition (Figure 4.1a). The stability of construct was monitored for a period of 5 months that showed no significant degradation (Figure 4.1b).

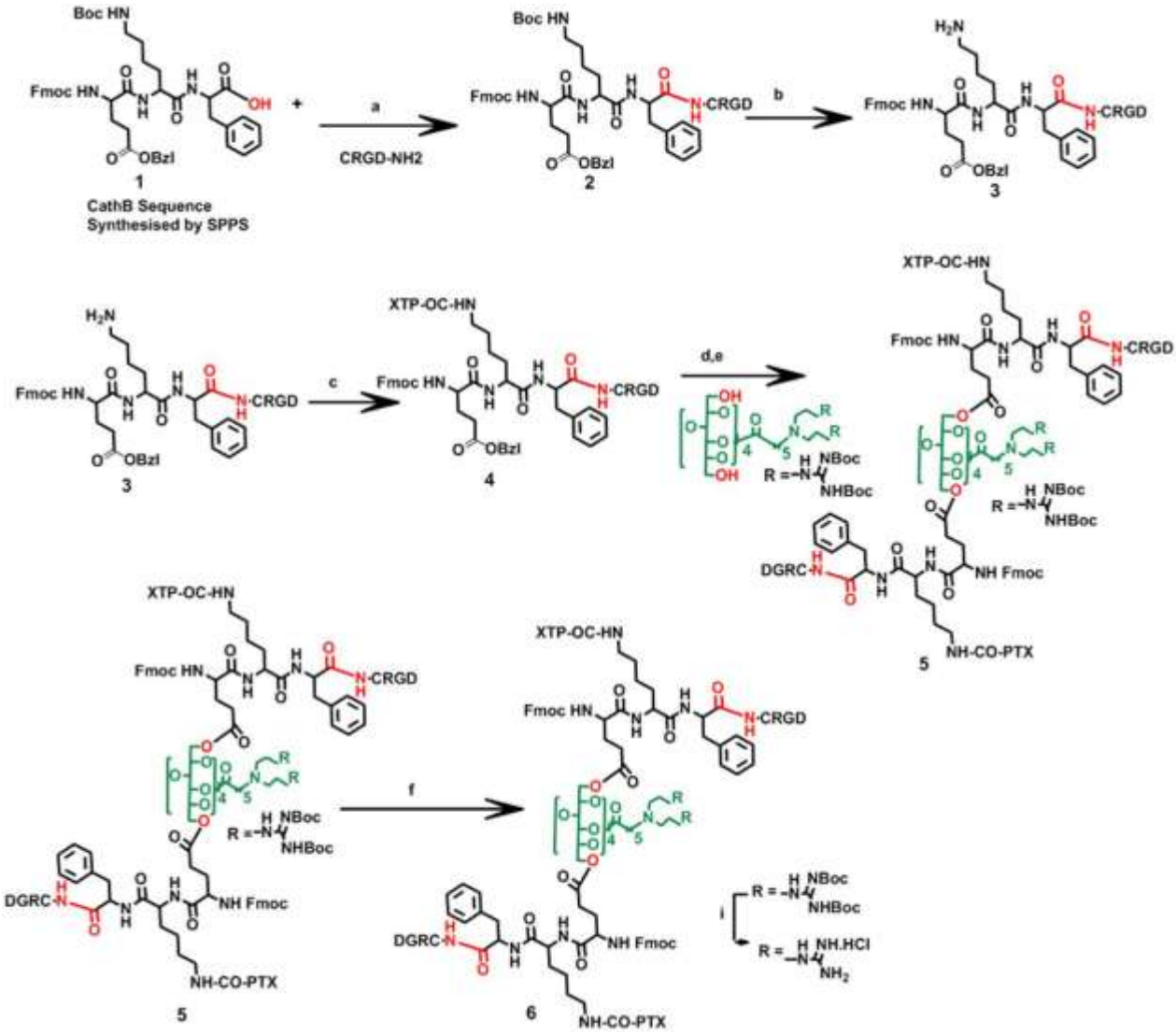

Scheme 4.2: Synthesis of SMTDDC: (a)EDC, HOBT, DIPEA, CH_2Cl_2, RT, N_2,16h,(b)HCl(g), saturated with EtOAc, RT, 4 h, (c) PTX-COOH,EDC, HOBT, DIPEA, CH_2Cl_2, RT, N_2, 26h,(d)Pd/C 10 mol %.,2hrs, (e)EDC, DMAP, CH_2Cl_2, RT, N2, 24h,(f) Ethyl acetate saturated with HCl (g),4h

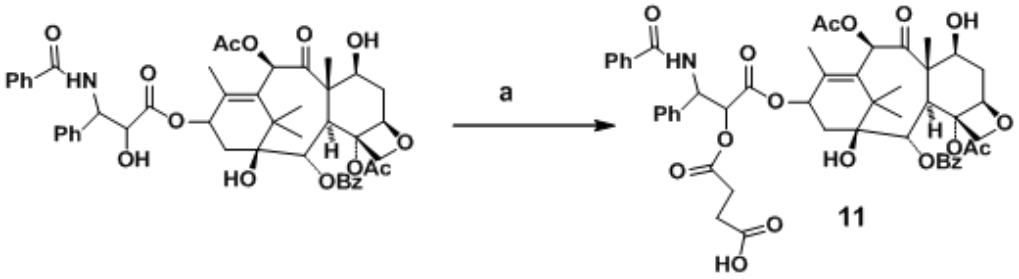

Scheme 4.3: synthesis of paclitaxel hemisuccinate; a) Succinic anhydride, Pyridine (catalytic), DCM, RT, 72hr.

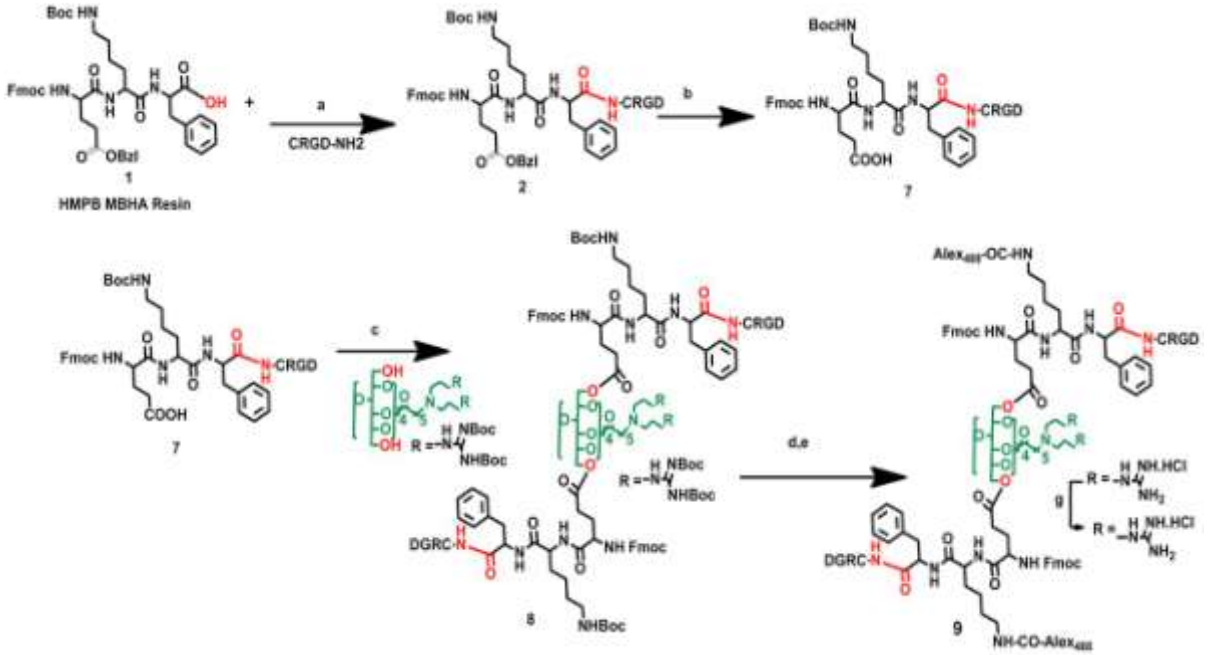

Scheme 4.4: Synthesis of SMC: (a) EDC, HOBT, DIPEA, CH_2Cl_2, RT, N_2, 16h. (b)Pd/C 10 mol %,2hrs(c) EDC, DMAP, CH_2Cl_2, RT, N2, 24h. (d) Ethyl acetate saturated with HCl gas,4h. (e) Alexa 488 Succinimidyl ester, TEA, MilliQ water, 6h.

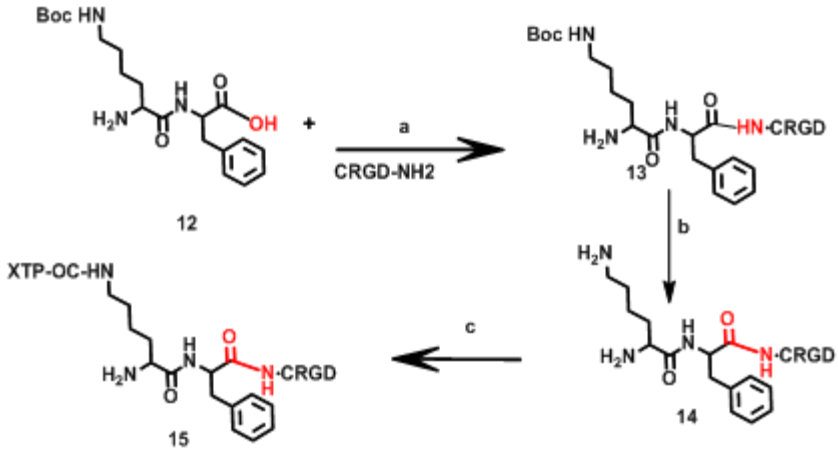

Scheme 4.5: Synthesis of Fragment: (a) EDC, HOBT, DIPEA, CH_2Cl_2, RT, N_2, 16h. (b) Ethyl acetate saturated with HCl(g) reagent, RT, 4hr (c) EDC, HOBT, DIPEA, CH_2Cl_2, RT, N2, 24h.

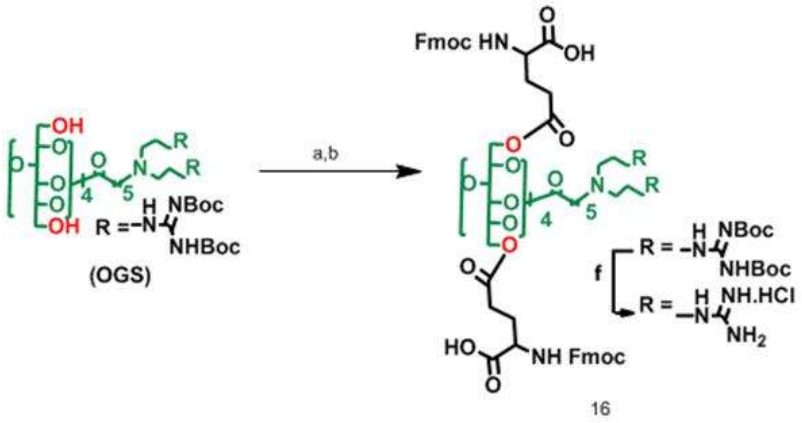

Scheme 4.6: Synthesis of Fragment 2: (a) EDC, DMAP, DIPEA, CH_2Cl_2, RT, N_2, 16h. (b) Ethyl acetate saturated with HCl (g) reagent, RT, 4hr

4.3.2 Release profile of SMTDDC by HPLC

In order to investigate the cleavage of cath B peptide sequence and release of active PTX-conjugate (Figure 4.2a), the SMTDDC was incubated with cath B enzyme for 24 h and analyzed by HPLC. The peaks at a retention time (t_R) of 4.1, 5.3 min appeared which was resembled with t_R of synthesized fragments FR1 & 2 (Figure 4.1a). The peak at t_R-5.3 started appearing after 30 min which was resembled to FR2 i.e. PTX-conjugate and shorter retention time t_R-4.1 identified as FR1 i.e. sorbitol appended carrier. The maximum drug release was noticed at around 12 h (Figure 4.2b).Moreover, the stability of the cat B peptide substrate in SMTDDC was evaluated at a physiological pH, 7.4 and without cath B enzyme also, in both cases no significant drug release was observed. (Figure 4.2c, d).

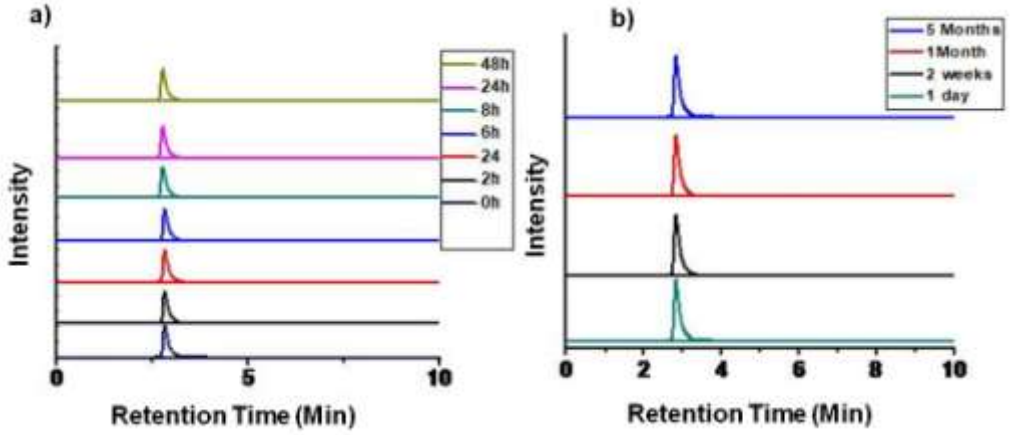

Figure 4.1: (a) Stability of SMTDDC in 10%FBS in PBS, (b) Stability of SMTDDC upon storage.

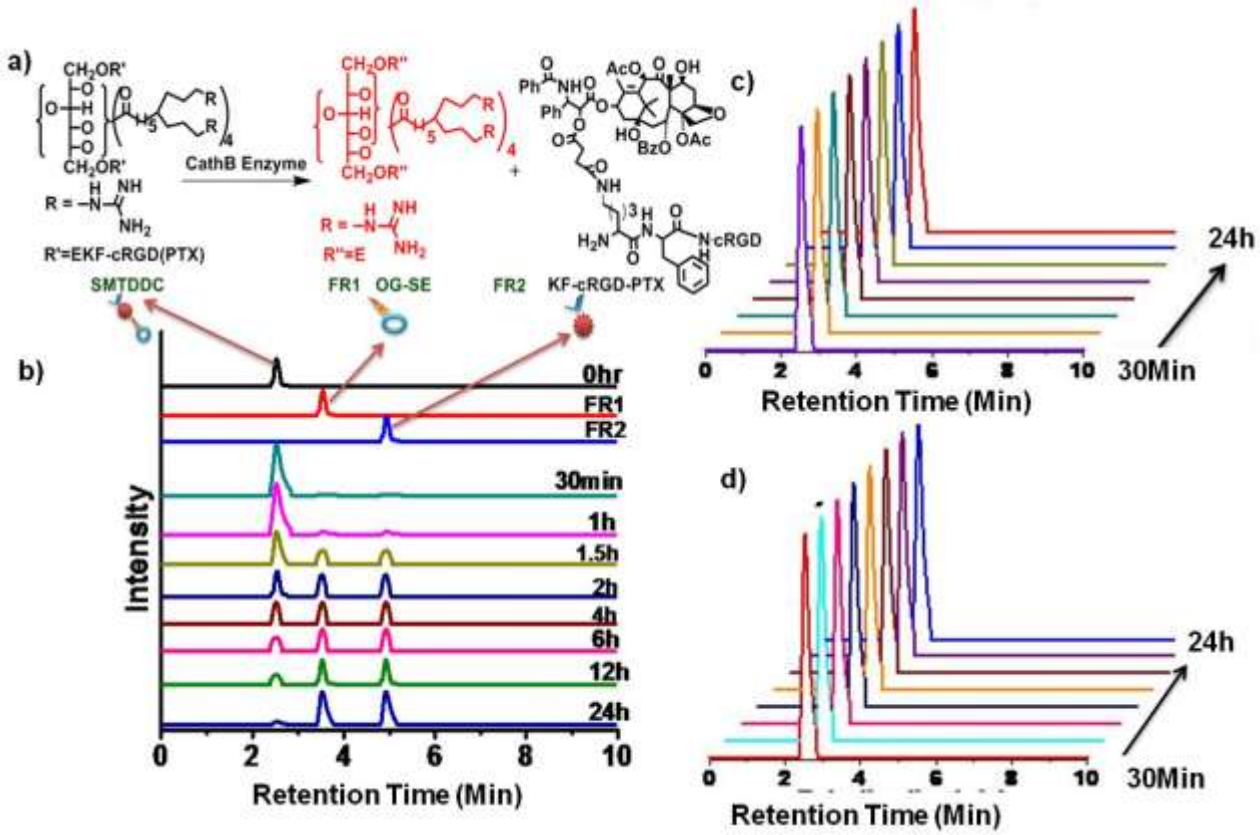

Figure 4.2: (a) Schematic representation of generation of active ligand after incubating with cath B enzyme at pH 5.5, b) HPLC release profile with cath B enzyme at pH5. c) HPLC release profile of PTX active ligand from SMTDDC with cath B enzyme at pH 7.4. d) HPLC release profile of PTX active ligand from SMTDDC without cath B enzyme at pH 5.5

4.3.3 Release profile of SMTDDC by Raman spectroscopy

SMTDDC release profile has been evaluated through surface enhanced Raman scattering (SERS) fingerprint of PTX-conjugate as a novel strategy)[30] . The SERS spectra were recorded from SMTDDC, Cath B-cRGD sequence and free PTX after incubating with colloidal gold nanoparticles (Au-NPs: 40 nm) as SERS substrate (Figure 4.3a).The conjugation of AuNPs with SMTDDC was confirmed by Uv-Vis spectroscopy (Figure 4.3b) The complex SERS-nanotag SMTDDC@ AuNP was readily formed by simple mixing of AuNPs solutions with SMTDDC in 9:1 ratio (v/v), at room temperature. The amine groups present in octa- guanidium moieties of SMTDDC facilitate the strong binding with AuNPs, which acted a key role for SERS fingerprinting. Prominent SERS peaks from SMTDDC @ $AuNP_S$ appeared at 707 cm^{-1} (C-N, C-O, C-C stretching) and 1080 cm^{-1} (C-O stretching, C-N stretching, phenylalanine) showed a significant decline of Raman intensity (Figure 4.3 c; Table1) after incubation with activated cath B enzyme (63 ng/ mL, 37 °C) indicative of the release of the payload from the octa- guanidium scaffold. The time dependent decrease in SERS intensity is due to the enzymatic activity leading to the cleavage of the cath B peptide substrate there by detaching the PTX-conjugate from AuNPs surface. However, a control experiment was also performed in the absence of cath B (Figure 4.3d).

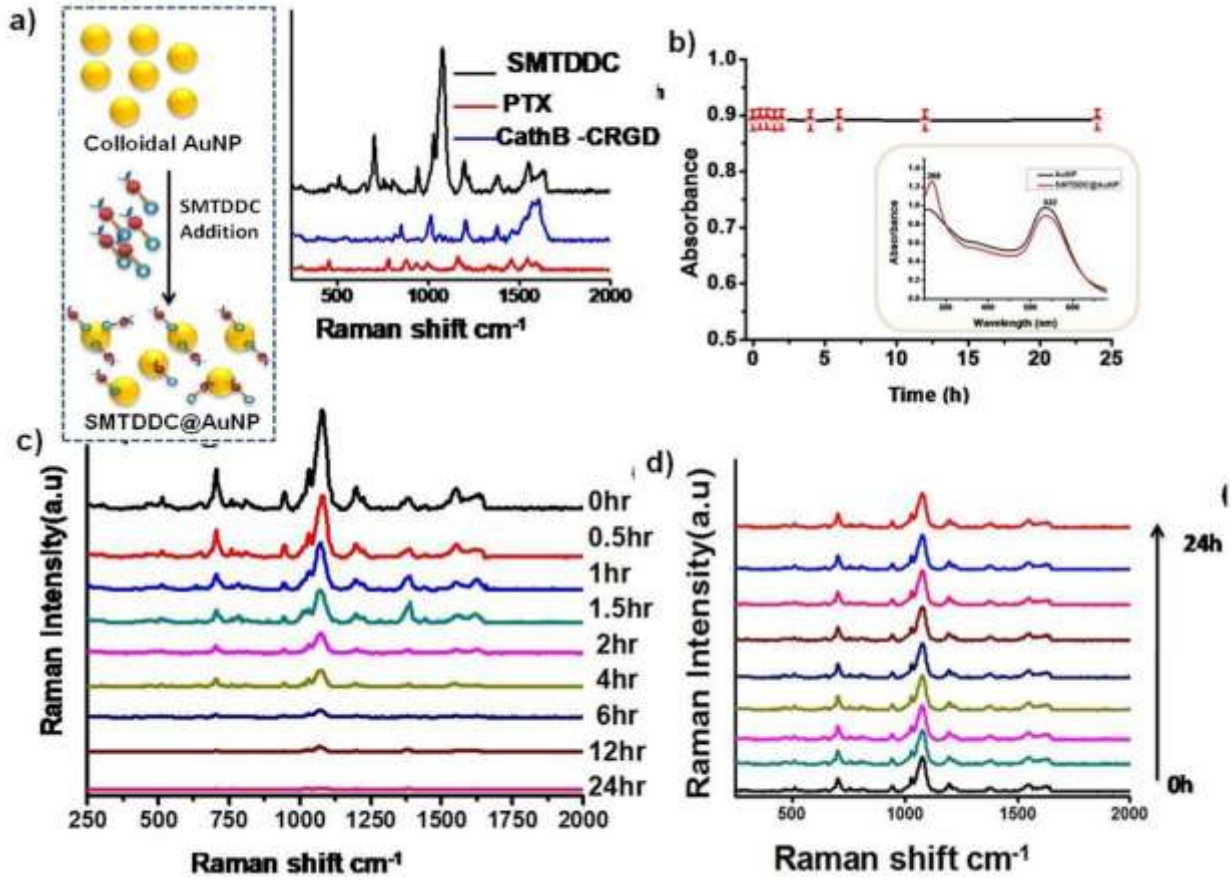

Figure 4.3: a) Schematic representation of preparation of SMTDDC@ AuNPs. a) SERS spectra of SMTDDC, CathB- cRGD sequence, free PTX, b)UV absorbance analysis of SMTDDC @AuNPs in presence of cathB enzyme at pH 5.5(Inset figure shows UV profile of AuNP and SMTDDC @AuNPs, c) Release monitoring by SERS in presence of cathepsin B enzyme at pH5.5,d) SERS profile of SMTDDC@AuNPs in presence of cathB enzyme at pH 7.4

4.3.4 Integrin status and cellular internalization of Molecular Transporter: SMC-tagged Alex 488

In order to assess the targeting efficiency of SMTDDC, first the cell surface integrin expression status in U-87 MG glioblastoma cells and WI-38 normal human fibroblast cells was evaluated by flowcytometric analysis using antibodies directed against the integrin (Figure 4.4a). The U-87MG showed significantly higher integrin expression compare to WI-38 cells. Based on this information the targeted cellular uptake of the synthesized transporter SMC tagged with Alex 488 was checked in U-87 MG cells by

confocal fluorescence microscopy. The cRGD can effectively target $\alpha_v\beta_3$ integrins on the glioblastoma cell surface and enter to the cytoplasm via receptor-mediated endocytosis[14]. From the image (Figure 4.4b) it is clear that most of the SMCs were internalized and localized within cytoplasm. Furthermore, intracellular co-localization was confirmed by investigation through cellular staining dye lysotracker red. Merged image showed SMC internalization rapidly and found to be highly co-localized with LysoTracker™ (Figure 4.4c).

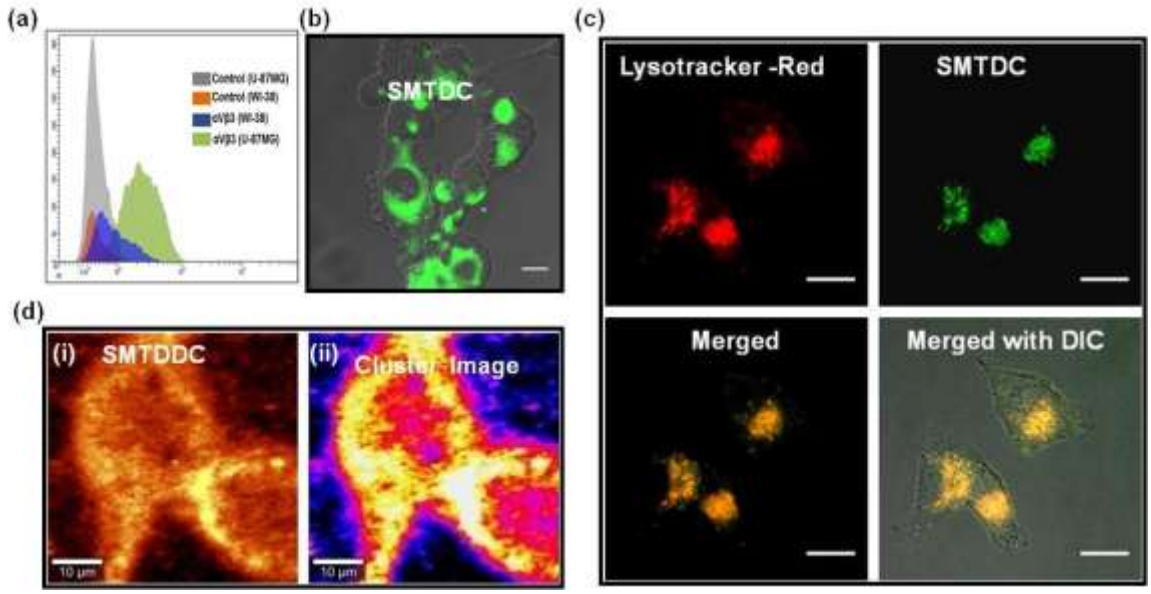

Figure 4.4: (a) Flow-cytometric analysis of $\alpha_V\beta_3$ integrin expression in glioblastoma cell line (U-87 MG) represented as green histogram and non-cancerous lung epithelial cell line (WI-38) represented as blue histogram. (b) Microscopic image represents significant cellular uptake of Alex-488 attached SMC in U-87 MG cell line. Microscopic image indicates Lysosomal localization of SMC(c). Scale bars correspond to 20 µm. (d) SERS Mapping (i) and corresponding cluster image (ii) of SMTDDC@ AuNPs. Scale bars correspond to 10 µm.

4.3.5 Intercellular SERS imaging of SMTDDC

The prevalent method to study intracellular distribution of drugs in biological systems is the fluorescent labeling. Most common difficulties of this method include low contrast and photobleaching, also the introduction of fluorescent labels may alter biochemical properties of parent molecules. In recent years Raman imaging and spectral analysis precisely applied to the recognition and visualization of intra cellular cargo-delivery[31,32], specially anticancer drugs within tumour cells[33]. In the present study the

uptake efficiency with SMTDDC by SERS imaging has been explored using confocal Raman microscopy. SERS mapping and its cluster analysis of U-87 MG cells incubated with SMTDDC@AuNP$_S$ revealed the intuitive Raman intensities which reflected higher in the cytoplasmic area due to intracellular localization of SMTDDC inside the cells (Figure 4.4d).Three dimensional representations of the images clearly indicated the enhanced peak information in contrast with the surroundings (Figure 4.5a,b). 3D images and histogram of the relative intensity of the two most intense peaks, 707cm^{-1}, 1080cm^{-1} from the SMTDDC@AuNP$_S$ treated cells deciphered the significant signal enhancement. Raman spectra (Table 1) abstracted at various regions of the Raman image exhibited characteristic fingerprint SERS peaks.

Peak position	**SERS band assignment**
X = **512cm^{-1}**	C-OH$_3$ torsion (methoxy group)
X = **707cm^{-1}**	C-N,C-O,C-C stretching
X = **759cm^{-1}**	Thyrosine (ring breathing)
X = **817cm^{-1}**	tyrosine C-C twisting mode, cystine C-S stretching mode
X = **946 cm^{-1}**	C-C stretch
X = **1025 cm^{-1}**	Stretching C-O
X = **1080cm^{-1}**	C-O stretching, C-N stretching ,phenylalanine
X = **1200 cm^{-1}**	Aromatic C-O (cRGD thyrosine, CH$_2$ stretching deformation)
X = **1386 cm^{-1}**	CH$_2$ scissor deformation,CH$_3$ band
X = **1558 cm^{-1}**	Tyrosine

X = **1600-1640cm^{-1}**	(C=C stretching modes ,C=C stretching mode of tyrosine , C=C phenylalanine, Amide I , C=O stretching

Table 41: SERS Spectral interpretations[34]of SMTDDC@ AuNP, Samples were excited with a 633 nm excitation wavelength laser with 7 mW powers and Stokes shifted Raman spectra were collected in the range of 300-1800 cm^{-1} with 1 cm^{-1} resolution and an integration time of 0.5 and 20 accumulations

Peak position	**SERS band assignment**
X = 437 **cm^{-1}**	Cholesterol
X = 528 **cm^{-1}**	S-S disulfide stretching of proteins Cysteine, Cholesterol ester
X = 621 **cm^{-1}**	C-C twisting mode of phenylalanine (proteins)
X = 656 **cm^{-1}**	G, T (ring breathing modes in the DNA bases)
X = 756 **cm^{-1}**	Tryptophan(Symmetric breathing)
X = 826 **cm^{-1}**	Phosphodiester
X = 949 **cm^{-1}**	Skeletal modes (polysaccharides, amylose)
X = 1009 **cm^{-1}**	Carotenoids , Phenylalanine
X = 1065 **cm^{-1}**	(C-N)str
X = 1129 **cm^{-1}**	C-N stretching (proteins), C-O stretching (carbohydrates)
X = 1148 **cm^{-1}**	Cytosine, guanine
X = 1206 **cm^{-1}**	A, T (ring breathing modes of the DNA/RNA

	bases)-amide III (protein)
X = 1379 **cm^{-1}**	Guanine
X = 1450 **cm^{-1}**	CH2/CH3 deformation of lipids & collagen
X = 1503,1563 **cm^{-1}**	δ (C=C), phenylalanine, Phenylalanine
X = 1602**cm^{-1}**	Cytosine (NH2)

Table 4. 2: Spectral interpretations[34] of U-87MG cells administration of AuNPs. Samples were excited with a 633 nm excitation wavelength laser with 7 mW powers and Stokes shifted Raman spectra were collected in the range of 300−1800 cm^{-1} with 1 cm^{-1} resolution and an integration time of 0.5 and 20 accumulations

4.3.6 SERS imaging for *in vitro* release kinetics of SMTDDC

Apart from fluorescence modality *in vitro* SERS imaging techniques has been adopted for monitoring the release of PTX-conjugate (Figure 4.5c-h). Incubation of SMTDDS@$AuNP_S$ with U-87 MG cells at 37 °C appeared a gradual decrease in SERS intensity (Figure 4.5c) in a time dependent manner which attributed the cleavage profile of cath B peptide sequence from SMTDDC triggered by the presence of lysosomal cath B enzyme of U-87 MG cells. Initially, prominent SERS fingerprints (Table 4.1, 4.2) from SMTDDC@$AuNP_S$ were observed (the cell peaks were masked) corresponding to the Raman signatures of the SMTDDC. From time dependent imaging of U87 MG cells, clearly visualize the release profile in *in vitro* conditions (Figure 4.5 d-f). Cluster mapping analysis (Figure 4.5 g,h) of the SERS images taken at different time intervals shown in figure 4.5f panels. During subsequent intervals the SERS spectral intensity gradually decreases with the appearance of cell peaks which was also confirmed by a control experiment (Figure 4.6).

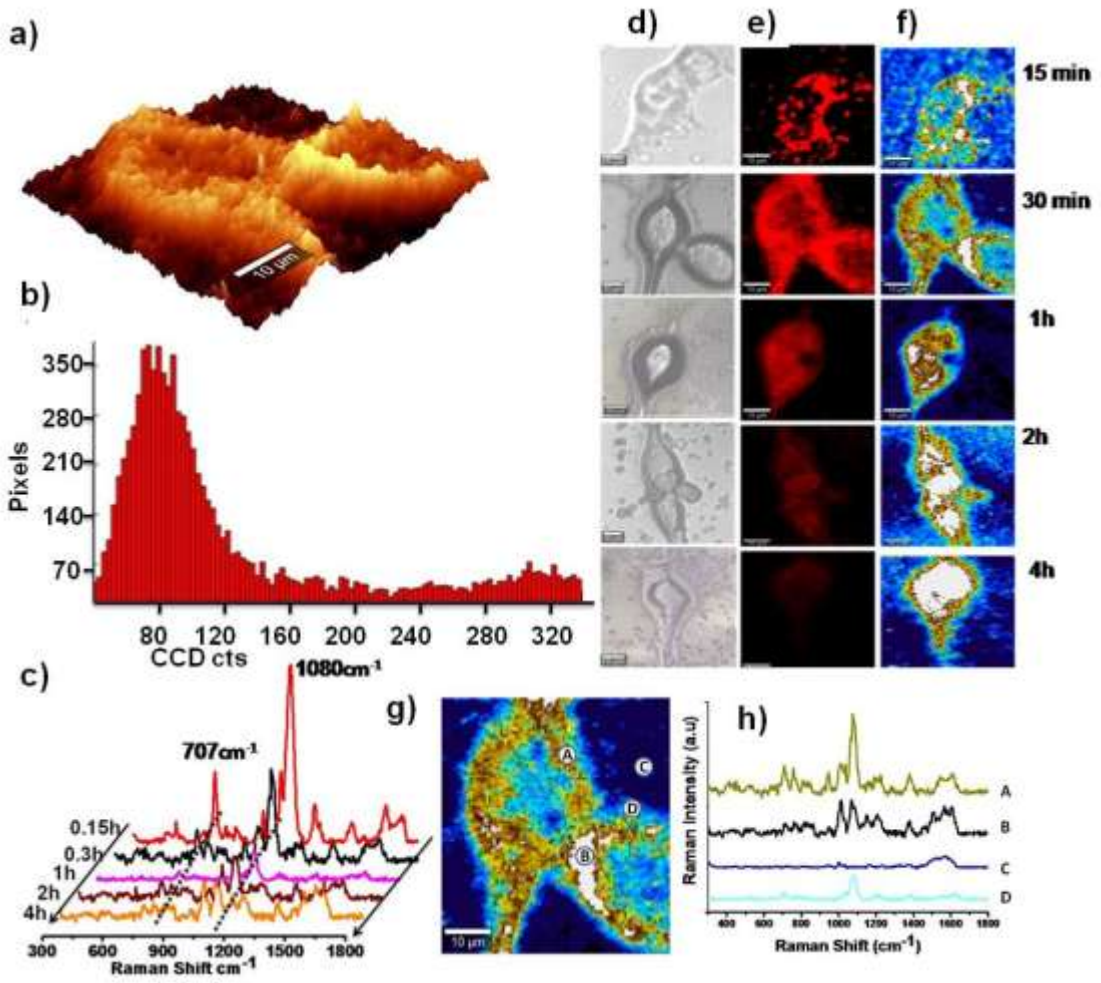

Figure 4.5: a) Three dimensional image and histogram (b) of the relative intensity of the two most intense peak coming from the SMTDDC (I1080/I707) with the gold nanoparticles in U-87MG cells. (c) Four cluster Raman map of U87-MG cells. (d) Average spectra corresponding to clusters in (A) the average spectra of SMTDDS (dark yellow),(B)cell peaks (black), (C), PBS buffer, (D) other regions (navy blue) (e) Bright-field microscopic image of U-87 MG cells, f) SERS mapping of U-87 MG cells with SMTDDC@ $AuNP_S$ were recorded after 15 min onward and continued up to 4 h. (g) Cluster analysis of SERS mapping (h), corresponding SERS spectra obtained from the cells . Scale bars correspond to 10 μm.

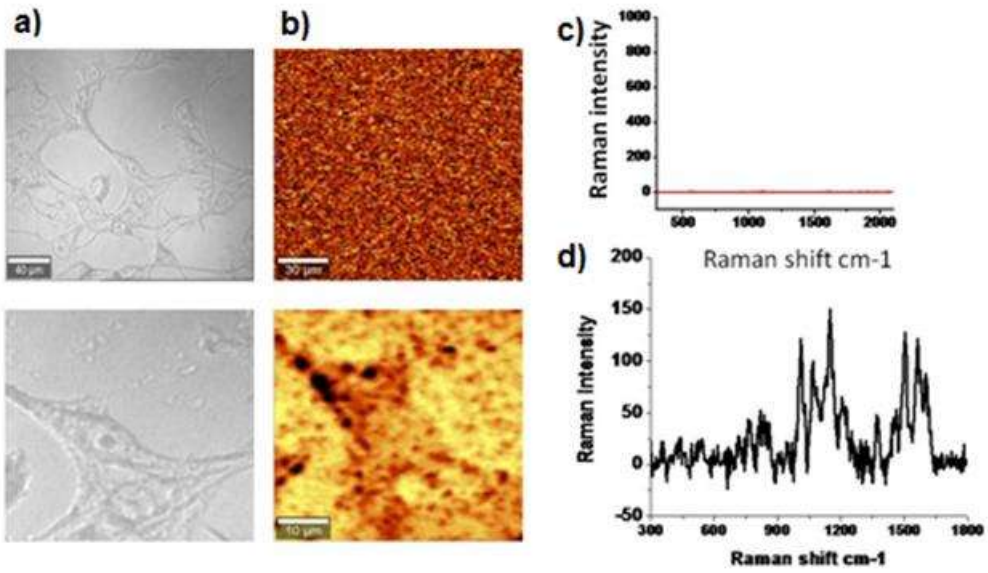

Figure 4.6: Cells without any external agent was used as control (a) and cells with AuNPS used as control ((a) down).The control 1 is not showing any significant Raman signals and Raman image (b) because of the very weak Raman scattering (c) signals from cells. While the cells incubated with AuNPs was showed significant cell spectra (d) due to presence of SERS substrate.

4.3.7 Haemolysis and *In vitro* lymphocyte proliferation of SMTDDC, SMC and PTX

In subsequent studies haemolysis assay has been performed to investigate the toxicity of SMTDDC, SMC and free PTX on red blood cells at three different pH of 7.4, 6.5 and 5.5. As shown in Figure 4.7a, the highest hemolytic activity obtained by free PTX under all the pH conditions investigated, which demonstrated concentration-dependent pH-independent lysis. On the contrary, the carrier SMC and PTX-conjugate were found to be devoid of any toxicity toward RBCs for all concentrations which ensures the safety profile and enables further clinical applications. Again, white blood cells play a major role in the primary immune response and external agents such as drugs always undergo interactions with lymphocytes in the circulation. In order to access the biocompatibility of the constructs, *in vitro* lymphocyte proliferation assay (Figure 4.7b) was performed. Free PTX even at a lower concentration of (0.5 μM) causes reduction in lymphocyte viability and toxicity increases in a dose dependent fashion. However SMTDDC was observed safer towards isolated peripheral lymphocytes, which highlights

the safety profile of the construct.

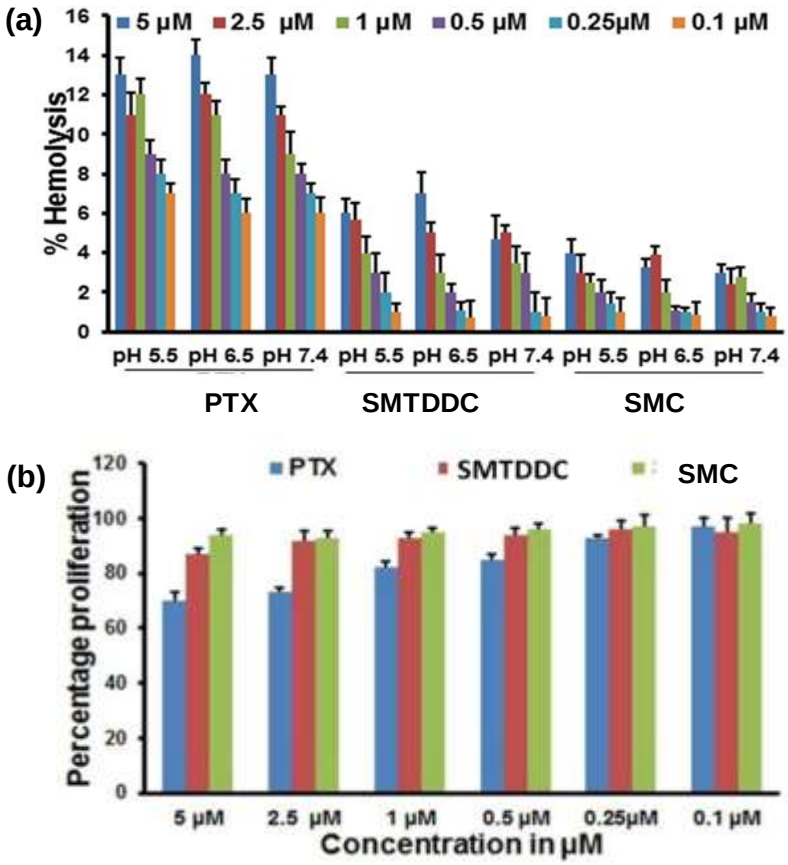

Figure 4.7: (a) Haemolysis experiment performed with SMTDDC, SMC, and free PTX at different concentrations and under various pH conditions. (b) *In vitro* lymphocyte proliferation assay.

4.3.8 Cytotoxicity studies of SMTDDC

The cytotoxicity profile of the SMTDDC conjugate has been investigated by MTT assay wherein, free PTX was treated as control. U-87MG cells were incubated with various concentrations (0.25 –8 µM) of SMTDDC and free PTX for 24 h. Interestingly, SMTDDC showed significant cytotoxicity in U-87MG cells (Figure 4.8a) whereas SMTDDC showed reasonably less toxicity against the noncancerous cell line WI-38 (Figure 4.8b). The transporter SMC alone didn't show any cytotoxicity after treatment.

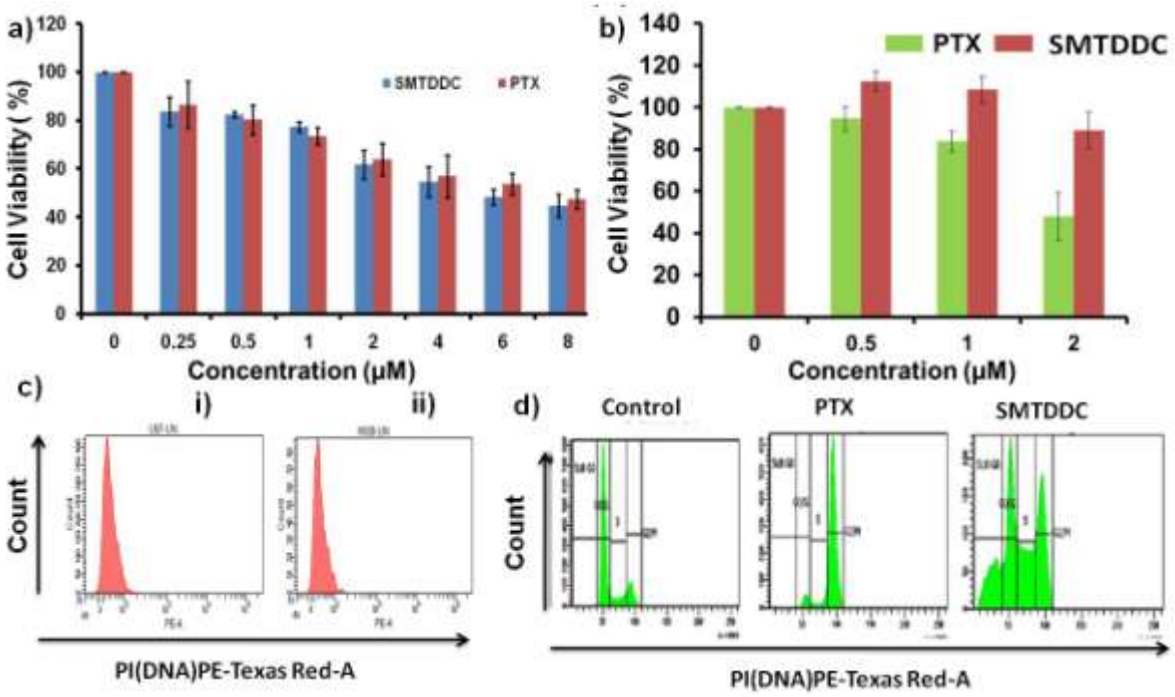

Figure 4.8: (a) cytotoxic evaluation of SMTDDC and PTX by MTT assay in U-87MG cells after 24h incubation. Data are the mean ± SD of six independent experiments. (b) Cell viability study of WI-38 after treatment with various concentrations of SMTDDC and paclitaxel., c) Flowcytometric analysis of the unstained U-87 MG (i) and WI-38 (ii) cells, d) Comparison of Cell cycle in U-87 MG after treatment of PTX and SMTDDC comparison to asynchronously growing control cells.

4.3.9 Cell cycle analyses

Similarly, role of SMTDDC in regulation of cell cycle progression has been evaluated in comparison to untreated (Figure 4.8c) and PTX treated cells (Figure 4.8d). Here, both PTX and SMTDDC showed inhibition of cell cycle progression at G2/M checkpoint. Interestingly, SMTDDC showed higher sub G0 population of cells, which represents a population of fragmented DNA containing apoptotic cells.

4.3.10 Effect on microtubule network

The precious evaluation of the changes in microtubule network has been monitored after treatment with free PTX and the SMTDDC for 24h (Figure 4.9a). The morphology of the microtubule network compared with untreated cells and it was noticed a significant damage of the network in the case of the SMTDDC compared to the free PTX treated U-87MG cells.

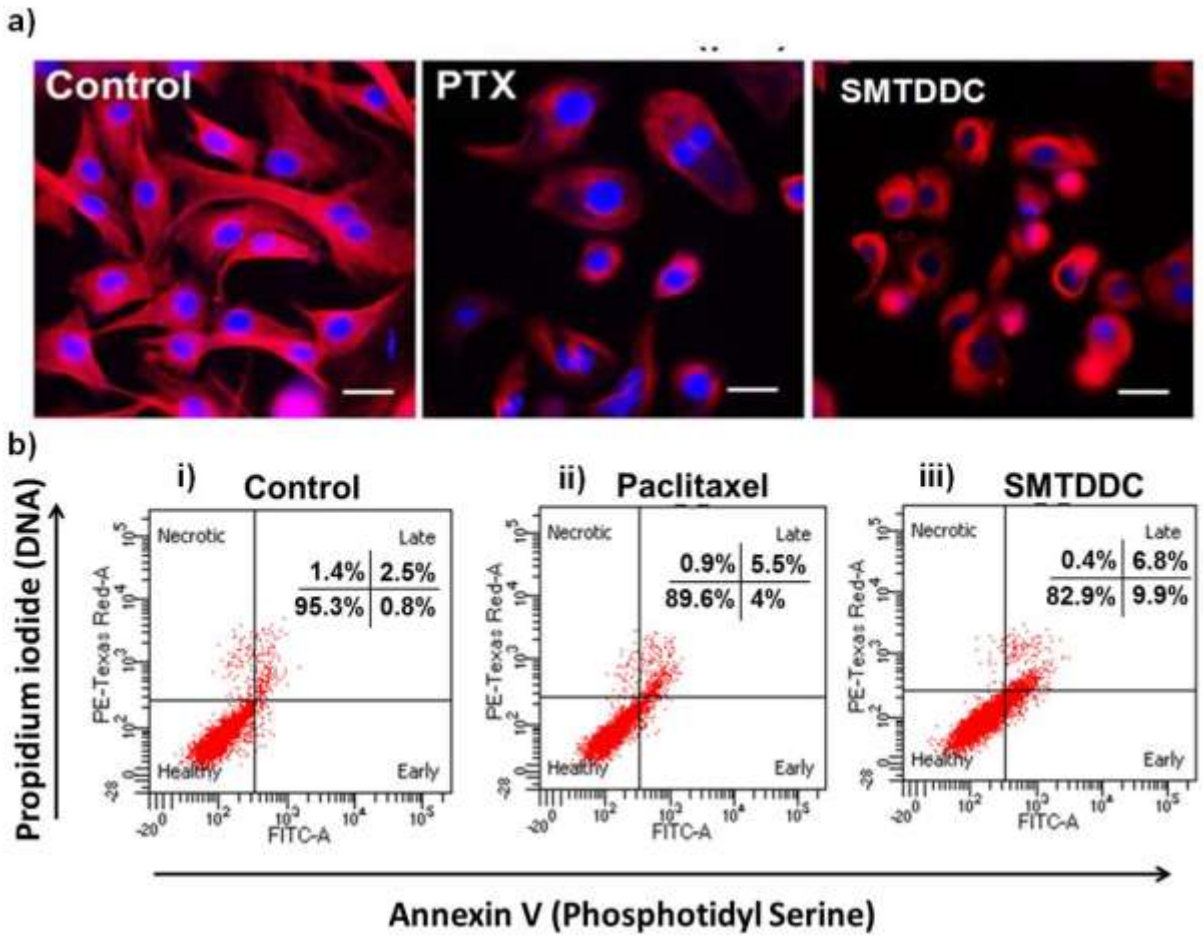

Figure 4.9: a) Effect of both PTX and SMTDDC on intracellular microtubule networks in U-87 MG in comparison to control cells. Scale bars correspond to 20 µm. b) Annexin V/PI method to analyze the apoptosis in U-87MG cell line in (i) Control (untreated), and after treatment with either (ii) Paclitaxel (PTX) at 10nM, (iii) SMTDDC at 10nM for 24h

4.3.11 Cell death evaluation

Finally, the apoptotic potential of SMTDDC and PTX has been assessed using flow cytometry by conventional annexin V and propidium iodide (PI) assay. Briefly, cellular apoptosis displays various molecular and structural events which regulate early and late phase of apoptosis. Further, exposure of phosphatidyl-serine (PS) at outer membrane of cell denotes ”eat me“ signal which is a signature event of early phase of apoptosis[35]. Annexin V is a known cellular protein which is regularly used to detect PS on cell surface because of its high binding affinity. Attachment of Annexin V FITC to the

cell surface of U-87MG cells indicated SMTDDC dependent apoptotic cell death. Further, late phase of apoptosis is denoted by cell membrane blebbing and its loss of selective permeability. Propidium Iodide (PI) is a cell membrane impermeable nucleic acid binding dye which is regularly used to detect the late phase of apoptosis. Thus, increase in PI cellular uptake reflects late phase of apoptotic cells. Herein, control denotes the untreated cells having maximum percentage of healthy cells. (Figure 4.9b). The flow cytometry data clearly indicates an apoptotic death of the U-87MG cells upon treatment with SMTDDC in compare to control and PTX.

4.4 Conclusions

In conclusion, a successful demonstration as a proof of concept has been executed using a dual targeted peptidomimetic carrier system with OG-S backbone for specific delivery of PTX in glioblastoma cell U-87MG. The OG-S drug conjugate i.e. SMTDDC exhibited significant stability, biocompatibility to RBCs and lymphocytes, high cellular uptake and excellent selectivity towards lysosomes. Again, PTX-conjugate showed significant response to enzyme activation. The successful delivery of PTX observed with SMTDDC could be due to its rapid integrin mediated cellular uptake and precise release of PTX conjugate triggered by lysosomal cath B activity which effectively monitored through HPLC and SERS spectral and imaging modality. Moreover, SMTDDC achieve target specific cytotoxity, programmed cell death and more precisely PTX conjugate exerts significant damage in microtubule networking observed in U-87MG cells. The SERS-guided spectral mapping enabled accurate profiling of internalization as well as release kinetics of PTX which otherwise could not be traced with conventional fluorescent modalities.

4.5 Experimental Section

4.5.1 Chemical Reagents and Characterizations

All non-aqueous reactions were carried out in oven-dried glassware under an inert atmosphere of dry nitrogen. Fmoc protected amino acids viz, Fmoc- Phe- OH, Fmoc-

Glu (OBn)- OH, Fmoc- Lys(Boc)- OH were acquired from Novabiochem, Globe scientific, and the cathepsin B amino acid sequence was synthesized by manual coupling of amino acids via solid phase peptide synthesis (SPPS) by Fmoc chemistry. The cyclic peptide cRGD (Cyclo-Arg-Gly-Asp-D-Tyr-Lys) was obtained from peptide international. The anticancer drug Paclitaxel™ was obtained from Calbiochem and Cathepsin B enzyme was purchased from Enzo life science. All the other common reagents and solvents were purchased from sigma Aldrich, Merk, and Spectrochem, was used without further purification. Analytical thin layer chromatographic(TLC) plates was procured from Merck 60 F254 silica gel plate (0.25mm thickness),TLC silica gel 60 RP-18 $F_{254}S$ (reverse phase TLC) and visualization was done with UV light (254nm and 365nm), or by spraying with a 5% solution of phosphomolybdic acid or ninhydrine solution followed by charring with a heat gun. Column chromatography was performed on Merck 60 silica gel (60-120 or 100-200 mesh), suphelclean™ LC-18 SPE Bulk and Sephadex LH20. High performance liquid chromatography (HPLC) was accomplished by Shimadzu HPLC system consisting of SCL-10Avp system controller, two LC-8A solvent delivery units, SPD-M20A UV-VIS photo diode array (PDA) detector, equipped with Multi PDA- LC solution(software) on a 250 mm x 4.6 mm i.d, 5µm, YMC-Pack R&D Octa-decanesilane (ODS) analytical column (9YMC Co., Ltd. Japan).NMR spectra were recorded on a Bruker AMX 300 (^{1}HNMR at 500MHz) spectrometer. Tetra methyl silane was used as reference for ^{1}H NMR, and the chemical shift were reported in ppm and the coupling constant in Hz. High resolution mass spectra were determined on a HR-EMI analysis of Thermo Scientific Exactive system, and MALDI-TOF mass spectra on a Shimadzu Biotech, AXIMA-CFR PLUS system. Liophilization was performed with lyophilizer, Scan Vacfreez drier model: coolsafe 110-4 PRO system (-110^{0}C).Surface enhanced Raman Scattering (SERS) spectra were recorded using confocal Raman microscope alpha 300 R WITeC Germany. The laser power source was directed to the sample via 20×objective (Numerical aperture [NA]-2.1mm) with 600 g/mm grating. The laser source of 633nm excitation wavelength was used for the whole experiments with a laser power of 5mW.All the Stokes Raman spectra were collected using a Peltier cooled CCD detector in the range of 400–3000 cm^{-1} with an integration time of 0.5 sec

and 30 accumulations for single spectra measurements and 0.05 sec integration time and 50X50µm area scan with 150X150 resolution for image scan.

4.5.2 **Chemical synthesis:**

4.5.2.1 Synthesis of SMTDDC

4.5.2.1.1 Solid phase peptide synthesis of Cath B Sequence[36]:-Compound 1

Preparation of Fmoc NH- EKF-OH (compound1, cath B peptide sequence) was initiated with activating the first amino acid using Di-isopropyl carbodiimide (DIC). Fmoc- Phe-OH (440mg, 1.13 mmol) was taken in dry dichloromethane (10mL) and DIC (0.218mL, 1.42 mmol) was added. This was stirred at 0-5 °C for 1h under N_2 atmosphere. The Fmoc- Phe-OH activated DIC complex was concentrated and then dissolved in DMF along with 2-3 drops of DIPEA and charged into the resin bed of HMPB-MBHA resin (200mg, 0.142 mmol) (commonly used for making acid terminal peptide sequences), which was swelled up in dry DCM (6mL) for 30 min. The reaction was continued for 8 h with shaking.The progress of the reaction was monitored by the Kaiser test (Colour test to monitor completeness of amino acid coupling). After completion of the coupling, the resin was washed with DMF (3 x 3 mL), and the Fmoc protection group was removed by treatment with piperidine in DMF (20%, 3 x 2 ml, 3 x 15 min). The reaction cycle was continued in a similar manner with Fmoc- Lys (Boc)-OH (260mg, 0.042 mmol), Fmoc-Glu (OBn) -OH (192 mg, 0.042 mmol) with HBTU, DIPEA in DMF. The resulting resin-bound tri peptide was washed with DMF (3 x 5 ml), dichloromethane (7 x 3 mL) and Hexane (3 x 3 mL), dried in vacuum(1 h) Finally the desired peptide sequence was released from the resin by using the cleavage cocktail, 2% trifluoroacetic acid in dichloromethane (10 x 2 mL). The resin washing was combined and concentrated under reduced pressure, and the residue co-evaporated with toluene. The residue was precipitated with cold ether (3 mL) and filtered the residue peptide that afforded of white solid (Fmoc NH-EKF-OH) (74 mg, 89%). ^{1}H-NMR (500MHz),[in $CDCl_3$ (Aldrich); referenced to δ 0.00 ppm for Tetramethyl- silane (TMS; Aldrich) used as internal standard (IS)]: δ 8.03 (s, 1H), 7.73 (d, *J=7.4 Hz*, 2H), 7.69 (d, *J=7.5Hz,* 1H), 7.56 (m, 3H), 7.48 (d, 2H), 7.39 (m, 5H), 7.29 (m, 2H), 7.28 (m, 2H), 5.09 (s, 2H), 4.70 (d, *J=6.9Hz,*

2H), 4.69(s,1H)4.54 (s, 2H), 3.52 (t, *J=6.2Hz,* 2H), 2.94 (s, 2H), 2.31 (m, 2H), 1.71 (m, 2H), 1.58 (m, 2H), 1.27 (s, 9H),1.21(m,2 H). HRMS: $[M+H]^+$ calculated for $C_{47}H_{57}N_5O_9$ is 835.4156, and found 835.4135.

4.5.2.1.2 cRGD attachment on Cath B peptide: Compound 2

Fmoc NH-EKF-OH (compound1) (1.35mg, 0.0016mmol), EDC (0.615mg, 0.00161mmol), HOBt (0.433mg, 0.0032mmol), and DIPEA (1.8 mL, 0.010 mmol) were stirred for 5 minutes and cRGD (1mg, 0.0016 mmol) was added. The mixture was stirred at RT for 16h under N_2 atmosphere. The crude product was purified using column chromatography to afford the product **2,** 62%.^{1}H-NMR (500Mz), [in $CDCl_3$ (Aldrich)]; referenced to δ 0.00 ppm for tetramethyl- silane (TMS; Aldrich) used as internal standard (IS)]: δ 8.56 (bs, 4H), 8.01 (s, 9H), 7.83 (d, *J=7.6Hz,* 2H), 7.75(m, 1H), 7.59 (m, 3H), 7.44 (d, *J=7.2Hz*, 1H), 7.38 (m, 5H), 7.30 (m, 2H), 7.26 (m, 2H), 7.10 (d, *J=7.2Hz*, 1H), 6.71 (bd, 2H), 5.50 (bs, 2H), 4.92 (m, 1H), 4.86 (m, 1H), 4.54 (s, 3H), 4.43(m, 2H), 3.31(s, 2H), 3.18 (s, 2H), 1.91 (bm, 6H), 1.69 (m, 6H), 1.57(m, 4H), 1.25 (s, 9H).). MALDI-TOF-MS: $[M+Na]^+$ calculated for, $C_{74}H_{93}N_{13}O_{17}Na$ is 1459.6710, found 1459.6725.

4.5.2.1.3 Synthesis of Compound 3

Ethyl acetate (4mL) saturated with gaseous HCl was added to a solution of **2** (2mg, 0.0013mmol) in ethyl acetate (1mL). The reaction mixture was stirred for 4h. Then the solution was concentrated and the residue was washed with ethyl acetate to remove less polar impurities to afford compound 3.The reaction was proceeded in to the next step without isolation and purification of compound 3.^{1}H-NMR (500Mz),[in CD_3OD (Aldrich); referenced to δ 0.00 ppm for tetramethyl- silane (TMS; Aldrich) used as internal standard (IS)]: δ (ppm): δ (ppm): 8.55 (bs,4H), 8.01 (s, 9H), 7.82(d, 2H), 7.74(m, 1H), 7.59(m, 3H), 7.43(d, 1H), 7.39 (m, 5H), 7.30 (m, 2H), 7.25 (m, 2H), 7.10(d, 1H), 6.72 (bd, 2H), 5.50 (bs, 2H), 4.54 (s, 3H),4.86(m, 1H), 4.91., (m,1H), 4.42(m, 2H), 3.31(s,2H), 3.18(s, 2H),2.03(bm,2H) 1.91 (b m, 6H), 1.69 (m, 6H), 1.57 (m, 4H). MALDI-TOF-MS: $[M+H]^+$ calculated for $C_{69}H_{86}N_{13}O_{15}$ is 1336.6366, found 1336.6331.

4.4.2.1.4 Synthesis of Compound 11.

Paclitaxel hemisuccinate[28] (PTX-COOH) was prepared using the method of Majoras *et al*[37]. Briefly, PTX (25 mg, 0.0293 mmol) was reacted with an excess of succinic anhydride (2.9mg.0.035 mmol) in anhydrous DCM in the presence of a catalytic amount of anhydrous pyridine. After the reaction was confirmed to be complete by thin layer chromatographic (TLC) analysis, pyridine was neutralized with dilute aqueous solution of hydrochloric acid and extracted. The residue, recovered from the organic phase after solvent evaporation, was re-crystallized with acetone/water to get needle like crystals of PTX-COOH in almost quantitative yield;-^{1}H-NMR (500Mz),[in CDCl3 (Aldrich); referenced to δ 0.00 ppm for tetramethyl-silane (TMS; Aldrich) used as internal standard (IS)]: δ 7.37 to 8.15 (m,10H), 7.33(m, 5H),7.24(d, 1H), 6.28 (s, 1H), 6.01 (dd, 1H), 5.72 (d, *J=5.3*, 1H), 5.52 (d, *J=6.1Hz* ,1H),4.97 (dd, 1H), 4.45 dd, 1H), 4.21 ,4.30 (dd, 2H), 3.81 (d,1H), 2.68-2.77 (m, 4H), 2.44 (s, 3H), 2.40 (dd, 2H), 2.22 (s, 3H), 2.20(dd, 2H),1.92 (s,3H), 1.68 (s,3H), 1.25 and 1.13(6H, S).HRMS: $[M+H]^{+}$calculated for $C_{51}H_{56}NO_{17}$ is 954.3548, found 954.4776$[M+H]^{+}$.

4.4.2.1.5 Synthesis of Compound 4

Paclitaxel-COOH (compound 11) (2.5mg, 0.00262 mmol), EDC (0.615mg, 0.00161mmol), HOBt (0.433mg, 0.0032 mmol), was stirred for 5 minutes then compound 3 (3.5mg, 0.0026mmol) was added. The mixture was stirred at RT for 24h under N_2 atmosphere. The crude product was purified using column chromatography to afford the product **4.** ^{1}H-NMR (500Mz),[in CD_3OD (Merk); referenced to δ 0.00 ppm for tetramethyl- silane (TMS; Aldrich) used as internal standard (IS)]: δ 7.26-8.23 (m, 29H), 6.72 (m, 2H), 6.98 (s, 1H), 6.23 (t,1H), 6.01 (dd,1H), 5.67 (d, 1H), 5.53 (d, 1H), 5.51(bs, 2H), 4.30-5.11 (m, 11H), 3.80 (d, 1H), 3.66 (s,2H), 3.29 (m, 2H),3.16 (s, 2H), 2.04-2.95 (m,11H), 1.93 (bm, 6H), 1.10-1.82 (m, 28H), MALDI-TOF-MS: $[M+H]^{+}$calculated for $C_{120}H_{138}N_{14}O_{31}$ is 2270.9652, found is 2270.9663.

4.4.2.1.6 Synthesis of compound 6

Bezyl deprotection of compound was done by global de-benzylation using Palladium carbon 10 mol% for 2hrs. The crude product was purified using celite column. The benzyl deprotected compound 4 was treated with EDC (0.4mg, 0.26X10^{-}

^{5}mmol) and Dimethyl amino pyridine, catalytic amount in dry DCM for 5 minutes. Further Octaguanidium sorbitol (OG-S, has been synthesized as per our previously reported synthetic route[8] (3.9mg, 0.13 X 10^{-5}mmol) core has been synthesized as per our previously reported synthetic procedure[1]was added to the reaction mixture. The mixture was stirred at RT for 24h under N_2 atmosphere to yield compound **5**.^{1}H-NMR (500Mz),[in CD_3OD (Merk); referenced to δ 0.00 ppm for tetramethyl- silane (TMS; Aldrich) used as internal standard (IS)]: δ (ppm):7.25-8.23 (m, 50H), 6.72 (m, 4H),6.98 (s, 2H), 6.23(t, 2H), 6.01(dd, 2H), 5.67(d, 2H), 5.53(d, 2H),5.52 (s, 8H) , 4.30-5.11(m, 22H), 3.80(d, 2H), 3.66 (s, 4H), 3.29(m, 4H),3.19(m,16H),3.16(s, 4H), 2.04-2.95(m, 62H), 1.93 (b m, 12H), 1.10-1.82 (m, 96H)., 1.32 (s, 144H). Which was further subjected to Boc deprotection using ethyl acetate saturated with HCl reagent. The residue was washed with ethyl acetate for removing less polar impurities to yield compound 6.The product 6 was further purified by supelclean™ C18-reverse phase silica gel (solvent: H_2O/MeOH). The purified product was dissolved in deionized water, filtered through poly tetra fluoro ethylene (PTEE) syringe filter, and lyophilized to give the transporter as a light orange foamy solid (HCl salt).^{1}H-NMR (500Mz),[in CD_3OD (Merk); referenced to δ 0.00 ppm for tetramethyl- silane (TMS; Aldrich) used as internal standard (IS)]: δ7.25-8.23 (m, 54H), 7.05-7.19 (m,10H) 6.01(m, 2H), 5.67(d, 2H), 5.53(d, *J*=7.3Hz, 2H),5.52 (s, 8H) , 4.30-5.11(m, 22H), 3.80 (d, *J*=7.45 Hz, 2H), 3.66 (s, 4H), 3.29 (m,4H), 3.19 (m,16H), 3.16(s, 4H), 2.04-2.95(m, 62H), 1.93 (b m, 12H), 1.10-1.82 (m, 96H), 1.32 (s, 144H) MALDI-TOF-MS:$[M+H]^+$calculated for $C_{289}H_{393}N_{56}O_{70}^{8+}$is 5767.8914 found 5767.8925 $[M+H]^+$.

4.4.2.1.7 Synthesis of compound 9:

The reaction is starting from global de benzylation of acid residue on compound 2 using Pd/C 10 mol%. Further the compound was purified using celite column to yield compound 7(SI Scheme 3). Then the primary hydroxyl groups on sorbitol (Octaguanidium sorbitol (OG-S, has been synthesized as per our previously reported synthetic route[8]) core were functionalized with compound 7 to yield compound 8.This was further subjected to Boc deprotection using ethyl acetate saturated with HCl reagent and the fluorophore, Alexaflour-488 sucinimidyl ester was attached to the free

amine terminal on lysine side chain (SI Scheme 2) to yield the first control compound 9,SMTDC. The product 9was further purified by supelclean™ C18-reverse phase silica gel (solvent: H_2O/MeOH). The purified product was dissolved in deionized water, filtered through poly tetra fluoro ethylene (PTEE) syringe filter, and lyophilized to give the control as a light orange foamy solid (HCl salt).The key intermediates and aimed products were characterized by NMR spectroscopy and MALDI-TOF, mass spectrometric analysis.^{1}H-NMR (500Mz),[in CD_3OD (Merk); referenced to δ 0.00 ppm for tetramethyl-silane (TMS; Aldrich) used as internal standard (IS)]:δ7.25-8.23 (m, 54H), 7.05(d,2H) 6.72 (m, 4H),6.98 (s, 2H),6.45,6.40 (m, 2H) 6.25(2H, S), 6.23(t, 2H), 6.11(s, 2H) 6.01(dd, 2H), 5.67 (d, 2H), 5.53(d, 2H),5.52 (s,8H) , 4.30-5.11(m, 22H), 3.80(d, 2H), 3.66 (s, 4H), 3.29 (m, 4H), 3.19(m, 16H),3.16(s,4 H), 2.04-2.95(m, 62H), 1.93 (b m, 12H), 1.10-1.82 (m, 96H)., 1.32(s, 144H) MALDI-TOF-MS: $[M+Na]^+$calculated for $C_{226}H_{304}N_{54}O_{46}{}^{8+}Na$ is 4536.1632 and found 4536.1523

4.5.2.2 Solid phase peptide synthesis of CathB dipeptide -Sequence: Compound 12

Preparation of Fmoc NH-KF-OH (compound 12, cath B sequence) was initiated with Fmoc- Phe-OH (440 mg, 1.13 mmol) which was taken in dry dichloromethane (10mL) and DIC (0.218 mL, 1.42 m mol) was added. This was stirred at 0-5 °C for 1h under N_2 atmosphere. The Fmoc- Phe-OH activated DIC complex was concentrated and then dissolved in DMF along with 2-3 drops of DIPEA and charged into the resin bed of HMPB-MBHA resin (200 mg, 0.142 m mol) which was swelled up in dry dichloromethane (6mL) for 30 min. The reaction was continued for 8 h with shaking. The progress of the reaction was monitored by the Kaiser test. After completion of the coupling, the resin was washed with DMF (3 x 3 mL), and the Fmoc protection group was removed by treatment with piperidine in DMF (20%, 3 x 2 ml, 3 x 15 min). The reaction cycle was continued in a similar manner with Fmoc- Lys (Boc)-OH (260mg, 0.042mmol), amino acid charged to the resin. The resulting resin-bound tri peptide was washed with DMF (3 x 5 ml), dichloromethane (7 x 3 mL) and Hexane (3 x 3 mL), dried *in vaccum* (1 h) Finally desired peptide sequence was released from the resin by treatment with 2% tri fluoro acetic acid in dichloromethane (10 x 2 mL). The resin washing was combined and concentrated under reduced pressure, and the residue co-

evaporated with toluene. The residue was precipitated with cold ether (3 mL) and filtered the residue peptide that afforded of white solid. ^{1}H-NMR (500Mz),[in $CDCl_3$] (Merk); referenced to δ 0.00 ppm for tetra methyl-silane (TMS; Aldrich) used as internal standard (IS)]:δ 8.13 (bs, 3H), 7.21-7.46 (m,9H), , 4.71 (m, 1H),4.39-4.51(m ,2H), 3.52 (m, 2H), 2.94 (d, J=6.2Hz, 2H), 2.32 (m, 2H), 1.71 (m, 2H), 1.58 (m, 2H), 1.27 (s, 9H), 1.22 (m, 2H). HRMS: $[M+H]^+$calculated for $C_{35}H_{42}N_3O_7$: 616.1822, found 616.1956$[M+H]^+$

4.5.2.3 Synthesis of compound 15:

Cathepsin B peptide sequence, Compound 12 (Fmoc NH-KF-OH, 1.35mg, 0.0016mmol), EDC (0.615mg, 0.00161mmol), HOBt (0.433mg, 0.0032mmol), and DIPEA (1.8mL, 0.010mmol) was stirred for 5 minutes and cRGD (1mg,0.0016mmol) was added. The mixture was stirred at RT for 16h under N_2 atmosphere. The crude product was purified using column chromatography to afford the product 13**.** Furthermore Cath B-CRGD-PTX attachment was done by coupling compound 11 (2.5mg, 0.00262mmol), EDC (0.615mg, 0.00161mmol), HOBt (0.433mg, 0.0032mmol), was stirred for 5 minutes then Compound 13(obtained after deprotection of Boc group from compound 12 using ethyl acetate saturated with HCl reagent) (3.5mg, 0.0026mmol) was added. The mixture was stirred at RT for 24h under N_2 atmosphere. The crude product was purified using column chromatography to afford the product 15.MALDI-TOF- MS: $[M+H]^+$ calculated for $C_{94}H_{118}N_{13}O_{26}$ is 1846.0123and found 1846.0632$[M+H]^+$

4.5.2.4 Synthesis of compound 16 (fragment 2)

Fmoc Glu-OH was treated with EDC (5mg, 0.026mmol) and Dimethyl amino pyridine, catalytic amount in dry DCM for 5 minutes. Further Octaguanidium sorbitol (OG-S, has been synthesized as per our previously reported synthetic route[8] (43 mg,0.013 mmol) core has been synthesized as per our previously reported synthetic procedure[1]was added to the reaction mixture. The mixture was stirred at RT for 24h under N_2.The product was purified by column chromatography. .This was further subjected to Boc deprotection using ethyl acetate saturated with HCl reagent. The product was further purified by supelclean™ C18-reverse phase silica gel (solvent:

H_2O/MeOH). The purified product was dissolved in deionized water, filtered through polytetrafluoroethylene (PTEE) syringe filter, and lyophilized to give the control as a white foamy solid (HCl salt). MALDI-TOF- MS: $[M+H]^+$ calculated for $C_{102}H_{165}N_{30}O_{20}$ is 2131.5826 and found 2121.8545 $[M+H]^+$

4.5.3 HPLC measurements

The HPLC analysis was conducted using Shimadzu RP- HPLC ODS column with mobile phase consisting of in MeOH (A) and in H_2O (B).The gradient was linearly increased from 0% to 80% B for 25 minutes at the flow rate of 1mL/min at ambient temperature. UV-VIS detection was monitored simultaneously at 254nm and 480nm wavelengths.

4.5.3.1 HPLC release[38] profile of active ligand

PTX ligand release from SMTDDC was measured after incubation of cathepsin B protease enzyme at 37°C at pH 5.5. 10µL (concentration= 120ng/µL) of enzymatically active cathepsin B substrate was added to 180 µL of 0.1mM SMTDDC compound in buffer (50mM of sodium acetate and 1mM of EDTA , in the ratio 9:1) . A blank was carried out without cathepsin B enzyme, using 100µl of SMTDDC buffer solution. All measurements were carried out at pH 5.5, 7.4 at specific time intervals from 0 to 24 hrs using HPLC.

4.5.3.2 Stability study:

To evaluate the stability of SMTDDC in blood circulation, we have dispersed the TDDS in PBS (pH=7.4) containing 10% fetal bovine serum (FBS) and incubated at 37^0C, and checked HPLC at different intervals of time[10]. The result indicates that there is no significant drug degradation providing possibility of enhancing drug accumulation in tumour tissue.

4.5.4 SERS Measurement

We evaluated the SERS performance of SMTDDC @AuNPS (vfm coverslips, CellPath Ltd., UK) using Confocal Raman Microscope system (alpha 300R WITeC Germany) The Raman system was coupled with a microscope in a back scattering

geometry. The SERS Raman spectra were acquired by a near-infrared-enhanced CCD detector (cooled at -60 ◦ C, Renishaw, UK) through a Czerny-Turner-type spectrograph (f = 250mm) equipped with a holographic grating (600 g/mm). A 633nm laser beam (maximum output of 30mW,Renishaw, UK) was focused onto analytes via an ultralong working distance 20X microscope objective Each SERS Raman spectrum was collected with an integration time of 2 s and laser power of ~2.5mW for SERS measurements All averaged spectra in this work were obtained from more than 10 different samples with a standard deviation of <5%.

4.5.4.1 Release profile Measurement by Confocal Raman spectroscopy

The SERS samples were prepared by different concentrations of SMTDDC, CathB-cRGD sequence , free paclitaxel molecules with AuNP colloid(40nm size, as SERS substrates)[39]a ratio of 1:9 (v/v). The samples were incubated at least for 5min atroom temperature prior to Raman analysis. For liquid-phase analyte detection, 10 μL of the sample was loaded onto a vfm coverslips, Cell Path Ltd., UK (sonicated in toluene and ethanol sequentially followed by drying in Hot air oven).Prominent Raman peaks located at around **512cm^{-1}(**C-OH_3 torsion of methoxy group), **707cm^{-1}**(C-N, C-O, C-C stretching), **759cm^{-1}**(ring breathing of Thyrosine), **817cm^{-1}**(C-C stretching) ,**946 cm^{-1} (**C-C stretch backbone),**1025 cm^{-1} (**Stretching C-O) , **1080cm^{-1}** (C-O stretching, C-N stretching, phenylalanine),**1200 cm^{-1}(**Aromatic C-O (cRGD thyrosine) CH_2 stretching deformation), **1386 cm^{-1}(**CH_2 scissor deformation,CH_3 band). **1558 cm^{-1} (**Tyrosine), **1600-1640**cm^{-1}(C=C stretching modes, C=C stretching mode of tyrosine, C=C phenylalanine, Amide I, C=O stretching) and are good enough to check release profile through Raman spectroscopy. The complexes of SMTDDC@ $AuNP_S$ and was readily formed by simple mixing of AuNPs solutions with SMTDDC at room temperature, the octa guanidium moieties of SMTDDC was key for its high payload onto AuNPS and leads to the intense SERS spectrum.The maximum SERS signal enhancement occurred with9:1 ratio (v/v) AuNPS Vs SMTDDC which is further reflected in a visible color change from red to blue attributed to the formation of SMTDDC@ AuNPS and AuNP aggregates. Subsequently, more hotspots are generated which significantly enhances the SERS intensity. The excellent SERS finger prints from SMTDDC@AuNPS was found

to be decreasing in intensity when it approaches target protease because the enzymatic recognition results in the cleavage of the cathB peptide substrate, which ultimately detaches active ligand PTX fragment) from AuNPs surface leading to the steady decrease in SERS signal intensity. The incubation of SMTDDC@ AuNPs with activated CathB enzyme (63ng/ml, 37 °C) resulted in significant decrease in the SERS signal intensity noticeably the peaks at 1080 cm^{-1}.

4.5.4.2 Cluster analysis

Cluster analysis is a statistical method of grouping the data, without a prior knowledge of its nature, purely based on its mathematical attributes. It is a particularly useful technique to characterize hyper spectral data. Moreover, it has been applied quite often in the analysis of data.[40]

4.5.5 Cell lines and Cell culture

U-87 MG, glioblastoma cell line and WI-38, Human lung fibroblast cell lines (Normal) were purchased from American Type Culture Collection (Manassas, VA) and National Centre for Cell Science (NCCS, Pune, India) respectively. All cells were cultured as anchorage dependent using 25 cm^2 tissue culture treated flask in 37^oC incubator with5% CO_2 humidified atmosphere condition. Cells were maintained in Dulbecco's modified eagle's medium (DMEM) containing 10% fetal bovine serum (FBS), penicillin (50 units/mL), kanamycin sulfate (110 mg/L), streptomycin (50 µg/mL). HEPES (25 mM) buffer and $NaHCO_3$ (3.6g/L) were added to maintain the pH of the culture. Cells were passaged after 70-80% of confluency attained. All the cell culture works were performed in sterile environment.

4.5.5.1 Flow-cytometric analysis of $\alpha_V\beta_3$ integrin expression

U-87 MG and WI-38 cells were detached using mild trypsin-EDTA and each cell was taken as a suspension in centrifuge tubes at a density of 5×10^6 cells/mL. Then cells were subdivided into unstained or antibody treated groups for each type of cells. Afterwards, the cell suspensions were incubated with anti- $\alpha_V\beta_3$ (1:100) antibody solution in serum free colorless DMEM and incubated at 37^oC for 2h. Followed by a single washing with 1X PBS (phosphate buffer saline) cells were further incubated

with cy3 labeled secondary (H/L) antibody (1:600) solution in serum free colorless DMEM. After 1 h of incubation cells were again washed with 1X PBS to removeresidual antibody solution and cells were resuspended with serum free colorless DMEM and analyzed under BD LSRFortessa™ FACS instrument.

4.5.5.2 Cellular uptake

U-87 MG cells were harvested overnight at a density of 20×10^3 cells/mL in a cover glass bottom dish. Then cells were washed with 1X PBS and incubated with 10μM of SMTDC for 2 h. Then cells were washed and analyzed under inverted fluorescence microscope at 488 nm fluorescent filters and DIC mode.

4.5.5.3 Lysosomal localization study

SMTDC and lysosome co-localization studies have been carried out using previously described method [41] Briefly, U-87 MG cells of 20×10^3 cells/mL density was harvested overnight followed by treatment with 10μM of SMTDC for 2h. Then cells were incubated with red fluorescent lysotracker for 45 mins. After a single wash with 1X PBS live cell microscopy has been performed using inverted fluorescence microscope using 488 nm, 561 nm fluorescent filters and DIC mode.

4.5.5.4 Live cell SERS Imaging

The instrument settings and experimental procedure adopted was detailed in Section 3.1. For cellular imaging, 20 μL (from a mixture of SMTDDC and AuNPs (100 μl [1: 9])) of SMTDDC @ AuNPs was added to U-87cells and was incubated at 37 °C for 30 min, and a negative control well without NPs was also maintained. The acquisition time of aim age scan was set to 0.05 s. A piezoelectric table was used to record 150×150 points per image, leading to a total of 22,500 spectra for one image. Data acquisition was performed using Image Plus software from WiTec.

4.5.5.5 Cell viability assay

Cell viability was analyzed using 5(6) carboxy fluorescence, 3-(4, 5-dimethylthiazol-2-yl)-2, 5-diphenyltetrazolium bromide (MTT) solution as earlier described method [41]. Briefly, cells (U-87 MG and WI-38 cell lines) harvested in 96 well tissue culture plates

were subjected to treatments with various concentrations (2 μM, 1 μM, 0.5 μM, 0.25 μM) of either PTX or SMTDDC. Then cells were incubated for 24 h and further incubated with MTT solution for 4 h. Methanol and DMSO (1:1) mixture has been used to solubilize the formazan. Then viable cells have been quantified using microplate ELISA reader (Thermo; Multiskan™ GO Microplate Spectrophotometer) at 550 nm of wavelength.

4.5.5.6 Haemolysis assay

The haemolysis assay [42] was conducted to monitor the effect of constructs on normal red blood cells and was evaluated using previously reported protocols with little modifications. Initially, for removing blood plasma and the surface layer the EDTA stabilized human blood samples were centrifuged at 1600 rpm for 5 min. The residual Red Blood Cells pellet will be washed 3 to four times with 6mL of PBS solution and RBCs will be diluted in 25 mL of PBS solution. To the 0.2 mL RBC suspension0.8 mL of compounds to be tested in PBS at different concentrations will be added. By adding 0.8 mL of 2% Triton X 100 and PBS, respectively to 0.2 mL of RBC solution was used as positive and negative control samples. Furthermore the samples will be incubated at room temperature for 2 h, shaken once for every 30 min to re-suspend the RBCs and compounds. The samples will be centrifuged after 2 h, at 1600 rpm and100 mL of supernatants will be transferred to a 96-well plate. Absorbance of hemoglobin in supernatants could be measured with a micro plate reader at 570 nm. Percentages haemolysis of the RBCs will be calculated using the following formula:

Percentage Haemolysis = (abs of sample - abs of negative control)/(abs of positive control - abs of negative control)

The experiments were performed after getting approval from Human ethical committee, RCC, Trivandrum. From three separate experiments we calculated hemolysis percentage values.

4.5.5.7 *In vitro* lymphocyte proliferation assay

Fresh human blood samples were layered on equal volumes of Ficoll-Paque™ Plus solution and centrifuged at 800 x g for 20 min at 18°C. The thin white middle

lymphocyte layer was collected and washed with PBS twice by centrifugation at 100 x g for 10 min at 18˚C. The supernatant was discarded and the cells were suspended in 10% RPMI-1640. The cell number was counted with a hemocytometer and the viability of the cells was examined using the trypan blue exclusion assay. Samples containing cells with ≥95% viability were suspended at a concentration of $2x10^4$ cells/well. The lymphocytes were incubated at 37˚C in a humidified atmosphere of 5% CO_2. The effect of SMTDDC on isolated lymphocytes was evaluated using the MTT assay as described before. The proliferation index (proliferation rate/100) was calculated.

4.5.5.8 Immunocytochemistry of cellular microtubule network

Microtubule network of U-87 MG cells were stained according to the previously described method[41] Briefly, cells were treated with 2 µM of either PTX or SMTDDC for 24h. Then cells were fixed and permeabilized and incubated with anti-α tubulin primary antibody solution overnight at 4 ^oC. Then cells were washed with PBS and incubated with cy3 labeled secondary antibody for 2h. Hoechst33258 was used to counterstain nucleus. Microscopy was conducted using 40X objective at 405 and 561 nm fluorescent filters.

4.5.5.9 Cell cycle

Cell cycle experiment was performed with PI/ Rnase A according to earlier published report[41]. Briefly, U-87MG cells ($1×10^5$ cells/mL) were harvested overnight in 6 well plate in 37 ^oC incubator. Then 6 well plates were grouped as 2 wells each for the treatment with 2µM of paclitaxel or SMTDDC for 24h. Untreated wells were defined as control. Then cells were detached and overnight fixed with 70% ethanol at -20^oC. Further, cells were washed properly with 1X PBS (Phosphate buffer Saline; pH 7.4) to remove residual ethanol. Then cells were incubated with freshly prepared PI/RNase A solution for 45 mins before analysis using BD LSRFortessa™ flow cytometer having emission filters at 610 nm.

4.5.5.10 Cell death analysis

To analyze apoptosis,annexinV/PI based cell death assay using BD LSRFortessa™ flow cytometer as previously discussed method[34]. Briefly, U-87 MG cells ($1×10^5$

cells/mL)were harvested overnight followed by treatment with either 10nM PTX or SMTDDC for 24h. Untreated cells were considered control cells. After treatment cells were collected in suspension and treated with both annexin V and PI in binding buffer for 15 mins. Then cells were washed with binding buffer and examined under respective channel uder flow cytometry.

4.6 References

(1) Davis, M. E. Glioblastoma: Overview of Disease and Treatment. *Clin. J. Oncol. Nurs.* **2016**, *20* (5), S2–S8.

(2) Minniti, G.; Muni, R.; Lanzetta, G.; Marchetti, P.; Maurizi Enrici, R. Chemotherapy for Glioblastoma: Current Treatment and Future Perspectives for Cytotoxic and Targeted Agents. *Anticancer Res.* **2009**, *29* (12), 5171–5184.

(3) Ali, I. U.; Chen, X.; Imaging, M.; Imaging, B.; Institutes, N.; States, U. Penetrating the Blood À Brain Barrier : Delivery Vehicles. *ACS Nano* **2015**, *9* (10), 9470–9474.

(4) Groothuis, D. R. The Blood-Brain and Blood-Tumor Barriers : Delivery 1. *Neuro Oncol* **2000**, *2* (1), 45–59.

(5) Yang, X.; Liu, Z.; Li, Z.; Pu, F.; Ren, J.; Qu, X. Near-Infrared-Controlled, Targeted Hydrophobic Drug-Delivery System for Synergistic Cancer Therapy. *Chem. - A Eur. J.* **2013**, *19* (31), 10388–10394.

(6) Chen, Z.; Li, Z.; Lin, Y.; Yin, M.; Ren, J.; Qu, X. Bioresponsive Hyaluronic Acid-Capped Mesoporous Silica Nanoparticles for Targeted Drug Delivery. *Chem. - A Eur. J.* **2013**, *19* (5), 1778–1783.

(7) Stanzl, E. G.; Trantow, B. M.; Vargas, J. R.; Wender, P. A. Fifteen Years of Cell-Penetrating, Guanidinium-Rich Molecular Transporters: Basic Science, Research Tools, and Clinical Applications. *Acc. Chem. Res.* **2013**, *46* (12), 2944–2954.

(8) Maiti, K. K.; Lee, W. S.; Takeuchi, T.; Watkins, C.; Fretz, M.; Kim, D.-C.; Futaki, S.; Jones, A.; Kim, K.-T.; Chung, S.-K. Guanidine-Containing Molecular Transporters:

Sorbitol-Based Transporters Show High Intracellular Selectivity toward Mitochondria. *Angew. Chem. Int. Ed. Engl.* **2007**, *46* (31), 5880–5884.

(9) Maniganda, S.; Sankar, V.; Nair, J. B.; Raghu, K. G.; Maiti, K. K. A Lysosome-Targeted Drug Delivery System Based on Sorbitol Backbone towards Efficient Cancer Therapy. *Org. Biomol. Chem.* **2014**, *12* (34), 6564–6569.

(10) Jyothi B. Nair, Saswat Mohapatra, S. G. and K. K. M. Novel Lysosome Targeted Molecular Transporter Built on a Guanidinium-Poly-(Propylene Imine) Hybrid Dendron for Efficient Delivery of Doxorubicin into Cancer Cells. *Chem. Commun.* **2015**, *51* (12), 2403–2406.

(11) Paul A. Wender Christina B. Cooley, E. I. G. Beyond Cell Penitrating Peptides: Designed Molecular Transporters. *Drug Discov. Today. Technol.* **2012**, *9* (1), e49–e55.

(12) Futaki, S.; Nakase, I.; Suzuki, T.; Youjun, Z.; Sugiura, Y. Translocation of Branched-Chain Arginine Peptides through Cell Membranes: Flexibility in the Spatial Disposition of Positive Charges in Membrane-Permeable Peptides. *Biochemistry* **2002**, *41*, 7925–7930.

(13) Pan, L.; He, Q.; Liu, J.; Chen, Y.; Ma, M.; Zhang, L.; Shi, J. Nuclear-Targeted Drug Delivery of TAT Peptide-Conjugated Monodisperse Mesoporous Silica Nanoparticles. *J. Am. Chem. Soc.* **2012**, *134* (13), 5722–5725.

(14) Chen, K.; Chen, X. Integrin Targeted Delivery of Chemotherapeutics. *Theranostics* **2011**, *1*, 189–200.

(15) Chen, X.; Plasencia, C.; Hou, Y.; Neamati, N. Synthesis and Biological Evaluation of Dimeric RGD Peptide-Paclitaxel Conjugate as a Model for Integrin-Targeted Drug Delivery. *J. Med. Chem.* **2005**, *48* (4), 1098–1106.

(16) Zhong, Y.-J.; Shao, L.-H.; Li, Y. Cathepsin B-Cleavable Doxorubicin Prodrugs for Targeted Cancer Therapy (Review). *Int. J. Oncol.* **2013**, *42* (2), 373–383.

(17) Strojnik, T.; Zajc, I.; Bervar, A.; idanik, B.; Golouh, R.; Kos, J.; Dolenc, V.; Lah, T. Cathepsin B and Its Inhibitor Stefin A in Brain Tumors. *Pflugers Arch. Eur. J. Physiol.* **2000**, *439* (7), 122–123.

(18) Dal Corso, A.; Caruso, M.; Belvisi, L.; Arosio, D.; Piarulli, U.; Albanese, C.; Gasparri, F.; Marsiglio, A.; Sola, F.; Troiani, S.; et al. Synthesis and Biological Evaluation of RGD Peptidomimetic-Paclitaxel Conjugates Bearing Lysosomally Cleavable Linkers. *Chem. - A Eur. J.* **2015**, *21* (18), 6921–6929.

(19) Zhang, Z.; Mei, L.; Feng, S.-S. Paclitaxel Drug Delivery Systems. *Expert Opin. Drug Deliv.* **2013**, *10* (3), 325–340.

(20) Crown, J.; O'Leary, M.; Ooi, W.-S. Docetaxel and Paclitaxel in the Treatment of Breast Cancer: A Review of Clinical Experience. *Oncologist* **2004**, *9*, 24–32.

(21) Perez, E. Paclitaxel in Breast Cancer. *Oncologist* **1998**, *3* (6), 373–389.

(22) Kumar, S.; Mahdi, H.; Bryant, C.; Shah, J. P.; Garg, G.; Munkarah, A. Clinical Trials and Progress with Paclitaxel in Ovarian Cancer. *Int. J. Womens. Health* **2010**, *2* (1), 411–427.

(23) Ramalingam, S.; Belani, C. P. Paclitaxel for Non-Small Cell Lung Cancer. *Expert Opin. Pharmacother.* **2004**, *5* (8), 1771–1780.

(24) Zhang, P.; Hu, L.; Yin, Q.; Feng, L.; Li, Y. Transferrin-Modified c[RGDfK]-Paclitaxel Loaded Hybrid Micelle for Sequential Blood-Brain Barrier Penetration and Glioma Targeting Therapy. *Mol. Pharm.* **2012**, *9* (6), 1590–1598.

(25) Dal Corso, A.; Caruso, M.; Belvisi, L.; Arosio, D.; Piarulli, U.; Albanese, C.; Gasparri, F.; Marsiglio, A.; Sola, F.; Troiani, S.; et al. Synthesis and Biological Evaluation of RGD Peptidomimetic-Paclitaxel Conjugates Bearing Lysosomally Cleavable Linkers. *Chemistry* **2015**, *21* (18), 6921–6929.

(26) Nance, E.; Zhang, C.; Shih, T. Y.; Xu, Q.; Schuster, B. S.; Hanes, J. Brain-Penetrating Nanoparticles Improve Paclitaxel Efficacy in Malignant Glioma Following Local

Administration. *ACS Nano* **2014**, *8* (10), 10655–10664.

(27) Zhao, M.; Liang, C.; Li, A.; Chang, J.; Wang, H.; Yan, R.; Zhang, J.; Tai, J. Magnetic Paclitaxel Nanoparticles Inhibit Glioma Growth and Improve the Survival of Rats Bearing Glioma Xenografts. *Anticancer Res.* **2010**, *30* (6), 2217–2223.

(28) Satsangi, A.; Roy, S. S.; Satsangi, R. K.; Vadlamudi, R. K.; Ong, J. L. Design of a Paclitaxel Prodrug Conjugate for Active Targeting of an Enzyme Upregulated in Breast Cancer Cells. *Mol. Pharm.* **2014**, *11* (6), 1906–1918.

(29) Merrifield, R. B. Solid Phase Peptide Synthesis. I. The Synthesis of. *J. Am. Chem. Soc.* **1963**, *85* (14), 2149.

(30) Narayanan, N.; Karunakaran, V.; Paul, W.; Venugopal, K.; Sujathan, K.; Kumar Maiti, K. Aggregation Induced Raman Scattering of Squaraine Dye: Implementation in Diagnosis of Cervical Cancer Dysplasia by SERS Imaging. *Biosens. Bioelectron.* **2015**, *70*, 145–152.

(31) Ling, J.; Weitman, S. D.; Miller, M. A.; Moore, R. V; Bovik, A. C. Direct Raman Imaging Techniques for Study of the Subcellular Distribution of a Drug. *Appl. Opt.* **2002**, *41* (28), 6006–6017.

(32) Salehi, H.; Derely, L.; Vegh, A. G.; Durand, J. C.; Gergely, C.; Larroque, C.; Fauroux, M. A.; Cuisinier, F. J. G. Label-Free Detection of Anticancer Drug Paclitaxel in Living Cells by Confocal Raman Microscopy. *Appl. Phys. Lett.* **2013**, *102* (11), 113701.

(33) Yuen, C.; Zheng, W.; Huang, Z. Low-Level Detection of Anti-Cancer Drug in Blood Plasma Using Microwave-Treated Gold-Polystyrene Beads as Surface-Enhanced Raman Scattering Substrates. *Biosens. Bioelectron.* **2010**, *26* (2), 580–584.

(34) Movasaghi, Z.; Rehman, S.; Rehman, I. Raman Spectroscopy of Biological Tissues. *Appl. Spectrosc. Rev.* **2007**, *42* (5), 493–541.

(35) Segawa, K.; Nagata, S. An Apoptotic “Eat Me” Signal: Phosphatidylserine Exposure.

Trends Cell Biol. **2015**, *25* (11), 639–650.

(36) Nair, J. B.; Joseph, M. M.; Mohapatra, S.; Safeera, M.; Ghosh, S.; Sreelekha, T. T.; Maiti, K. K. A Dual-Targeting Octaguanidine-Doxorubicin Conjugate Transporter for Inducing Caspase-Mediated Apoptosis on Folate-Expressing Cancer Cells. *ChemMedChem* **2016**, *11* (7), 702–712.

(37) Majoros, J.; Myc, A.; Thomas, T.; Mehta, C. B.; Baker, J. R. PAMAM Dendrimer-Based Multifunctional Conjugate for Cancer Therapy : Synthesis , Characterization , and Functionality. **2006**, No. Mwco 3500, 572–579.

(38) Li, Y.; Gu, C.; Gruenhagen, J.; Yehl, P.; Chetwyn, N. P.; Medley, C. D. An Enzymatic Deconjugation Method for the Analysis of Small Molecule Active Drugs on Antibody-Drug Conjugates. *MAbs* **2016**, *8* (4), 698–705.

(39) Ramya, A. N.; Joseph, M. M.; Nair, J. B.; Karunakaran, V.; Narayanan, N.; Maiti, K. K. New Insight of Tetraphenylethylene-Based Raman Signatures for Targeted SERS Nanoprobe Construction Toward Prostate Cancer Cell Detection. *ACS Appl. Mater. Interfaces* **2016**, *8* (16), 10220–10225.

(40) Parthasarathy, R.; Thiagarajan, G.; Yao, X.; Wang, Y.; Wang, Y. Application of Multivariate Spectral Analyses in Micro-Raman Imaging to Unveil Structural/Chemical Features of the Adhesive/ Dentin Interface. *J Biomed Opt.* **2009**, *13* (1), 1–18.

(41) Mohapatra, S.; Saha, A.; Mondal, P.; Jana, B.; Ghosh, S.; Biswas, A.; Ghosh, S. Synergistic Anticancer Effect of Peptide-Docetaxel Nanoassembly Targeted to Tubulin: Toward Development of Dual Warhead Containing Nanomedicine. *Adv. Healthc. Mater.* **2017**, *6* (2).

(42) Joseph, M. M.; Aravind, S. R.; Varghese, S.; Mini, S.; Sreelekha, T. T. Evaluation of Antioxidant, Antitumor and Immunomodulatory Properties of Polysaccharide Isolated from Fruit Rind of Punica Granatum. *Mol. Med. Rep.* **2012**, *5* (2), 489–

496.

Chapter 5

NIR-Light Driven Dual Targeting P-Sulfonato calix[4]arene Appended Hollow Gold Nano Transporter to Resolve Drug Resistance and Cardio Toxicity in Cancer Therapy

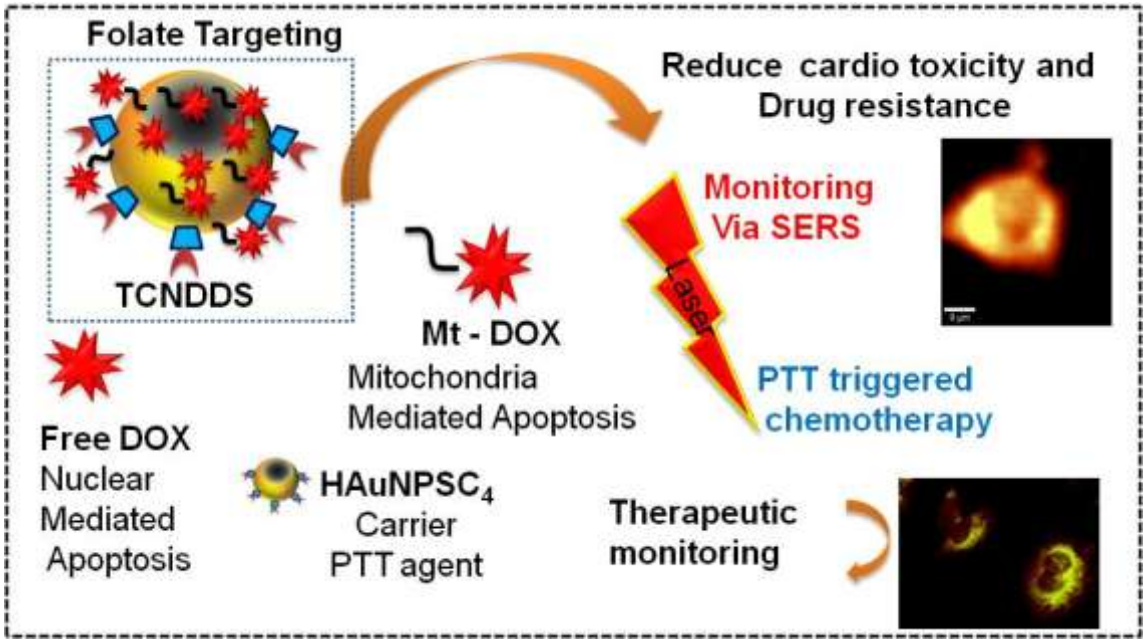

5.1 Abstract: *In order to overcome the problems associated with cardio toxicity, drug resistance and to increase therapeutic index, a new thermo responsive nano transporter was developed. A combination of doxorubicin (DOX) and mitochondria targeting peptide-substrate conjugated DOX (Mt Dox) was decorated on a folic acid targeted p-sulfonato calix[4]arene appended hollow gold nanoparticles designated as targeted combinational nano drug delivery system (TCNDDS). The synthesized transporter is able to produce NIR triggered photo thermal effect as well as temperature controlled drug release. The sub-cellular targeted chemotherapeutic cargo delivery along with photo thermal therapy improved the therapeutic index compare to conventional chemotherapy by the anticancer agents. The nano transporters are capable for targeted delivery DOX delivery towards cell nuclei and*

mitochondria, respectively. The as-synthesized mitochondrial targeted Mt DOX can induce mitochondrial membrane depolarization to cause cell death in cancer cells with a reduced toxicity in cardiac cells up on comparison with the clinically used free DOX. Cellular imaging using fluorescence and confocal Raman microscopic platforms revealed the delivery of DOX and Mt DOX towards nucleus and mitochondria respectively. Selective targeting and enhanced cytotoxicity was observed in folate over expressing cancer cells incubated with TCNDDS and subsequently irradiated with NIR light, attributable to both nano transporter-mediated photo thermal ablation and cytotoxicity of released free DOX and Mt DOX. These results indicated the promising potential of TCNDDS to overcome cardio toxicity in long-time anticancer chemotherapy.

5.2 Introduction

Nano-sized drug carriers were emerged as a budding platform in the delivery of versatile therapeutic cargoes. Among the different reported drug carriers liposomes and other lipid formulations[1] are the established one and some other polymeric nano carriers are in clinical trials. Over the past few years remarkable progress were made in the area of inorganic nano carriers'[2] and was used as an attractive platform for the delivery of many clinically approved drugs. Owing to the unique properties like easy fabrication strategies, unique chemical and physical properties, functional versatility, biocompatibility and low toxicity; gold nano particles (AuNPs) have attracted greater attention in pharma and medical industries[3]. AuNPs are currently used for both sensing, therapy, and is emerged as an attractive carrier for different anticancer therapeutics. [4] Various type of AuNPs like gold nanosphers, gold nanorod, nanostar, flowers etc. were already exploited as therapeutic vectors.[5] One key feature of these nano systems are, they can be readily customized to incorporate a diverse array of functionalized ligands such as in the case of aurimmune, a tumour necrosis factor (TNF) bound PEGylated colloidal gold nano particles is in phase II clinical trial for curing solid tumour[3,6].

Hollow gold nano particles (HAuNPs) are ideally suited for tuneable plasmon absorption in the NIR window, high photo thermal properties, tuneable diameter, availability of hollow interior for high drug loading and lack of cytotoxic surfactant

suggesting the greater potential for various biomedical applications.[7] Photo thermal therapy (PTT) is an established and emerging technique for treating solid tumours.[8] PTT utilizes the conversion of absorbed near-infrared (NIR) light to generate heat, which will in turn cause the desired effect. You *et al.* demonstrated the high loading efficiency of doxorubicin (DOX) in a photo thermal platform, HAuNPs and its light triggered release profiling.[9] DOX is the most widely used broad-spectrum anticancer chemotherapeutic drug due to its exact curative effect. However, continues usage of DOX can induce cardiac toxicity[10], and multi-drug resistance (MDR).[11] Thus, the development of new delivery strategy to improve the therapeutic outcome of currently employed chemotherapeutics is a challenging task. Simultaneous delivery of DOX to multi-subcellular target in tumour cell can augment the antitumour effect of DOX as well as reducing the drawbacks. [12,13]Mitochondria of cancer cell is also an important target of DOX, reports suggest that damage mitochondrial DNA (Mt-DNA) can cause mitochondria mediated apoptosis in tumour cells.[14] Thus, the approaches for the simultaneous delivery of DOX in to nucleus and mitochondria of cancer cells may lead to enhanced antitumour efficiency. It has been reported that CGKRK (Mt Peptide)[15] is a tumour homing peptide substarte, having mitochondria localisation property and internalized *via* energy and heparin sulfate receptor-dependent pathway and displayed higher affinity towards cancer cells.[16] So far, the development of multifunctional hollow nano particles as targeted delivery systems with simultaneous sub-cellular targeting, imaging, with enhanced therapeutic efficacy by overcoming cardio toxicity and drug resistance has not been reported.

To afford the comprehensive potential of chemotherapy and photothermal therapy, a novel programmable carrier system consisted of p-sulfonato calyx[4]arene (SC_4)[17], a supramoleular carrier and folic acid (FA),[18] a cell surface ligand for tumour targeting and a combination of therapeutic modalities was fabricated within a single nanoconstruct which was coined as targeted combinational nano-carrier drug delivery system (TCNDDS). The TCNDDS is taking the advantage of receptor binding property of ligand, intracellular organelle targeting moieties and photo chemotherapy for targeting, imaging and therapeutic applications. In the present work, by using FA as a tumour cell surface targeting ligand, a SC_4 appended HAuNPs ($HAuNPSC_4$) was carefully engineered. An optimized

ratio of 1(Dox): 100 (Mt-DOX) was loaded in the HAuNPSC$_4$ particles. TCNDDS was up taken by tumour cells followed by the laser irradiation causes the release of both DOX and Mt-DOX. Consequently, nano particles with Mt-DOX and DOX diffused to the mitochondria and nucleus respectively (scheme 5.1). The remarkable antitumour potential of TCNDDS was greatly improved in folate receptor expressing tumour cells as well as in DOX resistant tumour cells, facilitating reduced cardio toxicity. Thus, HAuNPSC4 is a promising nano system for delivering both DOX and Mt-DOX and can act as a moderator of dual-modality cancer therapy. The current findings may offer rationale to explore the use of hollow nanoparticles -based delivery systems for cancer therapy.

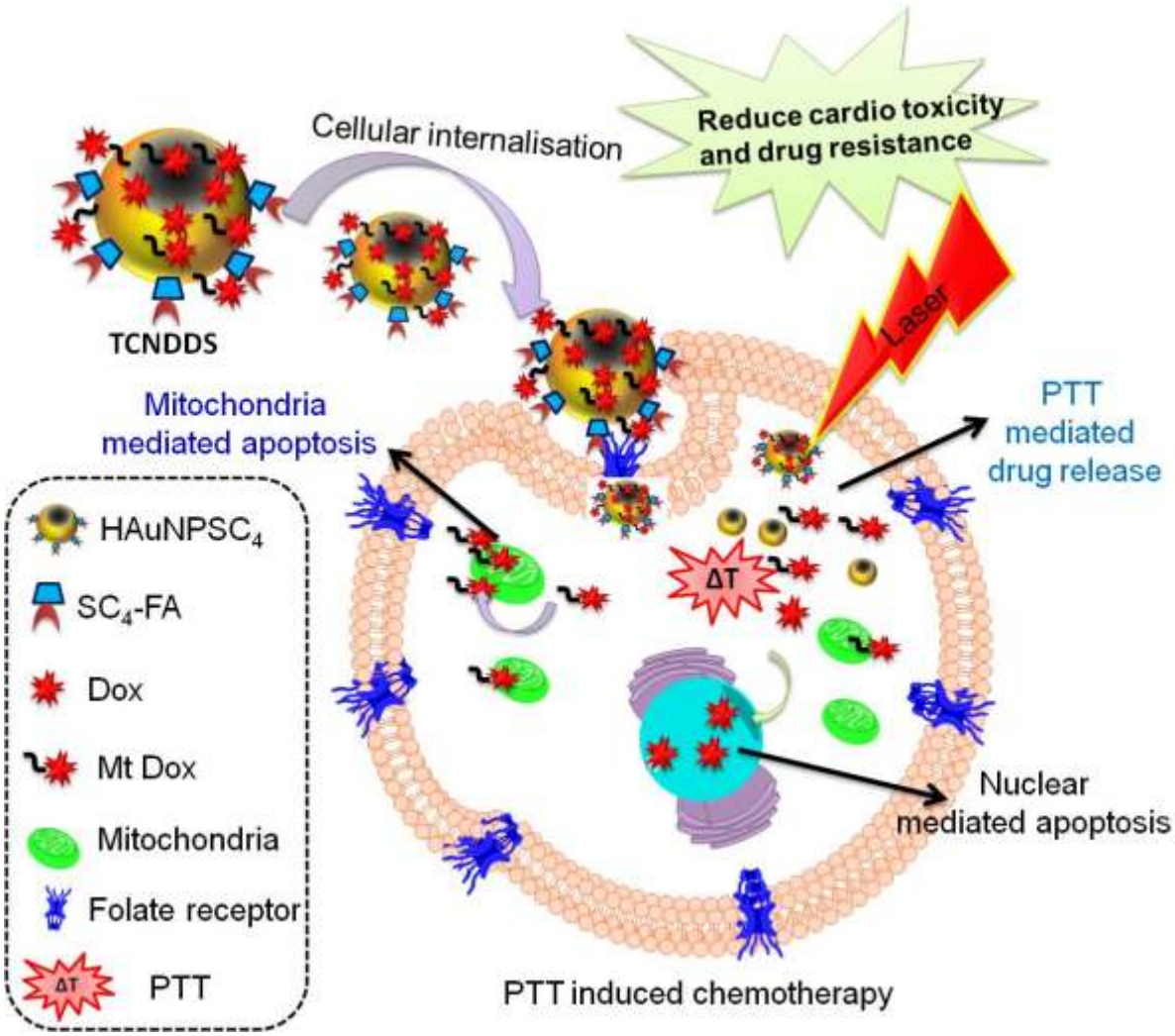

Scheme 5.1: Schematic representation; mode of action of TCNDDS.

5.3 Results and discussions

5.3.1 Synthesis and characterization of p-Sulfonato calix[4]arene appended hollow gold nano transporter

The fabrication of targeted combinational anticancer drug-delivery system was initiated by incorporating both chemo and photothermal therapeutic modality into a single nano construct. The primary goal is to develop a simple and reproducible method for synthesizing SC_4 appended HAuNPs which is tuned with strong SPR in the NIR region triggering photothermal therapy along with drug release profile in the target site. The method for the preparation of HAuNPs mainly based on templated galvanic replacement reaction, which is a general technique used in the fabrication of nano particles with hollow interiors and with good optical properties.[19] This is mainly based on the electrochemical processes between two metals, involving oxidation of any one of them and is also named as sacrificial galvanic replacement reaction. The metal having high reduction potential will be reduced and plated on the outside surface of the template. Therefore, the difference in the reduction potential between cobalt and gold was exploited to prepare HAuNPs with absorption in the NIR spectral window. Spherical cobalt nanoparticles were used as template for the galvanic replacement reaction to attain nano spheres with hollow interior in the presence of chloroauric acid according to the modified method of Schwartzberg *et al.*[20] The absorption spectra showed that the plasma resonance peaks for $HAuNPSC_4$ was tuned to the 710 nm NIR region (Figure 5.1a). Transmission electron microscopy (TEM) revealed the hollow morphology of the HAuNPs (Figure 5.1b) and indicated an average diameter of 34 ± 4.6 nm with gold shell thickness of 4-5 nm.

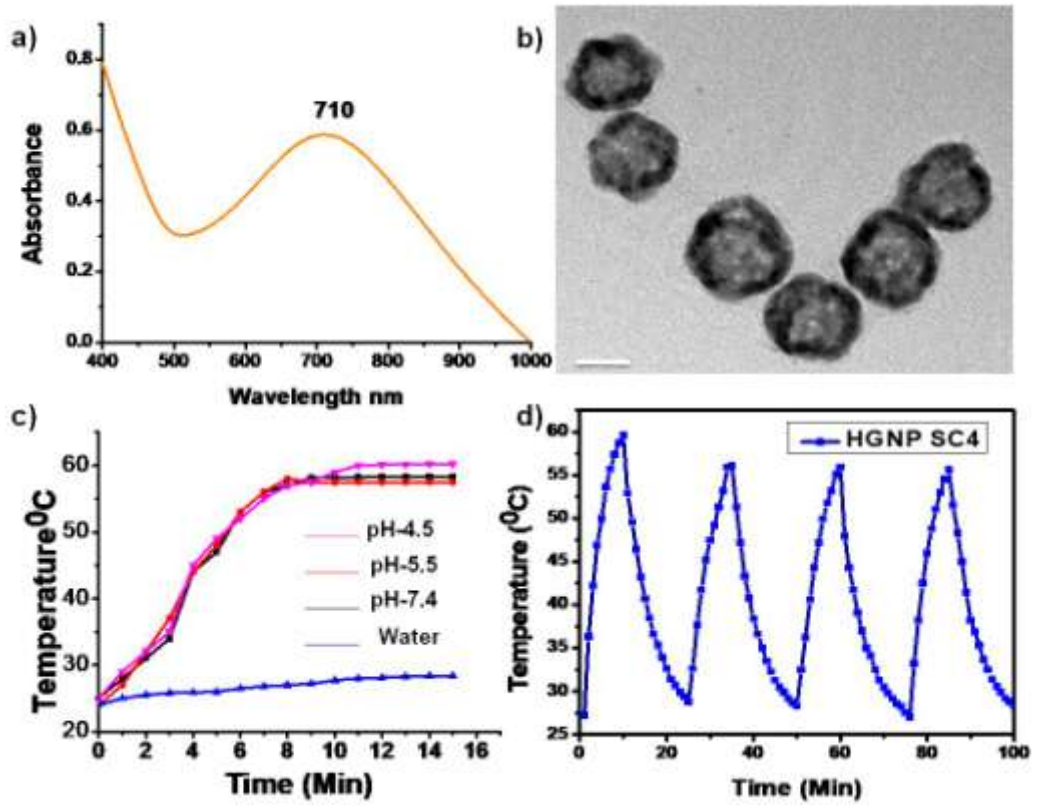

Figure 5.1: a) Absorption spectra of $HAuNPSC_4$. b) TEM images of $HAuNPSC_4$, Scale bar corresponds to 20nm. c) Photothermal efficiency of $HAuNPSC_4$ at various pH conditions. d) Photo stability of the nano transporter.

5.3.2 Photo thermal ability and stability of Nano transporter

Evaluation of photo thermal efficacy of the $HAuNPSC_4$ was performed by irradiating 808 nm lasers and found the temperature raise up to 59.8^{o}C over a period of 15 min (Figure 5.1c). Furthermore, the photothermal ability of the TCNDDS was also measured in order to check whether the conjugations will affect the hyperthermia, and found that the similar kind of increasing pattern upon NIR light indicating retained ability of the photo thermal effect of TCNDDS. Then, the photo stability was examined by repeating the irradiation of 808 nm laser for five cycles with same solution. The consistency in the higher temperature attained in all the five cycles indicates the excellent photo stability of the synthesized carrier (Figure 5.1d). Based on these studies, the possibility of making an efficient candidate for photo thermal therapy was confirmed. $HAuNPSC_4$, had a significantly higher colloidal stability. The particles showed good stability at different pHs and in phosphate-buffered saline (pH 7.4) supplemented with 10% fetal bovine serum at 37 °C (Figure 5.2a).

Moreover, no aggregation was observed when particles were stored in water at room temperature over a period of 3 months which disclosed same photo thermal property upon storage (Figure 5.2b).

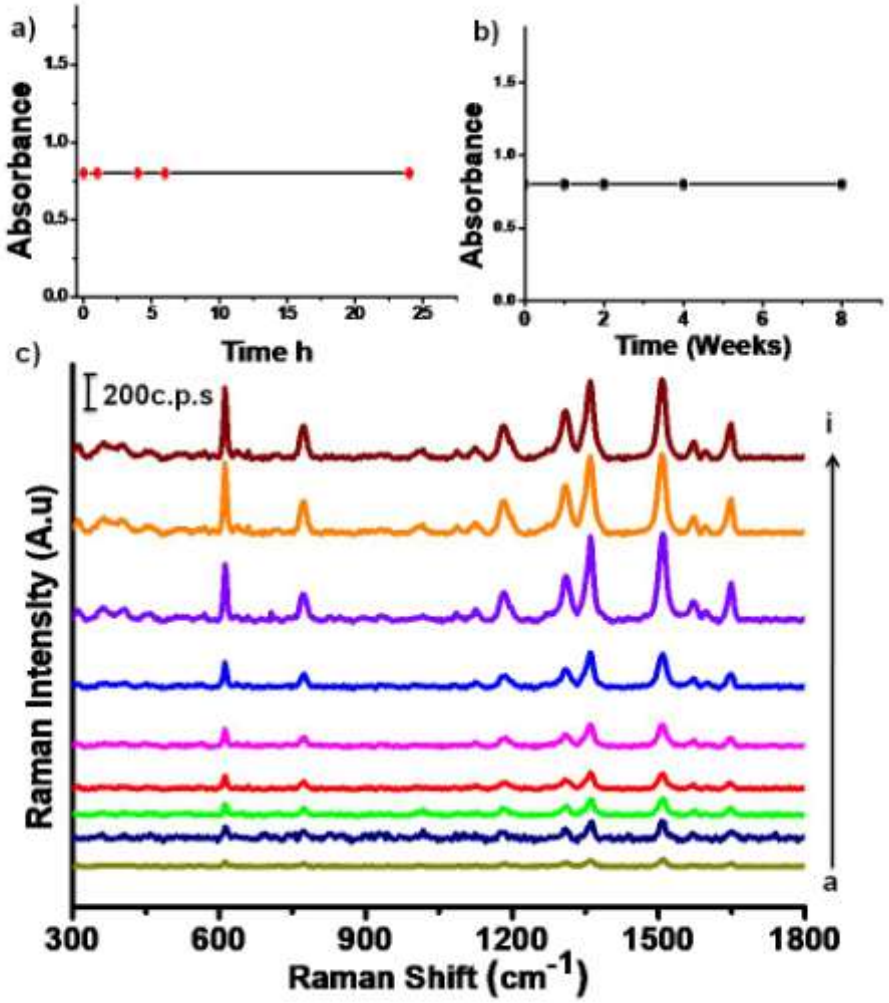

Figure 5.2: a) Stability of nano transporter with 10% fetal bovine serum in PBS (pH-7.4) at 37 °C. b) Stability upon storage, c) SERS fingerprints of Rh-6G by HAuNPs [a] represent Raman spectrum of 1M Rh-6G [b-m] represents the SERS spectra of increasing concentration of Rh-6G from 1 nM to 1M.

5.3.3 Evaluation of $HAuNPSC_4$ as an SERS substrate

To explore the efficiency of $HAuNPSC_4$ as SERS substrate for the enhancement of Raman fingerprints of the analytes, rhodamine 6G, a widely used Raman active molecule was used for the SERS spectral analysis. The most characteristic peaks around 1365 and 1514 cm^{-1} were detected even at very low dye concentration

(0.01nm) whereas the bare Raman fingerprints from the analyte was observed only at higher concentration of 1mM (Figure 5.2C, a). The results indicated the potential of $HAuNPSC_4$ as an SERS substrate. The peak at 1365 cm^{-1} obtained from C–C stretching vibrations and it was evaluated by decreasing the dilutions from 1mM up to limit of detection (Figure 5.2C, b-i). An enhancement factor of $2x10^7$, at an excitation wavelength of 633 nm, indicating the potential of $HAuNPSC_4$ as an SERS substrate.

5.3.4 Synthesis of Mt-DOX and conjugation with the delivery carrier

Next, the mitochondria targeting peptide sequence was synthesised *via* solid phase peptide synthesis by manual coupling of amino acids in HMPB-MBHA resin. (Scheme2) Further, the cleaved peptide was conjugated to DOX through amide coupling. The purified compound was subjected to HPLC analysis in order to check the purity; the absorbance of the compound was evaluated by UV-Vis spectroscopy, and was characterized by various spectroscopic methods. Subsequently the $HAuNPSC_4$ was evaluated for the drug encapsulation efficiency by incorporating DOX and Mt DOX separately and found 79% with free DOX and 94 % encapsulation efficiency with Mt-DOX. The increased encapsulation efficiency of Mt DOX could be due to the presence of cysteine residues which was bonded to the gold surface through sulphur terminal (Figure 5.3).

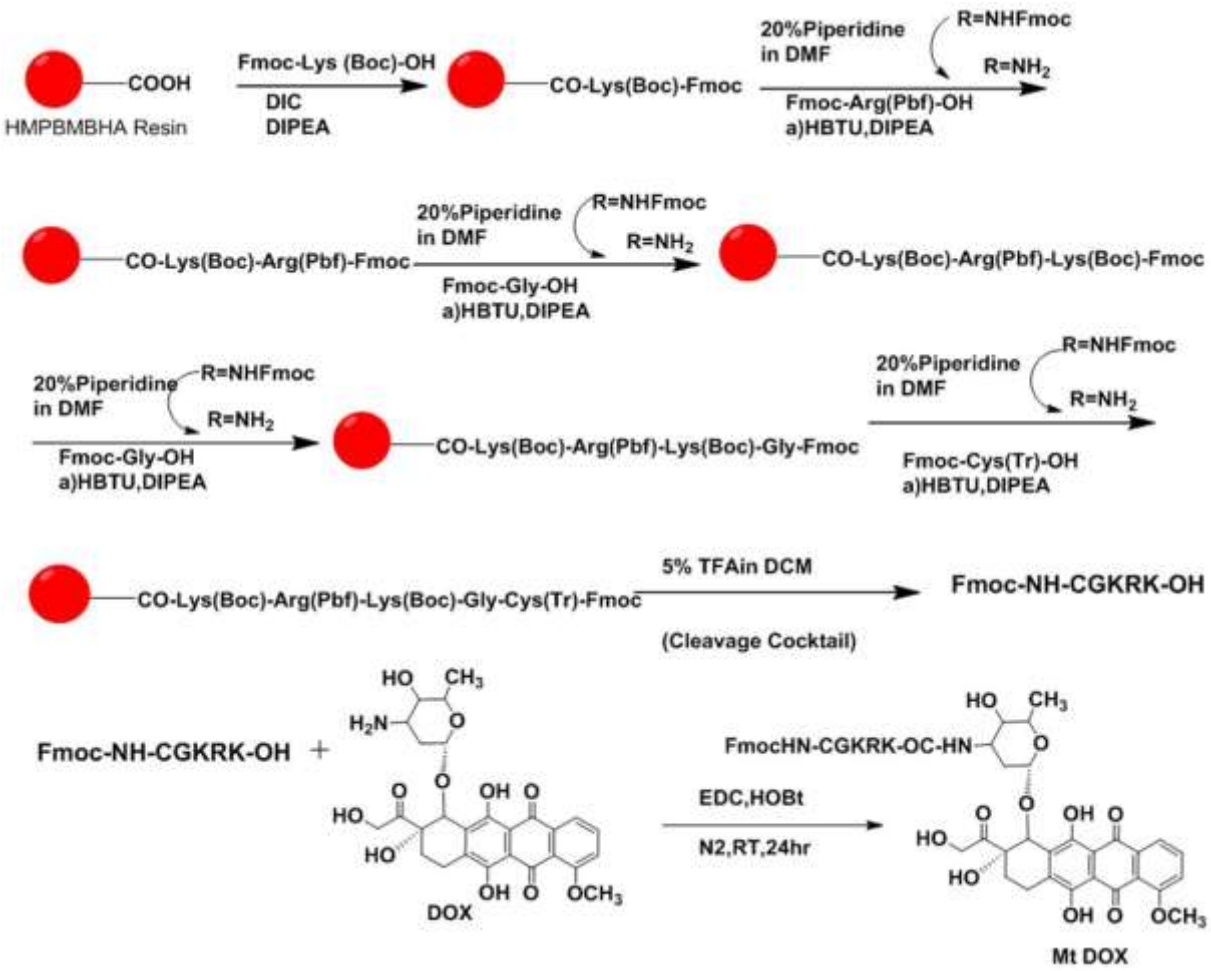

Scheme 5.2: Synthesis of Mt peptide *via* solid phase peptide synthesis and subsequent Mt Dox synthesis.

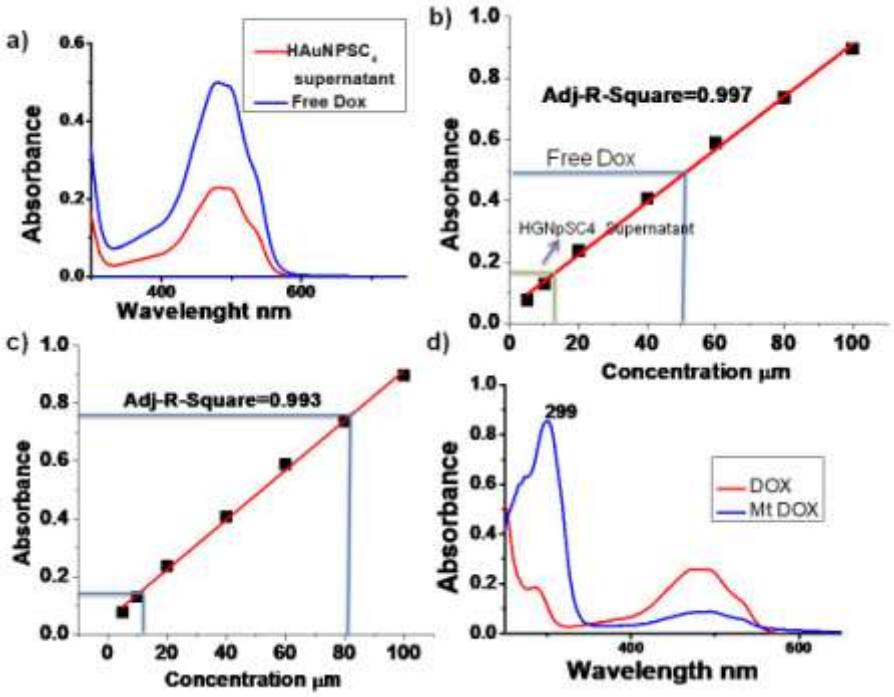

Figure 5.3: UV-Vis Spectroscopic profiling of free DOX and DOX remaining in the supernatant (unbound DOX). b) Standard cure for finding the concentration as well as encapsulation efficiency of DOX, c) Standard curve of Mt-DOX for finding encapsulation efficiency, d) Absorbance spectra of free DOX and Mt-DOX.

5.3.5 Evaluation of Raman signatures

The SERS spectra were recorded from DOX, Mt-DOX and Mt-peptide substrate after incubating with colloidal $HAuNPSC_4$ as SERS substrate. DOX displayed its characteristic Raman finger prints at around 449, 1258, 1387,and 1576 cm^{-1} corresponds to C=O in plane deformation, C-O stretch, CH_3 symmetric deformation, NH_2 deformation (amide ii band) respectively. Whereas Mt Peptide substrate showed Raman signature peaks at around 1001, 1231, 1291, 1371 ,and 1579 cm^{-1} coming out from the ring breathing mode, C-O-C stretch, C-O stretch, CH_3 deformation, and NH deformation (amide ii band) respectively. The Mt-DOX showed all the characteristic peak patterns from bare DOX and Mt peptide (Figure 5.4). The excellent peak pattern from the spectra indicating the SERS ability of the substrate, and also the interaction between the drugs and the carrier molecules (Figure 5.4).

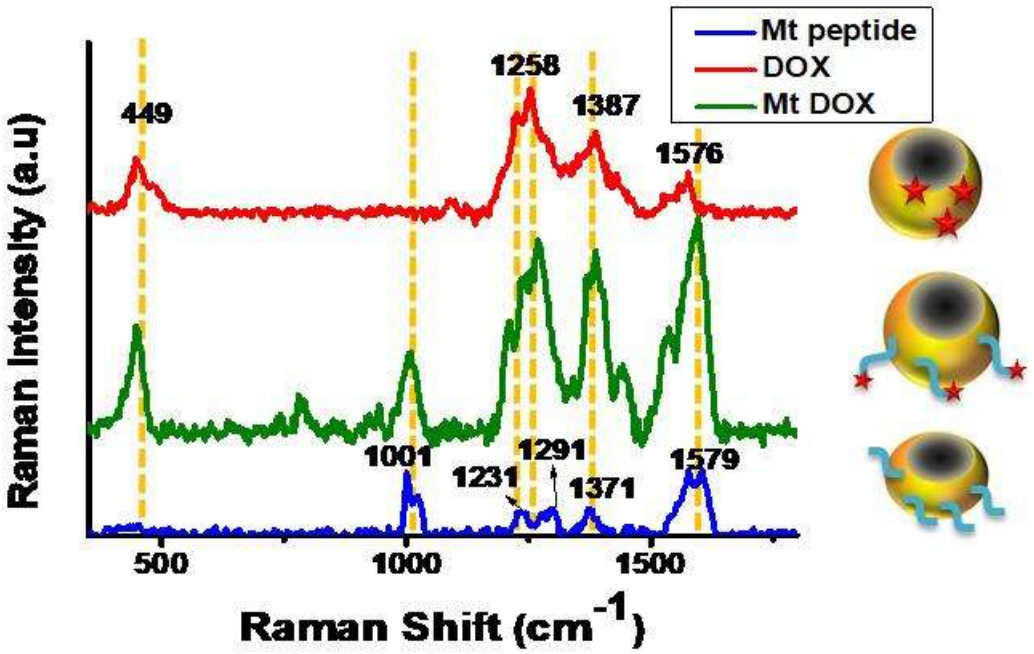

Figure 5.4: SERS analysis of DOX, Mt-DOX and Mt Peptide in presence of $HAuNPSC_4$.

5.3.6 Sub-cellular localisation of the synthesised Mt-DOX and free DOX

Drugs approaching into intracellular milieu required further targeting if their targets reside in membrane bound compartments. The free DOX first enter in to cytoplasm and diffuse towards the nucleus and bind to the nuclear DNA causing apoptosis which is a well established mechanism of action. Whereas the CGKRK, Mt Peptide substrate appended DOX facilitate the penetration towards mitochondria and produce mitochondria mediated Mt-DNA trigger toxicity. To evaluate the internalisation efficacy of both DOX and Mt DOX, the compounds were incubated with cervical carcinoma cell line HeLa and murine cardiocyte H9C2 cells for 4 hrs. (Figure 5.5). Further the cells were co-stained with nuclear staining hoechst and mitotracker green dye and imaged under florescence microscope. The distinctive mitochondrial localisation of Mt DOX, and nuclear localisation of DOX was confirmed by checking co-localisation and was determined using intrinsic fluorescence from DOX and Mt DOX respectively. The yellow co-localised images revealed excellent co-localisation of Mt DOX in mitochondria indicates the successful mitochondria targeting property of the probe which was further confirmed by statistical analysis.

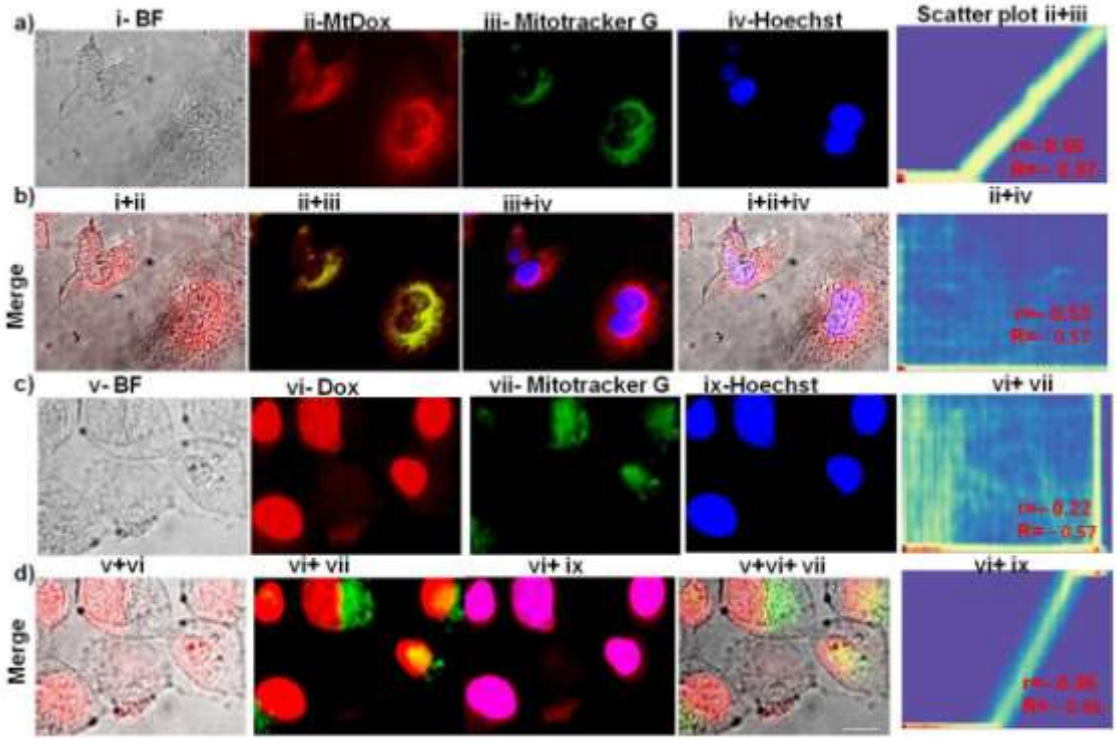

Figure 5.5: Fluorescence microscopic images of Mt DOX and DOX incubated HeLa cells and corresponding co-localisation with mitotracker green and nuclear staining dye hochest, after 4 hr incubation. a) HeLa cells with Mt DOX, i) bright field images,

ii)Mt DOX in the red channel, iii) mitotracker green in the green channel, iv)hoechst in the blue channel. b) Corresponding merged images. c) HeLa cells with DOX, v) bright field images, vi) DOX in the red channel, vii) mitotracker green in the green channel, viii) hoechst in the blue channel. d) Corresponding merged images .The fifth right panel represents scatter plots of merged images. In the scatter plot, r and R represents Pearson's correlation coefficient and Mander's overlap coefficient respectively. Scale bar 20 μm.

5.3.7 Evaluation of the subcellular distribution of drug conjugated nano transporter *via* SERS imaging

Apart from fluorescence imaging, SERS could be alternatively employed for finding the internalization of drugs or imaging agents. It can avoid the complications such as photo bleaching and low contrast generally observed with fluorescence imaging. HAuNPSC$_4$@DOX and HAuNPSC$_4$@Mt-DOX was incubated with HeLa (Figure 5.6a), A549 (Figure 5.6b), H9C2 (Figure 5.6c) and WI-38 (Figure 5.6d) cell lines and imaging were conducted with the aid of confocal Raman microscope. The SERS mapping of HAuNPSC$_4$@DOX incubated cells revealed localisation pattern from nuclear region where as HAuNPSC$_4$@Mt-DOX showed mostly cytoplasmic localisation indicating it is not going towards the nucleus.

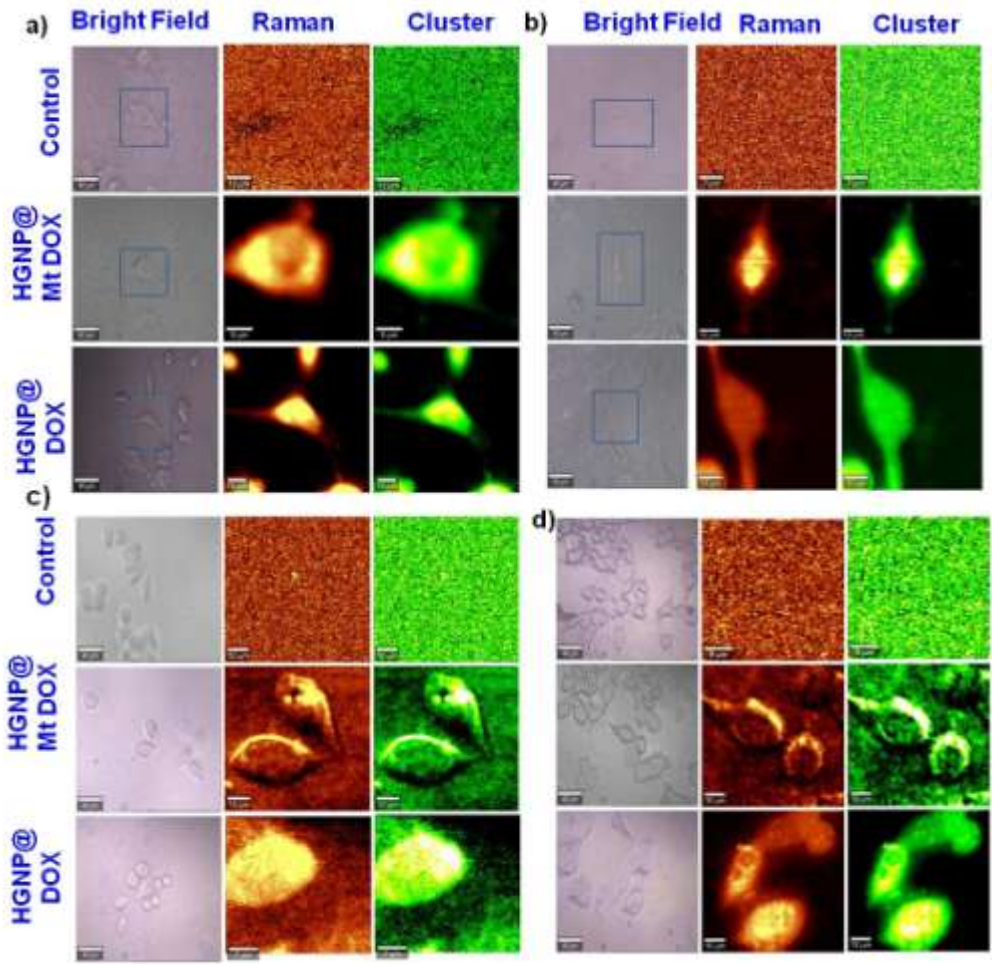

Figure 5.6: Cellular localisation *via* SERS in a) H9C2, b)WI-38, c) HeLa, and d) A549 cells incubated with the drug loaded nanotransporter.

5.3.8 Effect of DOX and Mt-DOX on mitochondrial membrane potential

Different studies showed that the mitochondria mediated apoptosis and Mt-DNA damage can be attributed to the loss of mitochondrial membrane potential. The effect of DOX and Mt DOX on mitochondrial membrane of HeLa cells was examined by using JC-1 staining**.** The decrease of red/green ratio of fluorescence intensity indicates depolarization of mitochondria. The ratio of red/green was significantly decreased in the case of Mt DOX indicating the change in membrane potential (Figure 5.7a, b). Additionally, one of the major roles of mitochondria is to produce ATP. P-gp is an ATP dependent pump and generally a higher mitochondrial membrane potential is essential for the production of ATP.[14] Therefore, the decrease in the mitochondrial membrane potential can lead to reduction of drug efflux

mediated by P-gp and the increase of the accumulation of antitumour drug in the drug resistant-tumour cells, subsequently enhancing the antitumour activity on drug-resistant tumour cells. The DOX targeted towards mitochondria can harvest different effects, i) disruption of mitochondria membrane through high affinity of DOX towards lipid bilayer, ii) it can cause release of mitochondrial enzymes such as cytochrome-c *via* disruption of membrane, and can lead to apoptosis in an intrinsic pathway iii) or it can induce production of free radicals in mitochondria and can cause calcium release, oxidative stress and peroxidation.

Furthermore, the membrane de-polarization was confirmed with tetra methyl rhodamine ethyl ester (TMRE) mitochondrial membrane potential assay. As shown in Figure 5.7c, the decrease in mitochondrial membrane potential was observed when cells were treated with DOX and Mt DOX. However, the decrease of mitochondrial membrane potential in the Mt DOX treated cells is more significant than that of the DOX treatment. These results suggested that mitochondria were damaged significantly by mitochondria targeted Mt-DOX than free DOX.

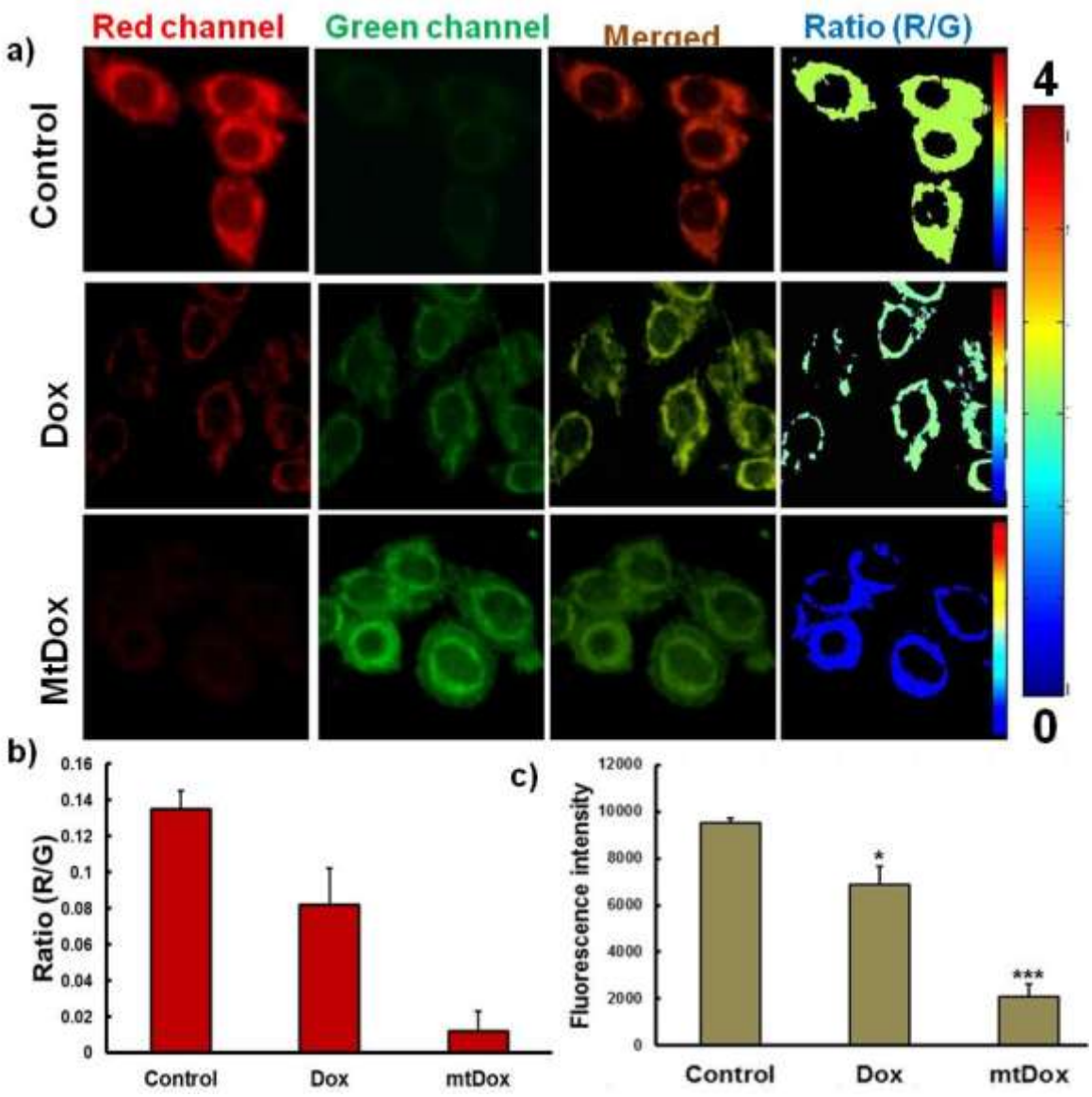

Figure 5.7: Mitochondrial membrane potential evaluation with a) JC-1 Assay, b) quantification of JC-1 assay and c) TMRE assay. Data are the meanœ ± SD of three independent experiments; **p<0.01, ***p<0.001, relative to control.

5.3.9 Synergistic therapeutic effect of DOX and Mt-DOX

As a preliminary screening, the combined effect of DOX and Mt-DOX was examined on cancer and normal cells. This drug combination showed synergistically increased anticancer activities *in vitro* without augmenting cardio myocyte toxicity (Figure 5.8, 9). Hence the ratio of Mt-DOX [100] : DOX [1] was selected for optimal cytotoxicity preferentially in cancer cells with less effects on cardiac cells. This ratio was selected for loading in to the TCNDDS.

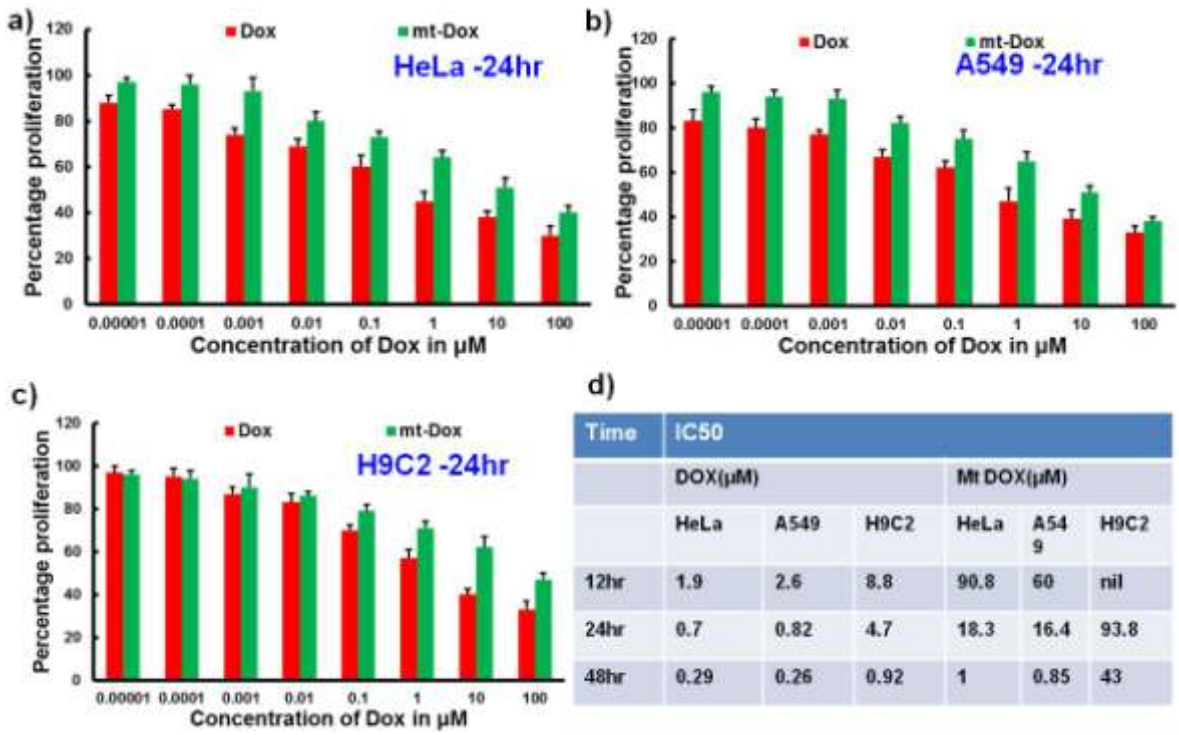

Time	IC50					
	DOX(µM)			Mt DOX(µM)		
	HeLa	A549	H9C2	HeLa	A549	H9C2
12hr	1.9	2.6	8.8	90.8	60	nil
24hr	0.7	0.82	4.7	18.3	16.4	93.8
48hr	0.29	0.26	0.92	1	0.85	43

Figure 5.8: Cytotoxicity evaluation of DOX and Mt DOX in different cell lines; a) HeLa b)A549, c) H9C2cells and d) the corresponding IC_{50} values. Data are the mean ± SD of three independent experiments.

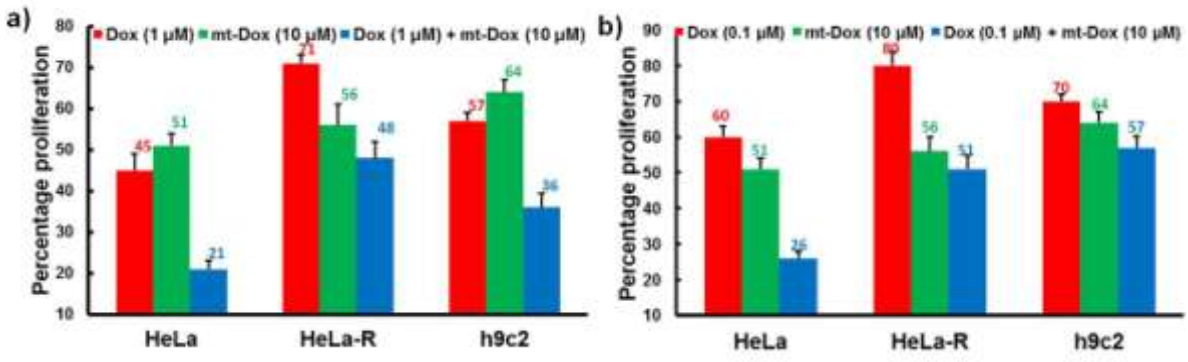

Figure 5. 9: Cytotoxicity evaluation of combination of DOX and Mt DOX in HeLa, H9C2 and HeLa R cells. a) DOX,1µM and Mt DOX10 µM, b) DOX, 0. 1µM and M DOX 10 µM. Data are the mean± SD of three independent experiments.

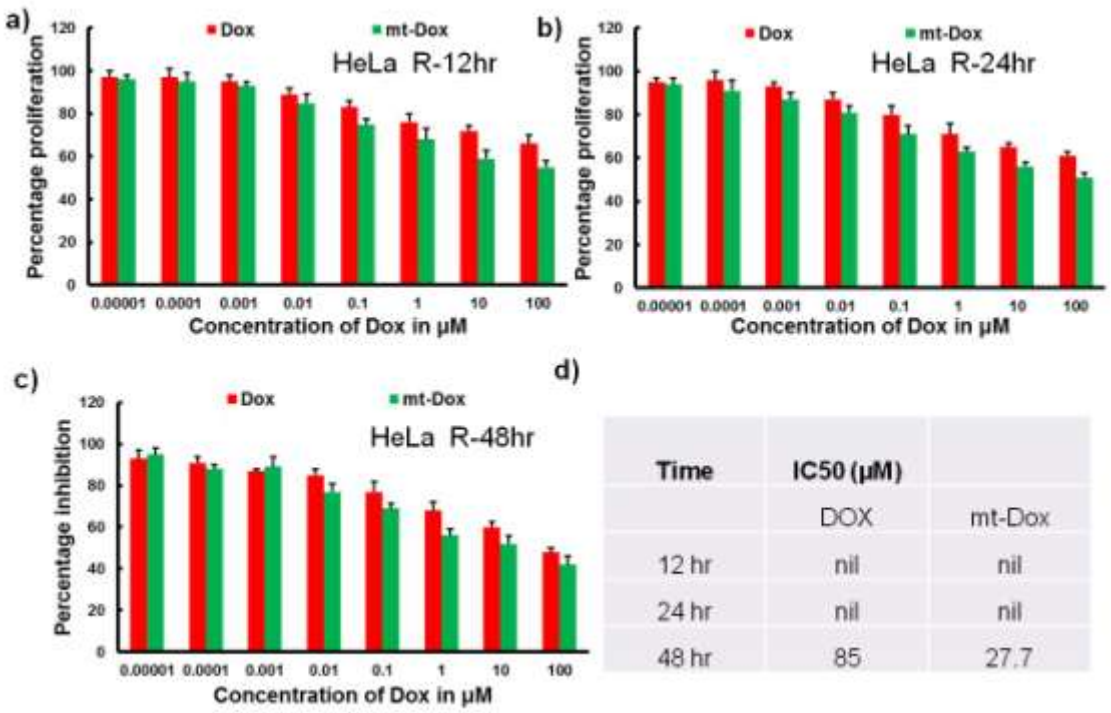

Time	IC50 (µM)	
	DOX	mt-Dox
12 hr	nil	nil
24 hr	nil	nil
48 hr	85	27.7

Figure 5.10: Cytotoxicity evaluation of DOX and Mt DOX in HeLa R cells; a) 12 hr b) 24hr, c) 48h, and d) the corresponding IC_{50} values. Data are the mean ±SD of three independent experiments.

5.3.10 Evaluation of cytotoxicity in drug resistant cells

Repetitive treatment of chemotherapeutic drugs produces drug resistance, which is the major bottleneck in the cancer treatment. As a result of this the cancer cells could effectively withstand with the drug provided after a few treatment cycles. Intelligent delivery systems were designed to overcome this clinical disadvantage. The cytotoxicity evaluation revealed the interesting property of Mt-DOX to produce cytotoxicity towards DOX resistant cell line HeLa R where the DOX was observed to be in effective (Figure 5.10).

5.3.11 *In vitro* drug release studies

The admirable photothermal effects of $HAuNPSC_4$ nano transporter encouraged to explore the NIR light responsive drug release profiling. The DOX was attached to $HAuNPSC_4$ *via* electrostatic interaction with amine, it was anticipated that the release of DOX from nano transporter would be temperature and pH dependent. In order to validate this assumption, the evaluation of DOX release from the nano transporter was assessed in the presence of NIR laser at different pHs. Interestingly, the DOX release from nano transporter was increased in acid environment (pH 5.0,

37 °C) in which the cumulative release of DOX exceeded ~ 80% after 12 hr of incubation compared with less than 70% of DOX release in pH 7.4 (Figure 5.11a). This was attributed to the increased solubility of DOX in an acid medium mimicking tumour microenvironment. Similar result was observed by controlling the release by on-off cycles upon NIR irradiation (Figure 5.11b) when repeated four times. In similar fashion, the Mt Dox release was monitored upon irradiation of NIR laser. The interaction between Mt DOX and nano transoprter is through Au-S interaction (from cysteine residue), the bond is indeed a thiolate–Au+ coordinative interaction. It has been reported that the thiol grafted coating on gold nanostar is labile to release the attached cargo upon NIR triggered hyperthermia.[21] The release kinetics of Mt-DOX upon laser irradiation displayed a similar kind of release pattern as observed with DOX. So the release of both DOX and Mt-DOX can be attributed by NIR triggered hyperthermia produced by the nano transporter (Figure 5.11c, d).

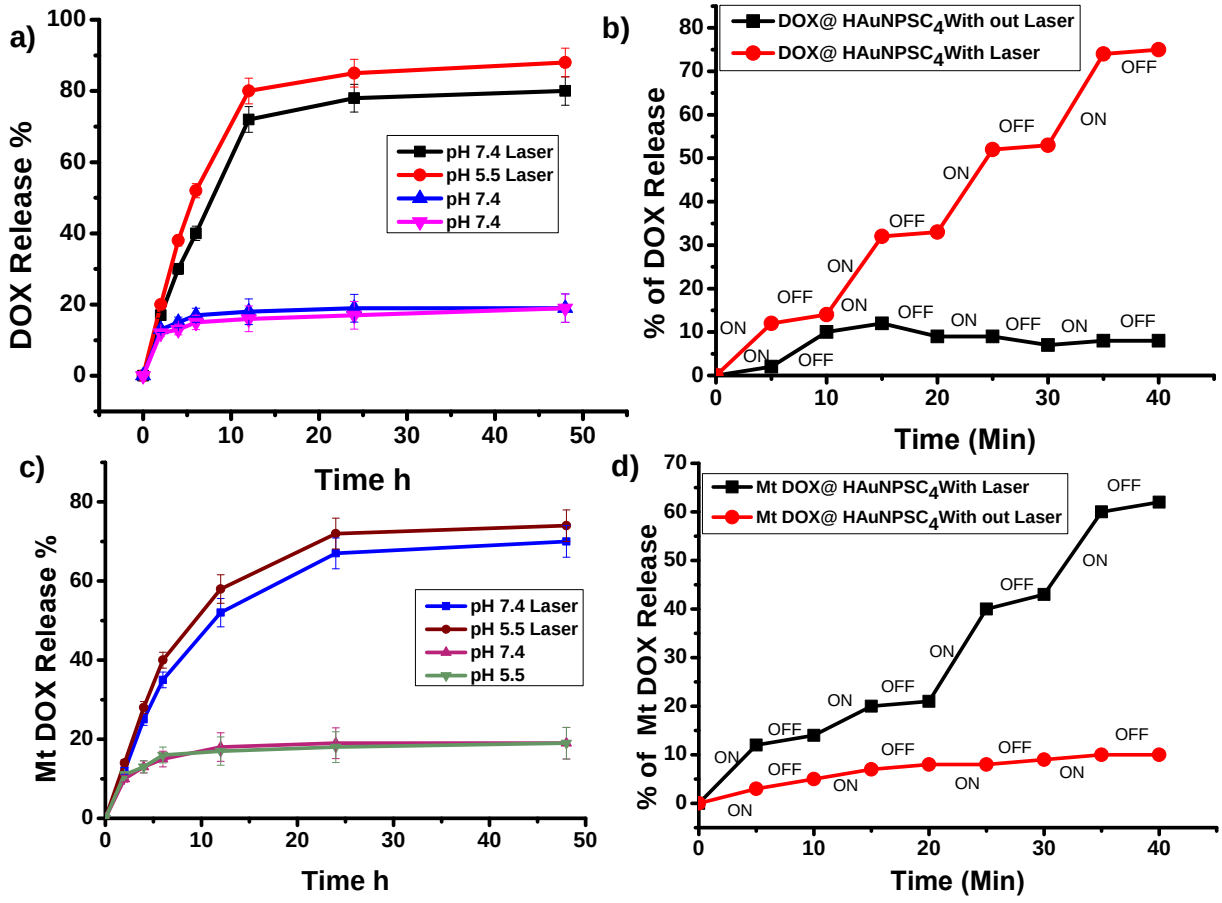

Figure 5.11: Evaluation of drug release kinetics. a) Release profiles of DOX from $HAuNPSC_4$ different media of pH values at 37 °C in presence and absence of NIR

laser (n=3). b) Release of DOX from DOX@HAuNPSC4 under repeated NIR laser exposure, c) release profiles of Mt-DOX , d) Mt-DOX release upon repeated NIR irradiation.

5.3.12 Fabrication of targeted combinational drug delivery system

The drug delivery platform was made a targeted system by adding SC_4 included with folic acid ligand. Later the drugs were added by simply mixing a ratio of DOX and Mt-DOX (1:100) with $HAuNPSC_4$ for 24 hrs. The solution was then centrifuged to remove unbound drugs. The final construct contain folic acid included SC_4 appended with a combination of DOX and Mt-DOX designed to produce maximum therapeutic index in cancer cells and minimal cardio toxicity can be named as targeted combinational nano-carrier drug delivery system (TCNDDS). The UV-Vis spectrum of TCNDDS confirms the formation of final nano construct (Figure 5.12a). After conjugation, the appearance of minor peaks at 499 and 532 nm along with the decrease in absorbance of broad NIR plasmon absorption peak at 710 nm, characteristic of $HAuNPSC_4$, indicating the conjugation of DOX and Mt DOX up on the nano transporter. Further TEM images revealed the conjugation uniform morphology of the nano transporter (Figure 5.12b).

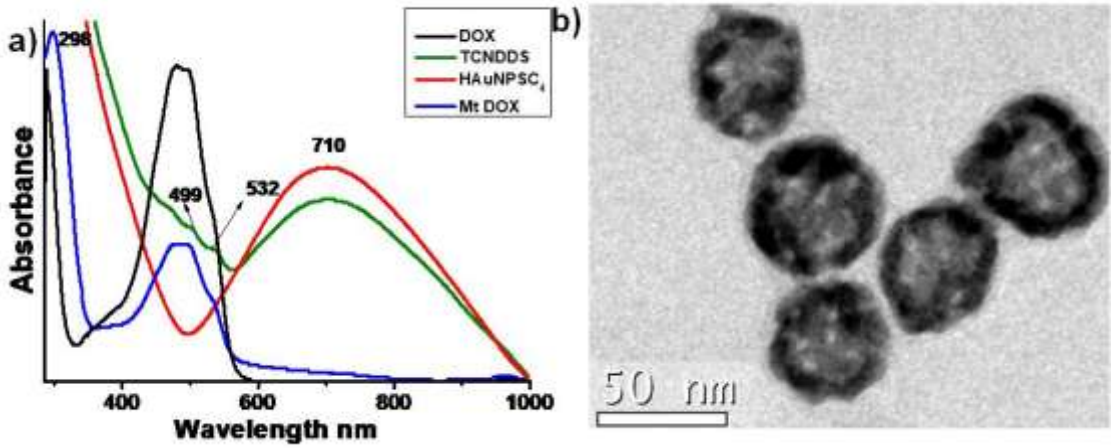

Figure 5.12: Absorbance spectra of free DOX (black), Mt-DOX (blue), $HAuNPSC_4$ (red), and TCNDDS (green).b) TEM images of TCNDDS

5.3.13 Cytotoxicity of TCNDDS

The cytotoxicity of TCNDDS with and without NIR laser irradiation was evaluated in cancer and normal cell lines Initially the photothermal effect of HAuNP and HAuNPSC4 (0.01µg/mL to 1000 µg/mL) on cells was tested (Figure 5.13). The NIR irradiation can attribute mainly three effects: 1) the photo thermal ablation effect produced by the nano construct *via* the thermal energy, 2) the increased concentration of drug molecules in the intracellular compartments due to NIR triggered release of therapeutic cargoes and 3) the synergistic effect of photo thermal chemotherapy. It has been reported that the increase in temperature above 40^{o}C can cause cellular injury and protein denaturation.[22] The exposure of NIR laser can cause either protein degradation or DNA, RNA degradation owing to the heat induced effect produced by the nano construct. Subsequently both DOX and Mt DOX was released by means of temperature dependent manner from the nano-carrier, and can effectively be taken up by the cancer cells and induce enhanced cytotoxicity. Moreover the synergistic photo thermal chemotherapy can cause significant cytotoxicity *via* hyperthermia induced by the nanoparticles and effect of chemotherapeutic agent. Both the free HAuNP and calixarene capped HAuNPSC$_{4,}$ showed nearly 80 % cell viability at maximal concentrations tested up on laser irradiation wherein without the laser, their cytotoxicity was negligible (Figure 5.13 a-c).

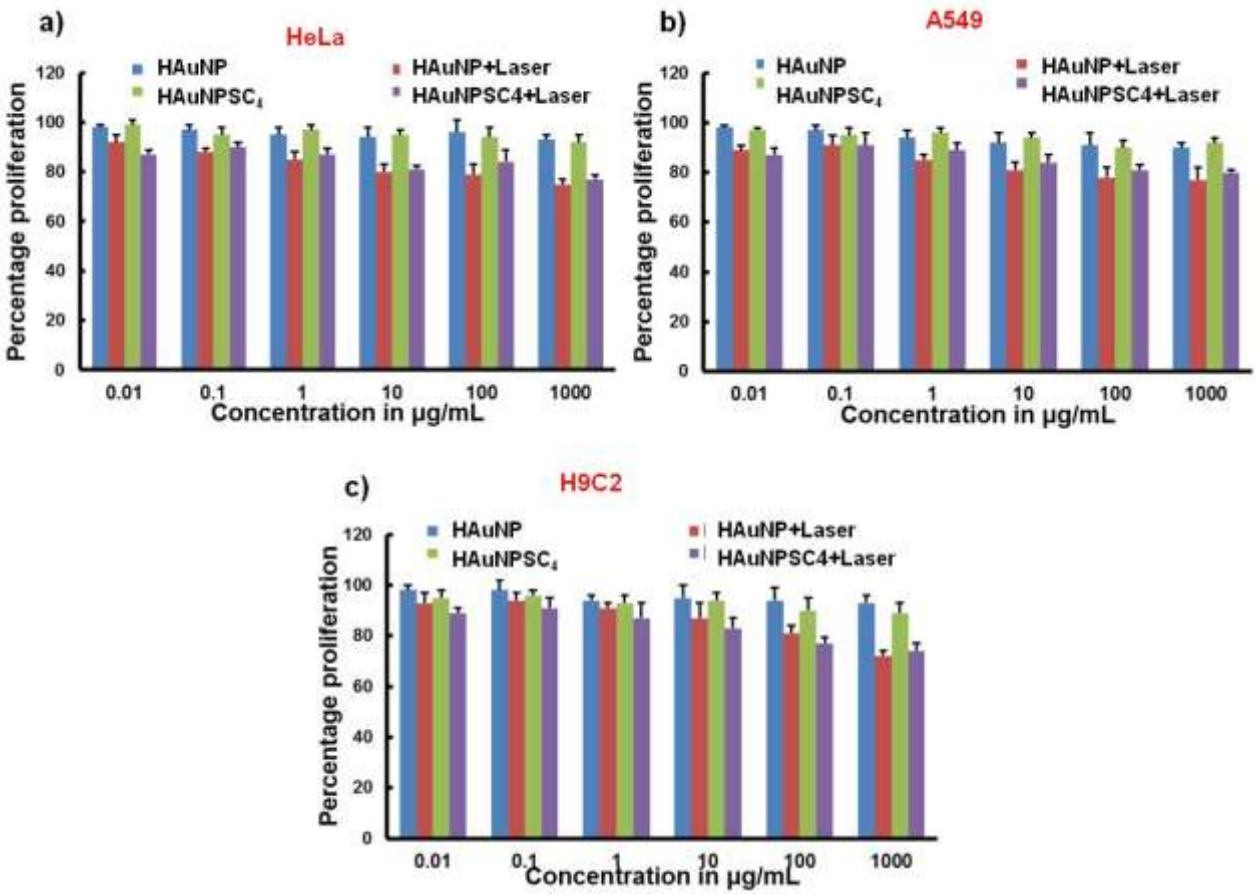

Figure 5.13: Cytotoxicity evaluation of HAuNP and $HAuNPSC_4$ by Brdu assay in a)HeLa cells, b) A549 cells, H9C2 cells. Data are the mean± SD of three independent experiments.

Next, the investigation of toxicity with TCNDDS in the absence and presence of NIR laser irradiation in folate receptor over expressing HeLa, folate receptor negative A549 and H9C2 cells were carried out from 0.1nm to 10 µM equivalent DOX concentrations 24 hr. TCNDDS showed dosage dependent cytotoxicity in FR positive HeLa cells where as in FR negative A549 and H9C2 cells no significant toxicity was observed. After NIR laser irradiation (0.5 W/cm^2 for 3 min per treatment, four treatments over a 2-h period), the TCNDDS displayed enhanced cell killing and reaches almost equivalent to the combination concentration of Free DOX+ Mt-DOX (Figure 5.14a-f). Corresponding IC_{50} values were shown in Figure 5.14, g.

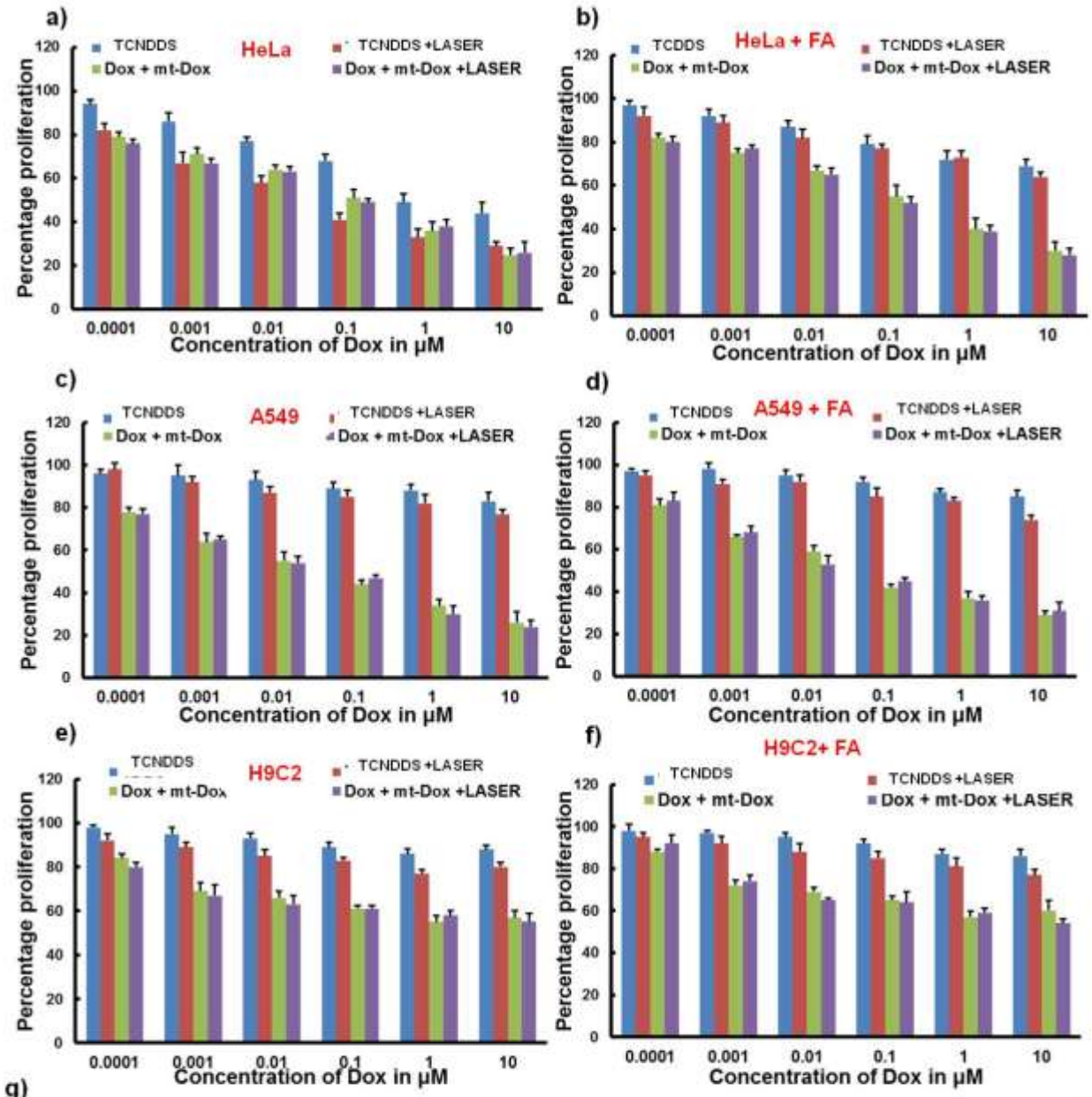

g)

IC_{50} Of	HeLa	Hela + FA	A549	A549+FA	H9C2	H9C2+FA
TCNDDS	0.95	NIL	NIL	NIL	NIL	NIL
TCNDDS+ LASER	0.52	NIL	NIL	NIL	NIL	NIL
DOX + Mt DOX	0.16	0.4	0.05	0.06	NIL	NIL
DOX+MT DOX +LASER	0.09	0.24	0.06	0.04	NIL	NIL

Figure 5.14: Cytotoxicity assay with cancer cells and normal cells treated with TCNDDS, TCNDDS+LASER, DOX+ Mt-DOX,DOX+ Mt-DOX+ LASER, with and without external folic acid (FA; 2 mm for 2 hr) after administration for 24 hr. a) HeLa cells, b) HeLa cells+ FA, c) A549 cells, d) A549 cells+ FA, e) H9C2 cells, f)H9C2cells + FA, g)

Table : corresponding IC_{50} values. Data are the mean ± SD of three independent experiments.

5.3.14 Apoptotic evaluation through molecular level changes in SERS platform

Analysis of Raman spectra from TCNDDS incubated HeLa cells in a time resolved manner was used to demonstrate the change in peak patterns after the incubation of targeted construct with cells for 4 hr. The characteristic biochemical changes happening during cell death mechanism after photothermal chemotherapy was evaluated.[23,24] The Raman spectral vibrations coming from various cellular components were evaluated after treatment, and observed a decrease in peak patterns of O-P-O stretching from backbone of DNA, proteins, and increase in intensity of N_7-H stretching of adenine guanine when compared to untreated cells (Figure 5.15). This phenomenon was attributed to the denaturation of DNA backbone of the cell during therapy.. The apoptotic DNA fragmentation occurred during photothermal-chemotherapy was effectively explored through SERS.

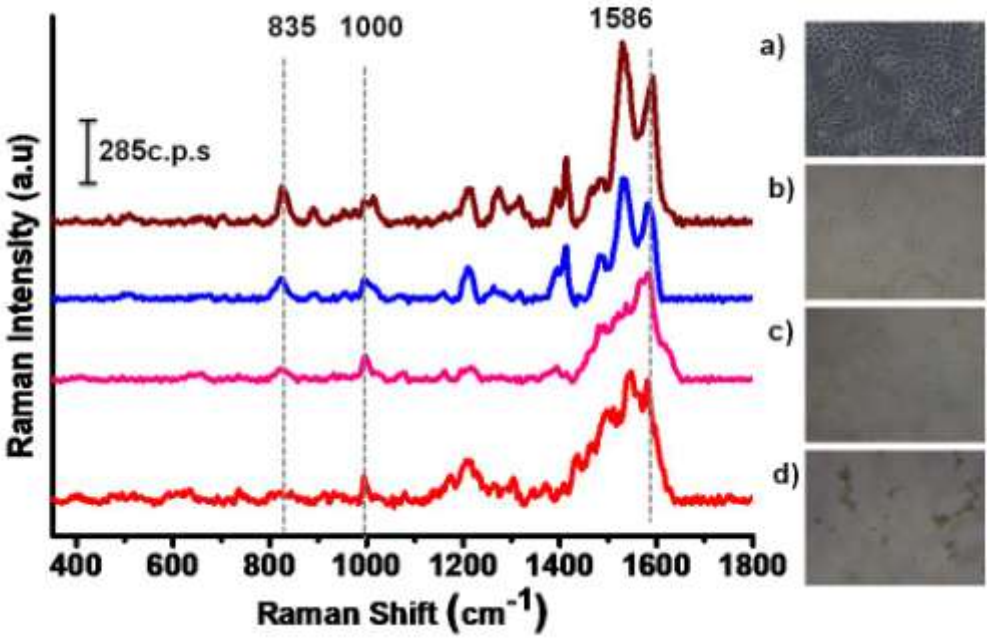

Figure 5.15: A) Time dependent SERS spectra of HeLa cells before and after photo thermal chemotherapy. Control cells without laser (brown) cells incubated with TCNDDS for 4 hr (blue), 6 hr (pink),12hr (red); a, b, c, d represents the corresponding bright field images of HeLa cells**.**

5.3.15 Haemolysis assay

The initial action of any chemotherapeutic agents occurs in blood components which makes it essential to check the effect of any therapeutic agent towards blood components. The cytotoxic agents can produce adverse effect such as haemolysis or thrombogenesis. Hence, evaluation of the haemolytic property of the carriers and TCNDDS, on red blood cells (RBC) under different pH conditions were performed. The positive and negative control samples were prepared with Triton X-100 and PBS respectively, and applied to RBCs. The highest activity was observed in the case of free DOX while the carrier and TCNDDS showed less haemolytic property, indicating high biocompatibility of the system (Figure 5.16).

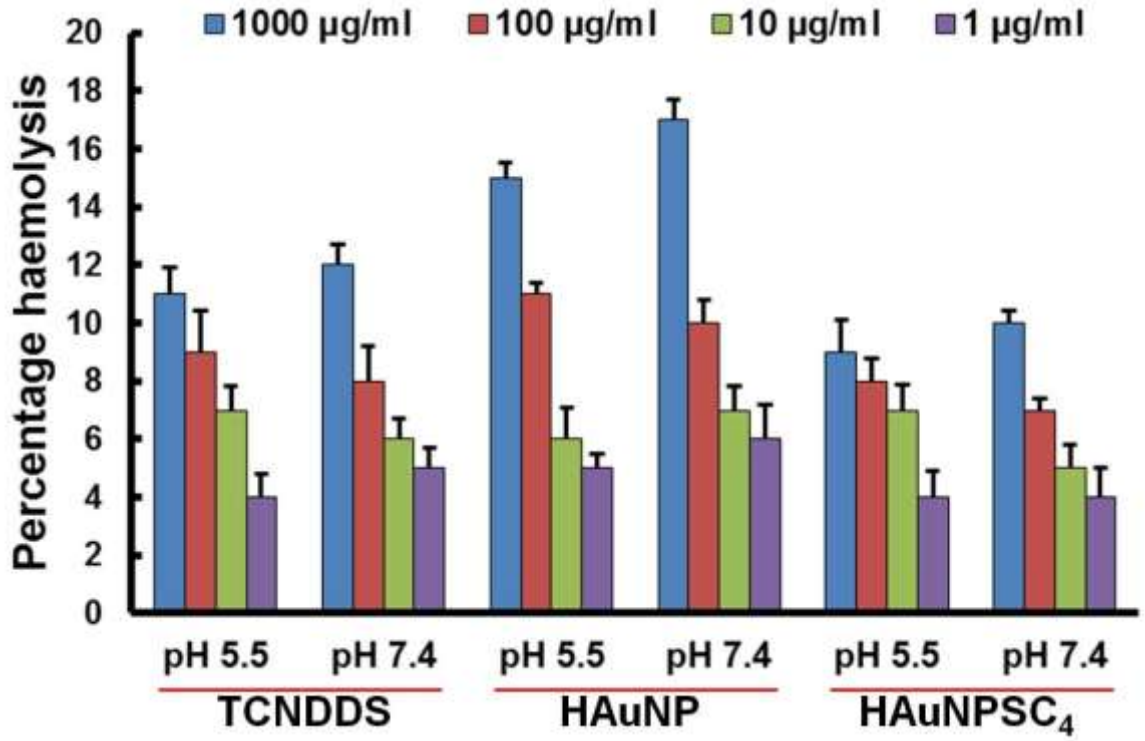

Figure 5.16: Hemolysis experiment performed with TCNDDS, HAuNP and $HAuNPSC_4$ at different concentrations and under various pH conditions; data are the mean ±SD of three independent experiments.

5.3.16 Annexin V binding assay

Morphological changes that occur in the early phases of apoptotic cells were detected by Annexin V-FITC staining, using flow cytometry (Figure 5.17). Annexin V binds to phosphatidylserine, which is externalized by plasma membrane permeability changes (measured by propidium iodide uptake), from the inner side

of the membrane. These events precede the morphological features of apoptosis. The early phase apoptotic cells stained with FITC are represented in the lower right quadrant of the FACS dotplot while the late phase apoptotic cells stained with both FITC and PI are represented in the upper right quadrant. The percentage of apoptotic cells on treatment with TCNDDS or vehicle at 24 h on HeLa cells without (Figure 5.17 a) and with laser (Figure 5.17 b) irradiation is summarized in Figure 5.17c. The induction of programmed cell death on the FR positive HeLa cells with a larger percentage of early and late apoptotic cells underlines the observations with SERS analysis. Further the experiment was repeated on FR negative A549 cells as well. The percentage of apoptotic cells on treatment with TCNDDS or vehicle at 24 h on A549 cells without (Figure 5.17 d) and with laser (Figure 5.17 e) irradiation is summarized in Figure 5.17f. There was minimal apoptosis event s suggesting the excellent targeted delivery of the drugs by the carrier.

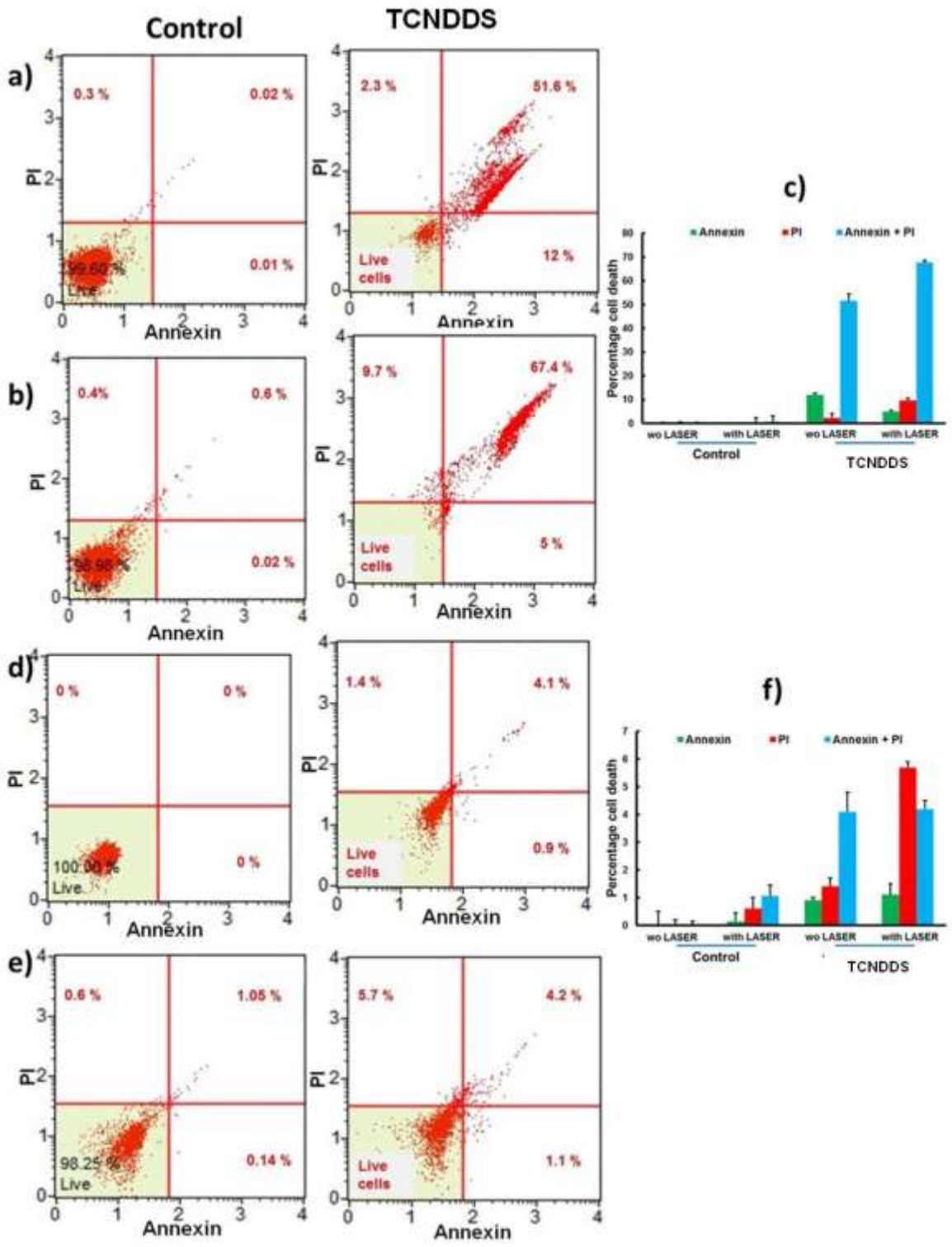

Figure 5.17: Flow cytometric dot plot analysis of PI/annexin V staining in cancer cells treated with TCNDDS. Apoptosis was evaluated by Annexin-V staining after treating HeLa and A549 cells without and with laser Flow cytometry analysis showing Annexin-V-FITC staining in the x-axis and PI in the y-axis. Percent of annexin-positive (apoptotic) cells is indicated in the respective quadrants. a) HeLa

without, b) with laser and c) represents cumulative effects. d) A549 without, e) with laser and f) represents cumulative effects.

5.4 Experimental section

5.4.1 Materials and methods

Doxorubicin hydrochloride, trisodium citrate dehydrate, cobalt chloride hexahydrate (99.99%), MTT reagent, JC1 Dye ,BrDU Kit, were obtained from Sigma-Aldrich (St. Louis, MO). Fmoc protected amino acids *viz*, Fmoc- Lys(Boc)- OH, Fmoc-Arg (pbf)- OH, Fmoc- Gly- OH, Fmoc- Cys (Tr)- OH were acquired from Novabiochem, Globe scientific and the CGKRK sequence was synthesized by manual coupling of amino acids *via* solid phase peptide synthesis (SPPS) by Fmoc chemistry. All the other common reagents and solvents were purchased from Sigma-Aldrich, Merk, and Spectrochem, was used without further purification. High performance liquid chromatography (HPLC) was accomplished by Shimadzu HPLC system consisting of SCL-10Avp system controller, two LC-8A solvent delivery units, SPD-M20A UV-VIS photo diode array (PDA) detector, equipped with Multi PDA- LC solution (software) on a 250 mm x 4.6 mm i.d, 5µm, YMC-Pack R&D Octa- decane silane (ODS) analytical column (9YMC Co., Ltd. Japan). NMR spectra were recorded on a Bruker AMX 300 (1HNMR at 500MHz) spectrometer. Tetra methyl silane was used as reference for 1H NMR, and the chemical shift were reported in ppm and the coupling constant in Hz. High resolution mass spectra were determined on a HR-EMI analysis of Thermo Scientific Exactive system, and MALDI-TOF mass spectra on a Shimadzu Biotech, AXIMA-CFR PLUS system. Lyophilization was performed with lyophilizer, Scan Vacfreez drier model: cool safe 110-4 PRO system (-110^{0}C). Surface enhanced Raman Scattering (SERS) spectra were recorded using confocal Raman microscope alpha 300 R WITeC Germany. The laser power source was directed to the sample via 20X objective (Numerical aperture [NA]-2.1mm) with 600 g/mm grating. The laser source of 633nm excitation wavelength was used for the whole experiments with a laser power of 5mW.All the Stokes Raman spectra were collected using a Peltier cooled CCD detector in the range of 400−3000 cm−1 with an integration time of 0.5 sec and 30 accumulations for single spectra measurements and 0.05 sec integration time and 50X50 µm area scan with 150X150 resolution for image scan.

5.4.2 Cell lines and cell culture

HeLa (cervical cancer cell line), A549 (lung adenocarcinoma), and H9C2 cardio myocyte were purchased from American Type Culture Collection (Manassas, VA). Human lung fibroblast cell line WI-38 was kindly gifted form Indian Institute of Chemical Biology (CSIR-IICB), Kolkata, India. HeLa R cell line was prepared in our lab. For the development of resistant cell line (HeLa R), HeLa wild-type (WT) cells were treated gradually with increasing concentrations of DOX starting from 2 nM. Drug concentration was increased at every passage at a rate of 0.2 nM until 1 lM resistance was achieved. All cells were cultured as anchorage dependent using 25 cm^2 tissue culture treated flask in 37°C incubator with 5% CO_2 humidified atmosphere condition. Cells were maintained in Dulbecco's modified eagle's medium (DMEM) containing 10% fetal bovine serum (FBS), penicillin (50 units/mL), kanamycinsulfate (110 mg/L), streptomycin (50 µg/mL). HEPES (25 mM) buffer and $NaHCO_3$ (3.6g/L) were added to maintain the pH of the culture. Cells were passaged after 70-80% of confluency attained. All the cell culture works were performed in sterile environment

5.4.3 Preparation of the carrier system

Hollow gold nano spheres (HAuNPs) and SC_4 appended hollow gold nano spheres ($HAuNPSC_4$) were synthesized with some modifications from previously reported protocols[7]. Initially, the cobalt nanoparticles were synthesized with extreme care given paid to cleanliness and removing air from the reaction vessel. All glassware was cleaned with glassware detergent, aquaregia distilled and then with water to ensure the elimination of all absorbents; the vessel was washed with ultrapure water thrice. To ensure completely air-free solutions, all solutions were vacuumed twice to remove oxygen on a vacuum line until gas evolution stopped and then bubbled with ultrapure nitrogen for 10 min.100 mL of ultra-pure water (MIlliQ Water 18MΩ) was taken in a 250 mL two-necked round-bottom flask, Purged with N_2 for 5 min. Subsequently 100 µL of 0.4 M cobalt chloride hexahydrate and 400 µL of 0.1M sodium citrate were added. Furthermore the whole solution was deaerated by purging with N_2 for 20 min without stirring. Afterwards a solution of 1M Sodium borohydride (100 µL) was injected and stirred for 40 min until the evolution of H_2 was ceased. The colour of the solution from pale pink to grey colour indicting *in situ*

generation the cobalt nano particles. Simultaneously 0.01 M, 100 µL SC_4 was injected as stabilising agent. Then, a 50 mL RB containing a solution of 10 mL water and 25 µL and was stirred at room temperature. To this stirring solution 30 mL of synthesised cobalt nanoparticles were added and keep stirring for another 5-8 min allowing reduction of Au^{3+}. a slow colour change from grey to dark green indicating the formation of hollow gold spheres. The average diameter and shell thickness of the sample are estimated from HRTEM analysis.

5.4.4 DOX and Mt DOX loading onto $HAuNPSC_4$

The loading of DOX and Mt DOX were evaluated separately. Aliquots of free DOX in ultrapure water were added into an aqueous solution of $HAuNPSC_4$ and the mixtures were shaken at room temperature for 12 hr. After centrifugation (10000 rpm for 10 min), the pellet was washed with MilliQ water and centrifuged, and the washing cycle was repeated until the supernatant became colourless. Supernatants collected were pooled together, and the amount of free DOX in the supernatant was determined by UV-Vis spectrometer. The encapsulation efficiency was calculated.

Encapsulation efficiency = (free dox-DOX in supernatant)/Free DOX x100

Similarly the loading of Mt DOX was also performed by shaking Mt-DOX and HAuNPs for 8 hr. Since Mt DOX containing cysteine residues, the interaction between SH and HAuNPs will be stronger. After 8 h the solution was centrifuged (10000 rpm for 10 min) and the pellet was repeatedly washed in order to remove unbound Mt DOX. The amount of Mt DOX remained in the supernatant was determined and calculated the encapsulation efficiency.

5.4.5 Drug release studies from HAuNPSC4

The release studies were performed by irradiating with 808 nm laser at room temperature. The DOX@$HAuNPSC_4$ and Mt DOX was taken in a 5-mL sample tube. A laser probe (10-mm spot diameter) was placed on the bottom centre of the tube. At pre-determined time intervals, the samples were irradiated with NIR laser centred at 808 nm at an output power of 0.5.0 W/cm2 for 3 min. Then the solutions were centrifuged (10000rpm, 20 min) and supernatants of the particles before and after NIR laser irradiation was analysed by UV-Vis spectroscopy and HPLC. The concentration of DOX in the supernatant was determined spectrophotometrically.

5.4.6 Screening of combination effect with DOX and Mt-DOX by BrdU assay

A total of $1X10^4$ cells were plated in 96-well plates and incubated for 24 hr to allow the cells to attach. The cells were exposed to free DOX and Mt-DOX from 100μM to 0.00001 μM concentrations. Then the cells were incubated at 37 °C for 12, 24, 48 hr respectively. Then the survival efficiency of the cell was evaluated by BrdU Assay kit (colorimetric – 11647229001, Roche Diagnostics, IN, USA) according to the manufacturer suggested procedures. The data reported represented the means of triplicate measurements, and the measurements were made at 450/690 nm.

5.4.7 Cellular internalization and organelle co-localisation study

Cellular uptake studies were performed with a fluorescence microscope and localization was performed after counter staining with nuclear staining dye hochest or mitotracker or lysotracker in HeLa, A549 and H9C2 cells. Cells were treated with DOX or Mt-DOX for 4 hr, then washed with PBS and counter stained with dyes. Imaging was performed under an inverted fluorescent microscope (Olympus 1X51).

5.4.8 Mitochondrial membrane potential evaluation

i) JC1 Assay: 5,5',6,6'-tetrachloro-1,1',3,3'-tetraethyl-benzimidazolyl-carbocyanine-iodide (JC-1) is an particular dye of mitochondrial membrane potential. When JC-1 interacted with normal mitochondria (having high mitochondrial membrane potential), it exhibits red fluorescence (590 nm). When JC-1 bond with damaged mitochondria (with low mitochondrial membrane potential), it exhibits green fluorescence (530 nm). [25] HeLa cells were seeded in 96-well plates(1×10^4 cells/well) for 24 hr. DOX and equivalent concentration of Mt-DOX were added and incubated for 4 hr, then the cell culture medium was removed. The cells were washed with HBSS, 3 times. Later, 100μL of JC-1 work solution (2 μ mol/L) was added and incubated for 20 min and viewed under fluorescence microscope, and finally cells were harvested and dispersed in JC-1 buffer solution (without JC-1). The fluorescence was quantitated by using fluorescent spectrophotometer.

ii) TMRE assay: Further the mitochondrial membrane potential measurement was confirmed by performing TMRE mitochondrial membrane potential assay kit (Abcam). Briefly, the HeLa cells were seeded in a 96-well plate with 1×10^4 cells each well. After incubation for 24 hr, the cells were treated with DOX and Mt-DOX and

incubated for another 24 hr. TMRE with a final concentration of 200 nM was then added to cells in the medium, and cells were further incubated at 37 °C for 20 min. The cells were then washed once with PBS, and then the fluorescence intensity of TMRE was recorded at an emission wavelength of 575 nm by using a microplate reader at an excitation wavelength of 549 nm. The FCCP-treated cells were used as positive control.

5.4.9 Preparation of targeted carrier system

The inclusion complex of folic acid and SC_4 was prepared by solution of folic acid in methanol and SC4 in water. The formation of inclusion was confirmed by UV-Vis Spectroscopy, The complex has been used in the intermediate step for the preparation of $HAuNPSC_4$ (In place of SC_4 0.01mM addition step). The addition of folic acid did not affect the spectral pattern of nano transporter and was confirmed by UV-Vis spectroscopy.

5.4.10 Live cell Raman imaging

Evaluating the efficacy of $HAuNPSC_4$ as a Raman substrate was done with the aid of a confocal Raman microscope (WI-Tec, Inc., Germany) with a laser beam directed to the sample through 20X objective with a Peltier cooled CCD detector. For cellular imaging, 10 µL of HAuNPSC4@DOX and HAuNPSC4@ Mt-DOX was added to HeLa, A549, H9C2, WI-38 cells and was incubated at 37 °C for 1 hr. SERS mapping was recorded by focusing the laser beam on the cell surface selected at a posit ion z = 0 µm using 0.05 as the integration time, 150 × 150 as points per line, and 50 × 50 µm mapping area along the X and Y directions. With the aid of a motorized scan stage the Raman and SERS cell maps were acquired and the images were computed from the 2D collection, after baseline subtraction of SERS spectra by integrating the intensity of a specific band over a defined wave number. Then Raman images were analysed by cluster. A minimum of three independent measurements were made for each sample.

5.4.11 Annexin staining:

Cells were seeded in T25culture flask and treated with TCNDDS or vehicle (PBS) for 24 hr. Cell death was determined by Annexin V-fluorescein isothiocyanate (FITC) and propidium iodide (PI) dual staining kit (BD Biosciences, San Jose, CA,USA).

Briefly, single cell suspensions obtained by trypsin digestion were pelleted by centrifugation at 5000 rpm for 5 min, and stained with Annexin V-FITC and PI for 20 min in the dark at room temperature. The cells were then analyzed by flow cytometry.

5.4.12 Statistical analysis

The data are expressed as the mean ± standard deviation (SD) of three replicates and were analyzed by using Graph Pad Prism software version 5.0 (Graph Pad, La Jolla, CA, USA). One-way analysis of variance (ANOVA) was used for the repeated measurements, and differences were considered to be statistically significant if $p<0.05$. IC_{50} values were calculated with Easy Plot software (version 2.8, Spiral Software, MD, USA).

5.5 Conclusion

The current chapter presents $HAuNPSC_4$ as a novel nano transporter for the targeted combinational delivery of DOX and Mt-DOX towards cancer cells. This approach is worth appreciable in quite a few aspects. First, $HAuNPSC_4$ showed exceptionally high drug loading ability and stability as exemplified by DOX and Mt-DOX owing to the unique physicochemical characteristics of $HAuNPSC_4$. Second, $HAuNPSC_4$ mediated strong photothermal effect owing to their strong surface plasmon absorption in the NIR region. This hyperthermia was exploited for controlled release of both DOX and Mt-DOX from TCNDDS using NIR light as release triggering agent. Third, dual sub cellular compartment targeting drug delivery eliminates drug resistance and cardio toxicity. Forth, The Dual therapy, ie, chemo and PTT were integrated in the nano transporter to produce photothermal effect produced by the carrier; mitochondria mediated cell death *via* release of Mt-DOX and nuclear mediated cell death *via* free DOX after NIR light irradiation. Additionally the SERS ability of the nano transporter enabled real-time Raman based internalisation studies and investigation of cell death mechanism. This approach is expected to significantly improve the therapeutic index, making it a promising approach to cancer therapy. The detailed investigation of apoptotic events tumour reduction capabilities in animal models and Raman analysis are the future perspectives of this work.

5.6 References

(1) Davis, S. S. Coming of Age of Lipid-Based Drug Delivery Systems. *Adv. Drug Deliv. Rev.* **2004**, *56* (9), 1241–1242.

(2) Sun, T.; Zhang, Y. S.; Pang, B.; Hyun, D. C.; Yang, M.; Xia, Y. Engineered Nanoparticles for Drug Delivery in Cancer Therapy. *Angew. Chemie Int. Ed.* **2014**, *53* (46), 12320–12364.

(3) Ajnai, G.; Chiu, A.; Kan, T.; Cheng, C. C.; Tsai, T. H.; Chang, J. Trends of Gold Nanoparticle-Based Drug Delivery System in Cancer Therapy. *J. Exp. Clin. Med.* **2014**, *6* (6), 172–178.

(4) Kumar, A.; Zhang, X.; Liang, X. J. Gold Nanoparticles: Emerging Paradigm for Targeted Drug Delivery System. *Biotechnol. Adv.* **2013**, *31* (5), 593–606.

(5) Lane, L. A.; Qian, X.; Nie, S. SERS Nanoparticles in Medicine: From Label-Free Detection to Spectroscopic Tagging. *Chem. Rev.* **2015**, *115* (19), 10489–10529.

(6) Wittenberg-lyles, E.; Demiris, G.; Oliver, D. P.; Washington, K.; Burt, S.; Shaunfield, S. Phase I and Pharmacokinetic Studies of CYT-6091, a Novel PEGylated Colloidal Gold-rhTNF Nanomedicine. *Clin Cancer Res* **2010**, *16* (24), 6139–6149.

(7) Ren, Q. Q.; Bai, L. Y.; Zhang, X. S.; Ma, Z. Y.; Liu, B.; Zhao, Y. Di; Cao, Y. C. Preparation, Modification, and Application of Hollow Gold Nanospheres. *J. Nanomater.* **2015**, *2015* (2015), 1–7.

(8) Liao, J.; Li, W.; Peng, J.; Yang, Q.; Li, H.; Wei, Y.; Zhang, X. T H E R a N O S T I c S Combined Cancer Photothermal-Chemotherapy Based on Doxorubicin / Gold Nanorod-Loaded Polymersomes. *Theranostics* **2015**, *5* (4), 345–356.

(9) Jian You, Guodong Zhang, and C. L. Exceptionally High Payload of Doxorubicin in Hollow Gold Nanospheres for Near-Infrared Light- Triggered Drug Release. *ACS Nano* **2010**, *4* (2), 1033–1041.

(10) Rahman, A. M.; Yusuf, S. W.; Ewer, M. S. Anthracycline-Induced Cardiotoxicity and the Cardiac-Sparing Effect of Liposomal Formulation. *Int. J. Nanomedicine* **2007**, *2* (4), 567–583.

(11) Shen, F.; Chu, S.; Bence, A. K.; Bailey, B.; Xue, X.; Erickson, P. A.; Montrose, M. H.; Beck, W. T.; Erickson, L. C. Quantitation of Doxorubicin Uptake, Efflux, and Modulation of Multidrug Resistance (MDR) in MDR Human Cancer Cells. *J.*

Pharmacol. Exp. Ther. **2007**, *324* (1), 95–102.

(12) Jean, S. R.; Tulumello, D. V.; Riganti, C.; Liyanage, S. U.; Schimmer, A. D.; Kelley, S. O. Mitochondrial Targeting of Doxorubicin Eliminates Nuclear Effects Associated with Cardiotoxicity. *ACS Chem. Biol.* **2015**, *10* (9), 2007–2015.

(13) Li, W. Q.; Wang, Z.; Hao, S.; He, H.; Wan, Y.; Zhu, C.; Sun, L. P.; Cheng, G.; Zheng, S. Y. Mitochondria-Targeting Polydopamine Nanoparticles to Deliver Doxorubicin for Overcoming Drug Resistance. *ACS Appl. Mater. Interfaces* **2017**, *9* (20), 16793–16802.

(14) Song, Y. F.; Liu, D. Z.; Cheng, Y.; Liu, M.; Ye, W. L.; Zhang, B. Le; Liu, X. Y.; Zhou, S. Y. Dual Subcellular Compartment Delivery of Doxorubicin to Overcome Drug Resistant and Enhance Antitumor Activity. *Sci. Rep.* **2015**, *5* (November), 1–19.

(15) Liu X, Braun GB, Zhong H, Hall DJ, Han W, Qin M, Zhao C, Wang M, She ZG, Cao C, Sailor MJ, Stallcup WB, Ruoslahti E, S. Tumor-Targeted Multimodal Optical Imaging with Versatile Cadmium-Free Quantum Dots. *Adv Funct Mater* **2016**, *26* (2), 267–276.

(16) Sharma, M.; El-Sayed, N. S.; Do, H.; Parang, K.; Tiwari, R. K.; Aliabadi, H. M. Tumor-Targeted Delivery of siRNA Using Fatty Acyl-CGKRK Peptide Conjugates. *Sci. Rep.* **2017**, *7* (1), 1–14.

(17) Guo, D.-S.; Liu, Y. Supramolecular Chemistry of P-Sulfonatocalix[n]arenes and Its Biological Applications. *Acc. Chem. Res.* **2014**, *47*, 1925–1934.

(18) Zwicke, G. L.; Mansoori, G. A.; Jeffery, C. J. Utilizing the Folate Receptor for Active Targeting of Cancer Nanotherapeutics. *Nano Rev.* **2012**, *1*, 1–11.

(19) Han, S.; Shi, X.; Zhou, F. Polyelectrolyte Hollow Sphere Lithographic Patterning of Surfaces: Construction of 2-Dimensional Well-Ordered Metal Arrays. *Nano Lett.* **2002**, *2* (2), 97–100.

(20) Schwartzberg, A. M.; Olson, T. Y.; Talley, C. E.; Zhang, J. Z. Synthesis, Characterization, and Tunable Optical Properties of Hollow Gold Nanospheres. *J. Phys. Chem. B* **2006**, *110* (40), 19935–19944.

(21) Borzenkov, M.; Chirico, G.; D'Alfonso, L.; Sironi, L.; Collini, M.; Cabrini, E.; Dacarro, G.; Milanese, C.; Pallavicini, P.; Taglietti, A.; Bernhard, C.; Denat, F. Thermal and Chemical Stability of Thiol Bonding on Gold Nanostars. *Langmuir*

2015, *31* (29), 8081–8091.

(22) Melamed, J. R.; Edelstein, R. S.; Day, E. S. Elucidating the Fundamental Mechanisms of Cell Death Triggered by Photothermal Therapy. *ACS Nano* **2015**, *9* (1), 6–11.

(23) Narayanan, N.; Nair, L. V.; Karunakaran, V.; Joseph, M. M.; Nair, J. B.; N, R. A.; Jayasree, R. S.; Maiti, K. K.;, M. A. Investigation of Apoptotic Events at Molecular Level Induced by SERS Guided Targeted Theranostic Nanoprobe. *Nanoscale* **2016**, *8* (22), 11392–11397.

(24) Kang, B.; Austin, L. A.; El-sayed, M. A. Observing Real-Time Molecular Event Dynamics of Apoptosis in Living Cancer Cells Using. *ACS Nano* **2014**, *8* (5), 4883–4892.

(25) Keil, V. C.; Funke, F.; Zeug, A.; Schild, D.; Müller, M. Ratiometric High-Resolution Imaging of JC-1 Fluorescence Reveals the Subcellular Heterogeneity of Astrocytic Mitochondria. *Pflugers Arch. Eur. J. Physiol.* **2011**, *462* (5), 693–708.